UNIVERSITY OF SOUTHAMPTON

Biological validation of acoustic backscatter and observations of biological/hydrographic interactions at the mesoscale

Sophie Fielding

Submitted for the degree of Doctor of Philosophy

September 2002

UNIVERSITY OF SOUTHAMPTON

ABSTRACT

FACULTY OF SCIENCE

Doctor of Philosophy

Biological validation of acoustic backscatter and observations of biological/hydrographic interactions at the mesoscale

by Sophie Fielding

The objective of this thesis was to study the distributions of zooplankton at the mesoscale, using acoustic backscatter data (from an Acoustic Doppler Current Profiler, ADCP and SIMRAD EK500 echosounder) taken concurrently with hydrographic data (from SeaSoar and CTDs) and net-sampled zooplankton (from a Longhurst Hardy Plankton Recorder, LHPR). A further aim was to validate acoustic backscatter data with concurrent net data.

Two cruises collected multidisciplinary datasets from two contrasting regions. RRS *Discovery* cruise 209 to the Arabian Sea (Indian Ocean) in August 1994 and RRS *Discovery* cruise 224 to the Alboran Sea (Mediterranean Sea) during November and December 1996.

The Arabian Sea was dominated by a strong oxygen minimum zone (OMZ) that extended from the thermocline (~50 m), to ~1100 m. From the analysis of sound scattering layers and net samples the OMZ appeared to play a major role in determining the vertical distribution of zooplankton. A persistent layer of high acoustic backscatter and high zooplankton biovolume indicated that the vertical extent of some zooplankton was restricted to oxygenated surface waters. Euphausiids, decapods and myctophid fish were observed to undertake dawn diel migration between the surface and depths of 300 – 400 m, well into suboxic waters, whilst the vertical distribution of polychaetes appeared to be independent of oxygen concentration and it is suggested that these taxa may possess morphological and physiological adaptations to low oxygen environments.

The Alboran Sea is the site of an intense geostrophic density front that has associated ageostrophic vertical components. It appeared that the front was exhibiting a fertilising effect on both phytoplankton and zooplankton. Observations of a layer of chlorophyll *a* fluorescence coincident with subducted surface waters indicated that phytoplankton were down and along isopycnals to a depth of ~200 m. Acoustic backscatter data and net samples indicated that increased numbers of euphausiids and chaetognaths occurred coincident with the drawn-down phytoplankton. Smaller zooplankton, copepods and possibly euphausiid larvae, which did not undertake diel migration, remained concentrated near the surface in the fast-flowing frontal jet.

A relationship between acoustic backscatter and net-sampled zooplankton abundance and biovolume is described using a direct comparison and acoustic scattering models. This thesis shows that observed acoustic backscattering volume is generally consistent with forward problem predictions. This consistency is true in terms of both total sample backscatter as well as the proportion of the acoustic backscatter contributed by each of six dominant sound scatterer types.

Contents

List of Figures

Chapter 5

Preface

The material included in this thesis has not been submitted for any other qualification at any other university. This thesis represents my own work.

This thesis has been produced under the supervision of Professor Paul Tyler[1] and Professor Howard Roe[2].

[1] School of Ocean and Earth Science, Southampton Oceanography Centre.

[2] Director, Southampton Oceanography Centre.

THE FAR SIDE® By GARY LARSON

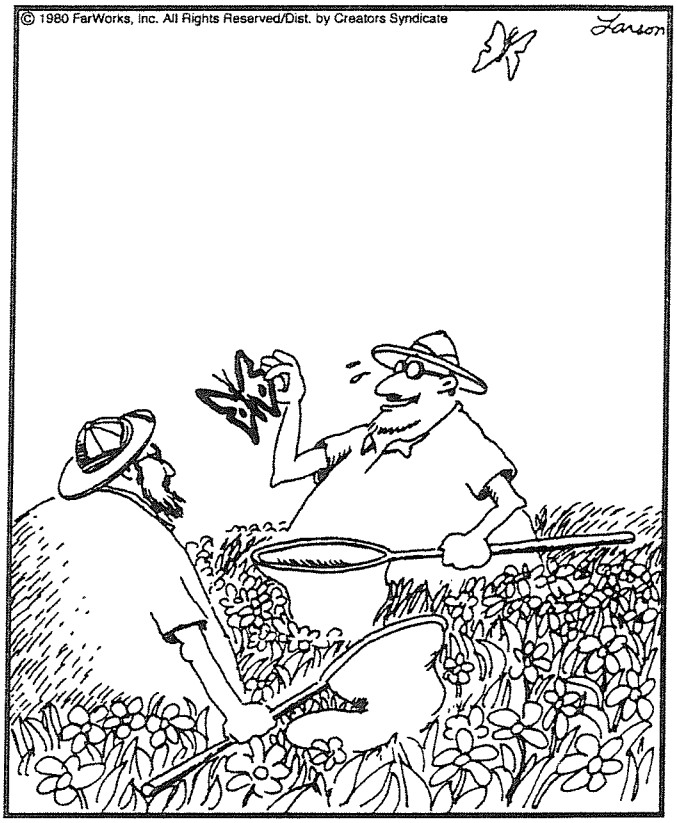

"An excellent specimen ... the symbol of beauty, innocence, and fragile life. ... Hand me the jar of ether."

Acknowledgements

First, I would like to thank Professors Howard Roe and Paul Tyler for their overall supervision of this work. Many thanks also to Professor Gwyn Griffiths for his valuable comments on the acoustic literature review and his help with the acoustic scattering models. I would also like to acknowledge the support of George Deacon Division for part-funding this thesis and for the provision of facilities.

Multidisciplinary observational surveys require many people to both collect and process the resultant data. I would like to thank the scientists, officers and crew who participated in RRS *Discovery* cruise 209 and especially those from cruise 224 who made it such a pleasurable experience to go to sea. For their initial processing of the hydrographic and acoustic data I would like to thank Dr. J. Allen, Mr N. Crisp and Mr M. Hartman. I would also like to thank Dr. M. Angel, Dr. P. Hargreaves, Dr. P Herring, Ms P. Howell, Ms G. Malzone and Dr. P. Pugh in identifying and sorting some of the supplementary net samples.

I would like to thank my friends here at SOC (Alex, thank you for not moaning too much about the mess in the lab), who have occasionally housed me (cheers Andrew), and from my school days, who have supported and encouraged me, and to David for taking me fishing!

Most of all I would like to thank my parents and my brother for their support. Dad – for the one you never wrote up.

List of abbreviations used

AMIW	Atlantic Mediterranean Intermediate Water
AOW	water of predominantly Atlantic origin
ARS	Arabesque Reference Site
ASW	Arabian Sea Water
AW	Atlantic Water
CTD	Vertical profiling system, incorporating Conductivity, Temperature and Depth sensors.
dB	Decibels
DVM	Diel Vertical Migration
DWBA	Deformed Wave Borne Approximation
EAG	Eastern Alboran Gyre
EOFC	Empirical Orthogonal Function Classifier
JGOF	Joint Global Ocean Flux Study
IOEW	Indian Ocean Equatorial Water
kHz	Kilohertz
LHPR	Longhurst-Hardy Plankton Recorder
LIW	Levantine Intermediate water
MMAW	mixed Mediterranean and Atlantic water
MOW	water of Mediterranean Surface water origin
MPC	Model Paramaterization Classifier
MSW	Mediterranean Surface Water
OAB	Observed Acoustic Backscatter
PGW	Persian Gulf Water
RSW	Red Sea Water
SSL	Sound Scattering Layer
TMEAB	Total Model-Estimated Acoustic Backscatter
TML	Temperature Minimum Layer
VM-ADCP	Vessel Mounted Acoustic Doppler Current Profiler
WAG	Western Alboran Gyre
WOCE	World Ocean Circulation Experiment

Chapter 1

Introduction and background to this thesis

1.1 Introduction to the thesis, objectives and layout

1.1.1 Relevance

"The spatial scale over which patchiness is measured defines the patterns and processes that can be observed"

(Folt and Burns, 1999)

A central aim of biological oceanography is to identify the major processes that control the dynamics of pelagic ecosystems (Legendre *et al.*, 1999). This information is vital for understanding and predicting changes in the pelagic ecosystem that result from natural and anthropogenic environmental changes and for the management of marine resources.

Zooplankton distributions in the ocean result from interactions between behaviour and the environment. These interactions lead to variability that is generically referred to as patchiness. Patchiness has been recorded on a wide variety of temporal and spatial scales, the dominant forcing function changing with scale (Haury *et al.*, 1978; Dickey, 1991). At the scale of ocean basins (>100 km), the physical processes of water mass formation and circulation set the distribution of zooplankton, forming the basis of zoogeography (Fager and McGowan, 1963; Pierrot-Bults *et al.*, 1986). At the smaller scale (1 mm to 10 m) variability is dominated by individual behaviours (e.g. mating and predator avoidance) that, in some instances, are capable of overriding physical processes (Folt and Burns, 1999). However, at the mesoscale, (10s - 100s kms) the spatial and temporal scales relevant for biological processes may interfere with the scales at which physical forces operate (Legendre *et al.*, 1986), thus variability is dominated by a complex interplay between the dynamics of fronts and eddies and biological behaviour (Strass, 1992; Roe *et al.*, 1996).

A fundamental requirement is the ability to sample biological data at the same spatial and temporal scales and rates as other environmental variables (Reeve, 1988). As the study of biological-physical interactions extends to finer scales and more fundamental processes, the demands increase for improved observational approaches. Remote sensing techniques now play a major role in such studies because of their ability to provide non-evasive measurements at a range of observational scales in both time and space. At one end of the spectrum satellite images of ocean colour provide an opportunity for studying the interaction of surface biological productivity with mega and mesoscale features. Below the surface of the ocean other remote sampling techniques are required.

One such technique is acoustics. Biological oceanographers have focused to a large extent on underwater sound as a tool to examine zooplankton distributions and dynamics

(Holliday, 1992). Conventional net and pump sampling cannot resolve even the mesoscale and the data are inevitably aliased leading to synoptic but simplified and inaccurate overviews (Nival, 1990). Whereas, acoustic methods provide a non-intrusive sampling technique that is capable of providing high-resolution qualitative and quantitative biological data over a range of time and space scales (Horne, 1998). The use of non-invasive techniques circumvents the potential response of zooplankton to the sampling instrument (e.g., net avoidance, Orr, 1981; Sameoto *et al.*, 1990; Cochrane *et al.*, 1991), eliminates behaviour-biased data (Smith *et al.*, 1992) and permits targeting of conventional sampling programmes.

Acoustic methods, combined with conventional net samples, provide a key tool in resolving zooplankton distributions at scales comparable with mesoscale physics, hence providing an ability to observe and resolve physical and biological forcing of zooplankton patchiness. The use of acoustics to resolve the dominant mesoscale physical and biological forcing governing zooplankton distributions in two different oceanic environments (the Arabian Sea and Alboran Sea) and the relationship between acoustic backscatter and zooplankton biomass are the key focii of this thesis.

The results from Chapters 4 and 5 of this thesis have been published as peer-reviewed papers (Appendix A).

Fielding, S. Crisp, N., Allen, J. T., Hartman, M. C., Rabe, B. and Hoe, H. S. J. (2001) Mesoscale subduction at the Almeria-Oran front: Part 2. Biophysical interactions. *Journal of Marine Systems*, **30**, 287-304.

Griffiths, G. Fielding, S. and Roe, H. S. J. (2002) Biological-Physical-Acoustical Interactions. In: The Sea: Biological-Physical interactions. A. R. Robinson, J. J. McCarthy and B. J. Rothschild (eds.). New York, John Wiley & Sons Inc. 441-474.

1.1.2 Tasks and objectives of the thesis

Three main tasks were completed in order to examine the biological distributions and physical interactions at two mesoscale features and investigate how acoustic backscatter data correlates with net-sampled zooplankton.

(1) Two multidisciplinary (hydrographic and biological) datasets were collected on the *RRS Discovery*. Cruise D209, 03 – 22 August 1994, in the Arabian Sea around 19 °N 59 °E (Herring, 1994; Chapter 3), and Cruise D224, 22 November 1996 – 17 January 1997, in the Alboran Sea within the western Mediterranean (Allen and Guymer, 1997; Pugh, 1997; Chapter 4).

(2) Net samples were analysed and used in partnership with acoustic and hydrographic data to describe the distribution of zooplankton and their interaction with their environment.

(3) Acoustic models were used to predict acoustic backscatter from the analysed net samples, which was compared with observed acoustic backscatter data.

The datasets and analyses were utilised to fulfil the following five objectives:

(1) Describe the distribution of zooplankton in relation to physical features and the oxygen minimum layer in the Arabian Sea.

(2) Describe the distribution of zooplankton in relation to the physical features and the water column structure in the Alboran Sea.

(3) Investigate the interplay between physical and biological forcing mechanisms on the distribution of zooplankton.

(4) Investigate the relationship between actual zooplankton net samples with observed acoustic backscatter in different oceanic regimes.

(5) Examine the use of acoustic models to relate acoustic backscatter to zooplankton in the *in situ* environment.

1.1.3 Thesis layout

Chapter 1 Introduction and literature review

In chapter one the work is introduced and its relevance and rationale discussed. A list of the main tasks and objectives is given. Subsequently literature reviews detail the dominant physical and biological forcing mechanisms controlling the distribution of zooplankton, and the development and use of acoustic methods.

Chapter 2 Methodology

This chapter provides a description of the collection, processing and calibration of the multidisciplinary datasets with particular emphasis on RRS Discovery Cruise 224 in which the author participated and played a greater part in the data collection.

Chapter 3 The Arabian Sea

A description of the major hydrographic features, water masses present and the water column structure of the Arabian Sea are presented in this chapter. Followed by a description of the hydrography and oxygen concentration at the Arabesque Reference site and the distribution of zooplankton examined using acoustic and net techniques.

Chapter 4 The Alboran Sea

A description of the major hydrographic features, the water masses present and the water column structure of the Alboran Sea, with particular focus on the Almeria-Oran front, are presented in this chapter. Followed by a description of the distribution of phytoplankton and zooplankton in relation to the physical environment. As in chapter 3 acoustic and net techniques are used to examine the distribution of zooplankton, these distributions are discussed in relation to the physical circulation and the Almeria-Oran front.

Chapter 5 An investigation into the relationship between zooplankton and acoustic backscatter

The relationship between acoustic backscatter and net-sampled zooplankton is investigated using both direct comparisons and predictions based on acoustic scattering models. Data from the Arabian Sea and the Alboran Sea are discussed separately.

Chapter 6 Summary, data limitations and future directions

A summary of chapters 3, 4 and 5 is given and data limitations and future directions are discussed.

1.2 Plankton patchiness

1.2.1 Introduction

Zooplankton are distributed in the oceans unevenly (i.e. patchily). They were long considered passive members of patches that were the product of physical processes (Pinel-Alloul, 1995). More recently, biological processes have been shown to contribute to zooplankton patchiness in addition to or overriding physical processes (Wishner and Allison, 1986; O'Brien, 1988; Zhou *et al.*, 1994). Because of the dynamic nature and variability of the oceans it is impossible to perform large-scale experiments to investigate the factors that influence the distribution of plankton. However, natural mesoscale phenomena exist that provide a means to investigate physical, chemical and biological influences on the distribution of plankton. The first aim of this thesis is to examine the distribution of zooplankton in relation to two different oceanic environments (the Arabian Sea and the Alboran Sea). In particular, the affect of the oxygen minimum layer on the distribution of zooplankton in the Arabian Sea, and the affect of an energetic geostrophic front in the Alboran Sea.

Modern technologies now provide us with a means to observe biological variability on similar scales as physical variability (e.g. Roe *et al.*, 1996; Fielding *et al.*, 2001). Acoustic methods are capable of collecting high-resolution qualitative and quantitative data on the distribution of zooplankton at scales equivalent to physical processes, permitting the identification and differentiation of the relative contributions of biology and physics to patchiness (Zhou *et al.*, 1994). However, the relationship between zooplankton and acoustic backscatter is complex (Holliday and Pieper, 1995) and acoustic research has diversified into the use of acoustics to measure the distribution of zooplankton in a qualitative fashion (e.g. Roe *et al.*, 1996; Wade and Heywood, 2001) and the assessment and interpretation of the relationship between acoustic backscatter and zooplankton (Wiebe *et al.*, 1996; Greene *et al.*, 1998; Stanton *et al.*, 1998a,b). The second aim is to use acoustic techniques as an aid to achieving the first aim and to assess the relationship between acoustic backscatter and zooplankton biomass, abundance and composition.

The following section (1.2) presents a general overview of the physical and biological forcing mechanisms that influence the distribution of plankton. Section 1.2.3 and section 1.2.4 discuss the more specific affects of oxygen minima and fronts on the distribution of zooplankton and in section 1.3 the theory and use of acoustics methods as a tool to measure zooplankton is reviewed.

1.2.2 Mechanisms that influence the distribution of plankton at the mesoscale

1.2.2.1 Introduction

The mesoscale covers length scales of ten to hundreds of kilometres and time scales of days to years (Flierl and McGillicuddy, 2002). Features that typically fall into the mesoscale category are eddies, fronts, jets and filaments. Physical processes associated with these features are understood to affect both the chemical and biological environment and this has been the subject of several reviews (Haury *et al.*, 1978; Owen, 1981; Olson *et al.*, 1994; Olson, 2002; Flierl and McGillicuddy, 2002).

In the 1960s and 1970s, physical oceanographers realised that mesoscale variability was ubiquitous within the oceans and that eddy flows were an order of magnitude stronger than the mean currents. Studies showed that the transport of momentum and heat by these transient motions could significantly alter the general circulation of the ocean (Robinson, 1983). Evidence that these mesoscale features could also profoundly alter the distributions and dynamics of the biota came later (e.g. Angel and Fasham, 1983).

At the mesoscale, because the scales at which physical processes operate are comparable with some behavioural scales (at a population level, e.g. diel migration, not an individual level), the distribution of plankton is determined by both biological and physical forcing. The net result of these forces can lead to strong cross-feature gradients in species composition, depth distributions and biomass (Grice and Hart, 1962; Ashjian and Wishner, 1993). The following review has been separated into physical forcing and biological forcing, however it must be remembered that they are not mutually exclusive.

1.2.2.2 Physical processes affecting the distribution of zooplankton

Mesoscale forcing can affect the distribution of zooplankton directly or indirectly. Direct affects occur where the fluid flow acts to transport the biology, both by translation of the water parcel and its contents (advection) and by dispersal to neighbouring water (dispersion). Indirect affects occur when the physical processes affect nutrient concentration and phytoplankton productivity and biomass that, in turn, produces a bottom up forcing of the higher trophic levels.

The flow fields associated with mesoscale features such as eddies, fronts and jets can directly influence the distribution of both phytoplankton and zooplankton through aggregation, dispersion, isolation, redistribution and advection (Owen, 1981; the Ring Group, 1981; Franks, 1992; Govoni and Grimes, 1992; Denman and Powell, 1994; Hood *et al.*, 1999).

Often associated with mesoscale geostrophic flows are ageostrophic vertical motions, produced either directly as part of the baroclinic flow or indirectly through interaction within the surface boundary layer (Allen *et al.*, 2001), that also influence the biological distribution (Fielding *et al.*, 2001). Vertical displacement of phytoplankton and zooplankton may have greater ecological effects than similar horizontal displacement because environmental gradients of temperature, salinity, light, pressure, oxygen, nutrients and flow are steepest in the vertical (Owen, 1981). In regions of upwelling, phytoplankton can be brought into higher light where they can potentially increase their photosynthetic rate and therefore their biomass given sufficient nutrients. Conversely in regions of downwelling, phytoplankton adapted to surface light conditions will typically not do well if they are moved deep in the euphotic zone (Olson *et al.*, 1994). Upwelling may also result in increased phytoplankton productivity and biomass through the supply of new nutrients into the euphotic zone or an oligotrophic region (Strass, 1992). In this way mesoscale features can enhance primary production (e.g. Prieur *et al.*, 1993; Videau *et al.*, 1994) that in turn can modify the distribution of zooplankton, through accumulation at a food source (an active response of the zooplankton, e.g. a bottom up effect). An increase

in nutrients may not only increase primary production but also result in a change of the dominant phytoplankton species, altering the trophic pathway of the ecosystem. This could cause movement away from the "microbial loop" food chain (Azam *et al.*, 1983) where little energy is passed up to the mesozooplankton (Cushing, 1989), the prevailing food chain in oligotrophic open ocean environments (Eppley and Peterson, 1979) where autotrophic picoplankton dominate, to the more "classic" food chain (Hardy, 1924), where larger autotrophic phytoplankton such as diatoms dominate. Larger phytoplankton are more suitable food for mesozooplankton, so consequently there may be a shift from a heterotrophic microzooplankton dominated system to a mesozooplankton-dominated system.

Vertical motions may also affect larger plankton. The ability of zooplankton to swim may determine the extent to which they can be redistributed by the flow field or may cause patchiness indirectly. For example, one indirect means of concentration of organisms in fronts occurs when the zooplankton cancels out the vertical fluid motion associated with cross-front circulation. That is the downward motion is cancelled by upward swimming owing to geotaxis or phototaxis, which would then lead to accumulation in the front (Olson, 2002).

As we progress up the food chain the ability to resist vertical motions increases, even though horizontal dispersion or concentration may still be affected by advection in ocean currents. Where swimming ability equals or exceeds physical forces enhancement in zooplankton biomass may arise through biological forcing (e.g. behaviourally mediated concentration).

1.2.2.3 Biological processes affecting the distribution of zooplankton

Four biological forcing mechanisms are consistently cited for their potential to cause zooplankton patchiness: Diel Vertical Migration (DVM), predator avoidance, finding food and mating (Folt and Burns, 1999). These may act alone or in combination to drive spatial heterogeneity.

DVM was first studied by Cuvier (1817) who described this phenomenon in freshwater Cladocera, and has since been reviewed numerous times (Russell, 1927; Kikuchi, 1930; Cushing, 1951; Banse, 1964; Roe, 1974; Angel, 1986; Forward, 1988). DVM is the increased acceleration of the continuous movement of motile plankton around sunset and sunrise (Roe *et al.*, 1984; Roe, 1984a,b). Typically, this is upwards at dusk and downward at dawn, but patterns may vary by taxa and stage, and observations of "reverse" migrations have been reported (Chae and Nishida, 1995; Heywood, 1996). Therefore as a result of DVM, organisms periodically aggregate at certain depths in an often-predictable

pattern. Much research has focused on distinguishing the physical and biological cues that alter DVM behaviour and variations in migration amplitude and depth has been related to variations in light (isolumes and rate of change), predators, food, oxygen and the zooplanktons endogenous rhythms (Roe, 1982; Richards *et* al., 1996; Manuel *et al.*, 1997; Dagg *et al.*, 1997; Herring *et al.*, 1998). In addition, the hydrographic structure of the water column may also affect DVM behaviour. Wishner and Allison (1986) and Ashjian and Wishner (1993) observed the constriction of the depth range over which DVM took place of some vertically migrating species in a strong cross-frontal environmental gradient.

Predators can create patchiness in prey spatial distributions both directly, by removing individuals (Folt *et al.*, 1993), and indirectly, by eliciting avoidance or escape responses (e.g. triggering DVM, Folt and Burns, 1999). The removal of individuals could also be classed as top-down pressure. The aggregation of zooplankton (whether through biological or physical forces) results in top down mechanisms. High densities of mesozooplankton are capable of exerting grazing pressure leading to fluctuations in phytoplankton biomass (Legendre *et al.*, 1999). In response to high densities of mesozooplankton, zooplanktivores may also aggregate resulting in gaps or grazing holes in the mesozooplankton distribution (Wishner *et al.*, 1988; Folt *et al.*, 1993; Macaulay *et al.*, 1995). At a smaller scale predator-induced avoidance or escape mechanisms may contribute towards maintaining aggregations. For example, predator chemicals increase the tendency of some cladocerans to aggregate horizontally (Pijanowska and Kowalczewski, 1997).

High food concentration is also potentially a strong driver of patchiness. In zooplankton this may result when physical processes concentrate them with phytoplankton passively, or when they orientate to food patches as individuals locate or remain in them. The ability to locate and remain within food patches has been observed in the copepod species *Acartia tonsa*, where they changed swimming speeds, turning angles and hopping rates in response to variations in food concentrations (Tiselius, 1992). This process also occurs at higher trophic levels. For example Carey and Robison (1981) show that when the swordfish *Xiphias gladius* moves across the Gulf Stream under a plankton-rich streamer of shelf water, it responds directly to the resultant decrease in light by raising in the water column.

Reproductive strategies are a dominating behaviour mechanism for any organism. Aggregation, swarming and mating are frequently linked (Larsson and Dobson, 1993). Since, for some zooplankton, mating frequency may depend entirely on chance

encounters, the maintenance of position within patches created by physical processes and migrations will be important.

1.2.3 The influence of oxygen minima on the distribution of zooplankton

1.2.3.1 Introduction

Midwater Oxygen Minimum Zones (OMZs) exist in all the worlds oceans, the most prominent are in the eastern Atlantic off NW Africa, the northern Indian Ocean (the Arabian Sea and the Bay of Bengal) and in the eastern tropical Pacific Ocean (Kamykowski and Zentara, 1990). They result from the degradation of primary producers, high oxygen consumption by zooplankton and bacteria, and reduced horizontal mixing below the thermocline (Wyrtki, 1962). In pronounced OMZs, oxygen concentration is high at the surface, decreasing abruptly below the thermocline to levels of less than 0.2 ml $O_2 l^{-1}$, and then below one thousand metres it increases with increasing depth (Saltzman and Wishner, 1997a).

1.2.3.2 The affect of oxygen minimum zones on the distribution of zooplankton

Oxygen is an important resource related to metabolism for most organisms (Eckert, 1983), and therefore it can be expected that OMZs will affect the distribution of plankton. Primary production in the surface mixed layer is not affected directly by the low oxygen layer, but the overall biological structure of the water column will be affected by the ability of particular species to endure oxygen deprivation within the OMZ (Herring *et al.*, 1998). In regions with pronounced OMZs, the distribution of zooplankton typically follows the trends of the oxygen concentration, with high plankton biomass in the mixed layer and a sharp decrease at the oxycline (Vinogradov and Voronina, 1961; Bottger-Schnack, 1996), in addition to a general decrease in biomass with depth (Angel, 1990). Deep-water oceanic species are either absent from oxygen-deficient regions or only from the OMZ. This may result in a secondary peak in biomass near the bottom of the OMZ (Sameoto, 1986). The OMZ may influence the distribution of zooplankton in three ways. Firstly, it may present a barrier to some zooplankton limiting their distribution to within the mixed layer and thermocline zones day and night (Herring *et al.*, 1998; Wishner *et al.*, 1998). For example, in the eastern tropical Pacific OMZ area 70 % of the zooplankton biomass in a 1230 m water column resided in the upper 100 m (Saltzman and Wishner, 1997a). Secondly, it may override behavioural mechanisms such as DVM, or limit the vertical extent of DVM (Herring *et al*, 1998). Different taxa are limited by different oxyclines, suggesting species-specific differences in physiological tolerance to low oxygen (Morrison *et al.*, 1999) As a result changes in species distribution occur with depth

(Brinton, 1979; Bottger-Schnack, 1996). It should be noted that the presence of DVM of some zooplankton, especially larger organisms, into suboxic waters has been observed (Morrison *et al.*, 1999; Luo *et al.*, 2000; Ashjian *et al.*, 2002). The physiology of these migrators remains unclear, although behavioural, physiological and morphological adaptations have been implied. The ability of some fish and zooplankton to move through suboxic zones, live anaerobically or alter their metabolism for limited periods has been reported (Baird *et al.*, 1973; Boyd *et al.*, 1980; Childress and Thuesen, 1992). More recently Herring *et al.* (1998) and Herring and Hargreaves (1998) comment on morphological adaptations such as extended gills and a softening of the carapace in an Arabian Sea decapod. Another indication suggesting a reduction in metabolism of animals within the OMZ is that many studies indicate higher daytime catches at depth than at the surface at night, suggesting that the animals during the day were less active most probably as a direct influence of oxygen limitation (Wishner *et al.*, 1998). The third influence of an OMZ is the occurrence of zooplankton at depth at the lower OMZ interface zone (Saltzman and Wishner, 1997b). Childress (1975) and Wishner *et al.* (1990) hypothesised that below the OMZ, even though the supply of organic matter is less, more food energy may be available because of higher oxygen concentrations and consequently lower metabolic cost.

1.2.4 The affect of fronts on the distribution of zooplankton

1.2.4.1 Introduction

Fronts form at interfaces between different water masses of different hydrographic, chemical and dynamic properties (Sournia, 1994) and can often be characterised by a rapid change in the horizontal density gradient. Four basic mechanisms are cited as responsible for the occurrence of fronts. These are (1) horizontal convergence associated with baroclinic instability and eddy formation (Pedlosky, 1979), (2) shearing flows acting on the density field (Cushman-Roisin, 1984), (3) gradients in vertical motion driven by forces such as winds (Charney, 1955), and (4) the conversion of vertical spatial gradients to horizontal gradients by diabatic mixing that eliminates the stratification on one side (Pingree, 1978).

Frontal zones harbour ecosystems where the patchiness of marine populations can be affected by the complex physical environment (Owen 1981; Haury, 1982; Fielding *et al.*, 2001; Olson, 2002).

1.2.4.2 The affect of fronts on the distribution of zooplankton

The response of organisms to a frontal environment varies by location and trophic level (Olson, 2002). The basic biological feature described in proximity to fronts is an

increase in biomass (Owen, 1981; Le Fevre, 1986;). This can be attributed to accumulation as a result of physical mechanisms (see Section 1.2.2.2), "an attraction to food" or frontal enhancement (bottom up forcing, see Section 1.2.2.3).

Increased biomass resulting from enhanced primary production in the proximity of fronts has been reported by numerous authors (*inter alia* Bainbridge, 1957; Olson, 1986; Strass, 1992). This increase in biomass is thought to result from various mechanisms including: vertical motion affecting the light field encountered by phytoplankton (Lillibridge *et al.*, 1990); mixing of phytoplankton and nutrients along the frontal interface (Yoder *et al.*, 1983; McClain *et al.*, 1990; L'Heguen *et al.*, 1993); death and subsequent remineralisation of foreign populations supporting higher endemic species growth, and along-front advection of populations in the presence of an along-front gradient in other environmental parameters (Olson *et al.*, 1994). In ageostrophic fronts, where cross-frontal secondary circulation exists, this production can be exported downwards along sloping isopycnals (Dewey *et al.*, 1991; Gorsky *et al.*, 1991; Videau *et al.*, 1994; Fielding *et al.*, 2001).

This enhanced phytoplankton standing stock may be passed to higher trophic levels (Le Fevre, 1986). Zooplankton populations have been shown to be influenced by fronts in passive response to physical factors, or through behavioural changes (e.g. Boucher, 1984; Govini and Grimes, 1992; Ashjian *et al.*, 1994; Thibault *et al.*, 1994). Increases in zooplankton abundance at frontal boundaries has been attributed to: behaviourally mediated concentration in the presence of convergence zones (Okubo, 1978; Olson and Backus, 1985; Franks 1992; 1997; Govoni and Grimes, 1992); close association with thermal gradients (Ortner *et* al., 1980; 1981; Magnuson *et al.*, 1981); orientation to density discontinuities (Murav'yev and Shirshov, 1984) or abundance of food (Bowman and Esaias, 1978; Crowder and Magnuson, 1983). Interpreting zooplankton distributions can be further complicated by zooplankton behaviour such as diel migration (e.g. Owen, 1981; Wishner and Allison, 1986). At the higher trophic levels behaviour becomes the prominent determinant in their distribution at fronts (Olson, 2002). Ontogenetic vertical migrations can maintain populations of organisms in highly advective frontal jet regimes by placing different life stages in different portions of the flow (e.g. Olson, 1991). Alternatively fronts may act as barriers, defining biogeographic provinces (Backus, 1986). For example, Wiebe and Flierl (1983) observed a rapid cross-front transition in euphausiid species from the temperate *Nematoscelis megalops* in a cold-core ring of the Gulf Stream meander to the subtropical *Stylocheiron affine* species in surrounding Sargasso Sea waters.

Localised increases in the abundance of larger organisms, such as large pelagic fish, squid and whales are also found (Podesta *et al.*, 1993; Waring *et al.*, 1993; Dawe and Brodziak, 1998). Although, at these organisms size range the manner in which they utilise the frontal ecosystem is often related to life cycle (Olson, 2002).

All these biological forcing mechanisms may act to enhance or counteract the physical forces that influence plankton distribution. Ultimately the scales of plankton patches depend on the type and scale of the driving mechanism, the eventual pattern being controlled by the organisms behaviour, food requirements and its response to the environment.

1.3 Acoustic methods for examining the distribution of zooplankton

The following section introduces the use of acoustic techniques as a tool to investigate the distribution of zooplankton. The history, basic principles, acoustic modelling, instruments and some examples of the techniques are discussed. In addition, the author recommends several reviews (Clay and Medwin, 1977; Medwin and Clay, 1998; Horne, 1998; Foote and Stanton, 2000; Griffiths *et al.*, 2002)

1.3.1 Background and History

The propagation of sound waves in the marine environment, and their scattering by discontinuities in the medium, provides the means for remote sensing of the environment. At acoustic frequencies greater than 1 kHz, a large proportion of oceanic volume reverberation is biological in origin (Farquhar, 1971; Anderson and Zahuranec, 1977; Clay and Medwin, 1977). A significant fraction of this reverberation is associated with large zooplankton and micronekton (Sameoto, 1976; Pieper, 1979; Greenlaw, 1979; Holliday and Pieper, 1980; Pieper and Holliday, 1984; Kristensen and Dalen, 1986; Greene *et al.*, 1988; 1989).

Observations of pelagic nekton with underwater sound dates from the 1930s (Sund, 1935; Balls, 1948). Scientific observation of mesopelagic organisms with underwater sound began in the late 1950s, and were largely focused on deep scattering layers which were hypothesised to result from the presence of mesopelagic fishes, such as myctophids (Hersey and Backus, 1954).

The development of echo counting (Craig and Forbes, 1969) and echo integration techniques (Ehrenberg and Lytle, 1972), meant it became practical to use single frequency echosounders to make quantitative estimates of biomass in diffuse layers of sparsely packed schools of fish. The addition of dual-beam (Ehrenberg, 1974; Traynor and

Ehrenberg, 1979) and split-beam (Ehrenberg, 1983; Foote *et al.*, 1986) technology allowed estimations of target strength of organisms *in situ*.

Holliday first defined an acoustic approach appropriate for zooplankton nearly two decades after the first application of fisheries acoustic methods (Holliday, 1977). This used a multi-frequency acoustic system, physics-based acoustic scattering models and a mathematical inversion technique to convert the data into a size distribution of the biological sound scatterers.

The methodology involved in using acoustics to study zooplankton has its roots in fisheries acoustics. Elements where they overlap are the sonar equation, echo integration, calibration and instrument platforms (Foote and Stanton, 2000). However, significant departures in zooplankton acoustic methodology from fisheries methods have resulted because of (a) the need for political policies to maintain standardised measurements of fish for stock assessments (Holliday and Pieper, 1995) and (b) the complexity of the organism studied. Fish, as acoustic scatterers, are relatively similar (excepting the presence or absence of a swimbladder) varying predominantly with size (e.g. Target Strength = m*log(length) + b where m and b are constants for any given species, Lillo *et al.*, 1996), whereas in the open ocean aggregations of zooplankton typically contain a number of species with vastly differing acoustic properties that vary not only with size but also between species as a result of composition (e.g. hard/soft carapaces, shape). In zooplankton acoustics, this diversity in species and thus acoustic scattering properties has led to the development of (1) multi-frequency echosounders spanning a range of frequencies, (2) mathematical inversion methods to infer biological parameters from multi-frequency data, and (3) advanced acoustic scattering models that have incorporated the major anatomical features of the zooplankton.

1.3.2 Acoustic theory and practise

1.3.2.1 Basic Principles

The active sonar equation (Urick, 1983; Medwin and Clay, 1998) is used to describe echo quantification. It is an engineering solution to the wave equation for a noisy, vertically bounded fluid medium, containing an acoustic source, targets and a receiver (Foote and Stanton, 2000). The equation is used for estimating echo levels from particular targets and for evaluating the performance of sonars in terms of target detection and maximum operating range.

1.3.2.2 Scattering strength

A single target is characterised by its backscattering cross section σ or Target Strength *TS*:

$$TS = 10\log\left[\sigma/\left(4\pi r_0^2\right)\right] = 10\log\left(\sigma_{bs}/r_0^2\right)$$

where σ is expressed in units of square metres, and r_o is a reference distance (typically 1 m). σ_{bs} denotes the differential backscattering cross section, where $\sigma_{bs} = \sigma/4\pi$ (Medwin and Clay, 1998). In an aggregation of unresolved single targets, the typical measure of scattering strength is the total scattering strength, $S_v + 10\log V$, where the Mean Volume Backscattering Strength (S_v or otherwise known as MVBS) can be described as follows:

$$S_v = 10\log\left(N\sigma/\left(4\pi V\right)\right)$$

where σ is the average backscattering cross section of N scatterers in the sampling volume V and units are generally given in logarithmic terms (dB).

1.3.3 Target strength models

Acoustic scattering from a target (hereafter assumed to be a zooplankton) is a complex function of size, shape, internal structure, material properties and orientation, as well as acoustic frequency. A measure of sound scattering can be determined empirically through measurements, mathematically through physics-based predictions (Anderson, 1950), or in some combination in which certain parameters of the mathematical model are experimentally determined (Stanton *et al.*, 1996). The scattering by a target can be described in terms of the incident sound pressure (P_0), the acoustic wave number (k_1 which is equal to $2\pi/\lambda_1$ where λ_1 is the wavelength and the subscript 1 denotes the surrounding fluid), a distance (r) between the receiver and target, and scattering amplitude (f) as

$$p_{scat} = P_0 \frac{e^{ik_1 r}}{r} f$$

Acoustic scattering descriptions focus on scattering amplitude at a reference distance implicitly assumed to be 1 m, which is the target strength (*TS*):

$$TS = 10\log\left|f_{bs}\right|^2$$

Where $|f_{bs}|^2$, the backscattering amplitude, is related to the backscattering cross section by the formula:

$$|f_{bs}|^2 = \sigma/4\pi = \sigma_{bs}$$

For further literature on the theory of acoustic scattering properties see Clay and Medwin (1977), Medwin and Clay (1998) and Foote and Stanton (2000).

1.3.3.1 Model Categories

The variety in, and complexity of, zooplankton size, morphology and material properties have resulted in a wide range of mathematical descriptions of their acoustic scattering. Using material properties as a governing factor, three categories of scattering models defined by Stanton *et al.* (1996) have become standard terminology in zooplankton acoustics. These are fluid-like (FL), elastic-shelled (ES) and gas-bearing (GB) (Figure 1.3.1). In each case they encompass a large number of zooplankton.

Fluid-like animals

Animals that are deemed fluid-like have material properties (mass density and sound speed) that are similar (within several percent) to the surrounding water. In addition their exoskeletons are considered thin enough to be assumed to be fluid-like and unable to support shear waves. Such objects with small contrasts in material properties and which do not support shear waves are referred to as "weak scatterers".

Scattering from copepods, euphausiids, amphipods, chaetognaths and salps are approximated using fluid-like models. Early models represented zooplankton as a homogenous fluid-filled sphere (Anderson, 1950; Greenlaw, 1977; 1979; Johnson, 1977; Stanton *et al.*, 1987). These models were successfully applied to field studies of the scattering of copepods (Pieper and Holliday, 1984; Holliday *et al.*, 1989). However, a sphere does not represent the shape of all zooplankton and hence increasingly sophisticated approaches have been used in order to take into account the complexity of the animals shape and material properties.

This commenced with the development of an infinitely long straight cylinder model which was applied to elongated zooplankton (Stanton, 1988a) and variations on this theme such as finite length, elastic and deformed cylinders (Stanton, 1988b; 1989).

The deformed cylinder model, whilst assuming the cross-section of the animals to be circular, can be used to describe the bend (Stanton, 1989), taper (McGehee *et al.*, 1998)

and roughness (Stanton, 1992, Stanton *et al.*, 1998a) of the body, as well as the variability of the material properties.

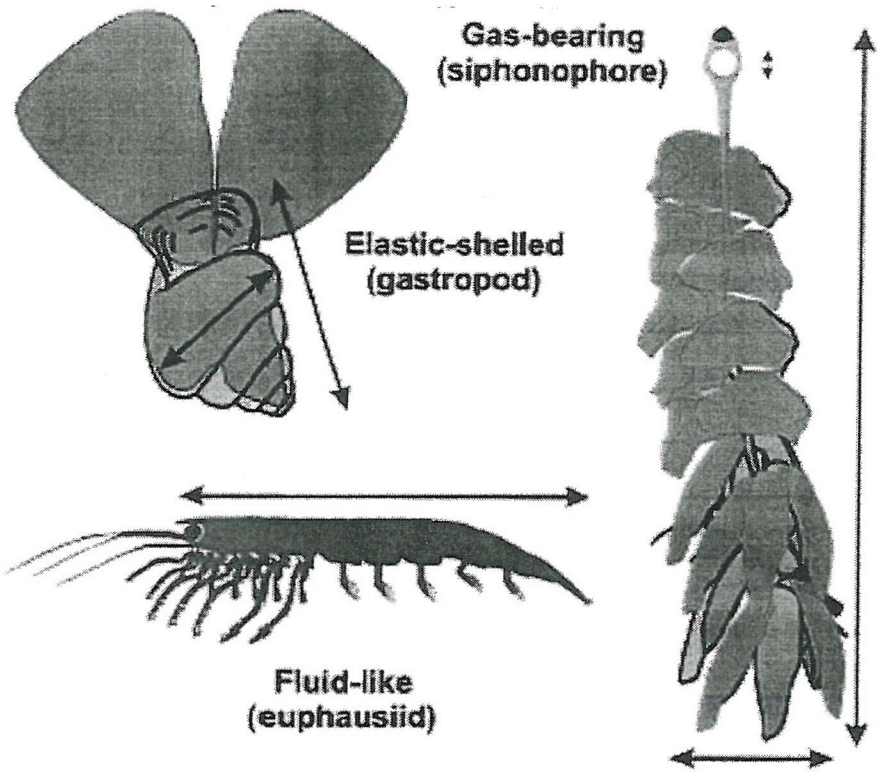

Figure 1.3.1 Sketches of zooplankton from the three major anatomical groups. The arrows indicate parts of the bodies over which the various dimensions measured are used in acoustic scattering models (Figure taken from Figure 1 of Stanton *et al.*, 1998a).

Initially the infinitely long cylinder model was developed and applied to elongated zooplankton using the approach based upon the exact modal-series solution (Stanton, 1988a; 1989; Wiebe *et al.*, 1990; Chu *et al.*, 1992; Miyashita *et al.*, 1996). This showed an improvement over the sphere model and was valid for a wide range of material properties, but was only valid for target orientations near broadside incidence (Partridge and Smith, 1995). More recently, the deformed cylinder model has been applied to zooplankton using the Deformed Wave Born Approximation (DWBA) (Chu *et al.*, 1993; Stanton *et al.*, 1993a, 1998a). The function of the DWBA-based deformed cylinder model assumes that the body is weakly scattering (i.e. the material properties are similar to the surrounding water) thus restricting the approximation with respect to material properties, but it is valid for all angles of orientation.

The general form of the DWBA formulation that accurately describes scattering from weakly-scattering bodies (Morse and Ingard, 1968) predicts the scattering of a body of arbitrary size, shape, orientation and material properties as well as arbitrary frequency.

Below is the DWBA-based deformed cylinder model (Stanton *et al.*, 1998a) used to predict scattering from euphausiids.

$$f_{bs} = \frac{k_1}{4}\int_{r_{pos}} (\gamma_k - \lambda_\rho) e^{2i(k_i)_2 \cdot r_{pos}} dv \times a \frac{j_1(2k_2 a \cos\beta_{tilt})}{\cos\beta_{tilt}} \left| dr_{pos} \right|$$

The terms γ_κ and λ_ρ are related to the density and sound speed contrasts (g and h, respectively) of the body where $g = \rho_2/\rho_1$, $h = c_2/c_1$, ρ is the mass density, c is the sound speed, and the subscripts 1 and 2 refer to the surrounding fluid and body medium, respectively. The term r_{pos} is the position vector of the body axis, J_1 is the Bessel function of the first kind of order one, k_2 is the acoustic wavenumber inside the body and β_{tilt} is the angle between k_1 (the incident plane wave) and the cross-section of the body at the point r_{pos} (Figure 1, Stanton and Chu, 2000). This deformed finite length cylinder formulation describes the scattering by finite-length elongated bodies whose cross-sectional radius (a), radius of curvature and material properties can vary along the axis.

Hence acoustic scattering by zooplankton is a complex function of animal size, shape, orientation and material properties (Table 1.1), as well as acoustic frequency (wavelength). The combination of size and frequency (i.e. k and a) will be discussed in section 1.3.3.3.

Shape

The shapes of the bodies of zooplankton are generally irregular. Low resolution models approximate the shape of zooplankton to be simple geometric shapes, whilst high resolution models take into account the bend of the body axis, the tapering of the body, and local irregularities such as legs (Figure 1.3.2). Rigorous representation of the shapes of bodies requires recording features of the order $\lambda/20$ and larger, this is now being achieved using Computed Tomography-scans to map the three dimensional image at resolutions of sub mm (Lavery *et al.*, 2002).

Material properties

Levels of scattering from an object depend on the contrasts of various material properties with the same physical properties as the surrounding medium. The critical material properties in zooplankton are the ratio of the sound speed through the scatterer to that in water and the ratio of the compressibility of the scatterer to the water. This relationship can be expressed by R, the reflection coefficient, and is a common variable in the acoustic scattering models and is described by:

Function	Model/observation	Effect	Reference
Size	Fluid sphere model	Model-estimated acoustic backscatter from a 2.5 mm copepod was 20 dB greater than from a 1 mm copepod.	Griffiths *et al.*, 2002
Shape	Bent cylinder model	The backscattering cross-section of a 23 mm euphausiid decreases by 6 dB if the animal bends by 1.4 mm at the ends of the cylinder.	Stanton, 1989
Material properties	Fluid cylinder model	A 5 dB difference was found when the extreme low and high values of g and h (Køgler *et al.*, 1987) were used to predict the target strength of *Meganyctiphanes norvegica*.	Griffiths *et al.*, 2002
Orientation	Tank observations	A change of 3-4 dB in target strength was observed with a change of mean angle of 10^0 from vertical of a 27 mm target.	Macaulay, 1994

Table 1.1 A table of the effect of size, shape, material properties and orientation on target strength. The model, effect and reference for each function is given.

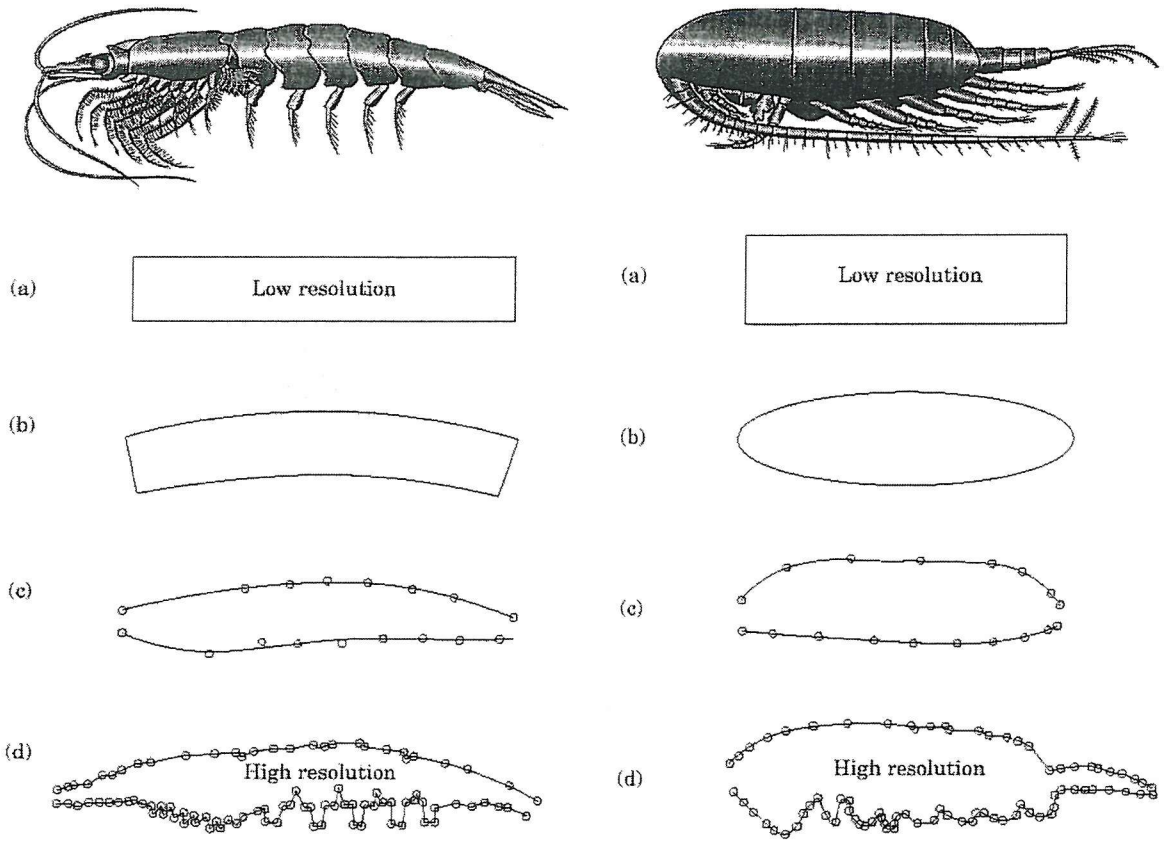

Figure 1.3.2 Euphausiid (*Meganyctiphanes norvegica*), copepod (*Calanus finmarchicus*) and various models of shape ranging from (a) low resolution to (d) high resolution). (Taken from Stanton and Chu, 2000).

$$R = (gh-1)/(gh+1)$$

where g is the mass density of the zooplankton body relative to that of the surrounding water and h is the relative sound speed in the animals. Both are obviously dependent on the biochemical composition of the zooplankton. Values of g and h have been obtained either through direct measurement of both dead and living animals (Køgler *et al.*, 1987; Foote, 1990) or inferences based upon scattering measurements (Stanton *et al.*, 1994a; Chu *et al.*, 2000). There are few published data regarding values of the density and sound speed contrasts, but they are generally within 1-2% of 1.04 for each value (Stanton and Chu, 2000). These values assume the body to be homogenous (i.e., they are bulk values). However, some authors have investigated the heterogeneity of the internal structure (Yayanos *et al.*, 1978; Foote, 1998). The density and sound speed contrasts have been shown to have seasonal and annual cycles (Køgler *et al.*, 1987) and in addition, to add complexity, Chu *et al.* (2000) noted that the sound speed contrast of a euphausiid also changed with depth.

R is critical not only in FL models but also for all other types (i.e. ES and GB). When R is high the animal is an efficient scatterer of sound (for example, a gastropod has a hard shell whose material properties are different from the surrounding water) and conversely when R is small the animal is a relatively inefficient scatterer (for example, a salp is principally composed of gelatinous material, whose properties are similar to the surrounding water). Variations in R can result in changes in the type of scattering associated with different zooplankton, hence the classification of FK, ES and GB. This can cause differences in scattering energy that can be so dramatic that the average echo energy per unit quantity of biomass of a 2 mm-long gastropod is about 19000 times that of a 30 mm-long salp (Stanton *et al.*, 1994a).

Orientation

Target strength of elongated zooplankton is recognised to vary with orientation (Greenlaw, 1977; Sameoto, 1980; Everson, 1982; Kristensen and Dalen, 1986; Macaulay, 1994; Hewitt and Demer, 1996; McGehee *et al.*, 1998). Very little information is available regarding the *in situ* orientation distribution of free-swimming animals or how it changes over a diurnal cycle. Krill in aquariums have been observed with mean orientations in the range of 20-40° relative to horizontal (where 0° corresponds to a horizontal body axis and positive angles refer to the head up) with standard deviations of ~ 20° (Kils, 1981; Endo, 1993; Miyashita *et al.*, 1996). These observations agree with Chu *et al.* (1993) who

inferred mean orientation of 20° for encaged krill, calculated using a DWBA-based model applied to two frequency data. Recently, with the increasing sophistication of the video plankton recorder, the orientation of copepods freely swimming over Georges Bank was observed to be peaked at about 90° (animal axis was vertical, with the head up) with a standard deviation of 30° (Benfield *et al.*, 2000). Such observations will provide valuable information for deciding the orientation function of the acoustic models.

Elastic-Shelled animals

Animals that are described as elastic-shelled include planktonic gastropods such as pteropods. The scattering from an elastic-shelled body is complex and is a summation of a number of processes. Initially it was simplified to assuming that the body was a solid dense fluid and that the scattering was dominated at high frequencies by the echo from the front interface of the body (Stanton, 1989; Stanton *et al.*, 1994a), although processes within the shell, within the internal fluid and surface waves propagating along the shell also contribute to the total backscattered energy (Stanton *et al.*, 2000; Griffiths *et al.*, 2002). However laboratory acoustic tank measurements identified another key scattering mechanism, that the shell was supporting circumferential (subsonic Lamb) waves, which would interfere with the shell interface echo (Stanton *et al.*, 1998a). The most recent models for elastic-shelled animals are from Stanton *et al.* (1998b, 2000):

$$f_{bs} \cong f_{\text{spec}} + f_{\text{op}} + f_{\text{Lamb}},$$

where

$$f_{\text{spec}} \cong \frac{a_{\text{spec}}}{2} R_{12} F_{\text{spec}} e^{-i2k_1 a_{\text{spec}}},$$

$$f_{\text{op}} \cong \frac{1}{2} a_{\text{op}} R_{12} F_{\text{op}} e^{i2k_1 a_{\text{op}}},$$

$$f_{\text{Lamb}} \cong -\frac{1}{2} G_L e^{i\phi} L\bar{a} e^{-2(\pi-\theta_L)} \beta_L \times e^{i2k_1\bar{a}[(c_1/\bar{c}_L)(\pi-\theta_L)-\cos\theta_L]-i\pi/2} F_L$$

$$\times \sum_{m=0}^{\infty} (-1)^m e^{-2\pi m\beta_L} e^{i2\pi m k_1 \bar{a} c_1/\bar{c}_L} e^{-(1/2)y^2\sigma_r^2}$$

where

$$\theta_L = \sin^{-1}(c_1 / c_L),$$
$$G_L \cong 8\pi\beta_L c_1 / c_L,$$
$$\bar{c}_L / c_1 \cong k_1 \bar{a}(\alpha_L + 1/2)$$

and

$$y = k_1\{2[(c_1 / \bar{c}_L)(\pi - \theta_L) - \cos\theta_L] + 2\pi m c_1 / \bar{c}_L + Bk_1\bar{a}[2(\pi - \theta_L) + 2\pi m]\}$$

The terms f_{spec} and f_{op} contain a reflection coefficient R_{12} owing to the interface they are associated with. f_{Lamb} contains a coupling coefficient G_L that describes the efficiency with which the incident signal couples with the shell and reradiates, B accounts for dispersion according to the relationship $c_1 / c_L = c_1 / \bar{c}_L + Bk_1\Delta_a$, where the mean speed $\bar{c}_L$ is c_L evaluated at $k_1\bar{a}$. The terms a_{spec} and a_{op} are the local radii of curvature that the incident wave sees. $\bar{a}$ is the average radius of the irregular sphere. β_L is the attenuation coefficient and α_L is the dispersion term of the Lamb wave. θ_L is the angle at which the Lamb wave launches and lands at the surface and ϕ_L a phase shift owing to the irregularity of the body. σ_r is the root-mean-square deviation of the shell radius from the mean value $\bar{a}$. F_{spec}, F_{op} and F_{L} are empirically determined terms that are used to weight the different scattered rays (Stanton *et al.*, 2000).

These equations predict scattering resulting from reflections and refractions within the fluid-like body of the animal, scattering from the back of the opercular opening, as well as flexural Lamb waves propagating along the shell (within the shell) and Franz waves propagating along the shell (within the surrounding fluid). The resonance structure of the scattering was found to be strongly dependent on orientation, although variation in material properties has not as yet been analysed (Stanton *et al.*, 2000).

Gas-bearing animals

These are animals that contain enough gas to produce a substantial echo as a result of the gas. In this case the acoustic backscatter results from both the gas inclusion and the surrounding tissue. The gas inclusion can be modelled as a fluid-filled sphere, where the fluid (in this case gas) has a low speed of sound and density. However, gas inclusions exhibit a resonance that augments the scattering significantly when the product of wave number and the equivalent spherical diameter of the target is greater than one. The general focus for gas-bearing models has been fish (Johnson, 1977; Reeder, 2000). In the past decade it has been recognised that gas bearing siphonophores can also be major acoustic scatterers. Initial models described scattering solely from the gas inclusion (Stanton *et al.*, 1996). More recently, the model describing the scattering from a gas inclusion has been

combined with the model describing fluid-like animals, thus including the scattering effects of surrounding tissue (Stanton *et al.*, 1998c)

1.3.3.2 The effect of size and acoustic frequency on Target Strength

Scatterer size and the frequency of sound used are also critical variables in the resultant Target Strength (TS) of the zooplankton. The general dependence of scattering on size and frequency is that when the product of the wave number for the sound ($k = 2\pi f/c$) and the scatterer size (a) is small, i.e., $ka \ll 1$, then the scattering is considered to be in the Rayleigh domain (where f = acoustic frequency and c = speed of sound). When $ka \gg 1$ the scattering is characterised as geometric and where $ka \approx 1$ the scattering is in the transition zone. 'k' can be fixed, which means that one can examine the dependence of scattering on variations in the size (a). Similarly 'a' can be kept constant and the variation of frequency can be studied. Examination of the variation in TS within a frequency range of 38 to 2000 kHz (which encompasses most zooplankton acoustic frequencies used at present) reveals several features (Figure 11.1, Griffiths *et al.*, 2002):

1) Small fluidlike animals (e.g. copepods, amphipods and chaetognaths) typically exhibit Rayleigh scattering within this frequency range.

2) Large copepods and euphausiids exhibit oscillatory target strength between $1 < ka < 10$.

3) The TS of a 2 mm long pteropod is comparable to that from a 30 mm long euphausiid at frequencies above 100 kHz.

4) The TS of a gas-bearing siphonophore is independent of frequency as the lowest frequency considered is above the resonant frequency of the gas bearing pneumatophore.

5) The TS of a siphonophore with a 2 mm equivalent diameter pneumatophore is ~15 dB greater than either a 2 mm long pteropod or a 30 mm long euphausiid.

These features are evident in model calculations from single animals. The model-predicted nulls (oscillatory characteristics) for single large copepods and euphausiids become less pronounced when the scattering volume contains more than one animal.

1.3.3.3 Sources of variability

Variability may arise from both the act of measurement and the modelling of zooplankton.

Measurement

This category encompasses variations in the instrument used, in the medium in which the measurements are taken and the behaviour of the targets themselves. It is generally assumed that instruments will perform consistently and in accordance with their calibration, with no variation over time. However, in reality performance may vary

resulting from changing conditions of operation, power and thermal effects. Acoustic measurements are affected by the state of the medium. For example, air bubbles introduced into the medium by turbulence or storm events may attenuate both transmitted signal and echoes. This may reduce the signal to noise ratio below the detection threshold or lead to an over estimation of zooplankton. Finally, zooplankton react to changes in their environment such as light and noise. This can result in variations in orientation, which may effect the estimations of numerical density.

Modelling

The mathematical models used to describe acoustic scattering are approximations, and as such are subject not only to their own accuracy but also that of the model parameters. The models require knowledge of the morphology and material properties of the animal. Determination of these characteristics can involve complex experimental procedures (Foote, 1998) subject to error.

1.3.4 Instruments and their applications

Sonar (SOund NAvigation and Ranging) is a general term applied to equipment and software that receives and possibly transmits sound. The echosounder is a particular kind of sonar, one whose acoustic beam is directed vertically downwards.

In a basic echosounder (Figure 1.3.3), the transmitter produces a burst of electrical energy at a particular frequency. The transmitter output is applied to a transducer, which converts the electrical energy to acoustic energy in the water. The transducer projects sound in a directional beam, with the width of this beam being inversely proportional to the frequency of the sound (assuming a fixed diameter transducer). The transmitted pulse of sound propagates through the water away from the transducer and encounters various targets, e.g. fish or the sea-bed. These targets reflect or scatter the pulse, and some energy returns towards the transducer. The backscattered sound (the echo) is detected by the transducer and converted to electrical energy as the received signal. The time at which the echo is received indicates the distance of the target from the transducer. Most sonar systems cannot be used in near-surface and near-bottom "dead-zones" where targets cannot be discriminated from the surface or substrate (Mitson 1983; Ona and Mitson, 1996; Misund, 1997).

Acoustic returns contain three types of data that can be directly extracted: time between pulse transmission and echo return (i.e. target range), pressure detected at a receiver (i.e. echo amplitude, in volts) and within-pulse phase (identification of single or multiple targets). Sound pressure at a receiver is measured as an intensity which is often

converted to a logarithmic ratio of an observed intensity to a reference intensity (in decibels).

1.3.4.1 Single Frequency acoustics

Single-frequency acoustics can provide reasonable biological information providing certain assumptions are valid. These are: 1. A single size organism dominates the acoustical scattering and that size is known, 2. There is a tractable, validated model for the organism, relating its size and the acoustic frequency used to its Target Strength (TS) in quantitative terms, 3. Multiple scattering effects and shadow effects are negligible, and 4. Any dependence of TS on any other parameter is known and one can sufficiently estimate the power in the echoes (Holliday and Pieper, 1995). Biomass estimates based on single-frequency acoustic surveys now represent an accepted and standard approach for enumerating many fish-stocks (Foote and Stefánsson, 1993; Holliday and Pieper, 1995). When measuring zooplankton these assumptions are rarely met, though a certain amount of biological information can still be obtained.

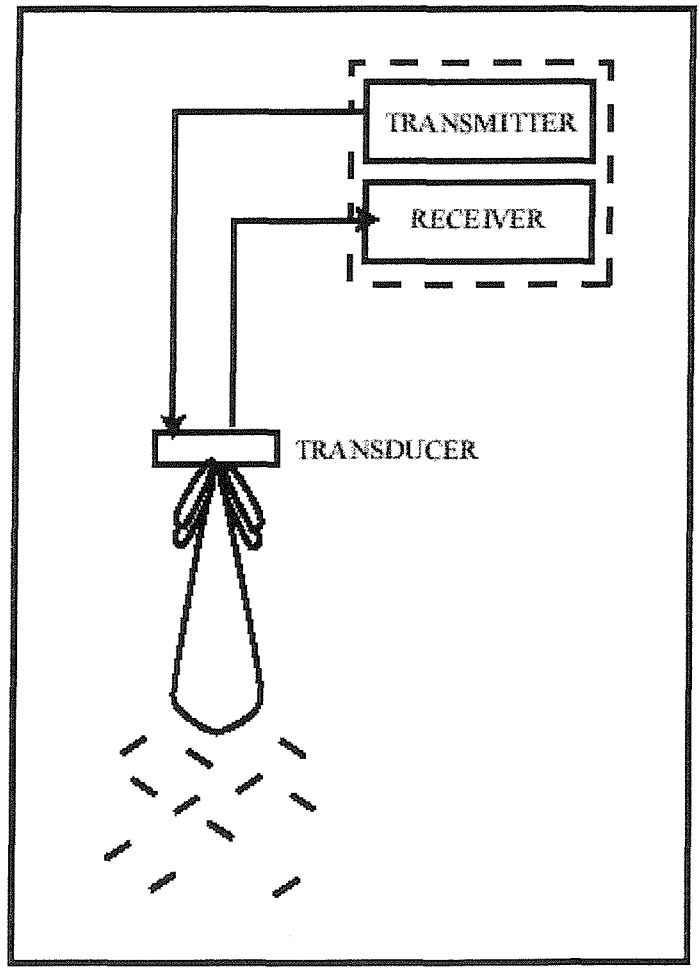

Figure 1.3.3 A basic echosounder (after Foote and Stanton, 2000).

Acoustic Doppler Current Profilers (ADCPs)

Acoustic Doppler Current Profilers (ADCPs) are one example of a single frequency acoustic system which have been used to provide biological information. ADCPs have, since the mid 1980s, become routine instruments for physical oceanographers (for review see Woodward and Appell, 1986). They use the change in the observed pitch of sound owing to relative motion between a source and receiver for measuring current velocities. Particles, which are perceived to be drifting passively in the water column, scatter the incident sound pulses and some of the scattered energy ends up back at the receiver. In the open ocean, it is assumed that these particles will be predominantly zooplankton and micronekton. Through this theory, Haury (1982) raised the possibility that ADCPs could provide biological data in addition to current velocities. This idea was developed by Flagg and Smith (1989a,b) and Plueddemann and Pinkel (1989).

Without further processing ADCPs produce uncalibrated acoustic backscatter (often termed relative) data on an arbitrary scale, which are useful for providing semi-quantitative distribution patterns. However, these "relative data" are not comparable over different hydrographic regimes or different depths because of the variation in sound absorption with temperature and salinity and variations in instrument performance with temperature. To improve these relative data studies in the last decade have calculated the Mean Volume Backscattering Strength (MVBS, units in dB) using the manufacturers calibration together with *in situ* salinity (Zhou *et al*, 1994), and temperature and noise levels (Weeks *et al.*, 1995). Roe *et al.* (1996) have taken this process one step further using concurrent temperature and salinity measurements (from the towed vehicle SeaSoar) to calculate directly the sound absorption coefficient α (see Francois and Garrison, 1982). This is then used with the manufacturers calibration (RDI, 1990) in the calculation of MVBS. This absolute MVBS has been used to describe the distribution of zooplankton in the Atlantic, Southern and Indian Oceans (Griffiths and Roe, 1993; Roe *et al.*, 1994; 1996; Herring *et al.*, 1998) on the same time and space scales as physical variables. Good correlation was found between backscatter data obtained from an ADCP (153 kHz) and a SIMRAD EK500 echosounder (120 kHz) (Griffiths and Diaz, 1996) indicating that the ADCP was producing acoustic backscatter data consistent with a commercially built well-calibrated biological echosounder.

ADCPs have been used on moored long-term interdisciplinary arrays, hull mounted systems, and have collected backscatter data together with CTDs or towed

hydrographic sensors (Heywood *et al.*, 1991; Fischer and Visbeck, 1993; Griffiths and Roe, 1993; Roe and Griffiths, 1993; Ashijan *et al.*, 1994; Flagg *et al.*, 1994; Zhou *et al.*, 1994; Herring *et al.*, 1998). They have been used to provide observations of diel migrations (Flagg and Smith, 1989a; Smith *et al.*, 1989; Ashijan *et al.*, 1994; Buchholz *et al.*, 1995; Heywood, 1996; Roe *et al*, 1996; Rippeth and Simpson, 1998; Wade and Heywood, 2001), reverse migrations (Heywood, 1996), speed of diel migrations (Wilson and Firing, 1992; Heywood, 1996), and the distribution of zooplankton at mesoscale features. For example, Roe and Griffiths (1993) and Roe *et al.* (1996) observed columns of high backscatter/zooplankton biomass in the eddy boundaries associated with the Iceland-Faeroes front and Ashijan *et al.* (1994) recognised diel, regional and meander associated patterns in zooplankton distributions in the Gulf stream.

Single frequency echosounders

Other single frequency systems are generally commercial echosounders, for instance, the SIMRAD EK120. Zooplankton acousticians now typically use acoustic wavelengths which approximate to the same size as the animals present in the study volume, this maximises the reflections obtained from relatively weak scatterers.

Zooplankton ecologists have used such systems to describe biological distributions and the influence of physical forcing on these in several areas. Sameoto (1976; 1980) used a 120 kHz echosounder to map and quantify the distribution of euphausiids in the Gulf of Lawrence. Nash *et al.* (1989) used a 70 kHz sonar to measure the distribution of peaks of acoustic backscatter in relation to depth and temperature at the edge of the Gulf Stream. They observed patterns of diel migration influenced by differences in the thermal structure between the Gulf Stream and a front, with a general selection by organisms for warmer water and an avoidance of cooler temperatures. Szczucka and Klusek (1996) used a 30 kHz echosounder to observe scattering layers in the South Baltic Sea, commenting on changing depths of vertical migration with changing seasons. Holliday (1992) used a 1.05 MHz echosounder on a moored system to record patterns in zooplankton distribution with time in Fish Harbor, USA. Variations in acoustic backscatter were assumed to have been caused by diel migration and the tidal advection of zooplankton assemblages past the moored sensor. Wiebe *et al.* (1996) used a 420 kHz echosounder to study volume backscattering over Georges Bank, showing that the volume backscattering structure varied between a well mixed and a stratified area. Internal waves were shown to modulate the depth of dense mid-depth scattering layers, thus providing evidence that the physical forcing of zooplankton patterns varied significantly between the two areas. Baussant *et al.*

(1992) described the distribution of scattering layers across a strong density front (the Ligurian front) collected using a 50 kHz echosounder. They found rapid horizontal changes in vertical distribution in and away from the front and concluded that these changes and observed seasonal changes were as a result of the distribution of chlorophyll biomass.

Acoustic methods can also be used to investigate predator/prey relationships. Macaulay (1993) and Macaulay *et al.* (1995) used a 120 and 200 kHz sonar (on separate cruises) to assess the distribution and abundance of the prey (copepods) of Right whales near Georges Bank. Observations showed distinct diel migrations of zooplankton with estimations of biomass of 1.0 - 25.0 g wet weight m^{-3}, which correlated with abundance measurements from MOCNESS tows. The behaviour of the whales was related to the spatial scales and abundance of their prey as shown by the use of acoustic estimates of target distribution and abundance.

Acoustic methods have been used intensively in the Southern Ocean for the stock assessment of krill. The Antarctic krill (*Euphausia superba*) is a key species in the food web of the Southern Ocean (Laws, 1985) and because of its high abundance is important as a major invertebrate fisheries resource (McClatchie *et al.*, 1994). Bioacoustical methods of various types have been used extensively to map and quantify the distribution of Antarctic krill (Burczynski, 1973; Kalinowski, 1982; Guzman, 1983; Miller and Hampton, 1989; Everson *et al.*, 1990; Greene *et al.*, 1991; Ricketts *et al.*, 1992; McClatchie *et al.*, 1994; Brierley and Watkins, 1996; Murray, 1996) and their behaviour (Kaufmann *et al.*, 1993). These measurements have typically used single-beam single frequency systems, operating at 120 kHz (Sameoto, 1976; Ricketts *et al.*, 1992; Brierley *et al.*, 1998a). Several problems were identified: Demer and Hewitt (1995) reported that surveys may be biased when the animals migrate above the observation window of down-looking transducers and adjusted the observed density observations with a temporal compensation factor. Hewitt and Demer (1996) used a more direct method estimating the abundance of krill in the near-surface layer using side-ways looking sonars. Standardised measurements of Antarctic krill abundance have primarily used single frequency systems. In addition, both dual-beam echosounders (Hewitt and Demer, 1996) and multifrequency acoustics (Foote *et al.*, 1990; Madureira *et al.*, 1993a,b) have also been used to measure Antarctic krill abundance.

Single frequency summary

Analyses of data from single-beam systems are confounded by the interaction between the target strength of an actual animal and its position in the beam. A dual-beam system circumvents this problem by analysing the single echoes returning from individual animals (Richter, 1985; Greene and Wiebe, 1988; Greene *et al.*, 1989; Wiebe *et al.*, 1990). Greene *et al.* (1989) and Greene and Wiebe (1990) used a dual-beam system combined with an echo integration analysis of corresponding volume backscattering data to estimate numerical abundance and biomass concentration and apportion it to different acoustical size classes. Calibration studies using a dual-beam echosounder operating at 405 kHz showed qualitative and quantitative estimates of animal distribution consistent with previous studies using more conventional sampling methods (Greene and Wiebe, 1988).

However the extraction of biological parameters such as biovolume from the acoustic volume backscatter of a mixed species/size assemblage still remains relatively unsolvable with single frequencies systems and currently available scattering models. The more frequencies used to make quantitative measurements of volume backscatter from an ensemble of zooplankton made up of several sizes, the better the ability to discriminate between the different sizes present (Holliday and Pieper, 1995). Hence the use of multi-frequency acoustics.

1.3.4.2 Multi-frequency acoustics

Multi-frequency acoustic systems are available both commercially (e.g. SIMRAD EK400, EK500 and EK60) and as unique developments (MAPS, Holliday *et al.*, 1989; BIOMAPPER, Wiebe, 1995; TUBA, Crisp and Harris, 2000)

Mitson *et al.* (1996) used a two-frequency algorithm to determine the size and abundance of plankton. The two frequency (120 and 38 kHz) method used a highpass fluid sphere model to determine mean size and density of animals (typically euphausiids). The results were compared with net samples and found to agree satisfactorily. The ratio of 120 to 38 kHz is well suited to studying the size group of euphausiids. Greenlaw applied this approach and Madureira (1993a,b) used this ratio to separate and distinguish the acoustic signal of three species of Antarctic zooplankton. ΔMVBS (= MVBS 120 kHz - MVBS 38 kHz, in dB) were used to distinguish *Euphausia superba, Themisto gaudichaudii* and *E. frigida* (ΔMVBS = 4.6, 9.7 and 15.6 dB respectively), with results being significantly different to allow the three species to be separated acoustically. Brierley and Watkins (1996) used this method to distinguish between *E. superba*, nekton (larger than krill) and zooplankton (smaller than krill). Later Brierley *et al.* (1998a) used this method with three

frequencies (200-38 and 200-120) to separate species of euphausiid, amphipod and copepods.

Guerin-Ancey and David (1993) and Van Cuyck *et al.* (1993) have used seven frequencies (between 75 - 130 kHz and 0.3 - 1.2 MHz respectively) to look at a mixed small zooplankton population and a monospecific plankton layer. Guerin-Ancey and David (1993) found distinct scattering layers at different depths with different frequencies and compared net sampled zooplankton with measured acoustic backscatter (see section 1.3.5.2). Johnson and Griffiths (1990) also commented on the use of different frequencies to target different size classes of zooplankton. They used two frequencies (120 and 200 kHz) to assess zooplankton abundance in areas where the Arctic bowhead whale is commonly found as part of a study to measure the energy requirements of the whales. Other multifrequency systems have been used to observe predator/prey relationships. For example, Orr (1981) used a multifrequency system operating between 10 and 600 kHz to detect predator-prey interaction, the passive response of zooplankton to fluid processes such as internal waves, lee waves, and the response of organisms to the presence of an oceanographic instrument in the water column. Observations suggested that internal waves influenced predator-prey distribution on the continental shelf and that the presence of oceanographic instruments was detected to ranges of 15 m.

The acoustic instruments discussed so far are commercially built (BIOSONICS or SIMRAD). Novel systems developed by research institutes include BIOSPAR (BIOacoustic Sensing Platform and Relay) and BIOMAPER (Bio-Optical Multifrequency Acoustical and Physical Environmental Recorder) (Wiebe, 1995). These systems map the distribution of zooplankton in the upper 150 m of the water column using two frequencies (120 and 420 kHz). BIOSPAR is a free drifting buoy that collects Eularian bioacoustic measurements, whilst BIOMAPER is towed from the back of a ship. Other novel systems have been developed which operate with more than three frequencies. Holliday *et al.* (1989) developed the Multifrequency Acoustic Profiling System (MAPS). It employs 21 circular disc transducers operating at different frequencies from 0.1 to 10 MHz. The acoustic measurements are converted to estimates of the scatterer density by size class using a model developed by Holliday and Pieper (1980).

Costello *et al.* (1989) have compared the MAPS and pump-sampling techniques for zooplankton density estimation. Biological samples were collected by filtering the water from a pump whose inlet was attached to the MAPS probe so that the same populations would be sampled by both methods. Close agreement was found between the

abundance and size distributions indicated by the pump and acoustic measurements. Peiper *et al.* (1990) have described zooplankton distributions revealed by MAPS and Pieper *et al.* (1990), and Napp *et al.* (1993) used MAPS to construct biovolume-size spectra for the Gulf Stream and the Southern California Bight.

TAPS (Tracor Acoustic Profiling System) measures acoustic backscatter at four frequencies (165, 420, 1100 and 3000 kHz) (Holliday and Pieper, 1995). With data from all frequencies different discrete vertical structures, e.g. scattering layers, can be identified as dominant at different frequencies and therefore composed of different sized zooplankton.

A new development at the Southampton Oceanography Centre is the Towed Undulating BioAcoustic sensor (TUBA) (Crisp and Harris, 2000). This is a seven-frequency echosounder (175 - 2400 kHz) which, when mounted on SeaSoar, can provide a wide range of bioacoustic data sampled concurrently with environmental data. Recent trials in the Strait of Gibraltar identified strong backscattering associated with the tidal bore, which has strong agreement with concurrent EK500 data (Griffiths and Crisp, pers. comm.). This system is about to start trials to compare acoustic backscatter data with Longhurst Hardy Plankton Recorder (LHPR) sampled zooplankton.

To provide more accurate zooplankton abundance, size, and biomass estimates and to calibrate acoustic scattering models, single frequency and multifrequency systems are often used in conjunction with other sampling methods.

1.3.5 Estimation of zooplankton size, abundance and biomass from acoustic backscatter.

Two different approaches have been predominant when estimating the abundance of zooplankton acoustically.

1.3.5.1 Empirical regressions (the "direct method").

The "direct method" is based on an estimated regression equation derived from acoustic measurements (single frequency) and data on biological samples (Pieper, 1979; Sameoto, 1980; Klindt and Zwack, 1984; Johnson and Griffiths, 1990). Flagg and Smith (1989a,b) and Heywood *et al.* (1991) correlated the intensity of the acoustic backscatter from a shipborne ADCP, with zooplankton biomass inferred from net samples, and demonstrated a relationship between backscatter and biomass. Iida *et al.* (1996) compared volume backscattering strength from four frequencies (25, 50, 100 and 200 kHz) with IKMT net sampled zooplankton (mesh size 2 mm). Results of regression analysis showed a linear relationship between the log of zooplankton density and the acoustic volume

backscattering strength, with the greatest correlation at 50 kHz. However, these relationships are not standard or reproducible over different hydrographic regimes. Defining the relationship between zooplankton size, abundance and biomass is now tending towards the use of acoustic scattering models.

1.3.5.2 Theoretical models.

Predicting backscatter can be described from the "forward problem" and the "inverse problem".

The forward problem

The **forward problem** is the prediction of the acoustic return from a scatterer based on a knowledge of the physical and geometric properties of the scatterer as well as the specification of the sonar system used. The development and theory of the acoustic scattering models was discussed in Section 1.3.3.1. These models require validation through comparison with observed acoustic measurements both in the laboratory and in more complex studies in the field. Model estimations have been compared with observations of encaged collections of euphausiids (Foote *et al.*, 1990; Everson *et al.*, 1990), individual free-swimming krill (Hewitt and Demer, 1991; 1996; Pauly and Penrose, 1998), tethered zooplankton (Martin *et al.*, 1996), and individual zooplankton in a controlled setting (Greene *et al.*, 1991). Live zooplankton are necessary as Greenlaw (1977), Greenlaw and Johnson (1983), and Richter (1985) all observed live and preserved zooplankton to have different acoustic scattering properties. Most models compare satisfactorily with laboratory constrained target strengths.

In addition to "controlled validation", recent studies have used acoustic scattering models to predict acoustic backscatter from field observations of mixed species zooplankton assemblages for comparison with *in situ* measurements of acoustic backscatter (Guerin-Ancey and David 1993; Wiebe *et al.*, 1996; Greene *et al.*, 1998). The field observations, typically net samples, are used to provide abundance and length data of different taxa, which are variables within the acoustic scattering models. Simplified, the model-estimated acoustic backscatter from a mixed species zooplankton population is assumed to be a linear combination of the model-estimated backscattering from all individual sound scatterers in the theoretical insonified volume (assumed to be the net sample). This model-estimation can then be compared with acoustic backscatter measurements taken in the vicinity of the net sample (Figure 1.3.4).

Guerin-Ancey and David (1993) used seven discrete frequencies (between 75 and 130 kHz) to study the distribution of small zooplankton in the Northeast Atlantic Ocean. Different frequencies showed different distinct scattering layers with depth. Estimated

acoustic backscatter (calculated using actual zooplankton size and abundance data collected using nets in Johnson's (1977) fluid-filled sphere model) were found to be very close to the observed values taken in the vicinity of the net sample.

Wiebe *et al.* (1996) and Greene *et al.* (1998) compared the acoustic backscatter observed *in situ* with those predicted from net sample data and different acoustic scattering models for different zooplankton groups. The results showed that the observed backscatter data were generally consistent with model estimations, and that this consistency ran true in terms of the proportion of acoustic backscatter contributed by each of the dominant sound scatterer types.

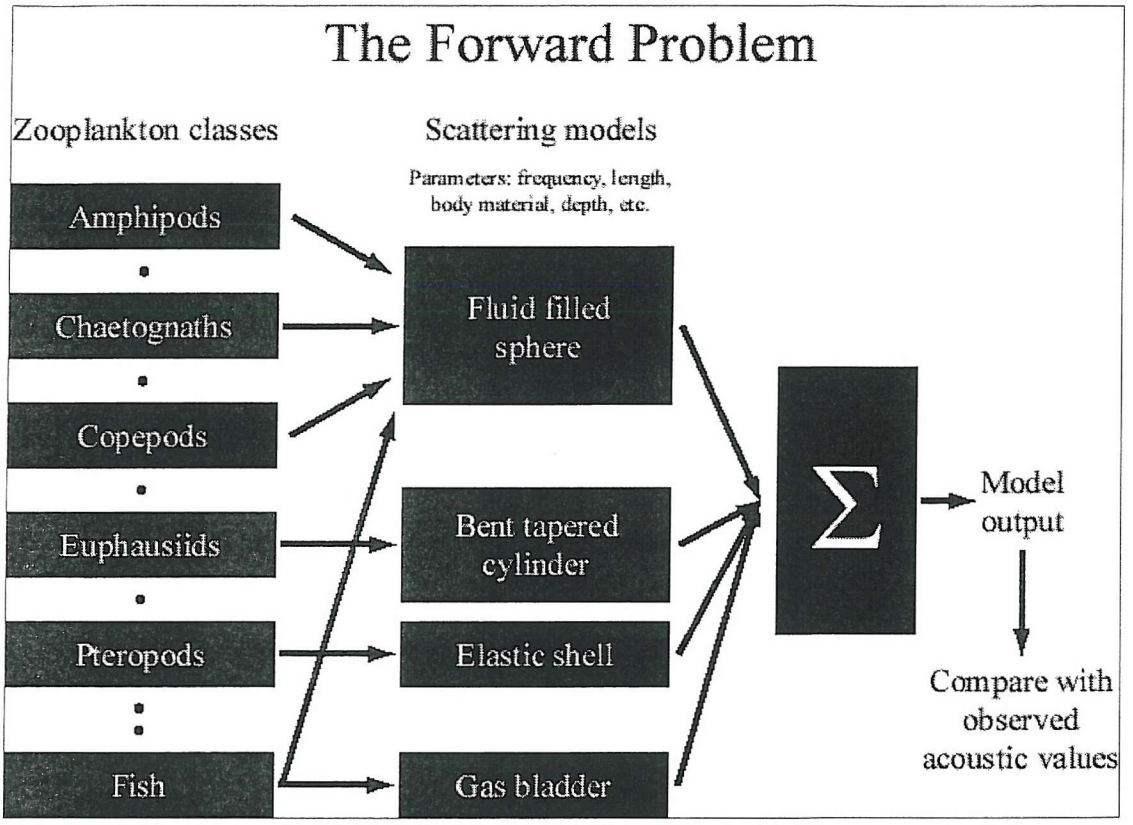

Figure 1.3.4 Schematic of the forward problem. Zooplankton classes and parameters such as length and abundance typically come from net samples.

Other modern zooplankton sampling techniques are increasingly being used concurrently with acoustic measurements to provide model variables. Using the OASIS (Optical-Acoustic Submersible Imaging System) instrument Jaffe *et al.* (1998) found that simultaneous optical and acoustic images permitted an exact correlation of Target Strength and taxa and that computer simulations from a model of the backscattered strength from euphausiids were in good agreement with the observed data. Certainly, because the taking

and processing of net samples is time intensive, modern techniques such as OASIS and video profilers (Benfield *et al.*, 1998) will increasingly play a part in providing the taxonomic abundance and length data required by the acoustic models. The combination of these instruments will supply a key tool for collecting data on zooplankton distributions.

The Inverse Problem

The **inverse problem** is the prediction of the properties of the scatterer based on a knowledge of the acoustic return and is more complex. Whilst "solving" the forward problem has had some success, we return again to the complexity of mixed species zooplankton populations composed of a mixture of shapes, sizes, orientations and composition. As yet studies using multiple acoustic scattering models to interpret the composition and abundance of mixed zooplankton populations have not been published. Holliday and Pieper (1995) have used a simplified approximation of numerical density of different size classes using multifrequency acoustic data from the instrument TAPS (Tracor Acoustic Profiling System), using only one simple acoustic scattering model (spherical model, Anderson, 1950) to describe all types of zooplankton. Where the numerical density can be estimated by means of a mathematical inversion in combination with an acoustic backscattering model of the animals present. The volume scattering coefficient for the *i*th frequency can be written as:

$$(S_v)_i = \sum_{j=1}^{N} \sigma_{ij} n_j$$

where n_j is the numerical density of the *j*th size class and σ_{ij} is the backscattering cross section of the *j*th class at the *i*th frequency. Given measurements of the volume scattering strength at each frequency and model calculations of all backscattering cross sections, then the numerical densities of the various size classes can be estimated through the method of non-negative least squares (NNLS) (Foote and Stanton, 2000). This method becomes far more complex when more than one acoustic scattering model is used.

Two alternative model-based approaches to zooplankton classification have been described by Martin *et al.* (1996). Two classifiers, model parameterization classifier (MPC) and empirical orthogonal function classifier (EOFC), make use of the consistent differences in acoustic backscatter signatures from different zooplankton groups (collected using a broadband sonar). In an at-sea on-deck experiment echograms of individual zooplankton were analysed and the MPC and EOFC correctly classified 95 and 87% of the

targets respectively. However, whilst this method is feasible with single targets, several advances are required before the technique can be used for *in situ* classification. For example, spatial resolution sufficient to resolve individual animals yet maintaining a sufficient signal to noise ratio over the full bandwidth.

Chu and Stanton (1998) used pulse compression techniques to characterise the temporal, spectral and statistical signatures of the acoustic backscattering by zooplankton with gross anatomical differences. This method has been used to examine the dominant scattering mechanisms from individual zooplankton for comparison with model-predictions. For example, the primary acoustic arrival from an elastic-shelled gastropod, as identified with this method, is the front interface and the secondary arrival corresponds to the subsonic Lamb wave that circumnavigates the surface of the shell. These arrivals correspond to the f_{spec} and f_{Lamb} functions of the acoustic scattering model (Section 1.3.3.1). Statistical studies demonstrated the ability of the Pulse Compression technique to size an individual animal and to differentiate the taxonomic group to which the zooplankton belonged.

1.3.6 Summary of acoustic methods

A variety of acoustic instruments and analytic techniques now exist to locate, map, count, size, and identify marine organisms. They can describe zooplankton distributions on the same time and space scales as physical data. Variation in backscattered intensity is influenced by choice of equipment, sampling conditions, organism morphology, and organism behaviour. Theoretical models exist which predict the target strength of various "dominant acoustic scattering" zooplankton groups, these models have been validated with laboratory measurements. Net, video and optical sampling methods are now used to collect biological data to predict acoustic backscatter that is comparable with observed data. Acoustic methods continue to progress in two areas, qualitative use and theoretical model-estimations. When (and if) these two directions finally converge acoustic methods will prove a powerful tool in zooplankton investigations.

Chapter 2

Methodology

This thesis draws on data resulting from two cruises to different hydrographic mesoscale regimes. For this reason the design and sampling strategy of the cruises have been separated into two sections, section 2.1 concerns *Discovery* Cruise 209 to the Arabian Sea and section 2.2 concerns *Discovery* Cruise 224 to the Mediterranean Sea. A greater emphasis and description has been made of the methodology and instrumentation used in the Mediterranean Sea as a result of the authors direct participation. Section 2.3 is generic to both datasets and discusses the analysis of the data, specifically the analysis of the zooplankton samples and the use of acoustic scattering models.

2.1 RRS *Discovery* cruise 209 – The Arabian Sea

2.1.1 Survey design

RRS *Discovery* Cruise 209 undertook biological and physical sampling of the oxygen minimum layer and hydrographic features of the Arabian Sea during the Southwest monsoon (3-22 August, 1994). It set out with two main objectives:

(1) To relate the biological distributions in the area around 19 °N 59 °E, extending from the shelf to deep water, to the physical and chemical oceanography of the area.
(2) To calculate a nutrient budget in an area extending from the shelf into deep water, using a sampling programme consisting of CTD profiles.

Sampling was undertaken within a box 120 km x 70 km in an area off the East Coast of Oman that gave access to oceanic, slope and shelf locations. The box was defined by a series of 15 full ocean depth CTD casts around its outer limits, and two SeaSoar surveys (SS1 and SS2) within these limits. (Figure 2.1.1). Acoustic backscatter data from a Vessel Mounted-Acoustic Doppler Current Profiler (VM-ADCP) were collected throughout the cruise.

The survey area was sufficiently small to permit detailed characterisation of mixed layer events, and was close to sections previously studied (section IV of Discovery 1963 transects, Currie (1992) and section D of Charles Darwin cruise 26, (Elliott and Savidge, 1990)). In the survey area the geographical position 19 °N 59 °E was designated as the UK Arabesque Reference Station (ARS) within the JGOFS Indian Ocean programme, allowing subsequent cruises to carry out long term monitoring of temporal changes in biogeochemistry (e.g. Mantoura, 1995).

The ARS was occupied several times during the cruise. On each occasion a full depth CTD was undertaken followed by a shallow (surface to 250 m) Longhurst Hardy Plankton Recorder (LHPR).

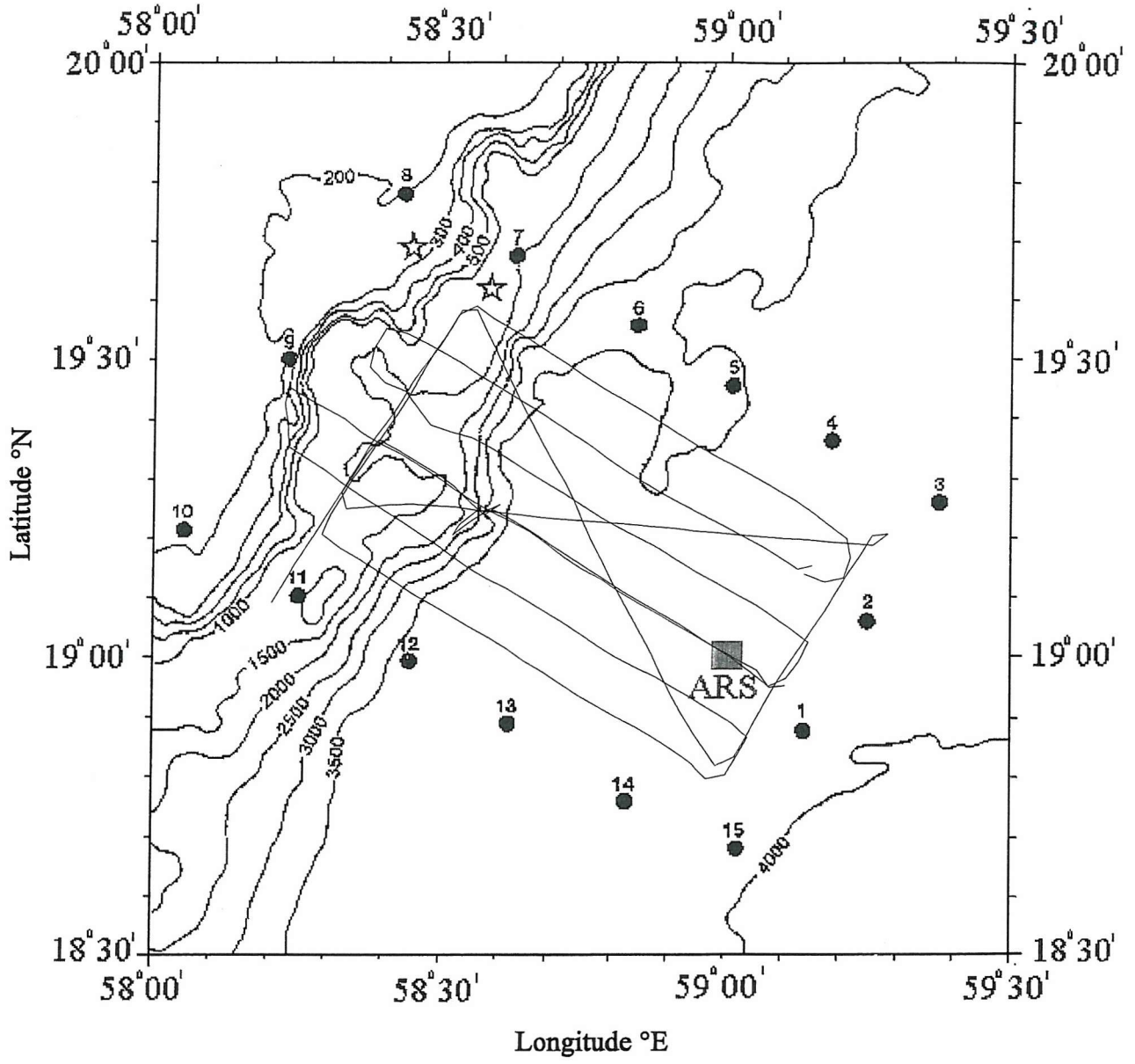

Figure 2.1.1 Topographic chart of survey area. CTD stations 1-15 are labelled. The ships tracks during SeaSoar survey 1 and 2 are shown. The symbol labelled ARS is the Arabesque Reference Station (from Herring *et al.* 1998).

2.1.2 Sampling methods

2.1.2.1 SeaSoar surveys

The first SeaSoar survey (SS1) had 7 parallel tracks, ~10 km apart, extending from the slope to deep water. It was carried out between 10 and 12 August and the track plot is shown in Figure 2.1.1. As a result of time limitations SeaSoar survey 2 (SS2) was restricted to a bow-tie shape pattern including a repeat of the first surveys leg 4 (Figure 2.1.1). SS2 was carried out between 16 and 18 August (Table 2.1).

SeaSoar is a platform, upon which sensors are attached, which flies in an undulating pattern through the water column (Pollard, 1986). A Neil Brown MKIIIB CTD and oxygen sensor, a Chelsea Instruments fluorometer and a 2_PAR irradiance sensor were mounted on SeaSoar. The CTD sensors were cross-calibrated with the underway thermosalinograph. The SeaSoar temperature and salinity data from this cruise are used solely to calibrate the acoustic backscatter data.

2.1.2.2 Collection of Vessel Mounted-Acoustic Doppler Current Profiler (VM-ADCP) data

The 153 kHz RD Instruments VM-ADCP recorded backscattered signal strength (acoustic backscatter) from each of our acoustic beams and averaged them every two minutes. Vertical resolution was 128 X 4 m bin depths giving a maximum range in excess of 500 m. The VM-ADCP transducers are set into the ship's hull at approximately 8 m depth (Wade and Heywood, 2001) and the VM-ADCP has a blank bin immediately below to allow the electronics time to recover between transmitting and receiving, therefore the first bin depth is at 12 metres. Acoustic backscatter is measured by the VM-ADCP as a function of the Automatic Gain Control (AGC). These data, from all four of the VM-ADCP beams, were averaged into two minute intervals. Mean Volume Backscattering Strength (MVBS) was calculated for each bin depth during the SeaSoar surveys following the manufacturers equation (RD Instruments, 1990) and allowing for a variable sound absorption coefficient (α) following the method outlined by Roe *et al.* (1996). Where α, which varies with temperature and salinity, was allowed to vary and calculated directly from *in situ* measurements of temperature and salinity from SeaSoar. Although the VM-ADCP could theoretically measure acoustic backscatter to depths greater than 500 m the signal noise to ratio was low at depth. This generally limited the backscatter data to depths shallower than 400 m during the day. At night there were so few targets below the oxygen minimum layer that the signal to noise ratio was low below depths of 80 metres. The data with low signal to noise ratio are omitted by following the practice of ignoring acoustic backscatter data from depth bins with suspect current velocities (Roe *et al.*, 1996).

Station Number	Gear	Date - Time (GMT)	Position	Depth	Comment
	SeaSoar (SS1)	10/8 – 1700 12/8 – 1300	19 08.4N 59 07.1E 19 08.2N 59 07.3E		
	SeaSoar (SS2)	16/8 - 2015 18/8 – 0430	18 56.3N 59 05.3E 19 05.3N 58 13.5E		
12661#3	CTD	5/8	18 59.9N 59 00.6E	0 - 3384	
12663#5	CTD	12/8	19 08.9N 59 05.9E	0 - 3263	
12670#3	CTD	21/8	18 60.0N 58 59.9E	0 - 2779	
12664#1	LHPR	12/8 - 1552-1819 (night)	19 07.1N 59 04 9E 18 58.3N 58 85.5E	0 - 290	Winch problems during recovery
12664#18	LHPR	14/8 - 1208-1516 (dusk)	18 59.6N 59 00.4E 18 45.3N 58 59.0E	0 - 210	Query regarding silks used
12664#37	LHPR	16/8 - 0900-1208 (day)	19 07.0N 59 05.9E 18 57.4N 58 58.0E	0 - 270	Swimming crab jammed wind-on
12666#1	LHPR	18/8 - 0927-1210 (day)	19 21.5N 58 22.7E 19 14.5N 58 13.0E	0 - 335	No paper chart (no flow or depth)
12670#4	LHPR	21/8 - 0507-0759 (day)	18 58.1N 58 59.2E 18 46.6N 58 53.2E	0 - 300	
12670#7	LHPR	21/8 - 1030-1312 (day)	18 45.5N 58 53.0E 18 35.1N 58 48.2E	0 - 310	Swimming crab jammed wind-on

Table 2.1 Station numbers, time, position and any problems that occurred with the SeaSoar surveys, CTDs and LHPR casts.

This also partially corrects for the non-linearity of the VM-ADCP, which is additionally corrected for by only accepting raw AGC counts at least 15 counts (~6.3 dB) above the noise level (identified from the deepest bin depth).

The resultant acoustic backscatter data were merged with navigational information so they could be contoured.

2.1.2.3 Collection of Conductivity Temperature and Depth (CTD) data

The CTD casts were made with a Neil Brown Mk IIIB CTD mounted on a 24 bottle General Oceanics multisampler. Additional sensors mounted on the CTD frame were a Beckman polarporaphic dissolved oxygen sensor, a Sea Tech 100 cm transmissometer and a Chelsea Instruments Mk II fluorometer. Salinity, oxygen and chlorophyll concentrations were determined from water bottle samples and used to calibrate the CTD and fluorometer (Herring, 1994; Herring *et al.*, 1998). Only the three CTDs at the Arabesque Reference Site (Stations 12661#3, 12663#5 and 12670#3) are presented in this thesis, their times and positions are given in Table 2.1.

2.1.2.4 Collection of Longhurst Hardy Plankton Recorder (LHPR) samples

The original single-net design of the Longhurst Hardy Plankton Recorder is described in Longhurst *et al.* (1966). Although it has been superseded by an improved twin net system (Williams *et al.*, 1983), a single net system was used on Discovery Cruise

209. The LHPR collects multiple samples (up to 100) during one tow. The system consists of a nose cone and a frame housing a conical 333 μm mesh aperture net, terminating in a cod-end unit. The cod-end unit contains two rolls of filtering gauze (mesh aperture 200 μm), which wind on to a third, sandwiching zooplankton samples between them (Figure 2.1.2). The gauzes are advanced on to the wind-on spool by an electric motor, thus giving a sequential series of samples. A flowmeter, mounted in the nose cone, measures the volume filtered for each sample. The nose cone diameter (20 - 40 cm) can be varied, depending on the concentration of plankton, as well as the sampling interval (30 seconds to 8 minutes). The LHPR can be towed at speeds up to 6 knots (3 m s^{-1}) and performs best when towed in a horizontal or upward oblique direction, providing both horizontal and vertical distribution data (Haury and Wiebe, 1982; Coombs *et al.* 1985; 1992; Williams and Conway, 1988). Its resolution, dictated by the wind-on motor, can be as fine as 5 - 20 m in the vertical and 15 - 100 m in the horizontal (Sameoto *et al.* 2000). Biases and errors associated with the LHPR include net hang up/residence time, inadequate discrimination between samples (Haury, 1973; Fasham *et al.*, 1974; Haury *et al.*, 1976) and, as with all net systems, extrusion (Nichols and Thompson, 1991) and avoidance (McGowan and Fraundorf, 1966).

Six LHPR tows were conducted during Cruise D209. The LHPR was towed in a V-shaped profile to a depth of ~ 300 m, estimated from the amount of wire paid out using the relationship described below:

$$\text{Depth} = \frac{\text{Wire Out}}{3}$$

The sampling period was set to two minutes, and a 280 μm mesh aperture conical net channelled the samples onto a 200 μm mesh aperture wind-on gauze. Actual depth and flow through the net for each two-minute sample were recorded on a paper chart, retrieved on recovery of the LHPR. Subsequent analysis of the LHPR tows showed that four were complicated either by instrument problems, or jamming of the wind-on mechanism by the swimming crab *Charybdis smithii* (Table 2.1).

Therefore, only two stations provide useful data for this thesis. Station 12664#1, a nighttime tow, made in the vicinity of the ARS, and Station 12670#4, a daytime tow, close to the ARS. The LHPR silks were preserved on-board in a 4 % buffered formaldehyde solution (Steedman, 1976), for subsequent analysis in the laboratory.

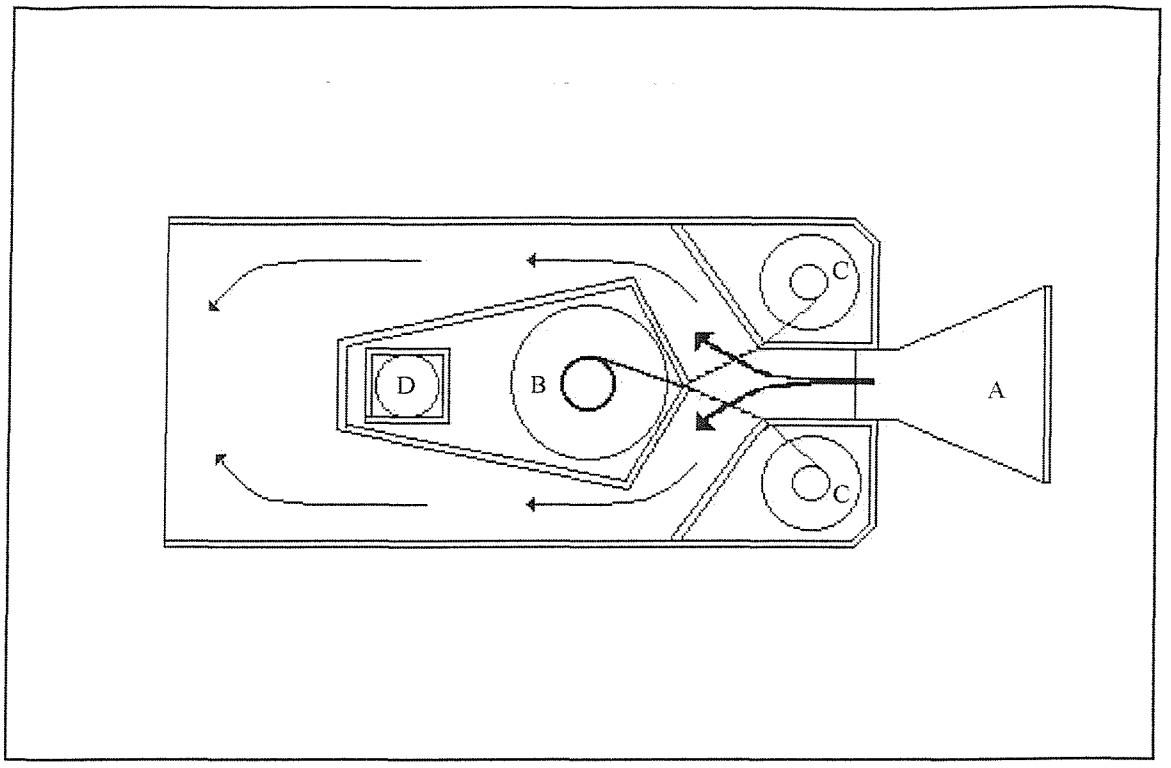

Figure 2.1.2 The Longhurst-Hardy Plankton Recorder (LHPR) cod-end unit, after Longhurst *et al.* (1966) (not to scale). A = intake tunnel from net to cod-end, B = wind-on spool, C = gauze spools and D = wind-on motor. Arrows indicate the flow of water through the cod-end.

2.2 RRS *Discovery* cruise 224 – The Alboran Sea

2.2.1 Survey design

As part of the EU MAST III funded project OMEGA (Observations and Modelling of Eddy scale Geostrophic and Ageostrophic motions), a multidisciplinary study was made of the Almeria-Oran front in the western Mediterranean (Figure 2.2.1) during December 1996 and January 1997.

The objective of the cruise was to provide the experimental field observations of eddy scale geostrophic and ageostrophic motions. A second objective was added, which is pertinent to this thesis, and that was to obtain concurrent physical, chemical and biological data at high resolution and on the same time and space scales to elucidate biophysical interactions at a mesoscale front.

Hydrographic, bioacoustic and biological data were collected aboard RRS *Discovery* Cruise 224, the first part of which comprised the second field experiment of OMEGA between 22 November and 29 December 1996 (Allen and Guymer, 1997).

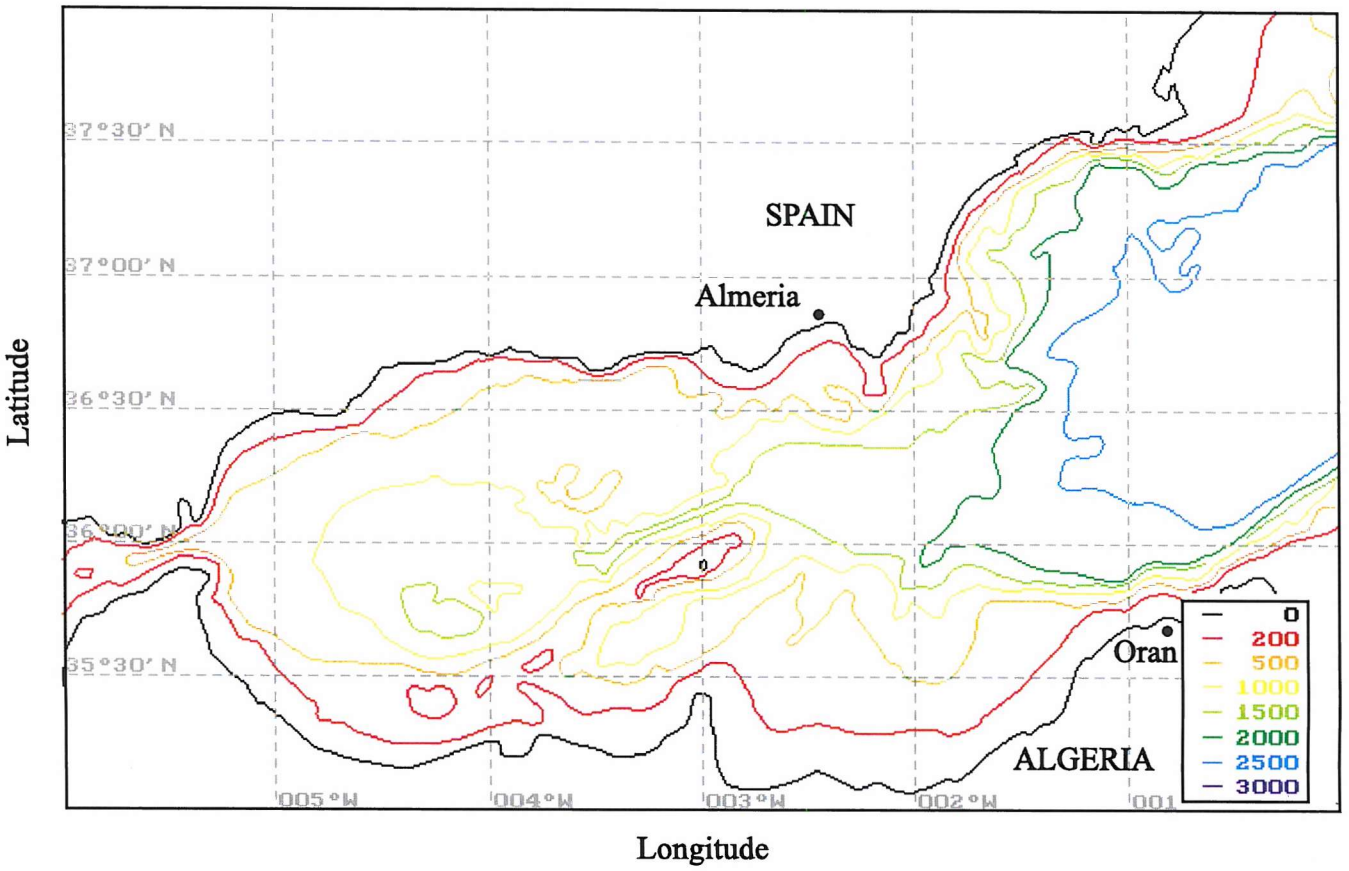

Figure 2.2.1 The topography of the Alboran Sea (Western Mediterranean Sea): reproduced from the GEBCO digital atlas, BODC. The Almeria-Oran front is typically positioned between Almeria, in Spain, and Oran, in Algeria.

During the second half of RRS *Discovery* Cruise 224, 31 December 1996 to 17 January 1997, traditional deep nets were deployed in the region of the Almeria-Oran front (Pugh, 1997).

Using the towed undulating vehicle SeaSoar (Pollard, 1986), two large scale and five repeat fine scale surveys were made of the Almeria-Oran front region in the western Mediterranean. Acoustic backscatter was collected throughout the cruise using both a Vessel-Mounted Acoustic Doppler Current Profiler (VM-ADCP) and a Simrad EK500 multifrequency echosounder. Between surveys, CTD stations and biological sampling with targeted Longhurst Hardy Plankton Recorder (LHPR) tows were carried out to determine nutrient profiles and verify biological distributions indicated by the acoustic data.

2.2.2 Sampling methods

2.2.2.1 SeaSoar survey

The repeated fine scale surveys had 10-11 parallel tracks, ~10 km apart (Figure 2.2.2) and their location was targeted at the Almeria-Oran front by near real-time analysis of underway thermosalinograph (TSG) data and AVHRR SST satellite imagery (Allen and Guymer, 1997). Three of the finescale surveys are the focus of this thesis (Table 2.2.).

SeaSoar is a platform, upon which sensors are attached, which flies in an undulating pattern through the water column (Pollard, 1986). Mounted on SeaSoar were a Neil Brown MKIII CTD, a fluorometer, a PAR sensor, a Sea-Tech light scattering sensor and a Focal Technologies Optical Plankton Counter (OPC). On Cruise D224 it had a typical depth range of 0 - 370 m, at a towing speed of 8 knots (4 m s^{-1}), using a fully faired conducting cable to communicate measurements in real-time to the ship. The CTD sensors were cross-calibrated with the underway thermosalinograph. The fluorometer (Chelsea Instruments SubAquatracker) provided an indicator of phytoplankton biomass, and the data are presented later as a measure of phytoplankton fluorescence yield, in instrument volts.

2.2.2.2 Collection of Vessel Mounted-Acoustic Doppler Current Profiler (VM-ADCP) data

For the duration of the SeaSoar surveys acoustic backscatter strength from the VM-ADCP was calibrated as Mean Volume BackScatter (MVBS), corrected for the variation of the sound absorption coefficient with changing salinity and temperature (from *in situ* SeaSoar CTD data) following the method used by Roe *et al.* (1996) (section 2.1.2.2).

It was not possible to tow a LHPR at the same time as SeaSoar, therefore *in situ* salinity and temperature from the environmental sensors on the LHPR were used to calibrate concurrent VM-ADCP MVBS data. As the LHPR temperature and salinity sensors were only calibrated on fabrication by the manufacturer, it was necessary to cross-

calibrate them with the calibrated underway thermosalinograph (Figure 2.2.3). These data were then interpolated across the tow to provide a two dimensional (in the vertical) description of the temperature and salinity of the water column (Figure 2.2.4). These data were then used to calculate α and hence calibrate MVBS following Roe *et al.* (1996).

Gear	Station Number	Date - Time (GMT)	Position
SeaSoar FSS1	FSS1	18:30 11/12/96 – 10:00 15/12/96	
SeaSoar FSS2	FSS2	21:10 16/12/96 – 17:30 20/12/96	
SeaSoar FSS3	FSS3	19:50 21/12/96 – 22:15 24/12/96	
CTD	13037	18/8 - 0927-1210 (day)	36.1689 N, 1.8527 W
CTD	13038	15/12 – 19:34 (day)	36.7327 N, 1.7537 W
CTD	13039	15/12 – 23:14 (night)	36.2903 N, 1.6673 W
CTD	13040	16/12 – 00:54 (night)	36.3614 N, 1.5758 W
CTD	13041	16/12 – 02:58 (night)	36.4226 N, 1.4835 W
LHPR	13036	15/12 – 14:40 – 17:05 (day)	36 16.15 N, 1 34.65 W 36 18.96 N, 1 41 43 W
LHPR	13048	21/12 – 09:17 – 11:42 (day)	36 14.66 N, 1 34.17W 36 10.35 N, 1 43.84 W

Table 2.2 Station numbers, time and position of the SeaSoar surveys, CTDs and LHPR casts.

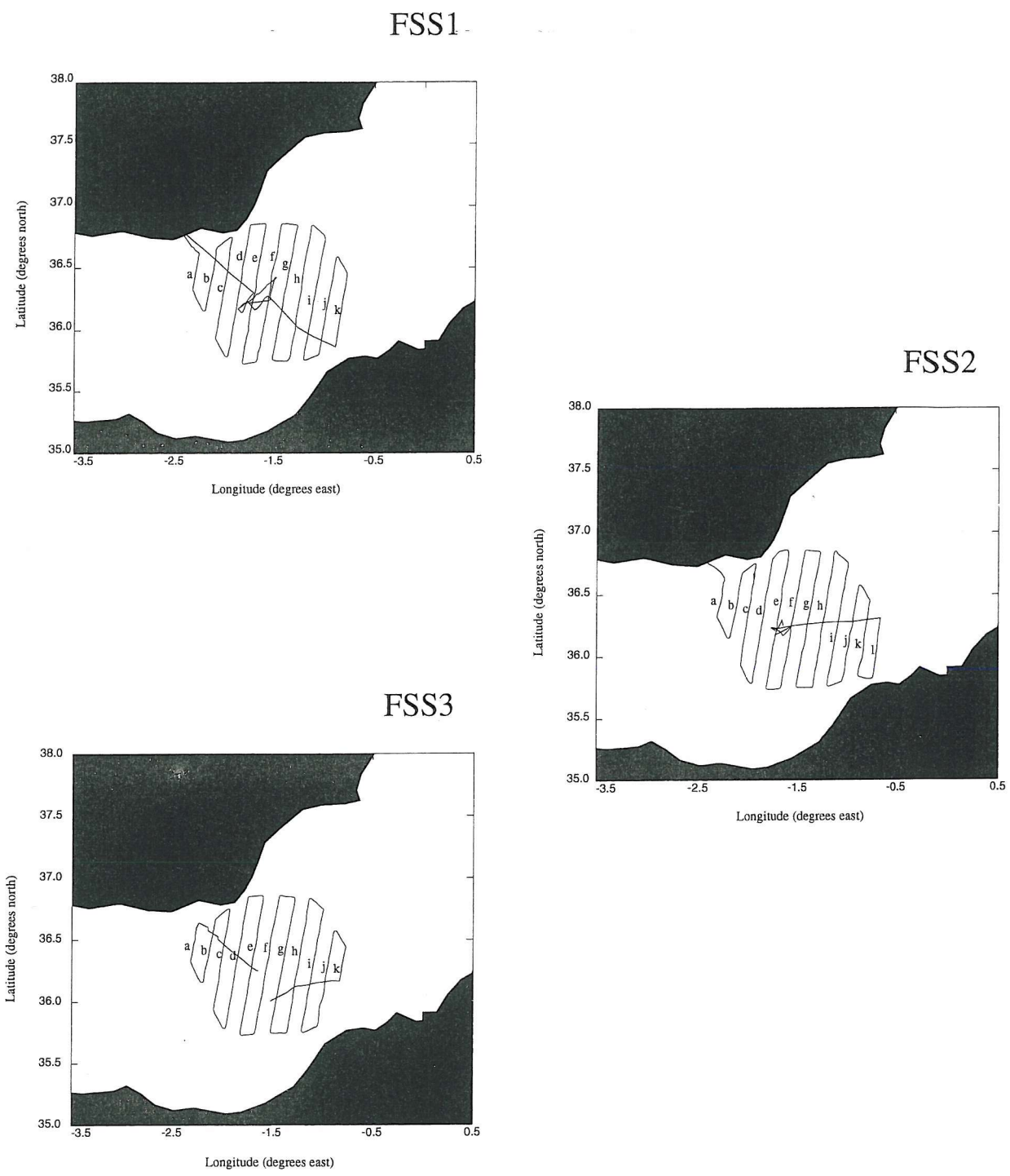

Figure 2.2.2 Cruise tracks for the first three Finescale Seasoar Surveys (FSS1-3) in the Alboran Sea.

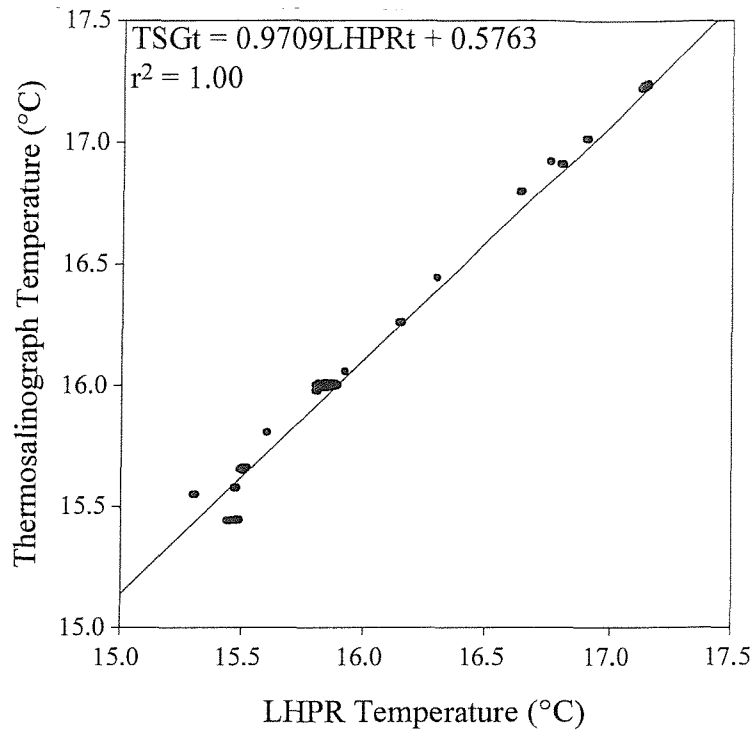

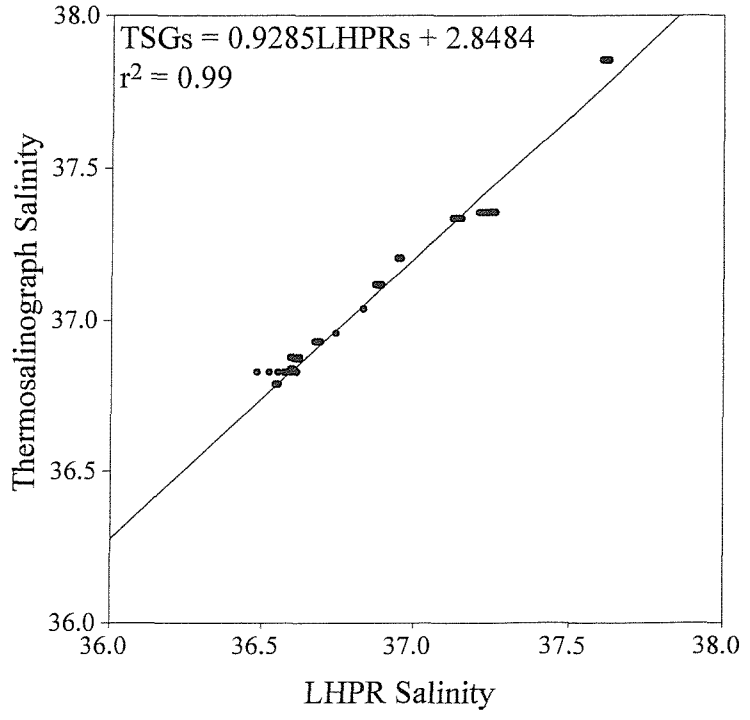

Figure 2.2.3 Regression analysis of LHPR versus ThermoSalinograph (TSG) measured (a) temperature and (b) salinity.

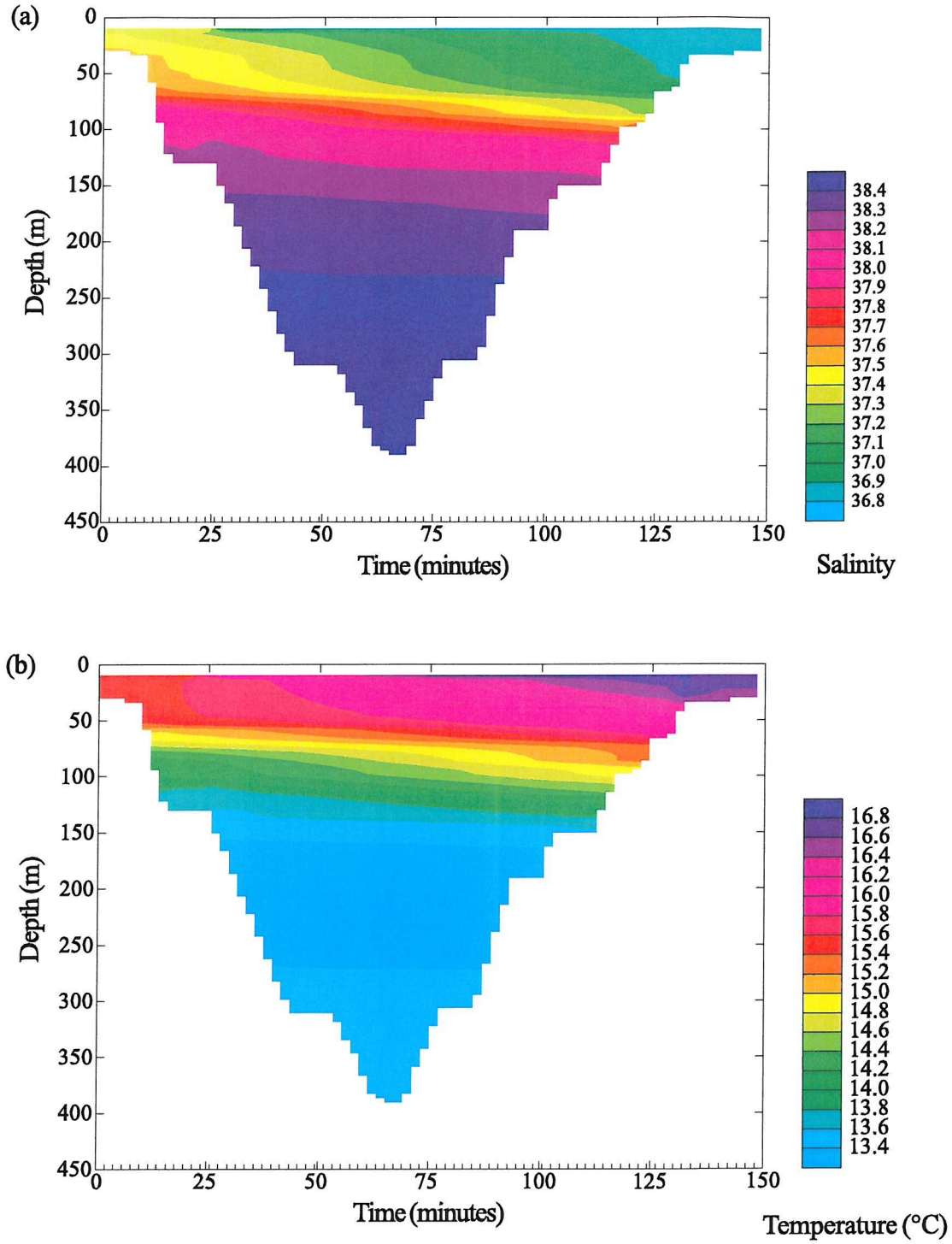

Figure 2.2.4 a) Interpolated temperature during LongHurst-Hardy Plankton Recorder (LHPR) Station 13036, b) interpolated salinity during LHPR Station 13036.

2.2.2.3 Collection of SIMRAD EK500 Echosounder data

The SIMRAD EK500 is a scientific multifrequency echosounder, operating at three frequencies, 38, 120 and 200 kHz. The 120 kHz and 38 kHz frequency transducers are split beam, made up of four separate transducers, and the 200 kHz transducer is a standard single beam unit. The split beam transducers are made up of quadrants and can transmit as one, but receive individually so that differences in the phase and amplitude of the returned signal can be used to give the position of the targets relative to the orientation of the beam. The EK500 has an extremely wide (150 dB) dynamic range that enables it to measure target strength reliably down to -120 dB and thus, as well as measuring individual targets, it is ideal for measuring Mean Volume BackScatter (MVBS). The validity of the manufacturer's target resolving algorithms has been questioned. In fact the British Antarctic Survey (BAS) do not use them for their krill census data (Brierley, pers. comm.). The distribution of numbers of high target strength values was plotted on the same time and space axis as the distribution of high MVBS and did not compare well. This may be a result of the algorithm's inability to resolve individual targets at high target densities. Therefore, the target resolving capability of the EK500 was not used in this study.

The EK500 was housed in a towed fish deployed from its own portable winch over the port side of the after deck of RRS *Discovery*. An attempt was made to calibrate the echosounder following standard echosounder procedure (Foote, 1983). However the relative motion of the ship, the towed fish and the calibration spheres was such that only on a few occasions were the spheres visible in the starboard quadrant of the beams (Allen and Guymer, 1997). As, in this study, the acoustic backscatter data are not being used to measure zooplankton quantitatively, it was decided to continue using it to describe the zooplankton distributions qualitatively and for direct comparison with net sampled zooplankton without calibration.

The acoustic backscatter data are presented here as acoustic backscatter calculated following the manufacturer's calibrations (SIMRAD, Crisp *et al.* 1998), with a vertical resolution of 1 m at 200 and 120 kHz and 2 m at 38 kHz. The horizontal resolution was set to two-minute averages, comparable with the VM-ADCP data.

2.2.2.4 Collection of Conductivity Temperature and Depth (CTD) data

Five CTD stations of Cruise D224 are of interest to this study. The CTD stations (RRS *Discovery* station numbers 13037-13041), were carried out in a line across the centre of the Almeria-Oran front (Table 2.2).

The CTD casts were made with a Neil Brown Mk IIIb CTD mounted on a 24 bottle General Oceanics multisampler, although only twelve 10-litre Niskin bottles were mounted in alternate positions around the rosette. Additional sensors mounted on the CTD

frame were, a Chelsea Instruments transmissometer and a Chelsea Instruments Mk II fluorometer. Temperature, from SIS reversing thermometers, and salinity, determined from water bottle samples, were used to calibrate the CTD sensors. The bottles were also used to provide water samples for the determination of Chlorophyll a biomass and nutrient concentration.

Determination of Chlorophyll a biomass

Water samples for the determination of chlorophyll *a* were taken at 5, 50, 100 and 200 m depth at each CTD station, with a further sample taken at the chlorophyll maximum (indicated by the CTD fluorometer). Chlorophyll *a* was extracted from each sample using 90 % acetone. The concentration of chlorophyll *a* in each sample was measured using a Turner Designs (TD) Fluorometer (model 10-000R, serial no. 00859), which was calibrated daily with a standard chlorophyll solution (1 mg Sigma™ chlorophyll *a* pellet dissolved in one litre of 90 % acetone) whose exact chlorophyll concentration was ascertained using a Pye Unicam SP6-500 spectrophotometer. Chlorophyll *a* and phaeopigment concentrations were calculated using the following equations (JGOFS protocol, 1994):

$$\text{Chlorophyll } a\,(mg\ m^{-3}) = FD\left(\frac{Fm}{(Fm-1)}\right)(Fb-Fa)\left(\frac{v}{V}\right)$$

$$Phaeopigments\,(mg\ m^{-3}) = FD\left(\frac{Fm}{(Fm-1)}\right)((Fm\times Fb)-Fa)\left(\frac{v}{V}\right)$$

Where: FD = Chlorophyll *a* Standard concentration / Chlorophyll *a* Standard fluorescence before acidification.

Fb, Fa = Fluorescence value before and after acidification of sample.

$Fm = \frac{Fb}{Fa}$ of Chlorophyll *a* Standard solution.

v = volume of 90 % acetone used in the extraction.

V = Volume of seawater filtered.

Since cruise D224 the standard method for measuring Chlorophyll *a* has altered, and acidification of the sample (and hence calculation of phaeopigment concentration) is no longer undertaken. The non-acidification technique (Welschmeyer, 1994) is found to provide more accurate estimates of chlorophyll a, ignoring aliases caused by phaeopigments and chlorophyll b.

Determination of nutrient concentration

The concentration of nutrients within the water column was measured from the CTD water samples from depths of 150 metres to over 2000 metres. A Chemlab™ autoanalyser was used to determine the concentration of silicate, phosphate and nitrate, following the AutoAnalyser mark II method of analysis (Allen and Guymer, 1997).

2.2.2.5 Collection of Longhurst-Hardy Plankton Recorder (LHPR) samples

Ten tows were made across the Almeria-Oran front to collect zooplankton, using a modern LHPR (see section 2.1.2.4, Sameoto *et al.*, 2000) designed by Spartel ™ . The LHPR was towed in a V-shaped profile across the front, which had been identified from underway temperature and salinity measurements (from the TSG). The modern LHPR has a large Aluminium frame with a polypropylene tail fin. A nose cone at the front, channels water through a 333 μm mesh aperture conical net to the cod-end. Attached to the frame, one each side, are two cylinders containing a rechargeable battery pack and the electronics for driving the cod-end, monitoring the sensors (a seabird conductivity meter, temperature probe and a depth sensor and flowmeter) and communicating with the surface. To assist the sampler to dive, a 45 kg depressor weight is attached to the underside front and a drogue streams from the back of the frame to assist stability.

The modern LHPR has been designed for real-time communication with the ship. However the lack of a conducting cable on Cruise D224 resulted in the LHPR being run in internal logging mode. This permitted a maximum time of 180 minutes in the water (the data holding capacity of the software cylinder before overwriting), including deployment and recovery. To err on the side of caution, tows were limited to around two hours and thirty minutes. A delay of six minutes before the first wind-on of the gauze was added to allow time for deployment.

Deployment of the LHPR was from the main A-frame over the stern of RRS *Discovery*, using the main towing warp. Twenty metres of wire was initially paid out at the start of each haul, and the LHPR held at the surface to allow at least one wind-on of the gauze (Figure 2.2.5). The wire was then paid out at 30 m per minute until the LHPR was at an estimated depth of around 400 m (this was equated to 1200 m wire out, section 2.1.2.4).

The LHPR was then held at its maximum depth for 5-10 minutes before hauling in at 30 m per minute. During hauling several depths of interest, identified by anomalies in VM-ADCP/EK500 acoustic backscatter, were stopped at and sampled for a further 5-10 minutes. Upon retrieval on deck, the cod-end was removed from the frame. The wind-on spool holding the "sandwiched" zooplankton was placed in 5 % formaldehyde and then both net and cod-end were washed in preparation for the next tow.

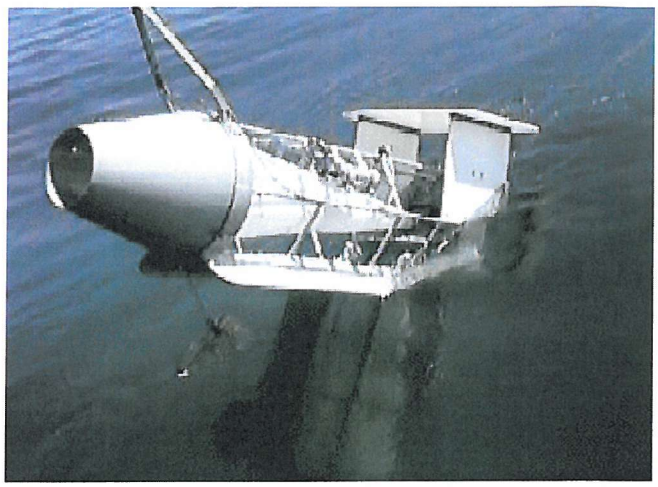

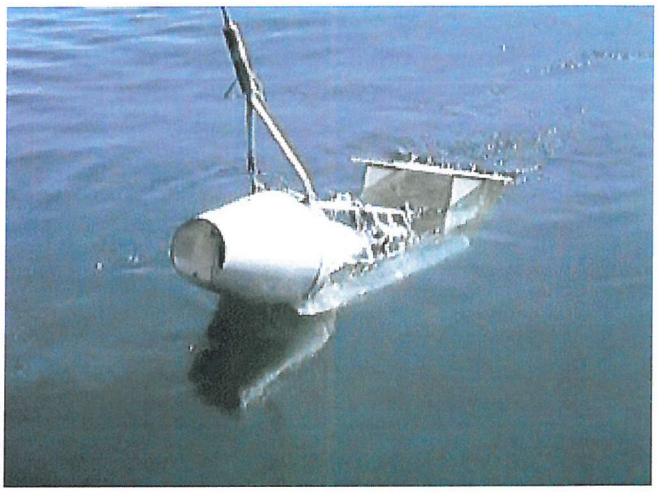

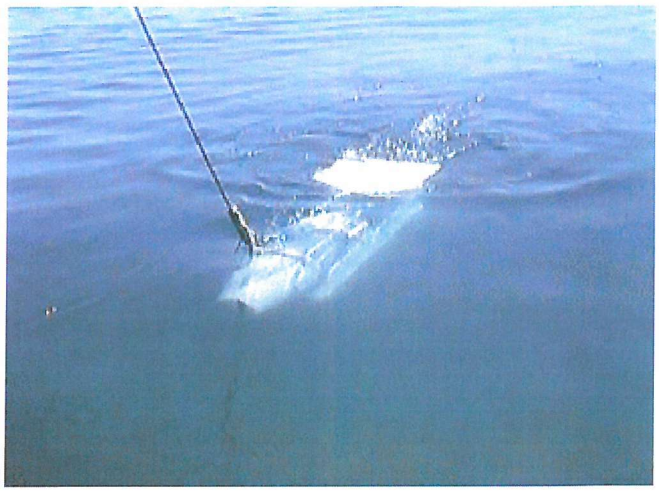

Figure 2.2.5 Photographs of the LHPR being held at the surface at the commencement of a tow (photographs courtesy of R. Pascal).

As part of this thesis two tows were analysed, these were chosen because they were either taken between two SeaSoar surveys, or had concurrent EK500 as well as VM-ADCP acoustic backscatter data associated with them (Table 2.2).

2.3 Data Analysis

2.3.1 Net samples

2.3.1.1 Identifying samples within a LHPR tow

Zooplankton samples obtained with a LHPR are sandwiched between two strips of gauze (Section 2.1.2.4). On return to the laboratory this gauze is unwound from the wind-on spool and, to aid identification of discrete samples, is laid out against a white background. Blank gauze separates each sequential sample, giving the gauze a striped appearance. Identification of discrete samples is aided by numbering each sample from the beginning of the haul (marked in permanent pen before deployment) and comparing with the recorded tow information. The gauze is then cut up into individual samples.

Each sample is washed off the gauze using a high pressure fresh water jet. This is necessary as the zooplankton (particularly chaetognaths) are frequently attached (squashed on) to the gauze as a result of water pressure during the tow and the sandwiching process on the wind-on spool. The samples are concentrated on a fine mesh and transferred into preserving fluid (2 % formaldehyde, Steedman 1976) in individual sample jars.

2.3.1.2 Identifying and counting zooplankton

Each sample was analysed for the abundance of zooplankton, identified to group level (e.g. euphausiids, copepods, chaetognaths, etc.) under a WILD M5 dissecting microscope. Zooplankton groups identified were amphipods, appendicularia, brachyura larvae, chaetognaths, cephalopods, copepods, decapods, euphausiids, fish, heteropods, medusae, mysids, ostracods, polychaetes, pteropods, siphonophores, stomatopods, and squilla larvae following Newell and Newell (1963). In each case the whole of the sample was analysed and each zooplankton group transferred to separate sample jars, except for copepods and the residue. This ensured that rare animals but strong acoustic scatterers, such as pteropods, were counted. A Folsom Plankton splitter was used to obtain a sub-sample from which the abundance of copepods were obtained. Whole animals and heads of animals were counted. Numerical abundances for each taxonomic group were standardised with the water filtered per sample and are displayed as No. m^{-3}.

2.3.1.3 Biovolume measurements

The total biovolume for each sample and, where possible, the biovolume for each group (only possible with samples from the Indian Ocean) were quantified using the normalised displacement volume (Beers, 1976; Postel *et al.*, 2000). Samples were sieved through a 200 μm mesh, blotted for excess fluid on absorbent paper, and then placed in a

known amount of preserving fluid in a measuring cylinder. The resulting rise in level (i.e displacement volume) is the biovolume, a measure of biomass. The biovolume measurements were standardised by the volume of water filtered per sample and are presented here as ml m^{-3}. This method is non-destructive and replicate measurements indicated the range of error to be 5-10 %, which could be caused by the inclusion of interstitial waters.

2.3.1.4 Length measurements

Length measurements of six groups of zooplankton (Amphipoda, Chaetognatha, Copepoda, Euphausiacea, Fish and Pteropoda) were made using a combination of a WILD M5 dissection microscope, drawing arm, digitising tablet and the PC based programme SIGMASCAN™. These groups were chosen as they represented zooplankton for which acoustic models are available. All measurements were made at either x 6 or x 12 magnification depending on size, and in all cases only complete animals were measured. The total length and the numbers of each group measured were:

Copepoda A split (taken using the Fulsam plankton splitter, numbers varying from 200 - 400) of copepods from each sample were measured as the lateral distance from the anterior tip of the cephalothorax to the posterior end of the uropods, excluding the terminal setae.

Euphausiacea Up to 100 euphausiids, where possible, were measured for Total body Length (TL), otherwise all complete euphausiids were measured. TL was measured as the lateral distance between the base of the eye-stalk and the posterior end of the uropods, excluding the terminal setae (reference measure Mauchline, biomass handbook No. 4).

Amphipoda All complete amphipods were measured as the lateral distance from the anterior tip of the cephalothorax to the posterior end of the uropods.

Chaetognatha Up to 100 chaetognaths were measured from each sample. Most were so squashed that to untangle them would rip and tear the organism. Therefore they were measured in a line following the middle of the organism, starting from the mouth to the tip of the caudal fin.

Fish All fish were measured as the lateral distance from the tip of the head to the posterior end of the caudal fin.

Pteropoda As a consequence of being kept in preserving fluid for at least two years (specific to the Indian Ocean samples) the calcite shell of some of the pteropods had dissolved. All Mediterranean pteropods, on removal from the main sample, were preserved in alcohol to maintain the integrity of the calcite shell. The length measured, where possible, was the distance from the embryonic shell to the mouth.

2.3.2 Observed/estimated acoustic comparison

The relationship between acoustic backscatter and actual zooplankton samples was examined. This utilised the downhaul of LHPR station 12664#1 and VM-ADCP 150 kHz acoustic backscatter data from Cruise D209 and the LHPR station 13048 and VM-ADCP and EK500 (200, 120 and 38 kHz) acoustic backscatter data from Cruise D224. Only the daytime haul was used from the Indian Ocean because, during the night, there was no acoustic backscatter data below 80 metres. This was a result of there being few targets below the oxycline. Also only the downhaul was used from St. 12664#1 as, when the depth and volume filtered of each sample was plotted, there were discrepancies between the up and downhaul values (Figure 2.3.1). This indicated that the sample interval of two minutes may not have been correct for some samples, hence only the downhaul samples were used. Although Pipe *et al.* (1981) found no statistical differences between the up and downhaul, Grant *et al.* (2000) also comment on greater reliability of the downhaul.

The observed acoustic backscatter/zooplankton relationship was investigated in three ways.

(1) comparing observed acoustic backscatter with zooplankton biovolume

(2) comparing observed acoustic backscatter with zooplankton abundance

(3) comparing observed acoustic backscatter with model-estimated acoustic backscatter, calculated using acoustic models.

Each variable (abundance, volume and model-estimated backscatter) was compared with the MVBS coefficient (observed acoustic backscatter) estimated by echo integration in the vicinity of the net sampled volume. Hence the first step was to identify, in time and space, observed acoustic backscatter data concurrent with the net samples.

2.3.2.1 Matching of acoustic and LHPR data records

All the acoustic data (VM-ADCP and EK500) were averaged into two-minute intervals so both acoustic and net data were available on the same sampling interval. The configuration of the equipment, where acoustic data were collected from immediately below the ship and the LHPR net samples from behind the ship, resulted in the net system always trailing some variable distance (L) behind the acoustic transducers (Figure 2.3.2). Therefore, the LHPR actually passed through the depth horizon (d) at a time (t_d) that differed by a variable period (Δt) after the VM-ADCP had sampled the same depth.

To match the data from the net with the acoustic information the corrected time (t_c) was calculated, where

$$t_c = t_d - \Delta t$$

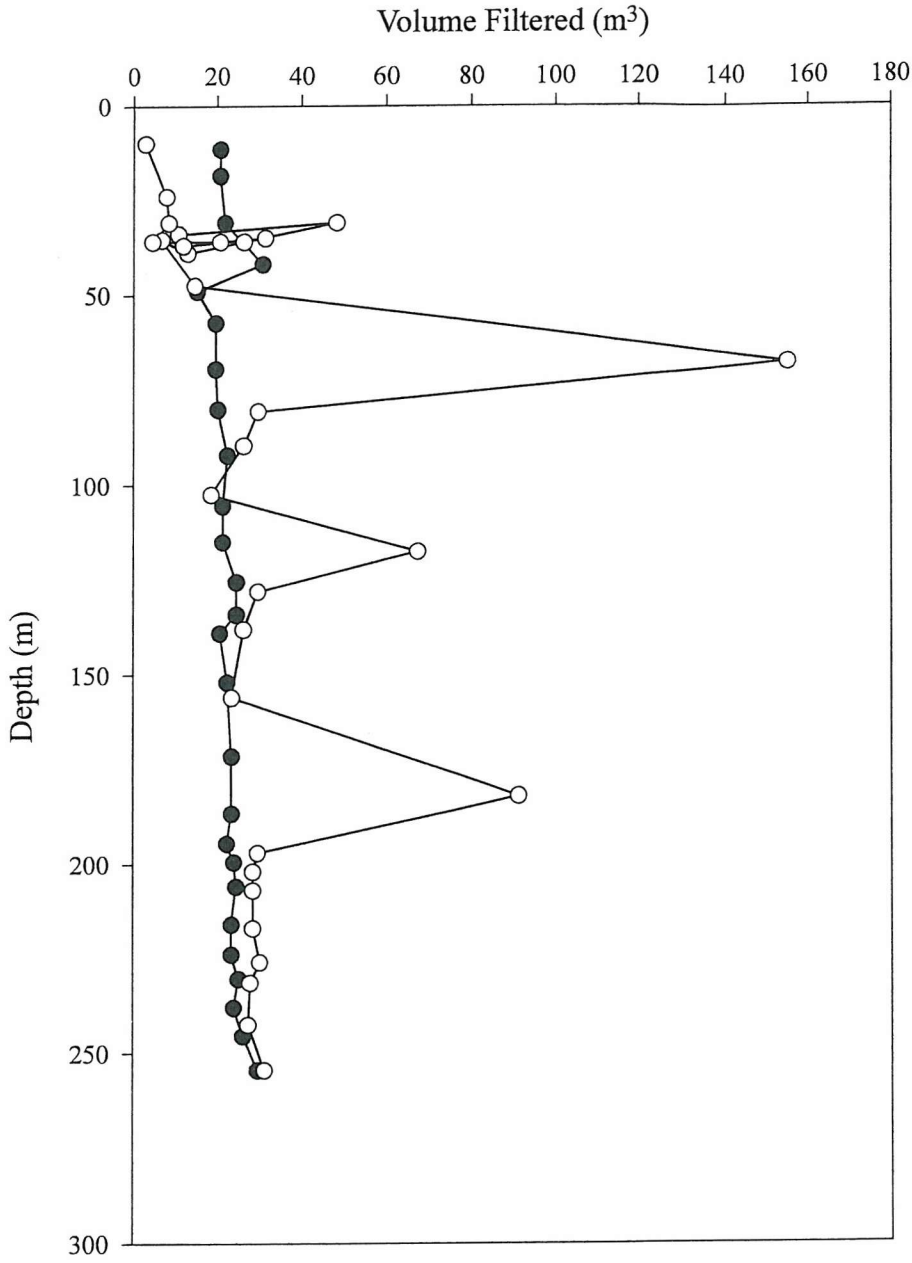

Figure 2.3.1 Volume of water filtered for each LHPR sample at Station 12664#1. Black circles are the downhaul data, white circles are the uphaul data.

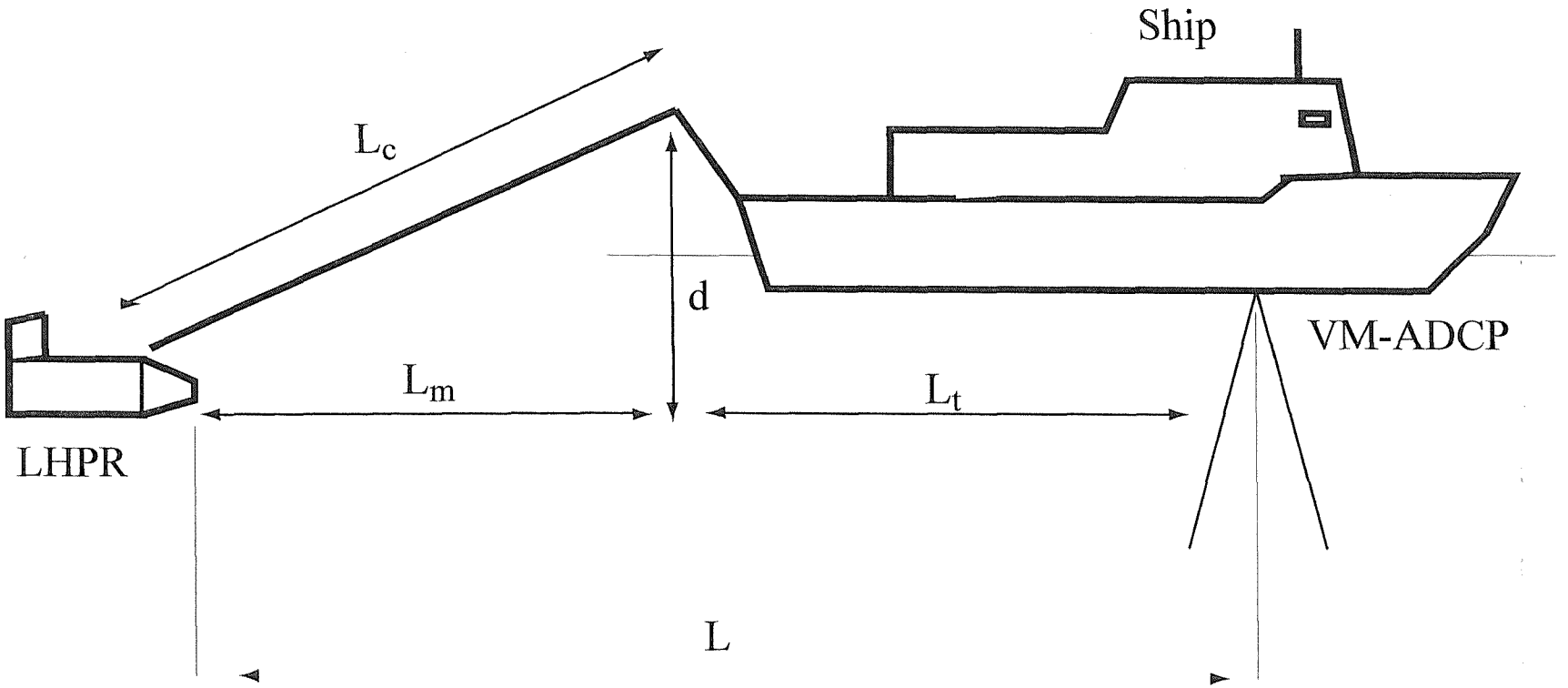

Figure 2.3.2 Diagram showing the geometry of the LHPR and VM-ADCP locations relative to the research vessel. L: horizontal difference of VM-ADCP beams from the LHPR; L_t: distance of the VM-ADCP forward of the A-frame; L_m: the distance of the LHPR behind the A-frame; L_c: the length of towing cable; d: the depth of the LHPR.

where t_d is the actual time at which the LHPR passed through depth d, and t_c is the time at which depth d passed through the VM-ADCP record. The variable time period, Δt, was calculated from (Figure 2.3.2):

$$\Delta t = \frac{\sqrt{L_c^2 - d^2}}{v}$$

where L_c is the length of towing cable between the LHPR and the A-frame, d is the depth at time t_d recorded by the LHPR CTD and v is the ship's speed (m s^{-1}). The towing speed of the vessel was fairly controlled at 2 m s^{-1} and the length of cable paid out during the deepest part (d = 395 m) of any tow was ~1200 m. Thus, the LHPR was towed through a given depth at periods ranging between 1 and 10 minutes after it had been sampled by the VM-ADCP.

LHPR tows were reconstructed through the VM-ADCP data using the variable time correction given by the equations above. Although the sampling interval of the acoustic data could be matched to that of the LHPR, the depth interval sampled by the LHPR was more variable. Therefore the acoustic data were integrated (in linear form) over the vertical range that the LHPR travelled during any two minute sampling period, where the LHPR travelled further (in depth) than one acoustic bin depth.

2.3.2.2 Abundance/biovolume/acoustic comparison

The abundance and biovolume of each LHPR sample was compared with observed acoustic backscatter. In all cases acoustic backscatter is presented as acoustic backscatter in dB, the log-transformed variable of backscattering cross section (Chapter 1). Therefore observed acoustic backscatter data are compared with log-transformed values of abundance and biomass.

For comparison with previous work the relationship between observed MVBS and log-transformed abundance and biovolume was examined using both a predictive regression, following Heywood *et al.* (1991) and Zhou *et al.* (1994), and a functional regression, following Wiebe *et al.* (1996) and Greene *et al.* (1998).

2.3.2.3 Acoustic scattering models

Model-estimated acoustic backscatter was calculated by solving the forward problem (Holliday and Pieper, 1995). It was determined for each two-minute LHPR sample by combining taxonomic and abundance data of zooplankton with appropriate scattering models (Chapter 1). In this case scattering models were used to calculate Total Model-Estimated Acoustic Backscatter (TMEAB) from six groups: large (>2 mm) and small (<2 mm) copepods, chaetognaths, amphipods, fish, pteropods and euphausiids.

<table>
<tr><th colspan="2">Acoustic model</th></tr>
<tr><th>Randomly-orientated fluid, bent cylinder model</th><th>Dense-fluid sphere model</th></tr>
<tr><td>$\sigma_{bs} = 0.08R^2L^2\beta_D^{-1}[1-\exp(-8\pi^2 f^2 D^2 s^2 c^{-2})\cos(\pi f D c^{-1}(4-\frac{1}{2}\pi(\pi f D c^{-1}+0.4)^{-1}))]$</td><td>$\sigma_{bs} = \frac{25}{144}\pi^4 D^6 R^2 c^{-4}\left(1+\frac{25}{9}\pi^4 D^4 f^4 c^{-4}\right)^{-1}$</td></tr>
<tr><td>R = reflection coefficient, determined empirically = 0.058 for all taxa
L = body length in metres
$s = \frac{\text{standard deviation of length}}{\text{length}} = 0$
β_D = ratio of body length to width
D = body width = $\frac{1}{\beta_D}L$</td><td>R = reflection coefficient, determined empirically = 0.5
D = spherical diameter</td></tr>
<tr><td colspan="2">f = acoustic frequency (Hz)
c = speed of sound (m/s)</td></tr>
</table>

Table 2.3 Model equations used to calculate representative backscattering cross sections from the net sample data.

Where the TMEAB for each two-minute LHPR sample was assumed to be a linear combination of the backscattering from all individual sound scatterers in the insonified volume (following Clay and Medwin, 1977). Thus the forward problem can be described by the following equation:

$$\text{TMEAB} = \sum_{i=1}^{t} \sum_{j=1}^{s} n_{ij} < \sigma_{bsij} >$$

Where TMEAB is the estimated volume backscattering coefficient, n_{ij} is the numerical abundance for size class j of taxon i, and s and t are the numbers of relevant size classes and taxa respectively.

The acoustic scattering models used in computing the forward problem were developed by Stanton *et al.* (1994a). The fluid-filled bent-cylinder model was used for the amphipods, chaetognaths, copepods, euphausiids and fish, and the dense fluid-filled sphere model was used for the pteropods. The equations for these models are presented in Table 2.3. All representative backscattering coefficients derived from the models were calculated for each frequency used respectively (i.e. 153, 200, 120 and 38 kHz).

Format of input files

The models that estimate acoustic backscatter from known zooplankton samples are run within the computer programme MATLAB™. The programme requires three input text files to describe each sample, set in the following manner:

Acc.asc containing one column of descriptive information: Total number of individuals, biovolume, observed acoustic backscatter and the station number.

Aliquot.asc containing one column, which holds the following information: station number, volume of water filtered by the sample (m^3) and percentage of each group which has been sampled.

Length.asc containing seven columns of length measurements, in the specific order of small copepods (csmlen), large copepods (clglen), amphipods (amplen), chaetognaths (chalen), euphausiids (euphlen), fish (fislen) and pteropods (ptelen).

Output of acoustic scattering models

The output for each sample is a value of estimated acoustic backscatter for each group and a total model-estimated acoustic backscatter (TMEAB). Through these data, the contribution to the total estimated acoustic backscatter of each zooplankton group can be defined. The total model-estimated backscatter was compared with observed acoustic backscatter using a students t-test.

2.3.3 Statistical analysis

A functional regression analysis was conducted to examine the relationship between observed and estimated acoustic backscatter. The slope of each regression line was then compared with the expected slope using a students t-test. In all cases the observed acoustic backscatter was placed as the horizontal (X) variable following previous work. These methods of analysis were analogous to those outlined in Wiebe *et al.* (1996) and Greene *et al.* (1998).

2.3.3.1 Functional regression analysis

A functional regression analysis (Ricker, 1973) was used to examine the correlation between the estimated and observed volume backscattering coefficients. A functional regression was chosen in favour of a predictive regression as it defines a central trend, minimising the sum of the products of the horizontal and vertical of each point from the line. Whereas a predictive regression minimises the sum of the squares in only the vertical or horizontal.

The equation for the functional regression line is:

$$Y = u + vX$$

Where X and Y are two variable quantities, u is the intercept and v is the slope of the line. In this case v can be calculated using:

$$v = \pm\sqrt{\frac{\sum y^2}{\sum x^2}}$$

Where x and y represent the quantities as measured from their means, i.e. $x = X - \overline{X}$; $y = Y - \overline{Y}$.

All regressions were calculated on log-transformed data. The correlation coefficient (r^2) value for a functional regression is the same as that for a predictive regression and has been calculated following the equation given by Ricker (1973):

$$r^2 = \left(\frac{\sum xy}{\sqrt{\sum x^2 \sum y^2}} \right)^2$$

2.3.3.2 Students t-test

A t-test (Fowler and Cohen, 1990) was used to compare the slope of the regression line with the slope of previous regression lines, where the null hypothesis (H_0) is that the gradients are not significantly different. The t-test was applied using the following equation:

$$t = \frac{(v - b)}{S.E._{(v-b)}}$$

Where t is the students statistic at the appropriated degrees of freedom, v is the gradient of the regression line, b is the gradient of the null hypothesis regression line and $S.E._{(v-b)}$ is the standard error of the difference between v and b which can be calculated using:

$$S.E._{(v-b)} = \sqrt{S_v^2 + S_b^2}$$

Where S_b can be described by the equation (Ricker, 1973):

$$S_b = \sqrt{\frac{v^2(1-r^2)}{N-2}}$$

The ability of the acoustic scattering models to estimate backscatter correctly was also examined using a t-test. In this case, if the models estimated backscatter correctly the slope of the regression line would be one. Therefore, the null hypothesis (H_0) was that the slope of the regression line was not significantly different from one, tested using the following equation:

$$t = \frac{(v-1)}{S.E._v}$$

Chapter 3

The Arabian Sea

3.1 Introduction

In this chapter the results from a multi-disciplinary survey of the Arabian Sea are presented. Section 3.1 introduces the survey region and previous observations. In section 3.2 the hydrography and oxygen distribution of the Arabian Sea in the vicinity of the Arabesque Reference Site (ARS) is presented and discussed. Observations of the distribution of zooplankton are presented in section 3.3 and section 3.4, and discussed in section 3.5. Finally in section 3.6 the findings are summarised.

3.1.1 The physical structure of the Arabian Sea

The North Indian Ocean can be classified into approximately three areas: The equatorial belt (stretching between 10 °S and 10 °N), the Bay of Bengal, and the Arabian Sea (Shetye *et al.*, 1994). The Arabian Sea is essentially enclosed on three sides by land. Its boundaries according to Robinson (1966), quoting the International Hydrographic Bureau (Sp. Publ. 23,1953), are defined as follows: the southern 'open ocean' boundary, by a line from Ras Hafun (Somalia, 10.29 °N 51.20 °E) to Addu Atoll (approximately 73.25 °E 0.58 °S); the Eastern boundary, follows the Western edge of the Maldives up to Sadashivgad Light on the west coast of India (14.80°N); and, the Western and Northern boundary by Somalia, Oman and Pakistan (Figure 3.1.1). Northerly input of water is from two marginal seas: (1) the Persian Gulf, through the Gulf of Oman which can be theoretically separated from the Arabian Sea by a line from Ras Limah (25.95°N) in Oman to Ras al Kuh (Iran, 25.80°N); and (2) the Red Sea, through the Gulf of Aden, which is separated from the Arabian Sea by the meridian of Ras Asir (Somalia, 51.25°E). What was essentially a poorly-studied region became, in the 1990s, the subject of numerous multi-national multi-disciplinary expeditions conducted in the framework of the JGOFS and WOCE programmes and published extensively in Deep Sea Research II (Vol. 45, No. 10-11 (1998); Vol. 46, No. 3-4 (1999), Vol. 46, No. 8-9 (1999); Vol. 47, No. 7-8 (2000); Vol. 48, No. 6-7 (2001), Vol. 49, No. 7-8 (2002) and Vol. 49, No. 12 (2002). The majority of data prior to this resulted from the International Indian Ocean Expedition (Zeitzschel, 1973).

Circulation of the Arabian Sea

The Arabian Sea is a tropical basin limited in its northern extent. It has annual reversals in atmospheric (the strong Southwest and weaker Northeast monsoons) and upper ocean circulation (Figure 3.1.2) (Tchernia, 1980; Shetye *et al.*, 1994). Defining characteristics of the Arabian Sea seasonal cycle of physical conditions are (1) strong

wind stress during the SW monsoon (June – August/September) that results in widespread upwelling and mixing, (2) moderate strength, relatively cool and dry winds during the winter NE monsoon (December – February) that promote evaporative cooling, forcing strong convective mixing in the offshore region, and (3) during the spring and autumn intermonsoon transition periods, weak winds and surface layer heating that produce strong stratification and shallow mixed layers.

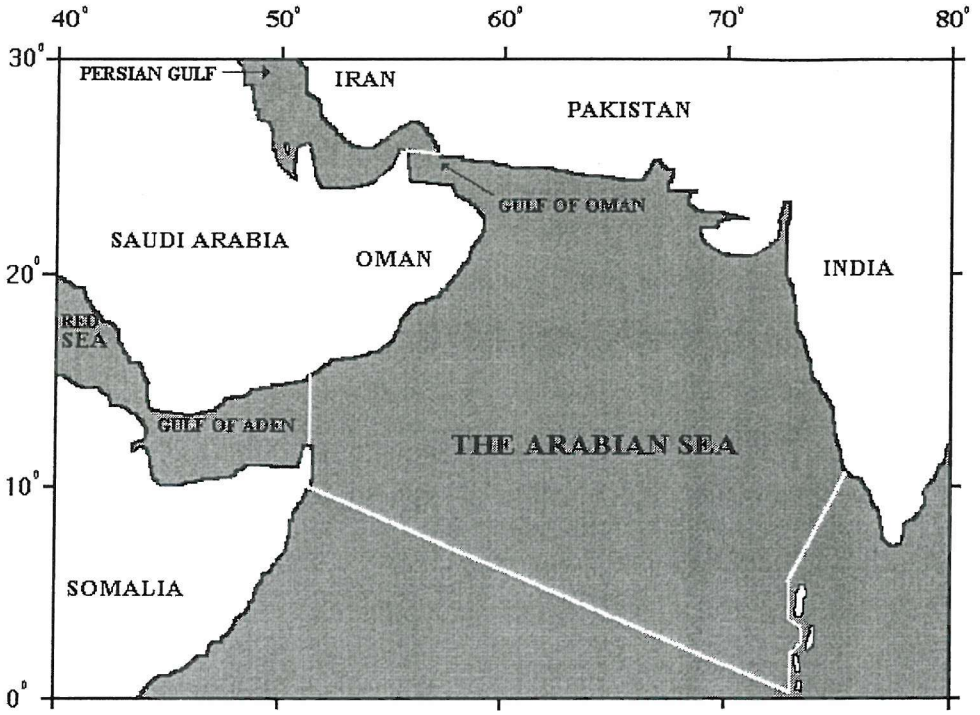

Figure 3.1.1 Schematic of the limits of the Arabian Sea.

Superimposed on top of the basin-scale circulation are mesoscale eddies and filaments (Wyrtki, 1973; Flagg and Kim, 1998; Lee *et al.*, 2000). During the SW monsoon there are, close to the Omani coast, alongshore winds that favour upwelling along the coast. Seaward of the coast the winds intensify to a strong offshore maximum wind jet, commonly called the "Findlater Jet" (Findlater, 1969), that manifests itself in a surface wind expression called the "Somali Jet". The decreasing southwesterly wind speeds cause negative wind-stress curl (Halpern and Woiceshyn, 1999), which drives strong Ekman pumping that deepens the surface mixed layer offshore (McCreary *et al.*, 1996). Associated with the coastal upwelling, are strong narrow jet-like currents that generally run in an offshore direction from the upwelling to about 700 km offshore (Brink *et al.*, 1996).

This strong physical forcing results in a large variability, both temporal and spatial, that result in dramatic seasonal changes in circulation and mixed layer depth.

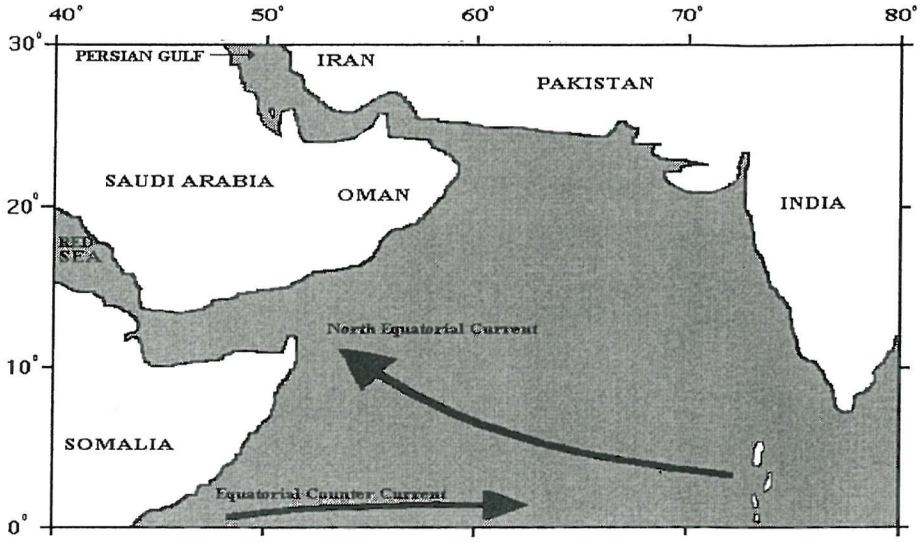

Figure 3.1.2a Schematic of the surface circulation in the Arabian Sea during the NE-monsoon (after Tchernia,1980).

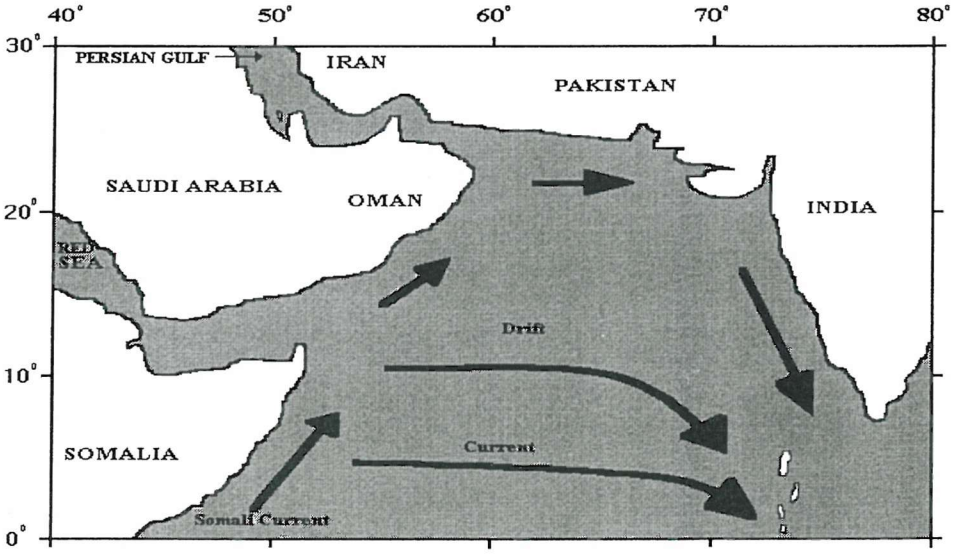

Figure 3.1.2b Schematic of the surface circulation in the Arabian Sea during the SW-monsoon (after Tchernia,1980).

Water masses of the Northern Arabian Sea

The basic hydrographic characteristics of the Arabian Sea have been the subject of much research (e.g. Sastry and De Souza, 1972; Wyrtki, 1973; Swallow, 1984; Brock *et al.*, 1992; Kumar and Prasad, 1999). Rochford (1964) provided the first description of the three different water masses present in the upper 1000 m of the Arabian Sea; Arabian Sea

High-Salinity Water (ASHSW), Persian Gulf Water (PGW) and Red Sea Water (RSW). Their typical temperatures, salinities, densities and depths are presented in Table 3.1.

Water Mass	Temperature (°C)	Salinity	Density (kg m^{-3})	Depth (m)
ASHSW	24-28	35.3-36.7	22.8-24.5	0-100
PGW	13-19	35.1-37.9	26.2-26.8	200-400
RSW	09-11	35.1-35.6	27.0-27.4	500-800

Table 3.1 Characteristics of the three water masses in the upper 1000 m of the Arabian Sea (after Kumar and Prasad, 1999). Water masses are ASHSW, Arabian Sea High-Salinity Water; PGW, Persian Gulf Water; and RSW, Red Sea Water.

Since then numerous studies have investigated the formation of PGW and RSW and its subsequent spreading within the Arabian Sea in the context of circulation and hydrography (Premchand, 1981; Premchand *et al.*, 1986; Fedorov and Meschanov, 1988; Brock *et al.*, 1992).

ASHSW forms at the surface in the northern Arabian Sea during winter (November to February) as a result of heat and fresh water flux into the atmosphere, and subsequently moves southward along the 24 σ_0 isopycnal surface. As it moves along the isopycnal surface it deepens and mixes with ambient low salinity water (Kumar and Prasad, 1999).

Warm and saline PGW forms because of an excess of evaporation over precipitation in the Persian Gulf (Premchand *et al.*, 1986), and flows into the Gulf of Oman at depths of 25-70 m through the Strait of Hormuz. In the Gulf of Oman it sinks to depths between 200 and 250 m forming a salinity maximum (~38). PGW enters the Arabian Sea at 200-250 m depth with salinities greater than 36.5, but its salinity and temperature decreases as it spreads southwards (Premchand *et al.*, 1986; Prasad *et al.*, 2001).

High salinity RSW also forms as a result of excess evaporation over precipitation (2 m yr^{-1}) and flows from the Red Sea into the Gulf of Aden through the shallow strait of Bab El Mandeb (Pickard and Emery, 1982). After mixing with Gulf of Aden water, RSW enters the Arabian Sea at depths between 600 and 900 m having a temperature of ~11 °C,

salinity of 35.5-35.7 and density of 27.15-27.35 (Rochford, 1964). Seasonal differences in the propagation of RSW through the Arabian Sea occur, in winter propagation of RSW along the Somali coast intensifies whilst in summer RSW propagates in a more easterly direction (Shapiro and Meschanov, 1991).

The Arabian Sea Oxygen Minimum Zone (OMZ)

There are three extensive regions of low oxygen concentration in the world's open ocean (Warren, 1994; see Chapter 1). The Arabian Sea is the second largest such area, where there is a permanent suboxic layer (Wyrtki, 1971, 1973; Qasim, 1982; Swallow, 1984), of oxygen concentration <0.1 ml O_2 l^{-1}, north of 6 - 10°N (Warren, 1994; Morrison *et al.*, 1999). Its upper boundary is marked by a steep oxycline (circa. 0.09-0.15 ml O_2 l^{-1}) at approximately 100 m depth, which coincides or lies directly below a sudden density change (Vinogradov and Voronina, 1961). Throughout the whole layer, which extends vertically for approximately 1 km, the oxygen content remains fairly low and constant (Shetye *et al.*, 1994). The lower boundary of the OMZ lies in waters with low-density gradients (Vinogradov and Voronina, 1961). These are favourable conditions for the mixing of deeper waters richer in oxygen, and there is a gradual reintroduction of oxygen from there. These interpretations follow the scheme of circulation of deep and bottom waters described by Warren (1992), where the bottom water in the Arabian Sea is derived from South of the equator (salinity varies between 34.730 - 34.737, and potential temperature between 1.090 - 1.330 °C; Shetye *et al.*, 1994). As the bottom water upwells in the Arabian Sea, it is transformed - salinity and temperature increase and dissolved oxygen decreases - into the North Indian Deep Water (1500 - 3500 m). At 2500 m depth, the mid-depth of the Indian Ocean deep sea water layer, salinity ranges between 34.769 - 34.783 and potential temperature between 1.910 - 2.109 °C (Wyrtki, 1971). Thus the North Indian Deep Water limits the vertical extent of the OMZ.

The processes affecting the generation and maintenance of the OMZ in the Arabian Sea (first proposed by Sewell and Fage, 1948) are a balance between consumption of oxygen by oxidation of organic matter and renewal of oxygen by advection and mixing. Oxygen consumption rates in the water beneath the oxycline are considered to be moderate, and are insufficient to exclusively cause or sustain the oxygen minimum (Warren, 1994). Warren (1994) suggested that the suboxic conditions are caused by a combination of the low oxygen concentration of incoming intermediate waters to the Arabian Sea and the consumption of oxygen by oxidation of organic matter. Incoming water to the Arabian Sea from the North (the Red Sea (RSW) and Persian Gulf (PGW))

have very high salinity and moderate oxygen concentrations (2.5-4 ml l^{-1} - Wyrtki, 1971), but lose oxygen rapidly downstream from the sills of the basins. The component inflow from the South, Indian Ocean Equatorial Water (IOEW) carries water of oxygen concentration 1.0 ml l^{-1} (estimated from data presented in Olson *et al.*, 1993). Therefore although processes within the suboxic layer are of only 'moderate' strength, they can have a significantly depleting effect on the already low concentrations of oxygen.

A relatively strong meridional gradient in latitude (from 6-10 °N) separates the region with low oxygen from the oxygen richer water to the south. The position of this gradient seems fairly stationary (Wyrtki, 1971; Sen Gupta and Naqvi, 1984), the identifying isopleths (1.0 to 0.5 ml l^{-1} at 500 m) were displaced by only about one degree of latitude between the summer and winter sections undertaken by RRS *Charles Darwin* in 1989 (Kearns *et al.*, 1989). Warren (1994) hypothesized that the zone is positioned by the distribution of wind stress, which imposes a separate horizontal circulatory regime on the Northern Arabian Sea.

The presence of suboxic conditions are known to have both chemical and biological consequences (Vinogradov and Voronina, 1961; Brinton, 1979; Wishner *et al.*, 1990; Morrison *et al.*, 1999), for example, the switching of facultative bacteria to the use of nitrate ions for oxidation of organic matter. This denitrification process represents a "sink" of free nitrogen (Codispoti, 1989). For larger pelagic organisms an OMZ can act as a barrier substantially impacting on their abundance and distribution (Vinogradov and Voronina, 1961). The chemical implications of the OMZ are beyond the scope of this thesis, its influence on the distribution of zooplankton is discussed later (Section 3.4, 3.5 and 3.6).

Upwelling off the Arabian Coast

There are three regions of strong upwelling in the Arabian Sea all located along the eastern boundaries (Swallow, 1984), which can be identified by cool sea surface temperatures (Bruce, 1974). The development of upwelling off Somalia is related to the southwest monsoon and also closely related to the strong western boundary current (the Somali Current) and its separation from the coast near 10 °N. This region has been reviewed extensively (Warren *et al.*, 1966; Bruce, 1974; Schott, 1983). The Somali Current flows northward (beneath the surface layer) and branches part passing between Socotra and the mainland into the Gulf of Aden, the other turning northeastward along the Arabian coast (Wyrtki, 1971).

The flow along the Arabian coast is similar in magnitude to that in other eastern boundary currents. Upwelling occurs along 1000 km of the Arabian coast (15 to 22 °N) and up to 400 km offshore. High vertical velocities and the great extent of the upwelling is caused by the strength of the southwest monsoon (6 dynes cm^{-2}) and the spatial distribution of wind stress. Thus upwelling commences around April, intensifies through July, and has a period of "quasi-consistent conditions" from July through to September (Duing, 1970). Arabian coast upwelling is induced by the coastal boundary causing a divergence in the Ekman flow, Smith and Botterro (1977) calculated this to be greater than 3×10^{-6} m^{-3} s^{-1}. Open ocean upwelling (defined as that from the inner continental slope to 400 km offshore) is a consequence of the Findlater Jet causing wind curls resulting in an additional Ekman divergence of 7×10^{-6} m^{-3} s^{-1}.

Smith and Botterro (1977) described the upwelling along the Arabian coast as strong (vertical velocities at 50 m depth of 3×10^{-3} cm s^{-1} over the continental shelf and $1-2 \times 10^{-3}$ cm s^{-1} in the offshore region). In comparison with the Somali upwelling, it is both broader and weaker permitting a greater time for the development of biological production to occur.

3.1.2 The distribution of phytoplankton in the Arabian Sea

The Arabian Sea displays distinct, predictable oscillations in phytoplankton biomass that are linked to the seasonal monsoons. Shipboard observations (Banse, 1987; Bauer *et al.*, 1991; Barber *et al.*, 2001; Shalapyonoh *et al.*, 2001) and CZCS images (Brock and McClain, 1992; Banse, 1994) show that the phytoplankton community responds dramatically to the wind-driven forcings associated with the NE and SW monsoons, with enhanced phytoplankton abundance, biomass and production occurring during the SW monsoon compared with the NE monsoon (Barber *et al.*, 2001; Shalapyonoh *et al.*, 2001). The increase in phytoplankton biomass during both monsoons leads to high rates of export production (Nair *et al.*, 1989), and therefore the Arabian Sea probably plays an important role in the production, export and remineralisation of particulate carbon.

Barber *et al.* (2001) observed that phytoplankton biomass during the SW monsoon was lower than their predictions based upon observations of high phytoplankton productivity. They attributed this to efficient grazing by mesozooplankton, particularly copepods.

3.1.3 The distribution of zooplankton in the Arabian Sea

Two features of the Arabian Sea are particularly important in determining the zooplankton communities. First, there are the seasonal monsoon reversals and second, there is the occurrence of the pronounced oxygen minimum zone.

The influence of the seasonal monsoon and associated physical processes on the distribution of zooplankton

In view of the marked inter-annual differences in phytoplankton populations, marked inter-annual variability in zooplankton populations should also exist. Surprisingly, Goswami *et al.* (1992) observed greater animal concentrations during the NE monsoon than the SW monsoon in the eastern Arabian Sea, in contrast to the phytoplankton. However, more recently and inshore of the Somali Jet, Smith *et al.* (1998) observed the maximum biomass of zooplankton during the SW monsoon compared with the other monsoon periods.

Smith *et al.* (1998), Wishner *et al.* (1998), Roman *et al.* (2000) and Ashjian *et al.* (2002) found a gradient in vertically integrated mesozooplankton biomass distribution in the Arabian Sea, which was highest at a position several hundred km off the Omani coast and declined seaward of the axis of the Somali Jet. The Somali Jet and associated filaments, that transport high concentrations of nitrate and chlorophyll several hundred kilometres offshore (Brink *et al.*, 1998; Barber *et al.*, 2001), has been recognised as potentially an important mechanism that could export zooplankton from the Omani upwelling zone offshore (Ashjian *et al.*, 2002).

The influence of the Oxygen Minimum Zone (OMZ) on the distribution of zooplankton

Since oxygen is an important resource related to metabolism for most organisms (Eckert, 1983), it can be expected that the OMZ will affect the vertical distribution of plankton. With the overall vertical distribution of zooplankton within the water column being controlled by a species' ability to endure oxygen deprivation within the mesopelagic realm. The affect of an OMZ on zooplankton distribution typically manifests itself in three ways: (1) concentration of organisms within surface oxygenated waters; (2) reduction of numbers in suboxic waters; and (3) a subsurface peak at the lower margin of the OMZ as oxygen concentrations begin to increase.

Previous studies in ocean regions showed that weak or moderate OMZs had little effect on zooplankton biomass (Brinton, 1979; Chen, 1986), however, within the Arabian Sea lower biomass within the OMZ has been consistently observed (Sewell and Fage, 1948; Vinogradov and Voronina, 1961; Sameoto, 1986; Wishner *et al.*, 1990; Herring *et al.*, 1998; Wishner *et al.*, 1998).

Wishner *et al.* (1998) were apparently surprised to find diel vertical migratory behaviour (DVM), into the suboxic OMZ during the day. However, this has been a prominent finding of several acoustic surveys in the Arabian Sea (Morrison *et al.*, 1999; Ashjian *et al.*, 2002) and from net data (Kinzer *et al.*, 1993). The physiology of the organisms undertaking DVM is unclear (Wishner *et al.*, 1998), although Herring *et al.* (1998) have mentioned morphological differences in the gills and carapace structure of euphausiids and decapods from the Arabian Sea (compared with the Atlantic); gills in suboxic regions were much larger and the carapace was less rigid.

Taxonomic analysis shows that only a few species contribute to the high biomass undertaking DVM in the Arabian Sea, and many species that would normally occur at depth in oxygenated waters are absent from the OMZ in the Arabian Sea (Wishner *et al.*, 1998). A dominant component of the migrating layers is mesopelagic myctophid fish (Banse, 1994; Herring *et al.*, 1998; Wishner *et al.*, 1998; Luo *et al.*, 2000; Ashjian *et al.*, 2002). As important consumers of mixed layer zooplankton animals (Dalpadado and Gjosaeter, 1988; Kinzer *et al.*, 1993; Smith *et al.*, 1998), these myctophid fish have a great impact on the balance of primary production.

The lower limits of an OMZ are frequently linked with a subsurface maximum in zooplankton biomass (Vinogradov and Vorinina, 1961; Böttger-Scnack, 1994; Wishner *et al.*, 1998). The interface in the Arabian Sea ranges between depths of ~500 to ~1500 m and increases in biomass compared with within the OMZ may be up to three orders of magnitude (Wishner *et al.*, 1998). This increase in biomass results from the concentration of fauna which cannot live permanently within the oxygen minimum layer.

3.2 Hydrography of the Arabesque Reference Site

Cruise D209, in the Arabian Sea, was undertaken during the SW monsoon period in August 1994. Wind speed and direction showed a seasonal pattern characteristic of the Arabian Sea; winds blew from the Southwest at speeds >7.5 m s^{-1} and up to 17.5 m s^{-1} knots (Herring *et al.*, 1998). The hydrography of the survey region (within 18.3 - 20 °N and 58 – 59.3 °E) was examined using a series of CTDs and two SeaSoar surveys. The following sections (3.2 - 3.5) are concerned with the hydrography and biology at the Arabesque Reference Site (ARS), interpretation of the SeaSoar data is given in Herring *et al.* (1998).

The vicinity of the ARS (19 °N and 59 °E) was occupied three times during cruise D209. The 5th of August (Station 12661), 12th of August (Station 12663-4) and the 21st

(Station 12670). On each occasion a CTD was performed followed by a series of RMT nets. In addition at the latter two stations (12664 and 12670) a LHPR tow was undertaken.

3.2.1 Water masses at the Arabesque Reference Site (ARS)

The characteristics of all the water masses encountered in the surface 500 m of the three CTD stations at the ARS are represented in the θ/S diagram in Figure 3.2.1. Salinity varied between 35.75 and 36. Persian Gulf Water (PGW), as identified by Rochford (1964), Currie (1992) and Morrison *et al.* (1998), was present between 100 and ~350 m with temperatures between 13 and 19 °C and salinities between 35.75 and 36.0. Compared with salinities within the Persian Gulf of about 38 (Premchand *et al.*, 1986), values at the ARS were always less than 36.0, suggesting considerable entrainment of ambient waters within the Gulf of Oman and the Arabian Sea. This water is characterised by spatial and temporal variability in θ/S characteristics arising from the complex water mass interactions that occur as it progresses through the Arabian Sea (see Section 3.1, Premchand *et al.*, 1986). Waters of temperatures above ~20 °C (σ_θ ~25) are described by Morrison *et al.* (1998) as Arabian Sea Water (ASW) and occurred in the surface 100 m.

3.2.2 The structure of the water column at the ARS

Figure 3.2.2 presents the vertical profiles of temperature, salinity, oxygen concentration and chlorophyll concentration within the upper 500 m of the water column (Figure 3.2.2b presents the same data on an expanded depth scale of 100 m). Over the 16 days between the first and last station the mixed layer (~40 m), defined by the depth of the thermocline, temperature intensified such that it was 1.5 °C warmer at station 12670, whilst the overall depth of the mixed layer remained relatively constant. The salinity profile is more complex, the surface waters had a highly variable salinity, between 35.7 and 35.9, indicating interleaving. Below 200 m salinity was relatively high (~35.8) and the temperature and salinity were indicative of PGW.

The most dominant feature of the water column was the presence of a distinct oxycline between 40 and 60 m. The depth of the oxycline shoaled from ~60 m at station 12661 to ~40 m at station 12670. At all stations the surface oxygen concentration remained consistently high (~250 μmol l^{-1}), whilst waters below the oxycline had concentrations < 10 μmol l^{-1}.

The OMZ, with minimum recorded bottle oxygen concentrations of 0 and 0.04 μmol l^{-1} (±0.02 μmol l^{-1}), extended to a depth of ~1100 m before the gradual

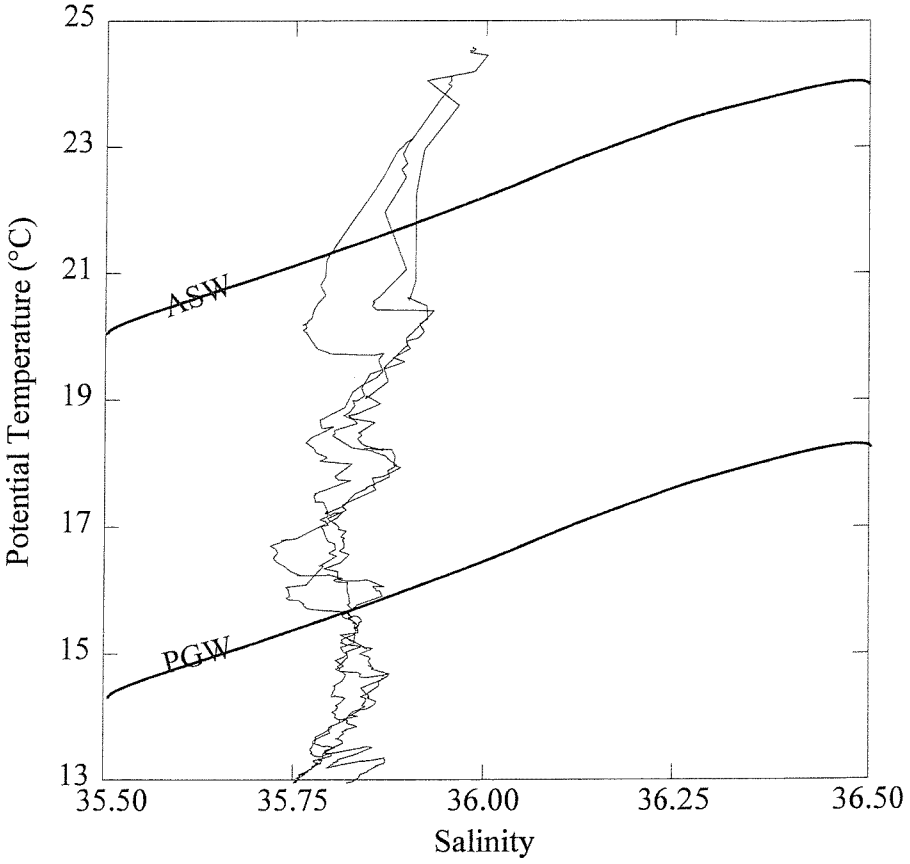

Figure 3.2.1 Potential temperature as a function of salinity for CTD stations 12661#3, 12663#5 and 12670#3.

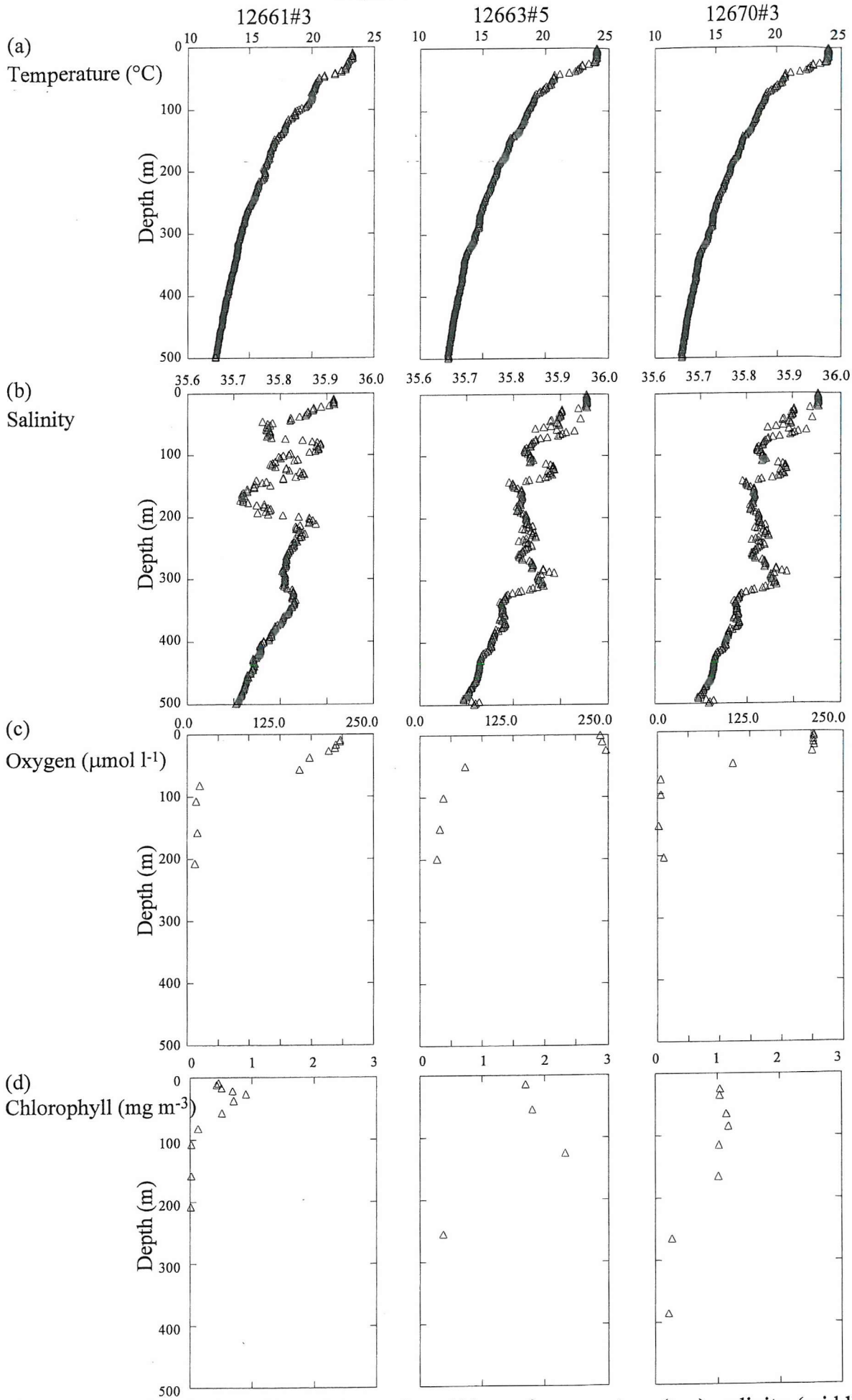

Figure 3.2.2a Vertical profiles of the surface 500 m of temperature (top), salinity (middle top), oxygen concentration (middle bottom) and chlorophyll concentration (bottom) at the ARS on the 5 (12661#3), 12 (12663#5) and 21 (12670#3) of August.

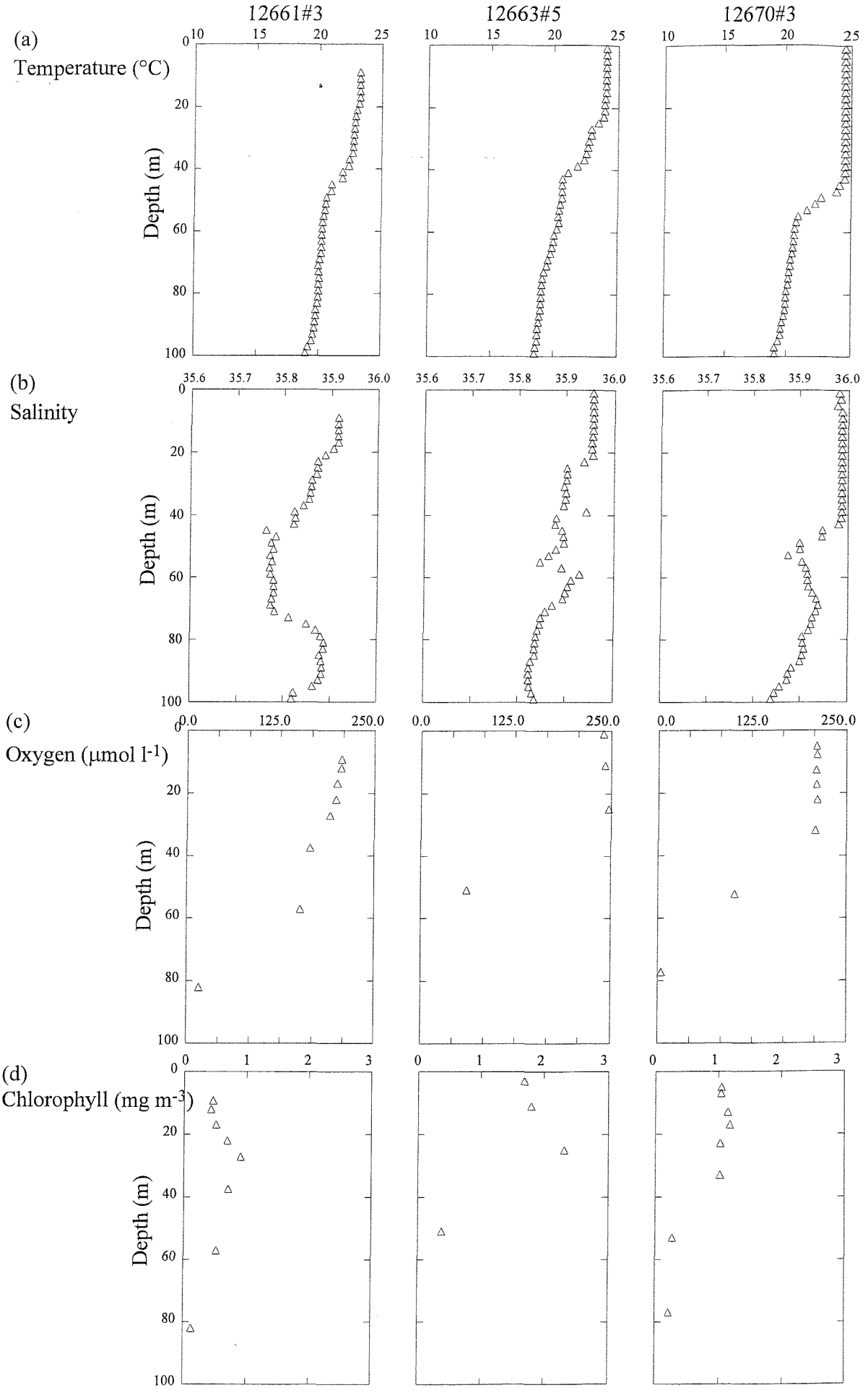

Figure 3.2.2b Vertical profiles of the surface 100 m of temperature (top), salinity (middle top), oxygen concentration (middle bottom) and chlorophyll concentration (bottom) at the ARS on the 5 (12661#3), 12 (12663#5) and 21 (12670#3) of August.

reintroduction of oxygen occurred (Figure 3.2.3) and at depths greater than 2000 m oxygen concentration was about half of the surface waters (>100 μmol l^{-1}).

The vertical distribution of phytoplankton showed great variability between the stations. At station 12661 chlorophyll concentration was low (0.5 mg m^{-3}) with a distinct subsurface chlorophyll maximum (SCM) of 1 mg m^{-3} at ~30 m. Chlorophyll was observed to a depth of 60 m, the distribution appearing to be controlled by the oxycline rather than the depth of the mixed layer. At station 12664 surface chlorophyll concentration (~1.7 mg m^{-3}) was three times greater than at station 12661, a SCM was still present but at elevated chlorophyll concentrations of 2.5 mg m^{-3}. At station 12670 chlorophyll concentrations throughout the surface 40 m were uniform, the SCM observed at the previous stations no longer present. Chlorophyll concentrations were lower than at station 12664 but greater than 12661. The chlorophyll was restricted to the surface 40 m within the oxygenated mixed layer.

3.2.3 Discussion of the hydrography, the OMZ and vertical distribution of phytoplankton at the Arabesque Reference Site (ARS)

The physical structure of the water column at the ARS showed the influence of PGW at depths of ~200 m and the intensification of the temperature of the thermocline.

The dominating feature of the water column, identified from the three repeat CTDs, was the presence of a distinct oxygen minimum zone. In this study the oxycline occurred at the base of or just below the thermocline (MLD), consistent with previous observations (Vinogradov and Voronina, 1961; Morrison *et al.*, 1999). Oxygen concentration was high at the surface (~200 μmol l^{-1}) and less than 10 μmol l^{-1} below the oxycline decreasing to <5 μmol l^{-1} at ~100 m, which is comparable with previous measurements of 8.9 μmol l^{-1} (Vinogradov and Voronina, 1961) and 5 μmol l^{-1} (Morrison *et al.*, 1999).

Reintroduction of oxygen commenced at depths >1000 m and hence the suboxic zone extended for ~1000 m, comparable with the observations of Morrison *et al.* (1999) for the North Arabian Sea.

The oxygen minimum appeared to have been the most important environmental factor observed here structuring the vertical distribution of phytoplankton. Phytoplankton were observed below the MLD to the depth of the oxycline at Station 12661. In the later stations, where the depth of the oxycline was the same as the MLD, the phytoplankton distribution was restricted to within the mixed layer. The increase in phytoplankton within

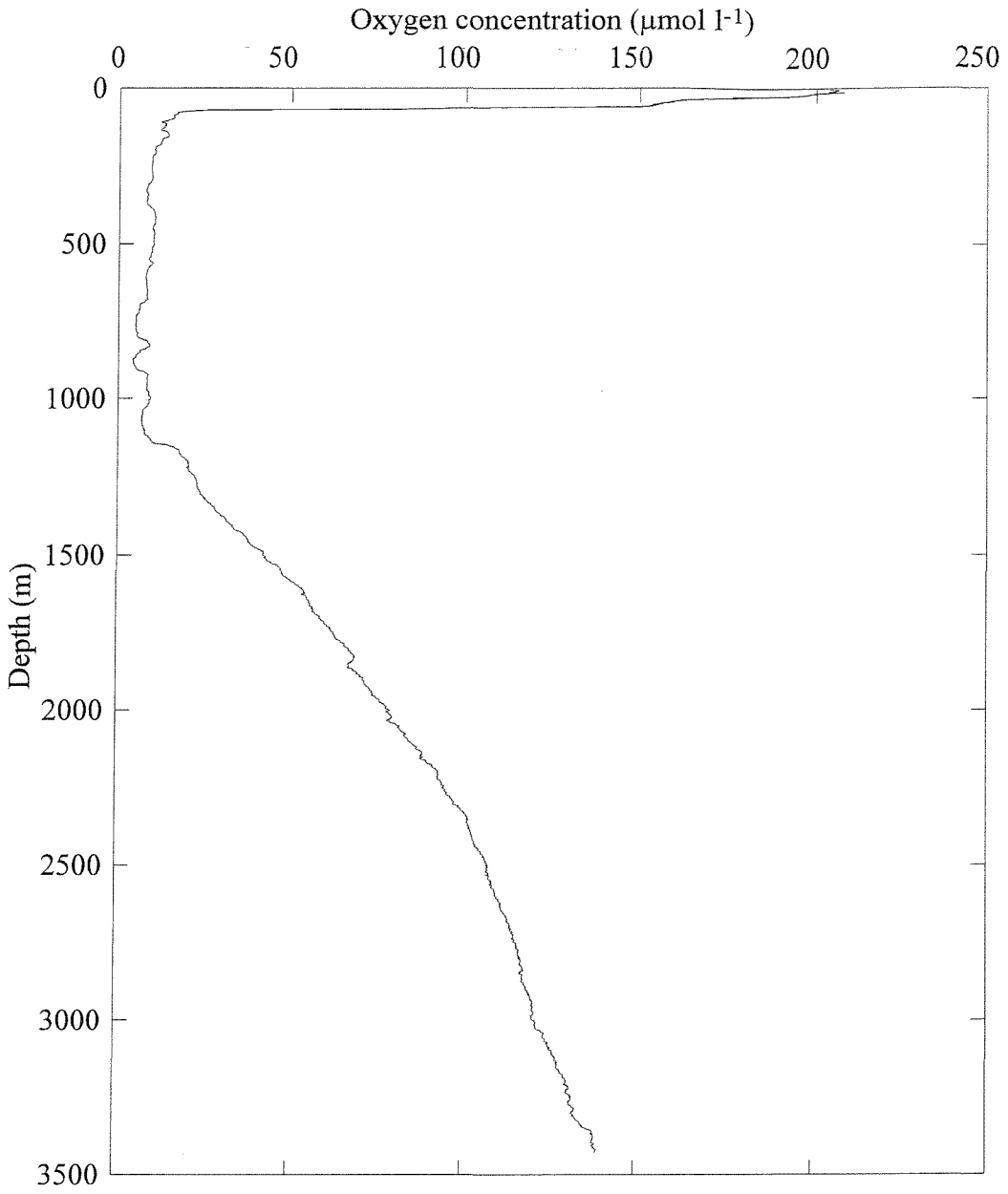

Figure 3.2.3 A vertical profile of oxygen concentration from CTD station 12261#3.

the mixed layer and the disappearance of the SCM was probably a result of an input in the nutrient concentration of the surface waters as a result of local upwelling or advection in from north of the survey region, identified by Herring *et al.* (1998).

3.3 The distribution of zooplankton at the Arabesque Reference Site (ARS)

The distribution of zooplankton within the vicinity of the ARS were assessed using LHPR net samples and VM-ADCP acoustic backscatter. The LHPR stations were taken nine days apart. LHPR station 12664 was taken on the 12th of August between 19:52 and 22:30 LT, immediately after CTD station 12663#5, and LHPR station 12670, taken on the 21st of August 09:07 and 11:37 LT, occurred immediately after CTD station 12670#3. In each case the LHPR was fished in a v-shaped profile to a depth of ~250 m. The CTD stations prior to each tow are used to describe the water column (see section 3.2). A problem with clogging of the net occurred during the upcast of LHPR station 12670 and as a result these data are not included (see Chapter 2).

3.3.1 The distribution of zooplankton biovolume at LHPR station 12664

Maximum values of total zooplankton biovolume occurred within the surface 50 m on both the down and upcast (Figure 3.3.1), although the profiles were not identical. During the downcast maximum total biovolume (~1.5 ml m^{-3}) occurred at the surface, with total biovolume consistently high (>0.8 ml m^{-3}) within the mixed layer (40 m). Measurements of identifiable zooplankton taxonomic group biovolume (where possible[1]) indicate that a dominant proportion of this biovolume (20-50 %) was copepods. Below this biovolume decreased to ~0.3 ml m^{-3} within the oxygenated waters. At the oxycline (~50 m) and below, biovolume decreased to <0.1 ml m^{-3} towards the bottom of the cast. Below the oxycline decapods and euphausiids were the significant contributors to biovolume.

During the upcast, biovolume was approximately half (~0.4 ml m^{-3}) that observed in the downcast. The maximum values (0.9 ml m^{-3}) throughout the upcast occurred at the thermocline. Below this biovolume was low (<0.1 ml m^{-3}) except for one sample at 75 m which contained 0.4 ml m^{-3}, similar to the surface values. Similar to the downcast, copepods contributed the greatest percentage (~40 %) at the biovolume maxima and below the oxycline the only measurable contributions were from euphausiids, decapods and chaetognaths (Figure 3.3.2).

[1] Measurements of group biovolume were not always possible as a result of the small sample size inherently collected by the LHPR and are therefore subject to large errors and bias towards large individuals of any one group. In addition there was also a residue (unidentifiable and detritus material) component to each sample. However, it is assumed that they will provide a qualitative indication of the dominant group present.

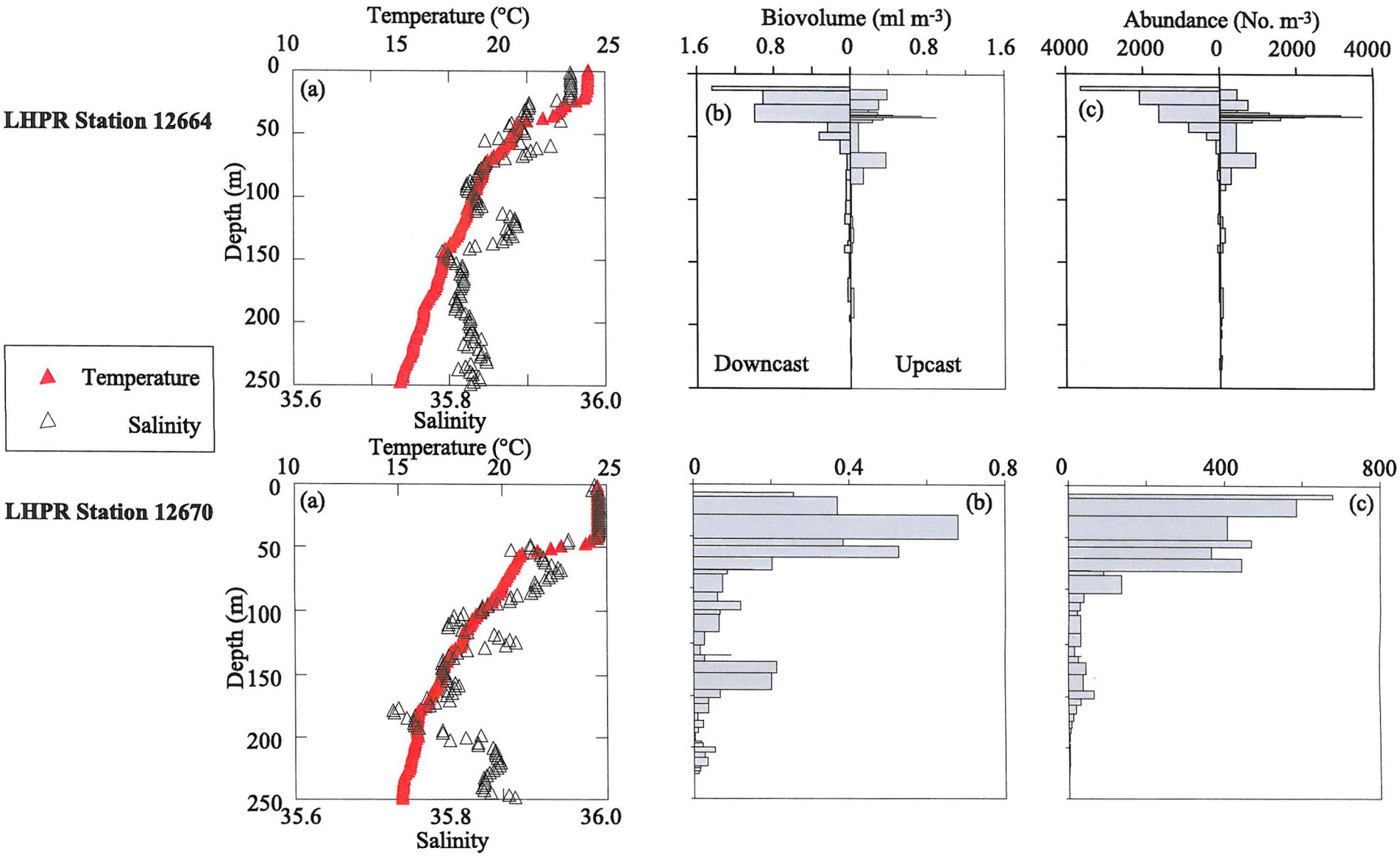

Figure 3.3.1 Vertical profiles of (a) temperature and salinity, (b) total zooplankton biovolume and (c) total zooplankton abundance for LHPR station 12664 (top) and 12670 (bottom).

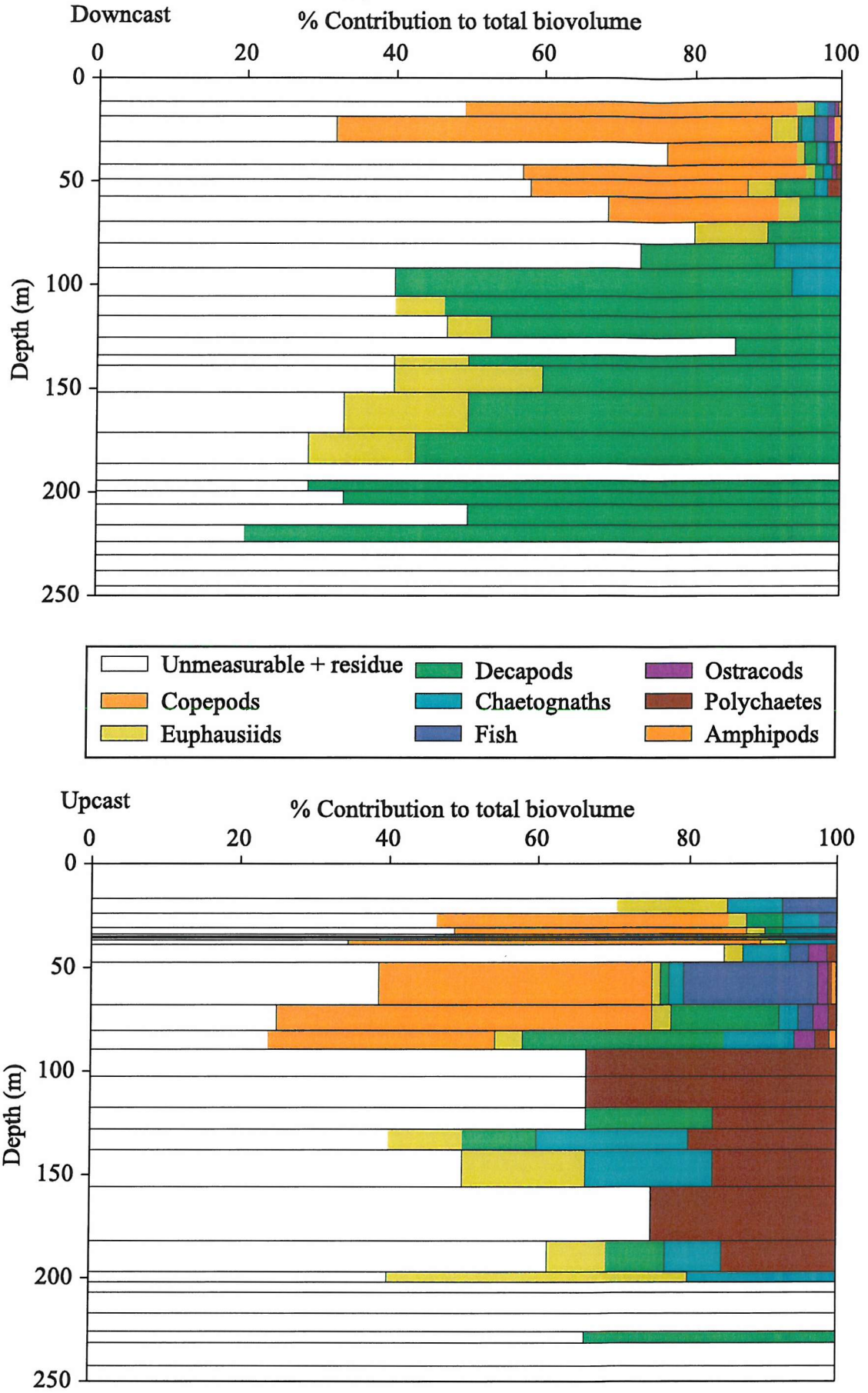

Figure 3.3.2 Percentage contribution of taxonomic groups to total zooplankton biovolume during the downcast (top) and the upcast (bottom) at LHPR station 12664.

Biovolume was integrated over the depth of the cast (250 m) and was greater on the downcast (46.8 ml m^{-2}) compared with the upcast (26.5 ml m^{-2}). Of this 79 % and 56 % respectively occurred within the mixed layer oxygenated waters.

3.3.2 The distribution of zooplankton abundance at LHPR station 12664

The vertical distribution of zooplankton abundance followed a similar pattern to biovolume (Figure 3.3.1). Highest abundances (~3800 No. m^{-3}) occurred within the two biovolume maxima, and although biovolume was less during the upcast than the downcast maximum abundances were comparable. Below ~60 m on the downcast and ~75 m on the upcast abundance was low ~50 No. m^{-3}.

Copepods were the most abundant group contributing >70 % to the total abundance at all depths (Figure 3.3.3), and at the maxima in total zooplankton abundance this contribution peaked at >95 %. Below the oxycline polychaetes were the second most abundant group, contributing between 5 and 20 % to the total zooplankton abundance. Polychaetes were present in greater numbers during the upcast than the downcast and this was reflected by an increase in their contribution to the total zooplankton abundance.

Vertical profiles of individual taxonomic groups indicated that the highest abundances of copepods, chaetognaths, euphausiids, fish, ostracods and amphipods all occurred above the shallow oxycline (Figure 3.3.4). The greater numbers of copepods and euphausiids occurring during the downcast compared with the upcast may have been responsible for the greater biovolumes observed during the downcast. The distribution of decapods and polychaetes appeared to be independent of either the mixed layer depth or the oxycline.

3.3.3 The distribution of zooplankton biovolume at LHPR station 12670

Maximum total zooplankton biovolume (0.7 ml m^{-3}) occurred at the depth of the thermocline and biovolume was relatively high (~0.4 ml m^{-3}) in all samples within the mixed layer above the oxycline (Figure 3.3.1). Below the oxycline biovolume was reduced to ~0.1 ml m^{-3} except at 150 m where it was slightly elevated (~0.2 ml m^{-3}) although still lower than surface values. Measurements of taxonomic group biovolume indicated that at least 20 % of the large surface biovolumes could be attributed to copepods (Figure 3.3.5). Chaetognaths, euphausiids and fish were the only other groups with measurable contributions in the surface waters. Below the oxycline euphausiids had the highest contribution to total biovolume (20-60 %), whilst smaller percentages of the total biovolume could be attributed to copepods, decapods, polychaetes and, at the bottom of the cast (250 m), fish.

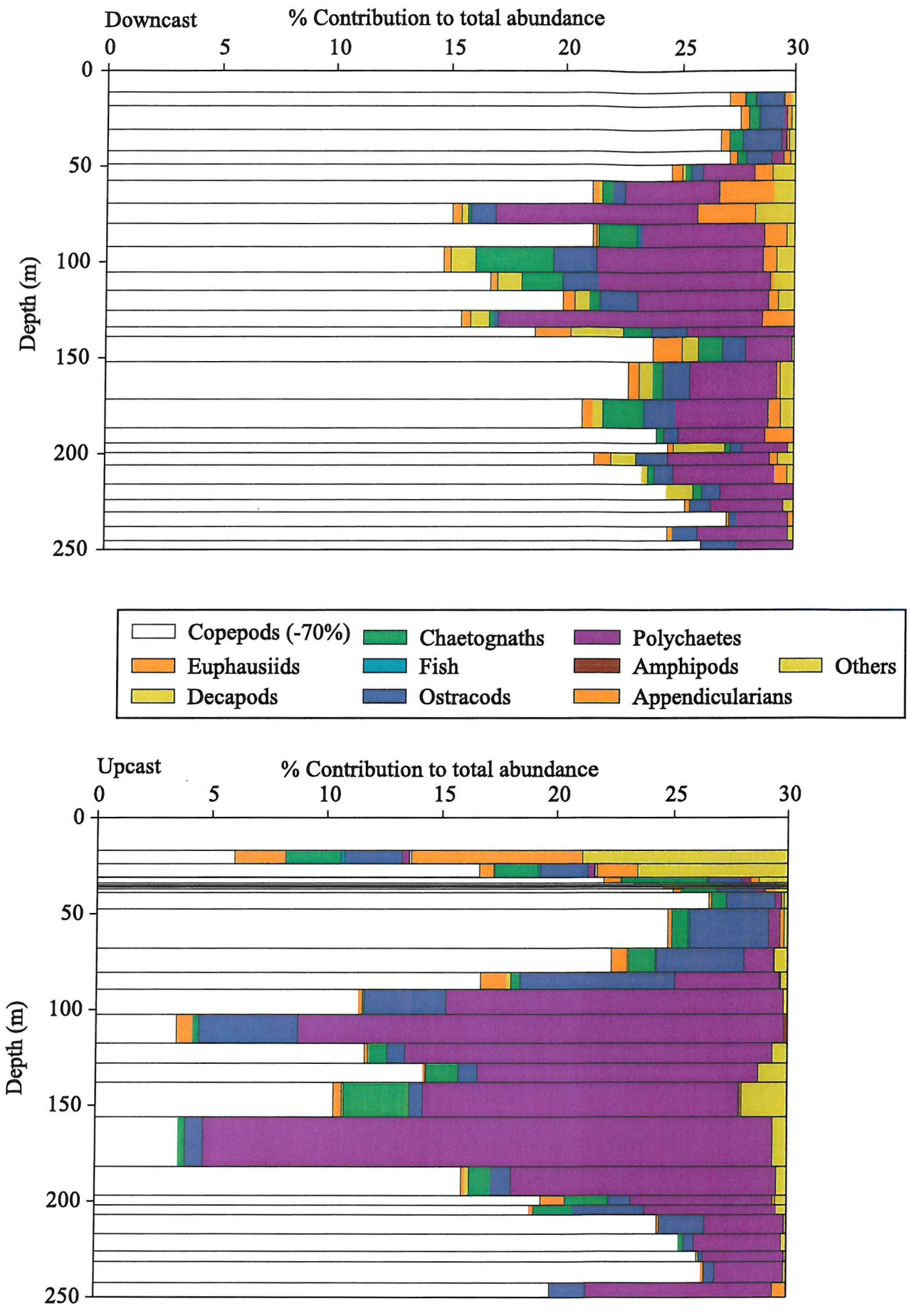

Figure 3.3.3 Percentage contribution of taxonomic groups to total zooplankton abundance during the downcast (top) and the upcast (bottom) at LHPR station 12664. In all samples the copepod group contributes an additional 70%.

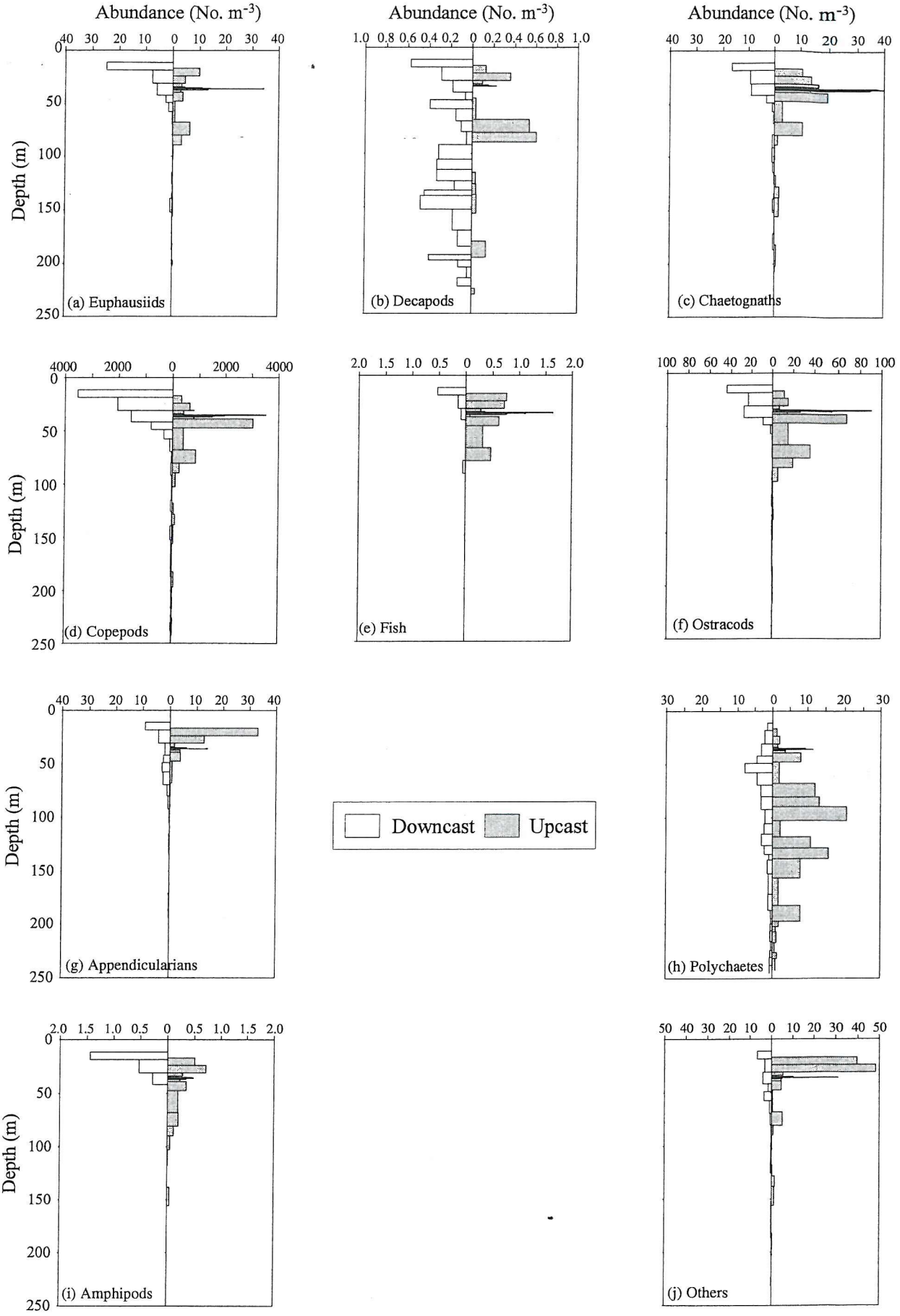

Figure 3.3.4 Vertical profiles of (a) Euphausiids, (b) Decapods, (c) Chaetognaths, (d) Copepods, (e) Fish, (f) Ostracods, (g) Appendicularians, (h) Polychaetes, (i) Amphipods and (j) others at LHPR station 12664.

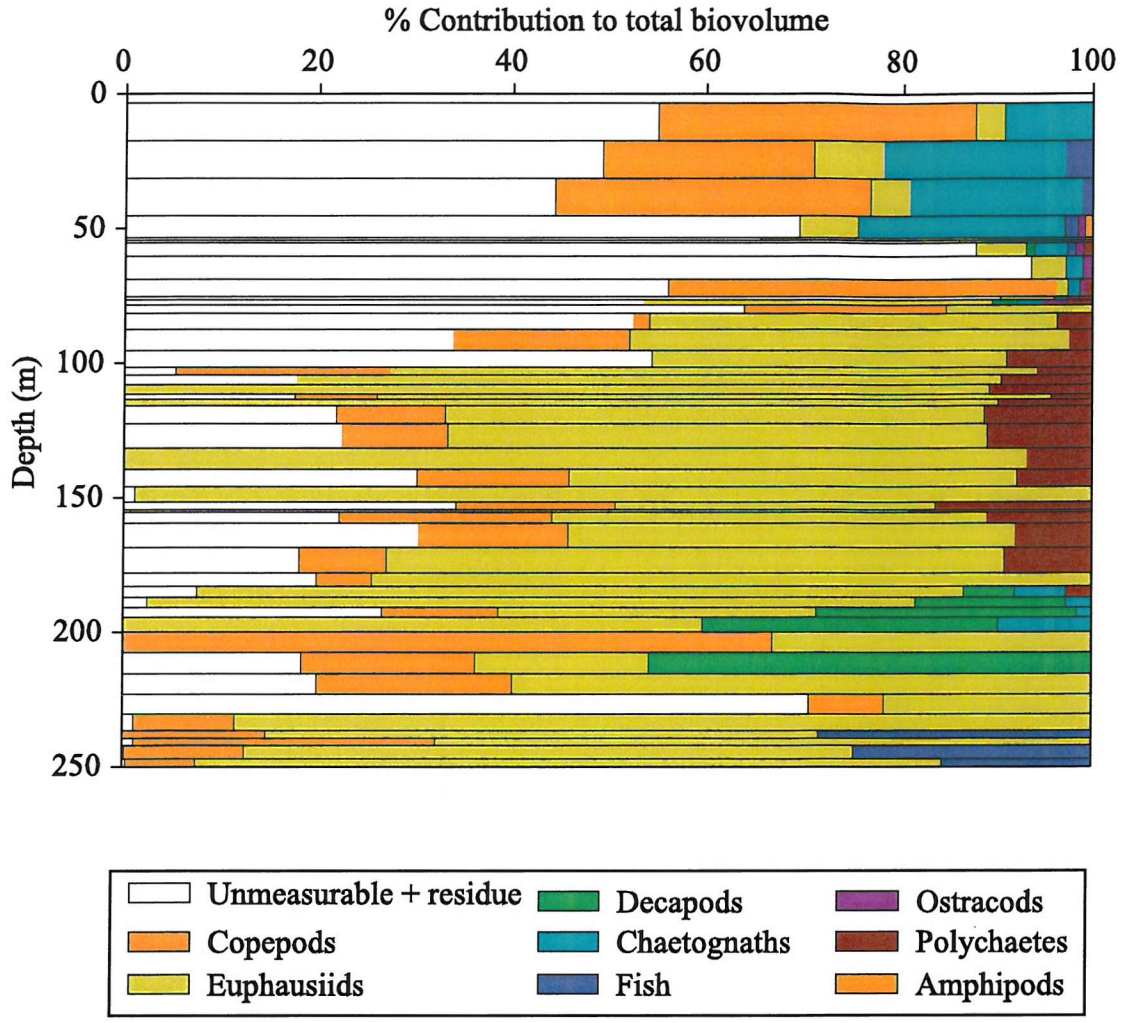

Figure 3.3.5 Percentage contribution of taxonomic groups to total zooplankton biovolume during the downcast at LHPR station 12670.

Integrated biovolume (45.17 ml m^{-2}) over the depth of the cast (250 m) was similar to that observed during the downcast of station 12664, although only 40 % of this was above the oxycline.

3.3.4 The distribution of zooplankton abundance and size at LHPR station 12670

The vertical profile of total zooplankton abundance was similar to total biovolume with abundance decreasing with depth at station 12670. This was comparable with station 12664, although surface abundances at station 12670 were a fifth of those observed at station 12664 (Figure 3.3.1). However, unlike station 12664, the highest abundance (~650 No. m^{-3}) occurred in the surface sample and not at the depth of the maximum in total biovolume. Total abundance was high (>400 No. m^{-3}) within the surface 80 m and appeared independent of the depth of the oxycline although abundance decreased rapidly below 80 m to ~50 No. m^{-3}.

Copepods contributed at least 60 % of the total abundance in all samples and within the surface 100 m this percentage was as much as 95 % (Figure 3.3.6). Within the oxygenated mixed layer chaetognaths were the next most abundant group, whilst below the oxycline euphausiids and polychaetes were more significant contributors to total abundance.

Vertical profiles of individual taxonomic group abundance show that the distribution of chaetognaths, appendicularians, ostracods, amphipods, pteropods and others (including siphonophores, brachyura larvae and medusae) were restricted to the surface oxygenated waters, whilst euphausiids, decapods and polychaetes show a distribution independent of the oxycline (Figure 3.3.7). The vertical profile of fish abundance indicates a bimodal distribution with fish either restricted to oxygenated waters or at depth. In all groups except chaetognaths and amphipods, abundances were significantly reduced above the oxycline compared with the night-time station 12664.

Length measurements of several taxonomic groups indicated that different sized individuals of each taxonomic group occupied different depths that could possibly be associated with variations in oxygen concentration (Figure 3.3.8). Several patterns could be identified. Firstly, for the groups restricted to the oxygenated surface waters (amphipods and pteropods) there was a slight increase in mean length with depth, with the largest individuals occurring at the base of the mixed layer at the oxycline. Secondly, the mean length of chaetognaths had a bimodal distribution The largest chaetognaths were found at the base of the mixed layer and at depth (~200 m). Within the oxygenated surface waters mean chaetognath length varied between 10 and 25 mm, whilst below the oxycline

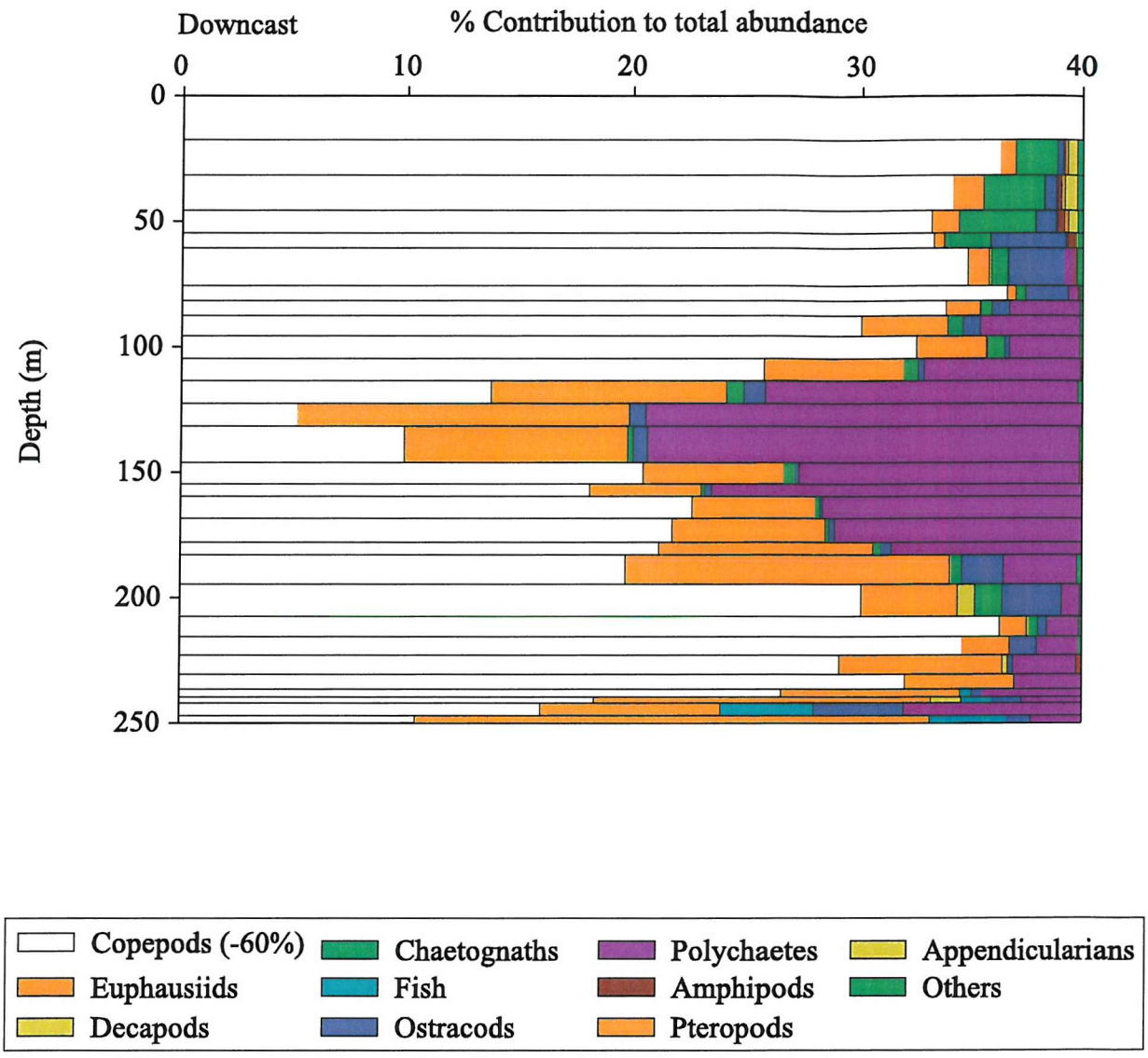

Figure 3.3.6 Percentage contribution of taxonomic groups to total zooplankton abundance during the downcast at LHPR station 12670. In all samples the copepod group contributes an additional 60% (note different from previous graph).

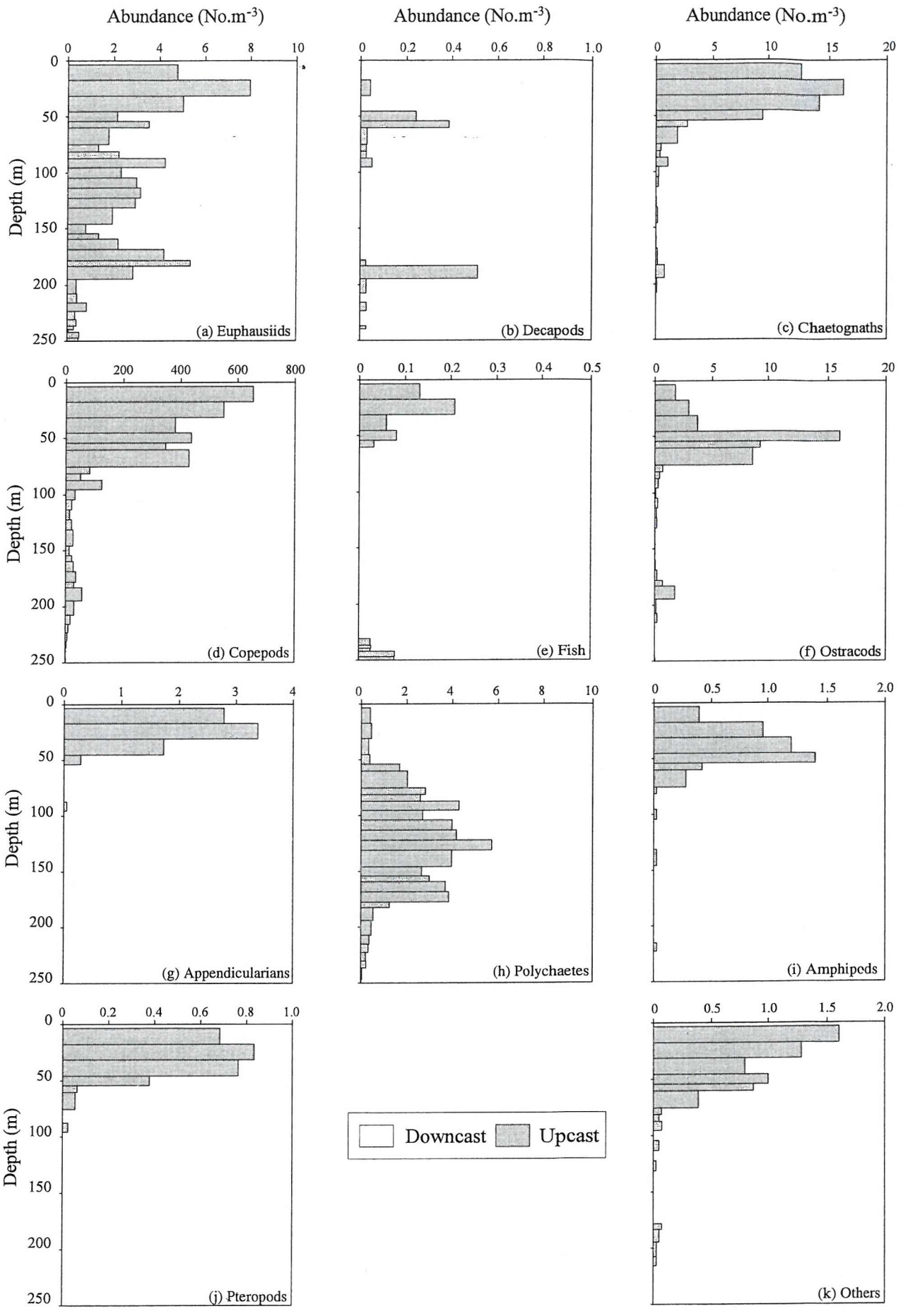

Figure 3.3.7 Vertical profiles of the abundance of (a) Euphausiids, (b) Decapods, (c) Chaetognaths, (d) Copepods, (e) Fish, (f) Ostracods, (g) Appendicularians, (h) Polychaetes, (i) Amphipods, (j) Pteropods and (k) others at LHPR station 12670.

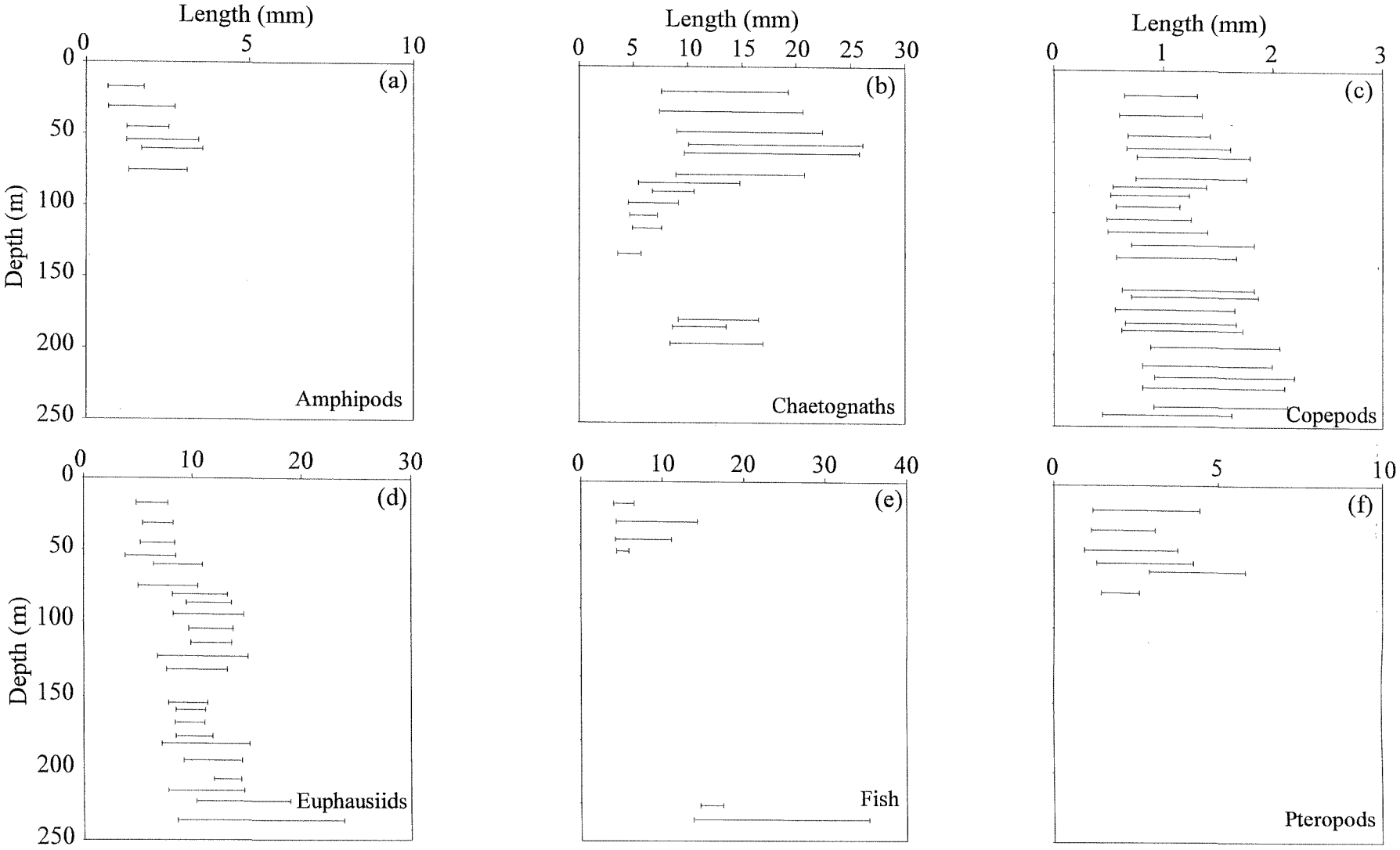

Figure 3.3.8 Vertical profiles of the mean length of (a) Amphipods, (b) Chaetognaths, (c) Copepods, (d) Euphausiids, (e) Fish and (f) Pteropods at LHPR station 12670.

mean length was smaller and varied between 5 and 15 mm. Thirdly, both copepod and euphausiid mean length increased with depth. The distribution of mean euphausiid length appeared to contain three tiers. From the surface to ~80 m mean euphausiid length was <10 mm, from 80 to 180 m mean length was between 10 and 14 mm, and below 180 m mean length was >14 mm. Finally, fish caught at the surface were smaller than those at depth. The mean length of fish caught at the surface was between 5 and 15 mm, whilst those at depth varied between 15 and 35 mm.

3.3.5 Comparison between LHPR station 12664 and LHPR station 12670

Comparison between the two LHPR stations is complicated by the nine-day time delay between the two stations and the difference in the time at which they were undertaken. LHPR station 12664 was a night-time station occurring one hour after dusk (19:00 LT), whilst station 12670 occurred during the day two hours after dawn (07:00 LT). To investigate differences in the down and upcast of Station 12664 and day/night variations in the distribution of zooplankton; total biovolume, total abundance and abundance of the taxonomic groups were integrated (Σ_{250}) over the depth of the cast (250 m). In addition the affect of the oxygen minimum zone was examined by calculating the percentage of the Σ_{250} occurring in the surface oxygenated waters (above 50 m) (Table 3.2). Three features were evident: a proportion of the zooplankton population appeared to be diurnally vertically migrating into and out of the OMZ; the distribution of a large proportion (>60 %) of amphipods, appendicularians, chaetognaths, fish and pteropods were restricted by the OMZ; there was a discrepancy between the biovolumes and abundances observed during the downcast and the upcast of LHPR station 12664.

During the night-time LHPR (station 12664) >90 % (downcast) and >62 % (upcast) of total zooplankton biovolume occurred above the oxycline. Day-time (station 12670) total zooplankton biovolume was surprisingly and significantly reduced above the oxycline compared with station 12664 (t-test, $P>0.01$, $n = 2$). Similar calculations for total abundance were inconclusive. This was caused by the reduced numbers of copepods caught during the upcast of station 12664 that affected the total zooplankton abundance. Recalculating the percentage of abundance of all zooplankton except copepods above the oxycline showed that a greater percentage of the zooplankton abundance (minus copepod abundance) resided above the oxycline at night than during the day (t-test, $P>0.05$, $n = 2$). From this it is evident that some zooplankton were undertaking diel vertical migration into the suboxic waters during the day.

		Abundance (No.m^{-3})											
Depth (m)	**Biovolume (mlm^{-3})**	**Euphausiids**	**Decapods**	**Chaetognaths**	**Copepods**	**Fish**	**Ostracods**	**Polychaetes**	**Amphipods**	**Pteropods**	**Appendicularians**	**Total abundance**	**Total abundance -copepods**
Station 12664 Downcast													
50	39.05	445.22	12.74	411.05	83754.61	8.23	1124.65	145.53	23.71	1.46	197.83	86298.83	2544.22
250	46.89	477.07	46.74	470.6	90809.81	8.75	1193.79	492.91	23.71	1.46	261.92	94011.23	3201.42
% within 50 m	83.30	93.32	27.27	87.45	92.23	94.06	94.21	29.52	100	100	75.53	91.80	79.47
Station 12664 Upcast													
50	16.58	335.88	5.27	592.98	24925.12	27.36	609.66	92.74	20.04	0.04	895.28	34058.95	9133
250	26.51	486.30	21.52	923.59	53940.11	37.49	1608.27	1341.39	28.98	0.04	932.46	66032.08	12091.97
% within 50 m	62.54	69.07	24.47	64.20	46.21	72.99	37.91	6.91	69.15	100	96.01	51.58	75.54
Station 12670 Downcast													
50	23.42	249.46	2.99	666.92	24136.23	5.47	288.21	18.88	51.68	34.09	99.42	25608.57	1472.33
250	45.18	695.38	15.71	808.44	39930.69	7.03	598.99	455.10	67.16	38.06	103.05	42800.41	2869.72
% within 50 m	51.83	35.87	19.04	82.49	60.44	77.79	48.12	4.15	76.95	89.59	96.48	59.83	51.31

Table 3.2 The percentage of total biovolume, total abundance and zooplankton group abundance occurring above the oxycline (~50 m) at LHPR stations 12664 and 12670.

Decapods were the only group that showed a significant difference between night and day abundances above the oxycline indicating diel vertical migration into and out of the OMZ. However the percentage of euphausiids and amphipods above the oxycline during the day were also less than observed night-time values, although not significantly. The lack of a significant statistical result may be a result of both type 1 and 2 errors (Fowler and Cohen, 1990) associated with the small sample size.

Whilst the vertical distribution of several taxonomic groups appeared to be restricted and controlled by the oxycline, the distribution of polychaetes, decapods and to a lesser extent euphausiids appeared to be more variable. Both decapods and euphausiids exhibited a degree of vertical migration with a significant proportion (>88 % and >69 % respectively) of individuals occurring below the oxycline during the day. The small percentage of polychaetes above the oxycline though both the day and night indicates that their vertical distribution was independent of the oxygen concentration of the water column. The high numbers and percentage of the polychaete population below the oxycline may indicate that this group of zooplankton were the best adapted to suboxic conditions.

Values of Σ_{250} showed that greater abundance and biovolume was observed during the downcast (46.8 ml m^{-3} and 94011 No. m^{-3}) compared with the upcast (26.5 ml m^{-3} and 66032 No. m^{-3}) at station 12664. This may have been caused by instrument error such as clogging of the net or angle of the sampling vehicle (see Chapter 2), or as a result of the patchiness of zooplankton distributions. Σ_{250} of individual zooplankton groups showed that more copepods and decapods were observed during the downcast, whilst more chaetognaths, fish, ostracods, polychaetes and appendicularians were observed on the upcast and the numbers of euphausiids and amphipods were comparable. These variations suggest that zooplankton patchiness rather than instrument problems may have been responsible for the variation between the down and upcast.

3.4 Underway acoustic backscatter observations in the vicinity of the ARS

Underway acoustic backscatter data were collected from a 153 kHz VM-ADCP throughout cruise D209, and are used here to describe the distribution of zooplankton larger than a few millimetres in length using the assumption that an increase in acoustic backscatter is related to an increase in zooplankton biomass (following Flagg and Smith, 1989a,b; Plueddemann and Pinkel, 1989; Roe *et al.*, 1996). Absolute acoustic backscatter data, computed with a varying α (sound absorption coefficient) calculated using concurrent *in situ* measurements of temperature and salinity from the SeaSoar vehicle (see

Roe *et al.*, 1996), during the two SeaSoar surveys (SS1 and SS2) in the vicinity of the ARS (see Chapter 2), were colour-contour plotted and are presented in Figure 3.4.1.

The presence of the strong oxycline at 50 – 80 m depth resulted in the definition of two patterns in the acoustic backscatter, a strong diurnal migration signal labelled Sound Scattering Layer 1 (SSL1) and the presence of relatively high acoustic backscatter in surface waters both day and night, labelled Sound Scattering Layer 2 (SSL2).

SSL1 was most evident during SS1 as a result of its longer temporal duration, although it was present during both surveys. High acoustic backscatter (-70 to –55 dB) was observed in the surface ~ 80 m during the night, a thin layer of high acoustic backscatter occurred throughout the water column at dawn and dusk and high acoustic backscatter (-70 to –50 dB) was found at depth (>200 m) during the day, caused by zooplankton descending at dawn and rising to the surface at dusk. A pattern of diel migration is a common feature of acoustic datasets. At night the zooplankton biomass remaining within the suboxic waters was so low that no VM-ADCP signal was detectable below 100-200 m. Even during the day waters between the oxycline and >200 m were characterised by a low acoustic backscatter signal (-91 to –79 dB). Daytime acoustic returns from below 200 m were strong (>-70 dB) and dawn and dusk migrations obvious.

SSL2 is described here as the presence of a permanent layer of high acoustic backscatter within the surface 80 m that persisted through day and night (contributing to SSL1 at night). Daytime values of acoustic backscatter within the oxygenated surface waters varied between –76 and –64 dB, at night acoustic backscatter values increased to between –64 to –58 dB.

Colour-contoured sections of acoustic backscatter of legs 2,3,4 and 5 from SS1, overlaid with two isopycnal surfaces (25.4 and 26.4 σ_0) indicate that the vertical extent of SSL2 was limited by the 25.4 isopycnal (Figure 3.4.2), whilst the depth of SSL1 during the day appeared to be independent of isopycnal surfaces. The depth of the 25.4 σ_0 isopycnal surface is consistent with the base of the mixed layer and the associated oxycline. This therefore reinforces the hypothesis that the zooplankton responsible for SSL2 were limited in their vertical extent by the concentration of oxygen within the water.

DVM behaviour within the Arabian Sea surveyed region

SSL1 exhibiting DVM behaviour was a clear feature of the acoustic dataset. Figure 3.4.3 presents the day and night vertical profiles of VM-ADCP data averaged for the first and second SeaSoar surveys. Light data were not available for cruise D209, so it was assumed that night time data took place between the upwards migration that occurred

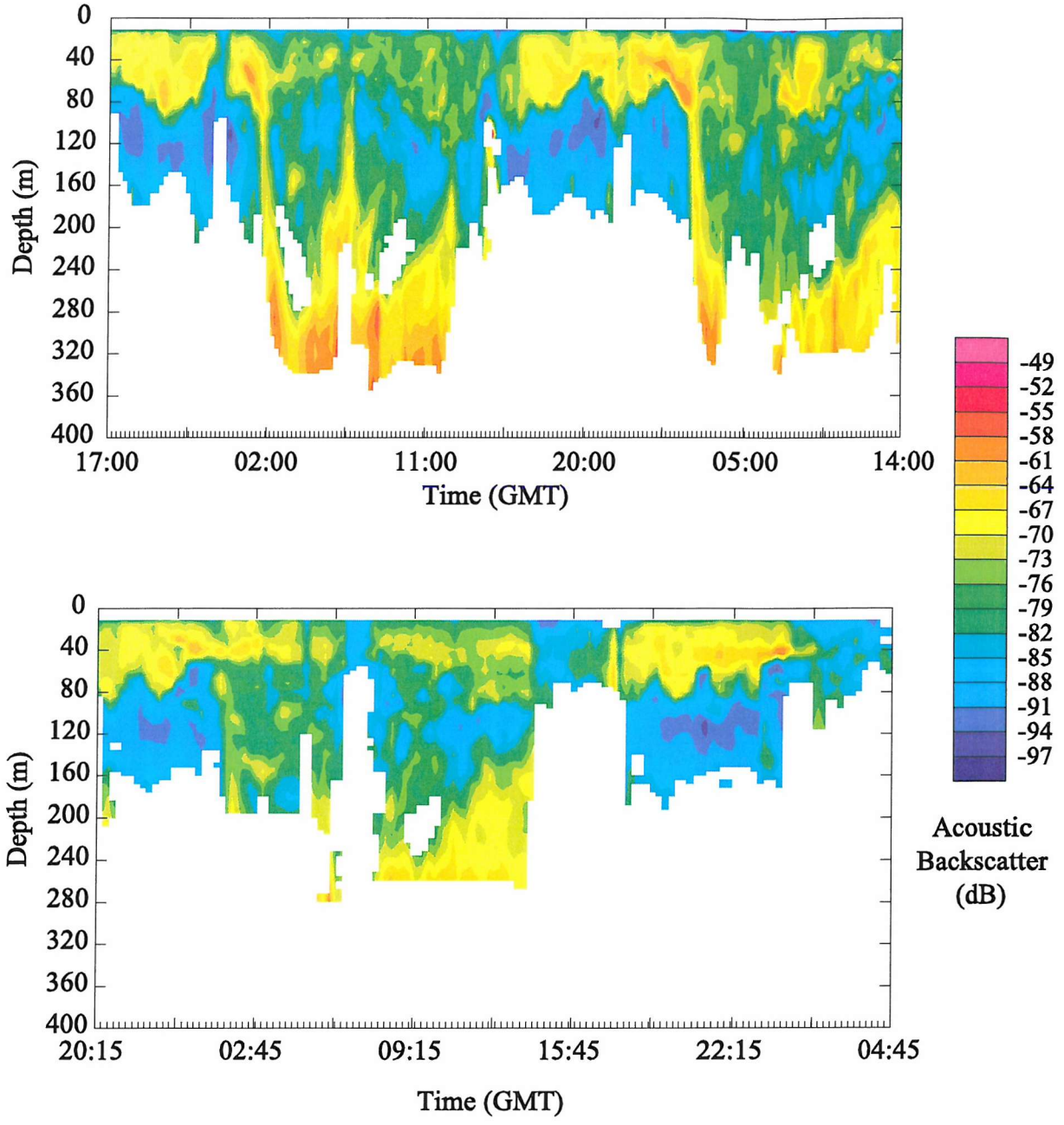

Figure 3.4.1 Colour-contoured VM-ADCP acoustic backscatter from SS1 (top) and SS2 (bottom).

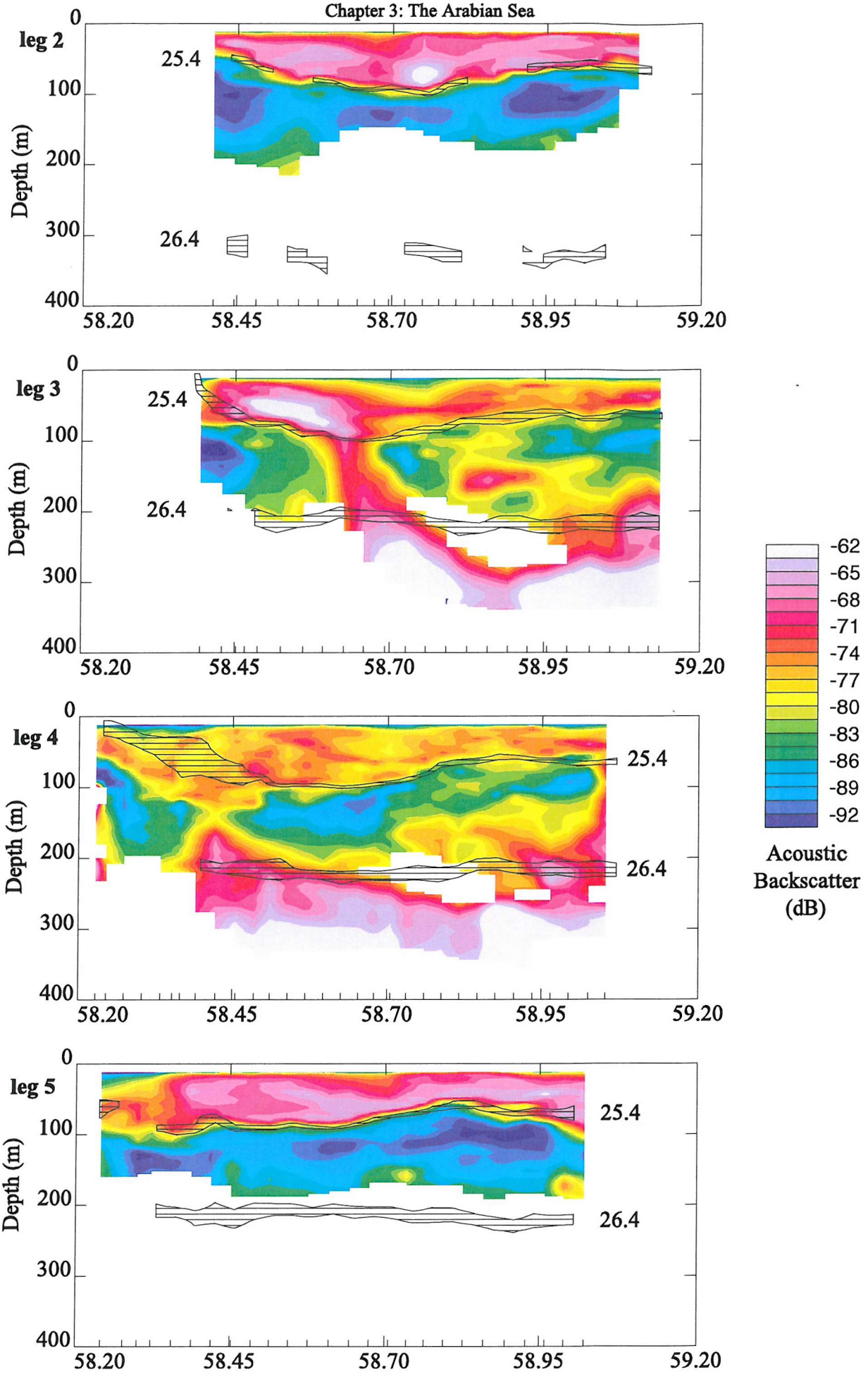

Figure 3.4.2 Colour-contoured sections of VM-ADCP acoustic backscatter from legs 2 (top), 3 (middle top), 4 (middle bottom) and 5 (bottom) of SS1. The 25.4 and 26.4 σ_0 isopycnal surfaces are overlayed.

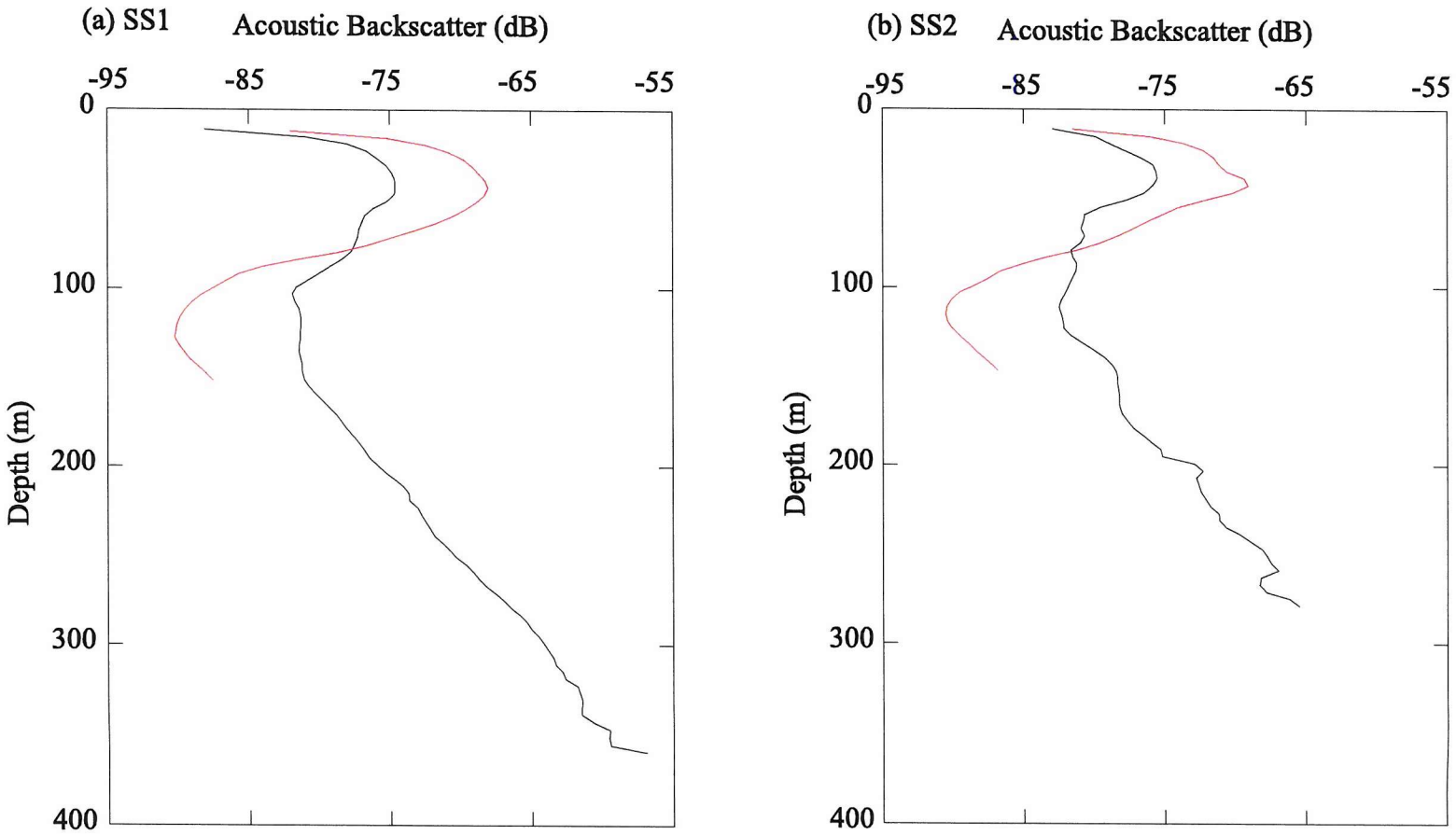

Figure 3.4.3 Day (black) and night (red) vertical profiles for the average VM-ADCP acoustic backscatter during (a) SS1 and (b) SS2

between 13:00 and 15:30 GMT (17:00 and 19:30 LT) and the dawn downwards migration that occurred between 01:00 and 02:30 GMT (05:00 and 06:30 LT). The actual periods of dawn and dusk diel migration (as above) were removed from the dataset as it was assumed that during these periods zooplankton would be vertically migrating. Thus the period of night time was similar to that approximated by Herring *et al.* (1998) of 15:00-03:00 GMT.

Figure 3.4.3 exhibits a clear DVM signal of increased acoustic backscatter in the surface 100 m at night compared with during the day. The night time values were maximum (~-68 dB) at approximately 50 m during both SS1 and SS2. During the day, above 100 m the maximum acoustic backscatter again occurred at ~50 m, although was 7 dB less. Just below 100 m the minimum values of acoustic backscatter (-90 dB) occurred during the night time and day time values were 8 dB greater. Below 150 m, acoustic backscatter intensity increases with depth during the day and is non-existent at night as a result of insufficient scatterers. The strong, deep day time and weak night time signals at depth and strong surface night time compared with day time intensities indicate that at least some, possibly all, of the zooplankton and micronekton responsible for the deep scattering layer were migrating to the surface oxygenated waters at night.

Supplementary RMT8 (Rectangular Mid-water Trawl, 8 m^2) net samples, undertaken during cruise D209, indicate that some chaetognaths, decapods, euphausiids, and fish undertook diel migration and that the abundance of zooplankton and micronekton was ~5 times larger (20500 x 10^{-4} No. m^{-3}) at night above the oxycline compared with daytime values (4000 x 10^{-4} No. m^{-3}). Below 100 m net sample volumes were low, correlating with the lack of targets within the VM-ADCP data. Between 100 and 200 m the daytime population was dominated by siphonophores and medusae, whilst at night the population was more mixed. The siphonophores and medusae may have contributed to the slightly higher acoustic signal observed during the day. Below 200 m decapods and myctophid fish (*Diaphus* and *Hygophum*) were the main components. Myctophid fish possess a gas bladder that resonates, thereby augmenting their acoustic scattering (Johnson, 1977). These fish were probably responsible for the large acoustic signal observed >200 m during the day.

The speed of the diel migrations was estimated following two methods; the speed of movement of backscattering bands representing the migration of zooplankton (e.g. Mauchline and Fisher, 1969; Maucline, 1980) and using VM-ADCP derived vertical velocities (e.g. Roe and Griffiths, 1993; Roe *et al.*, 1994; Tarling *et al.*, 2001; Wade and Heywood, 2001).

The speed of a backscattering band was estimated following:

$$c = \frac{\Delta Z}{\Delta t}$$

where c is the speed in cm s^{-1}, ΔZ is the change in depth of the band (cm) and Δt is the time (s) in which this change occurred.

As a result of a lack of definition of diel changes in the SS2 dataset only data from SS1 was examined and, as a result of the short duration of this survey, only two periods of dawn downward migration and one period of dusk upward migration are examined. Figure 3.4.4 presents colour-contoured plots of acoustic backscatter and VM-ADCP derived vertical velocities from three periods: jday 223 01:00-02:20; jday 223 13:00-15:30; and jday 224 01:00-02:30. Calculations of c for the "leading" edge of the jday 223 and 224 dawn migrations indicated a speed of 12 and 14.6 cm s^{-1} (respectively) which are not dissimilar from the VM-ADCP derived vertical velocities of a downwards speed of 11 cm s^{-1} for the leading edge. A clear feature indicated by the measurement of vertical velocities was that migration speed was not uniform throughout the "backscattering band" and that the fastest speeds were associated with the beginning (leading edge) of the downward migration. As a result of the paucity of data during the dusk diel period, speeds were not estimated (Figure 3.4.4). Additionally a layer of low acoustic backscatter, ~20 m thick, separated the surface scattering layer and the deep layer presumed to be migrating zooplankton.

3.5 Discussion of the distribution of zooplankton

The distribution of zooplankton observed through VM-ADCP acoustic backscatter and LHPR samples showed several features: the vertical extent of some zooplankton was limited by the oxycline; diel vertical migration of zooplankton into the OMZ during the day occurred; and the distribution of two taxonomic groups appeared to be relatively uninfluenced by the OMZ.

The oxycline limited the vertical distribution of some zooplankton

A dominating feature of the acoustic backscatter was a permanent layer of high acoustic backscatter (SSL2) present within the well-oxygenated surface waters. This layer persisted both day and night and had greatest intensities at ~50 m depth consistent with the depth of or just above the oxycline. LHPR samples support this observation where, during the day, maximum zooplankton biovolumes occurred at the thermocline. Although there are several observations of acoustic backscatter in the Arabian Sea (Herring *et al.*, 1998;

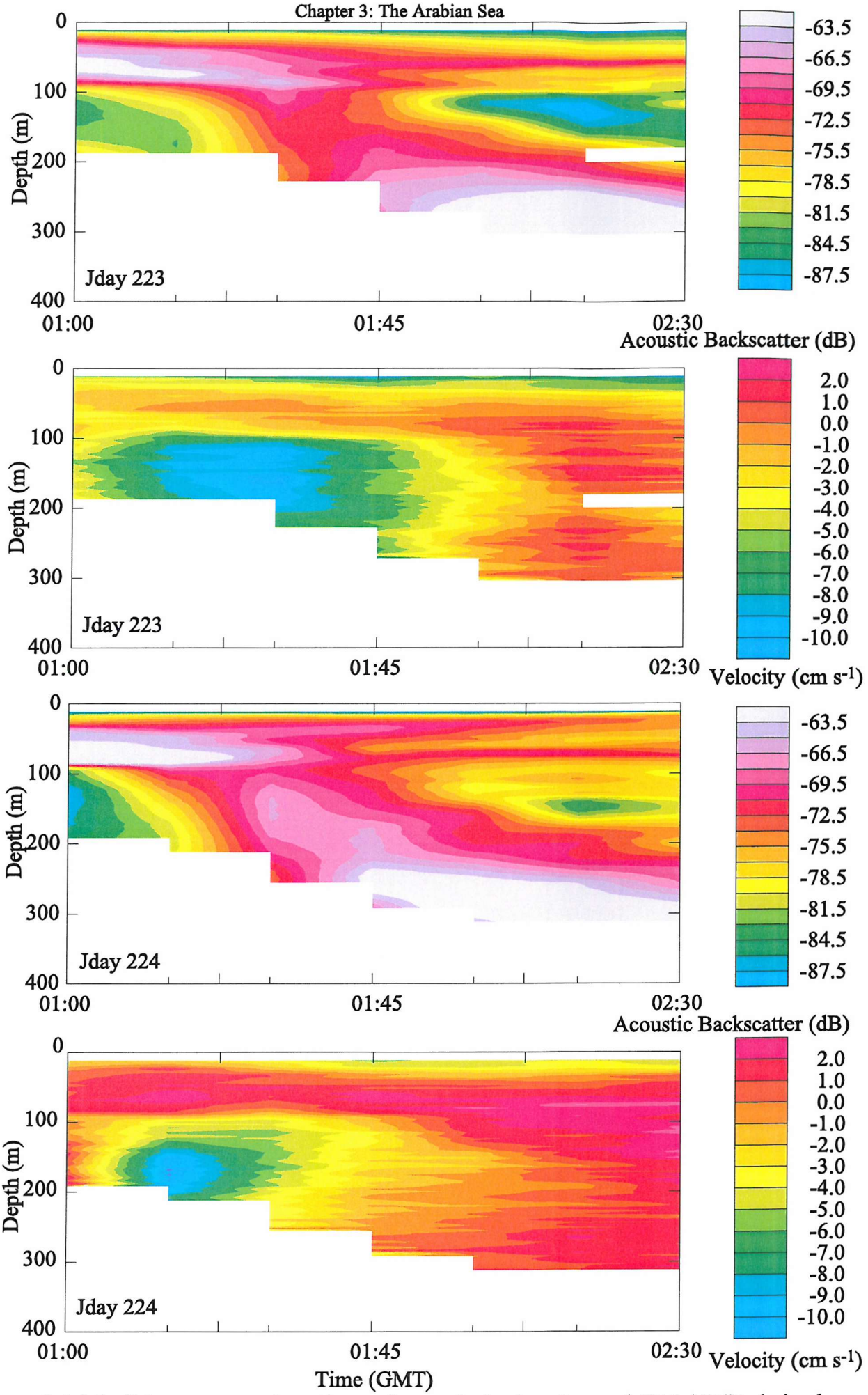

Figure 3.4.4ab Colour-contoured sections of acoustic backscatter and VM-ADCP derived vertical velocities from the dawn periods jday 223 (top) and 224 (bottom).

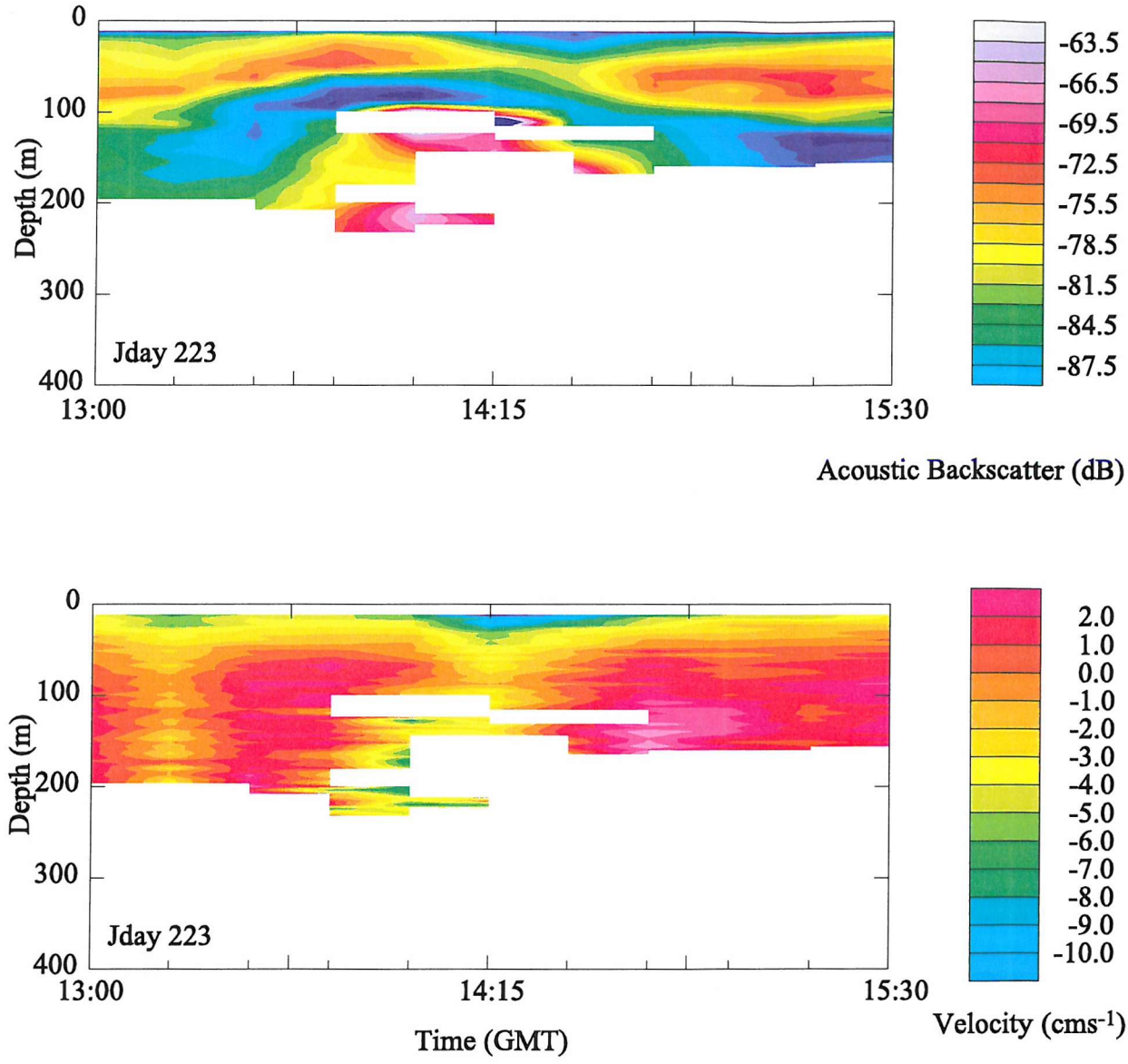

Figure 3.4.4c Colour-contoured sections of acoustic backscatter and VM-ADCP derived vertical velocities from the dusk period of jday 223.

Wishner *et al.*, 1998; Luo *et al.*, 2000; Ashjian *et al.*, 2002) this feature has not been previously reported.

Measurements of total zooplankton abundance and biovolume from the LHPR samples indicated that at least 50 % of the zooplankton sampled resided above the oxycline during the day. At night (ignoring the contribution from copepods) this percentage increased to greater than 75 %. This agrees with previous studies that show a large percentage of the zooplankton residing within the surface layers (>96 % of Σ_{500} in the surface 100 m, Vinogradov and Vorinina, 1961; >85 % of Σ_{300} in the surface 100 m, Smith *et al.*, 1998; >69 % of Σ_{1000} in the upper 200 m, Wishner *et al.*, 1998).

Hence a substantial portion of the zooplankton population were limited in their vertical distribution by the oxycline. This was more evident for some taxonomic groups such as amphipods, appendicularians, chaetognaths, pteropods and fish. For each of these groups > 75 % of their integrated abundance (Σ_{250}) was concentrated above the oxycline during the day. Studies have shown that many complex animals such as fish and crustaceans are able to satisfy their routine metabolic needs at oxygen concentrations of about 0.15 ml l^{-1} (6.7 μmol l^{-1}) by means of aerobic metabolism supported by periods of anaerobic metabolism (Childress, 1975). However, Childress and Thuesen (1992) suggest that simpler forms of zooplankton such as medusae and chaetognaths lack physiological systems that could be obviously adapted to support aerobic metabolism at low ambient oxygen concentrations. Those animals that do not have low oxygen adaptations may be restricted from OMZs (Yang *et al.*, 1992). Those taxonomic groups mentioned above appeared to be the most influenced by the OMZ, however none of the taxonomic groups was completely excluded from the OMZ. The different vertical patterns exhibited by the different taxonomic groups may be indicative of their different tolerances to minimum oxygen concentrations.

DVM in the Arabian Sea

SSL1 was the dominant signal in the acoustic backscatter data and has been observed on numerous occasions (Herring *et al.*, 1998; Wishner *et al.*, 1998; Morrison *et* al., 1999; Luo *et al.*, 2000; Ashjian *et al.*, 2002). The vertical migration of zooplankton and micronekton (e.g. large copepods, euphausiids, and fish) into oxygen deficient zones on a diel basis has been previously reported (Vinogradov and Voronina, 1961; Longhurst, 1967; Brinton, 1979; Herring *et al.*, 1998; Smith *et al.*, 1998; Wishner *et al.*, 1998; Luo *et al.*, 2000; Ashjian *et al.* 2002). Ashjian *et al.* (2002) identify the taxa responsible for this layer as myctophid fish, pelagic crabs and euphausiids. RMT and LHPR samples in this

study also indicated that fish and euphausiids were undertaking diel migrations as well as other taxa. The most frequently discussed DVM behaviour within the Arabian Sea is that of the dominant mesopelagic myctophid fish (Kinzer *et al.*, 1993; Herring *et al.*, 1998; Luo *et al.*, 2000; Griffiths *et al.*, 2001; Ashjian *et al.*, 2002). Kinzer *et al.* (1993) identified that all of the myctophid fish were residing during the daytime at depths of extremely low oxygen levels and foraging in the oxygen-rich surface layer at night. Recently Luo *et al.* (2000) estimated fish vertical migration speeds to have maximum values of 10-13 cm s^{-1}, not dissimilar to those observed during this study supporting the hypothesis that the dominant zooplankton and micronekton contribution to SSL1 was from myctophid fish.

The two LHPRs one a night-time station the other a day-time station, although nine days apart, also indicate that some zooplankton were diel vertically migrating into the OMZ during the day and out of it at night. By day the total biovolume below the oxycline was low but at night it became minimal. The increase in the relative importance of copepods, decapods, euphausiids and fish above the oxycline at night reflects their movement into the oxygenated surface waters. These migrations are emphasised in the VM-ADCP acoustic backscatter data, which identify the paucity of zooplankton below the oxycline by an inability to measure an acoustic signal as a result of insufficient targets at depth during the night.

In this study the LHPR data indicate that some copepods, euphausiids, decapods and fish were vertically migrating, residing in the OMZ during the day. However the vertical extent of their migrations differ. Whilst decapods, euphausiids and fish were found throughout the water column or at depths of ~200 m, a significant proportion of the copepods observed below the oxycline occurred within 40 m of it. Past studies have indicated that some copepods and euphausiids are tolerant of oxygen concentrations down to 4.4 μmol l^{-1} (Sameoto, 1986; Sameoto *et al.*, 1987; Vinogradov *et al.*, 1991). Whilst the oxycline occurred in this study between 40 and 60 m, oxygen concentrations were > 5 μmol l^{-1} to ~100 m (and < 5 μmol l^{-1} below to depths greater than 500 m). Hence, the copepods observed in this study may have been limited in their vertical distribution not by the oxycline but a particular threshold in oxygen concentration.

The physiology of the vertical migrants is unclear, although morphological adaptations such as increased gill surface area have been suggested (Wessel and Johnson, 1996; Herring *et al.*, 1998) and physiological alterations to metabolism permitting some animals to live anaerobically for certain periods (Childress and Thuesen, 1992). The decapods caught within the OMZ appeared to have a soft carapace and gills extending

below the carapace possibly indicating a morphological adaptation to low oxygen concentrations. In addition the higher daytime abundance of euphausiids at depth within the OMZ compared to night-time abundances in surface water may suggest that during the day the euphausiids were relatively inactive and hence more easily caught.

Distributions independent of the oxycline

Perhaps the most surprising result from this dataset was the distribution of planktonic polychaetes, which appeared to be independent of the OMZ and did not exhibit a pattern typical of diurnal migration. The distribution of polychaetes was similar during both the day and night LHPR stations and their peak abundances occurred well within the suboxic waters. Previous studies have tended to concentrate on the organisms capable of migrating into or only remaining above the suboxic zone. An interesting question here is "are the polychaete group the best adapted to low oxygen conditions?". Levin *et al.* (2000) observed polychaetes to be the dominant benthic fauna (86-99 %) with the OMZ on the Oman margin in the NW Arabian Sea. Investigation of these macrobenthic polychaetes identified morphological adaptations of branchiae enlargement and increased branching in response to hypoxic conditions (Lamont and Gage, 2000). These adaptations were hypothesised to result from either a direct response by the phenotype to intensity of hypoxia or to represent early genetic differentiation among depth-isolated sub-populations, and suggest that the polychaete community are adapted to low oxygen environments.

3.6 Summary

(1) An intense OMZ was present throughout the survey region, with a strong oxycline at ~50 m separating oxygen rich waters at the surface from suboxic waters below.

(2) The OMZ was the dominant forcing mechanism controlling the vertical distribution of zooplankton.

(3) The vertical distribution of chaetognaths, amphipods, pteropods and appendicularians was predominantly restricted to within oxygen rich surface waters.

(4) Some zooplankton (decapods and euphausiids) and fish undertook diel vertical migrations into and out of the OMZ. Morphological and physiological adaptations to low oxygen environments have been suggested for these groups.

(5) The vertical distribution of polychaetes appeared to be independent of water oxygen concentration and it is hypothesised that this group may be the best adapted to a low oxygen environment.

Chapter 4

The Alboran Sea

4.1 Introduction

In this chapter the results from a multi-disciplinary survey of the Almeria-Oran front are presented. Section 4.1 introduces the previous observations within the surveyed region. In section 4.2 the hydrography of the Alboran Sea and the Almeria-Oran front is presented and discussed. Observations of the distribution of phytoplankton are discussed in section 4.3 and section 4.4 discusses the influence of the Almeria–Oran front on the distribution of zooplankton. Section 4.5 summarises the conclusions drawn. The discussion has been wrapped into the results, for the ease of the reader, as a result of the large amounts of data presented in this chapter.

4.1.1 The physical structure of the Mediterranean Sea, Alboran Sea and the Almeria-Oran Front

Basin-scale circulation of the Mediterranean Sea

The Mediterranean Sea is a semi-enclosed sea, its only communication with the world's Ocean through the Strait of Gibraltar. The primary circulation within the Mediterranean is thermohaline, resulting from excess evaporation (an inverse estuarine circulation) (Heburn, 1994). It is a two-layer flow where relatively fresh, warm Atlantic Water (AW) enters the Western Mediterranean basin in an upper layer through the Straits of Gibraltar and generally flows to the east. These waters of Atlantic origin eventually reach the Levantine Basin in the eastern Mediterranean. By which time they have been modified, through evaporative processes and mixing in specific areas of deep winter mixing (Malanotte-Rizzoli *et al.*, 1999), to such an extent that they sink to intermediate depths (~400 m) forming the water mass referred to as Levantine Intermediate Water (LIW) (Gascard and Richez, 1985; Heburn, 1994). This LIW then gradually flows westwards, through the Strait of Sicily, into the Ligurian and Alboran basins and eventually exits the Mediterranean via the Strait of Gibraltar below the incoming surface AW layer.

Within this basin-scale concept, the detailed circulation of the Mediterranean Sea is highly complex, consisting of a number of semi-permanent gyres and mesoscale eddies interconnected by meandering jets and currents (Figure 4.1.1) (Millot, 1991; 1999).

Water Masses and circulation of the Alboran Sea

The Alboran Sea is the first Mediterranean basin encountered by the inflowing AW and has a very complex bottom topography (Figure 4.1.2). This topography is composed of both an East and West deep basin (1000 – 2000 m depth) as well as the Alboran Island and associated shallow banks, which extend south-westward towards the Algerian Coast.

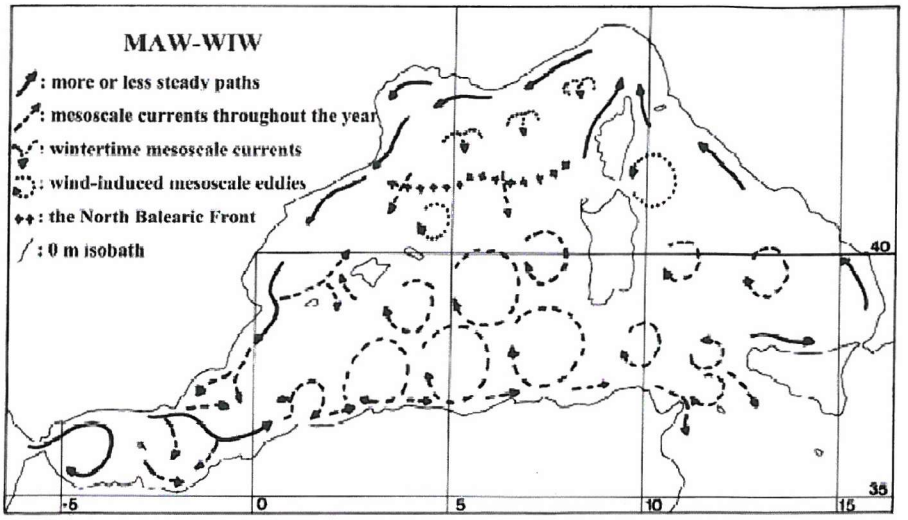

Figure 4.1.1 The circulation of Modified Atlantic Water (MAW) and the Winter Intermediate Water (WIW) in the western Mediterranean Sea (From Millot, 1999).

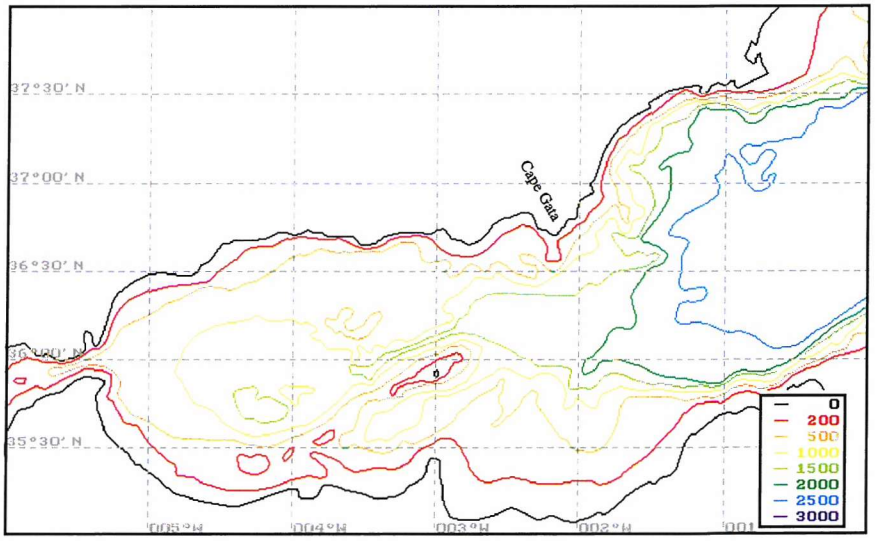

Figure 4.1.2 The topography of the Alboran Sea (depth in metres): reproduced from the GEBCO digital atlas, BODC.

The influence of this abrupt topography on the circulation in the Alboran Sea is not yet fully understood (Tintore *et al.*, 1994).

Atlantic Water entering the Alboran Sea, through the Strait of Gibraltar, is generally modified in its eastward migration, and is typically referred to as Modified Atlantic Water (MAW, $36.5 < S < 37.5$). MAW usually occupies the upper 2-300 m of the water column in the Alboran Sea and interacts below with LIW and to the east with Mediterranean Surface Water (MSW, $S > 37.5$) (Tintore *et al.*, 1994). Gascard and Richez (1985) refer to Atlantic-Mediterranean Interface Water (AMIW) as the water that forms as a result of the interaction between Atlantic waters and Intermediate waters, although more recent authors refer to it as MAW (Viudez *et al.*, 1996).

The large scale circulation of the Alboran Sea is generally well known. The main inflow path of the AW modified to MAW, entering from the Strait of Gibraltar, is around two anticyclonic gyres (Figure 4.1.3). Satellite imagery indicates that, on occasions, one or both gyres can disappear (Heburn and La Violette, 1990). These gyres are referred to as the Western and Eastern Alboran Gyres (WAG, EAG). The formation of, mean position, and shape of the WAG, initiated by the inflowing jet of AW, are controlled by the narrowness of the Strait of Gibraltar, the angle of the Strait with respect to the Alboran Sea, and Coriolis force (Preller and Hurlburt, 1982; Heburn, 1985, 1987). The WAG has been studied intensively (Gascard and Richez, 1985; La Violette, 1990; Heburn and La Violette, 1990; Tintore *et al.*, 1991) and is considered a quasi-permanent feature. The EAG is less well-studied but is known to break down more readily than the WAG (Heburn and La Violette, 1990; Prieur and Sournia, 1994; Viudez and Tintore, 1995).

The Almeria-Oran front

In the easternmost Alboran Sea near Cape Gata, where MAW meets MSW flowing slowly west, an intense density front (the Almeria-Oran front) is present. Its size and position appears to be partly influenced by the size and position of the EAG (Tintore *et al.*, 1988; Arnone *et al.*, 1990) and, when the EAG is present, the front is found at the eastern boundary of the EAG. This makes its position highly variable, and the Almeria-Oran Front (AOF) has been found in a median (Tintore *et al.*, 1988) and a southern position (Prieur and Sournia, 1994). Associated with the AOF is a strong geostrophic current (~1 m s^{-1}) on the EAG side of the front (Folkard *et al.*, 1994). A secondary, ageostrophic, circulation is present that is weaker than the primary circulation by 1-2 orders of magnitude. The spatial extent of the AOF in length is greater than 200 km, ~10 km in width. Physical and biochemical data indicate that the front is limited to the upper 200 m. The secondary ageostrophic circulation associated with instability of the jet

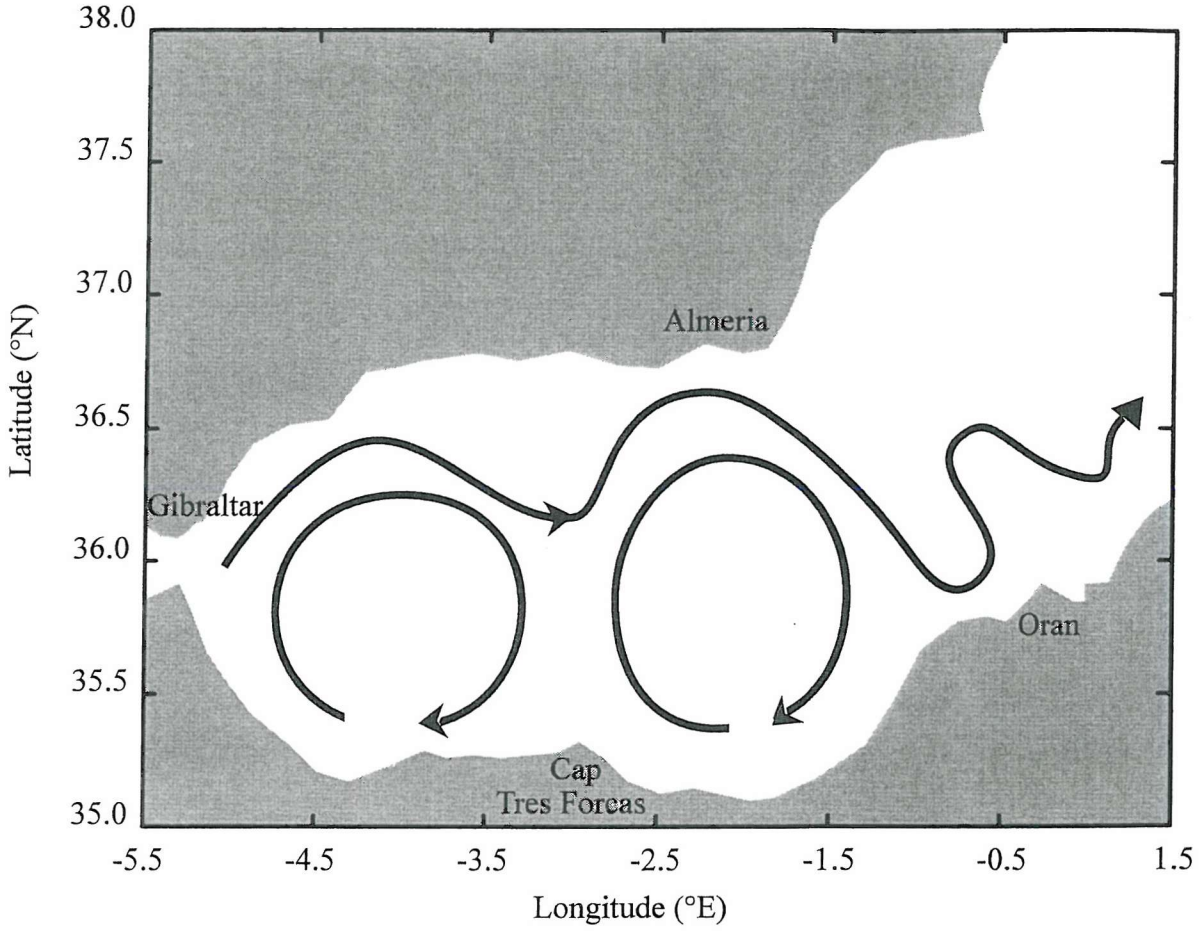

Figure 4.1.3 Cartoon of the two gyre surface circulation of the Alboran Sea, following Arnone *et al.* (1990) and others.

is characterised by surface convergence and periodic isopycnal sinking and upwelling (Tintore *et al.*, 1988; Prieur and Sournia, 1994; Allen *et al.*, 2001).

As a result of the strong gradients, intense flows, restricted horizontal dimensions and quasi-permanency, the AOF has been the subject of recent interdisciplinary programmes such as ALMOFRONT-1 (Prieur and Sournia, 1994), ALMOFRONT-2 (Prieur, pers. comm.) and OMEGA (Allen *et al.*, 2001; Fielding *et al.*, 2001).

4.1.2 The distribution of phytoplankton and zooplankton at the AOF

The affect of the AOF on primary production

Frontal enhancement[1] of phytoplankton populations has been observed at the Almeria-Oran front (Lohrenz *et al.*, 1988; Videau *et al.*, 1994; Fiala *et al.*, 1994). In fact, Prieur and Sournia (1994) describe them as anomalously high, with maximum chlorophyll concentrations of 23 mg m^{-1} measured by Gould and Wiesenberg (1990) at a depth of 54 m. Diatom and nanoplankton abundance, chlorophyll content and primary production have been observed to be higher in the jet, measured from satellite data (Arnone and La Violette, 1986; Lohrenz *et al.*, 1988; Arnone *et al.*, 1990) or *in situ* shipboard data (Prieur *et* al., 1993; Fiala *et al.*, 1994; Videau *et al.*, 1994). This suggests that the frontal-jet system exhibits a fertilising effect on the otherwise oligotrophic waters of the Alboran Sea. Such a frontal enhancement is thought to result from the vertical input of nutrients caused by upwelling (Claustre *et al.*, 1994; Fiala *et al.*, 1994; Videau *et al.*, 1994) and is supported by observations from L'Helguen *et al.* (1992) and Videau *et al.* (1994) who describe a shallower nitracline in frontal waters than in Mediterranean waters (18-30 m and 30-60 m respectively). During ALMOFRONT-1 Videau *et al.* (1994) observed some of this enhanced production exported down below the thermocline to depths of 110 m, along the 28.0 σ_0 isopycnal.

The affect of the AOF on zooplankton

Fewer studies have been made of the distribution of zooplankton at the Almeria-Oran front. Coincident with the observations of high phytoplankton biomass at the front during the project ALMOFRONT-1 Thibault *et al.* (1994) and Seguin *et al.* (1994) observed higher total standing stocks of zooplankton, including higher copepod abundances, in the frontal jet compared with surrounding waters. Baussant *et al.* (1993) investigated the distribution of micronekton and macrozooplankton using a 38 kHz echosounder, multi-net sampling and video profiling across the Almeria-Oran front. They showed that the region was dominated by several deep scattering layers, which could be

[1] Enhancement is used here to describe increased rates of primary production and increased biomass.

attributed to fish such as Myctophid and *Cyclothone* spp. or euphausiids. These layers were observed at different depths on each side of the front (50 metres deeper on the Mediterranean side). Anderson and Sardou (1992) also refer to the existence of a non-migratory species of myctophid fish present at the Ligurian front in the North Western Mediterranean.

4.2 Hydrography of the Alboran Sea and the Almeria-Oran front (AOF) during cruise D224

4.2.1 General description of the Alboran Sea

The surface temperature field derived from remotely-sensed data, of the Alboran Sea, on the 31st October, 19th November and 2nd December 1996 are shown in Figure 4.2.1. Purple and blue represent cool waters, green and yellow warm, and the Spanish and North African coastlines are clearly discernable. Satellite IR images were provided and processed by the Southampton Oceanography Centre (SOC) and the University of Pisa (UP).

The most outstanding feature in these data are the warm-cored anticyclonic gyres, which, in terms of temperature gradient, are most prominent in October. During November, the Western Alboran Gyre appeared to move eastwards to be replaced by a new Western Alboran Gyre resulting in the presence of three gyres (Figure 4.2.1b). Between the 19th of November and the 2nd of December the "central" and Eastern Alboran Gyres had coalesced (Allen *et al.*, 2001) and the Alboran Sea circulation had returned to the more "traditional" two Alboran Gyre flow regime (Figure 4.2.1c) (Tintore *et al.*, 1988; Heburn and La Violette, 1990).

Thus the satellite IR imagery indicates that during the Finescale SeaSoar Surveys of OMEGA (16-28/12/1996) the Almeria-Oran Front (henceforth denoted as AOF), as the eastern boundary of the Eastern Alboran Gyre (EAG), was located in its median position.

4.2.2 Water masses in the vicinity of the AOF

The characteristics of all the water masses encountered in FineScale Surveys 1-3 (FSS1-3) are represented in the θ/S diagram in Figure 4.2.2. The lowest salinity waters, ~36.63, are surface waters of recent Atlantic origin and are referred to here as Modified Atlantic Water (MAW) (Arnone *et al.*, 1990; Sparnocchia *et al.*, 1994). There is a mixing line between the MAW and high salinity low temperature Mediterranean intermediate waters (LIW). These waters have been identified here as Atlantic-Mediterranean Interface Water (A-MIW) following Gascard and Richez (1985) and include any waters of < 15.5 C and S < 37.5. Mediterranean Surface Waters (MSW, S > 37.5, t > 15.5 °C)

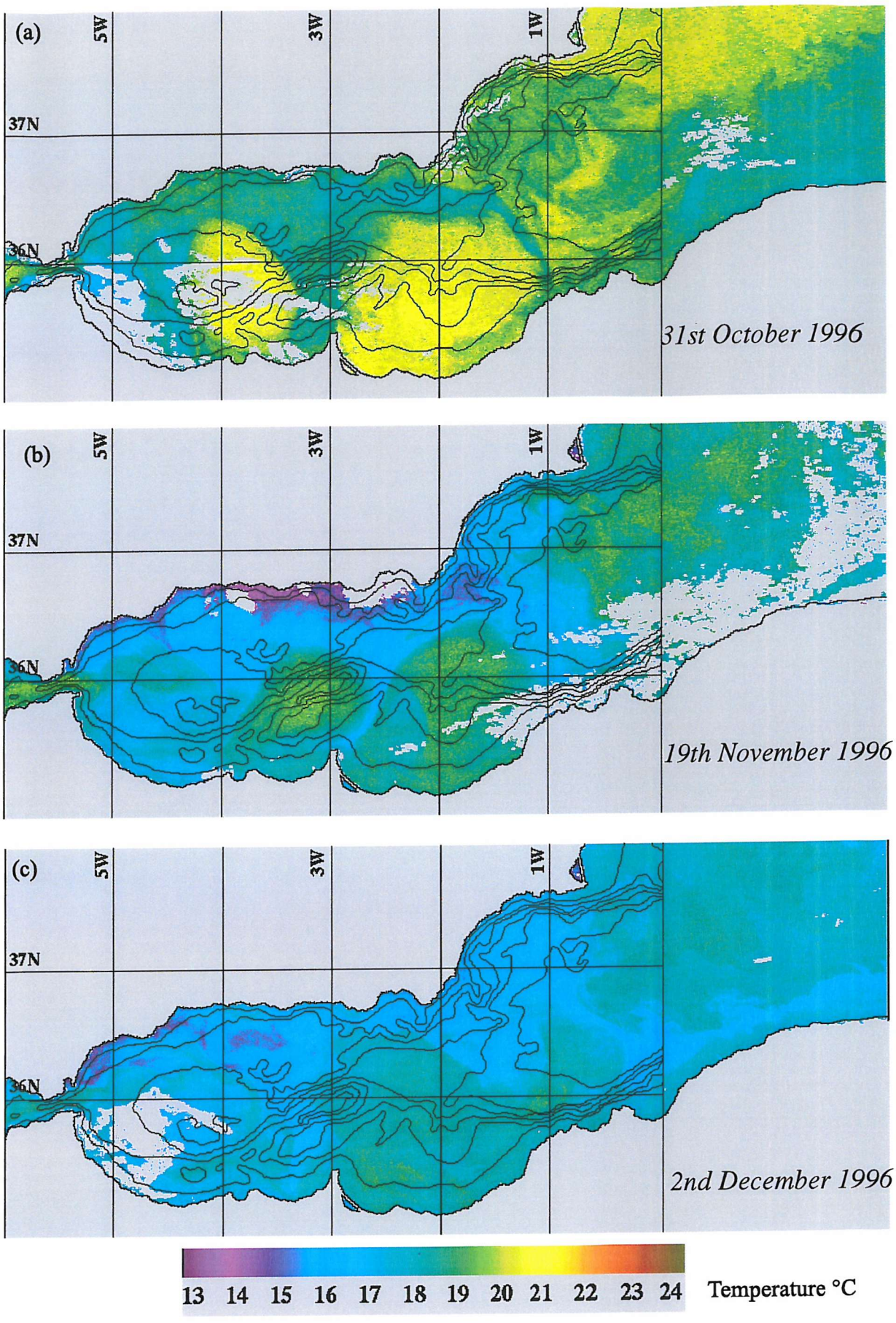

Figure 4.2.1 NOAA-14 AVHRR images provided by the Natural Environmental Research Council through the Southampton Oceanography Centre and processed at the University of Pisa (Baldacci *et al.*, 1998)

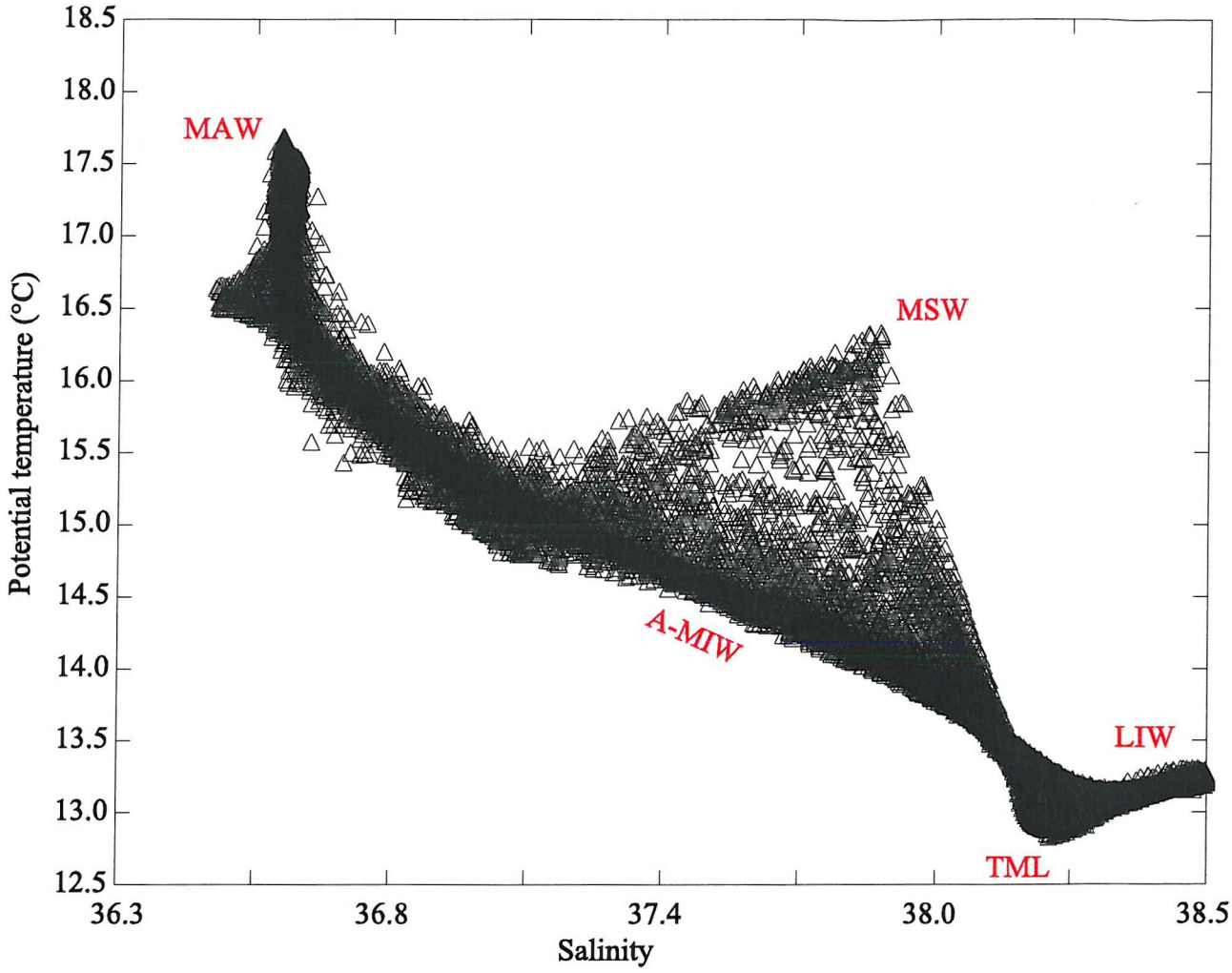

Figure 4.2.2. Potential temperature as a function of salinity for all the SeaSoar data collected during the three finescale surveys. Note the relatively fresh surface modified Atlantic waters (MAW) in the eastern Alboran gyre, the warm salty Mediterranean surface waters (MSW), Atlantic-Mediterranean interface water (A-MIW), the Levantine water (LIW) and the temperature minimum layer (TML).

(Arnone *et al.*, 1990) were found in the North East corner of FSS2 and FSS3. This water appeared to have flowed slowly southward along the Spanish coast and appeared at the surface near Almeria. The signature of MSW is less well defined than that of MAW, as MSW is predominantly old MAW that has remained at the surface in the Western Mediterranean (Benzohra and Millot, 1995).

Below the surface waters, a Temperature Minimum Layer (TML) of water with salinity of ~ 38.2 and temperature below 13.5 °C was present to depths of 250-300 m. This has been called "Riviera Water" and forms through cooling of Atlantic waters along the French Riviera (Gascard and Richez, 1985). At maximum SeaSoar depths of ~370 m a tight θ/S signature of Levantine Intermediate Waters (LIW) was observed that formed a distinct salinity maximum (Sparnocchia *et al.*, 1994).

4.2.3 The horizontal structure of the AOF

The position of the surface signature of the AOF is denoted by a steep change in surface temperature and salinity observed in the thermosalinograph datasets (Figure 4.2.3). Its position and shape was seen to change significantly from FSS1 through to FSS3. Between FSS1 and FSS2 the position of the front at the surface had (most notably in the middle legs) moved Southwest (Figure 4.2.3a-b,d-e). Then between FSS2 and FSS3 it returned to its more northeasterly position (Figure 4.2.3c,f).

The high temperature, low salinity signature of MAW was observed in the southwest part of the survey area throughout FSS1-3, the temperature of the MAW increasing and salinity decreasing towards the centre of the EAG. Northeast of the front was water of higher salinity and lower temperature, identified as AMIW. During FSS2 and FSS3 the salinity of the AMIW northeast of the front, near Almeria, intensified so that the water had properties more typical of MSW (S > 37.5).

The near surface currents (at 14 m) measured with the VM-ADCP indicate that associated with the AOF was a strong current, with speeds up to ~ 100 cm s^{-1} (Figure 4.2.4). The surface horizontal velocities were greatest and had a coherent structure on the southwest, EAG, side of the front, and decreased in intensity towards the middle of the EAG. On the northeastern, or "Mediterranean", side of the front, horizontal velocities were reduced (~20 cm s^{-1}) with no regular structure. The fast velocities associated with the surface of the front followed the changing position of the front (identified in surface temperature and salinity fields) between FSS1, FSS2 and FSS3. Comparison of the surface currents with horizontal velocities at 54 m and 150 m depth indicated that velocities decreased with depth, such that no obvious coherent flow could be associated with the front at 150 m depth (Figure 4.2.5).

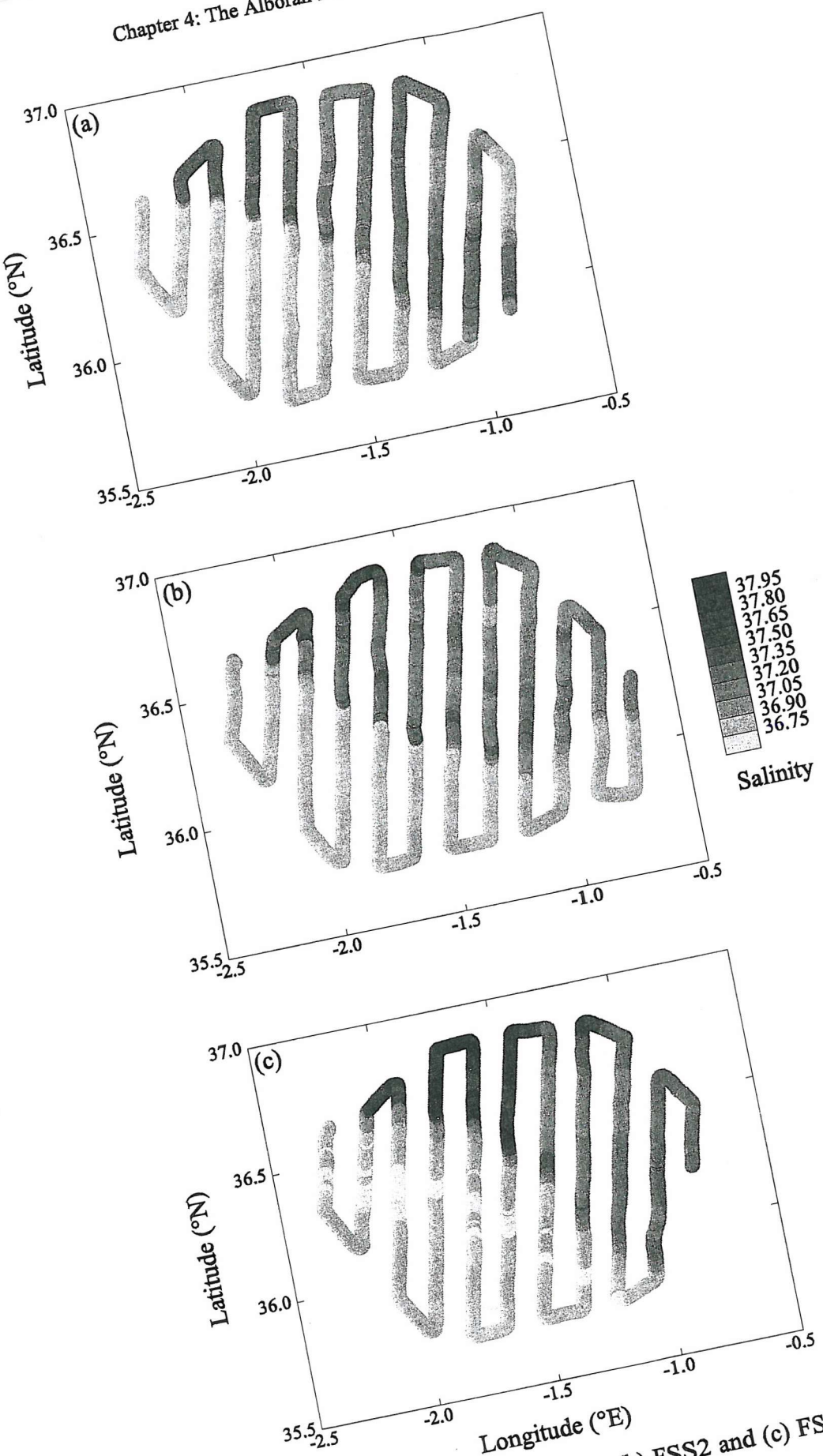

Figure 4.2.3a-c. Maps of surface salinity for (a) FSS1, (b) FSS2 and (c) FSS3 measured using the underway thermosalinograph.

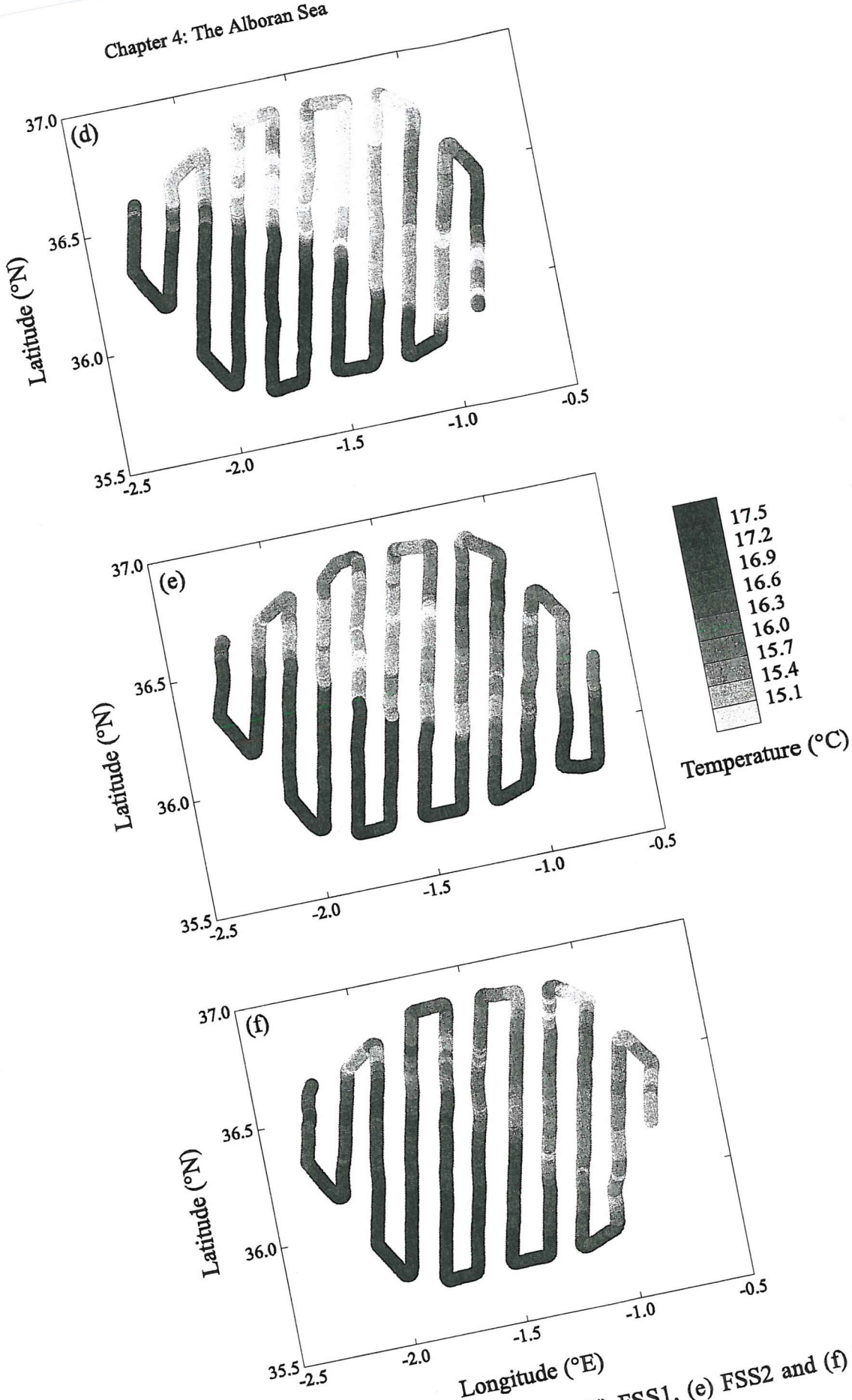

Figure 4.2.3d-f. Maps of surface temperature (°C) for (d) FSS1, (e) FSS2 and (f) FSS3 measured using the underway thermosalinograph.

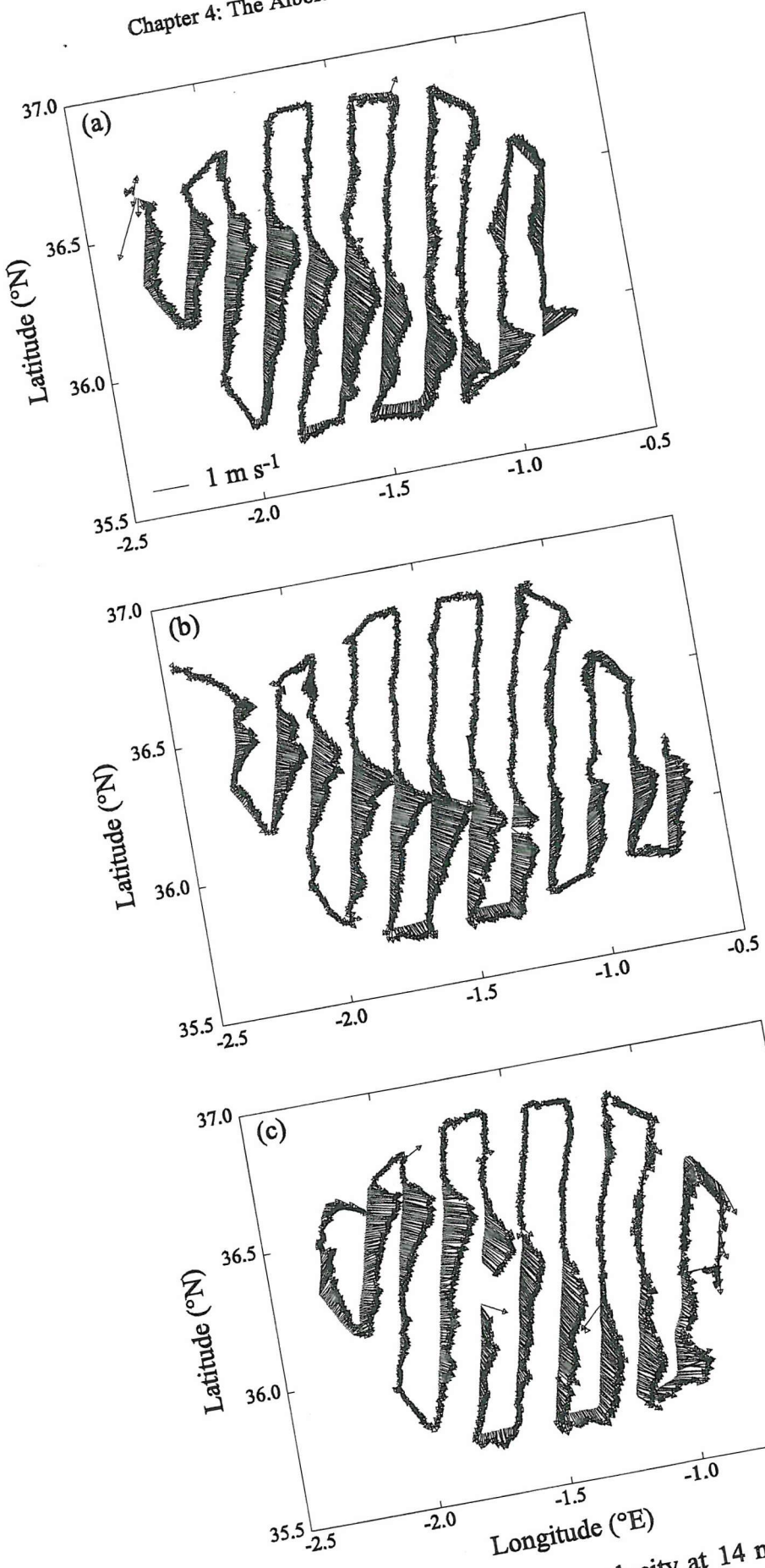

Figure 4.2.4. Maps of VM-ADCP derived current velocity at 14 m depth for (a) FSS1, (b) FSS2 and (c) FSS3.

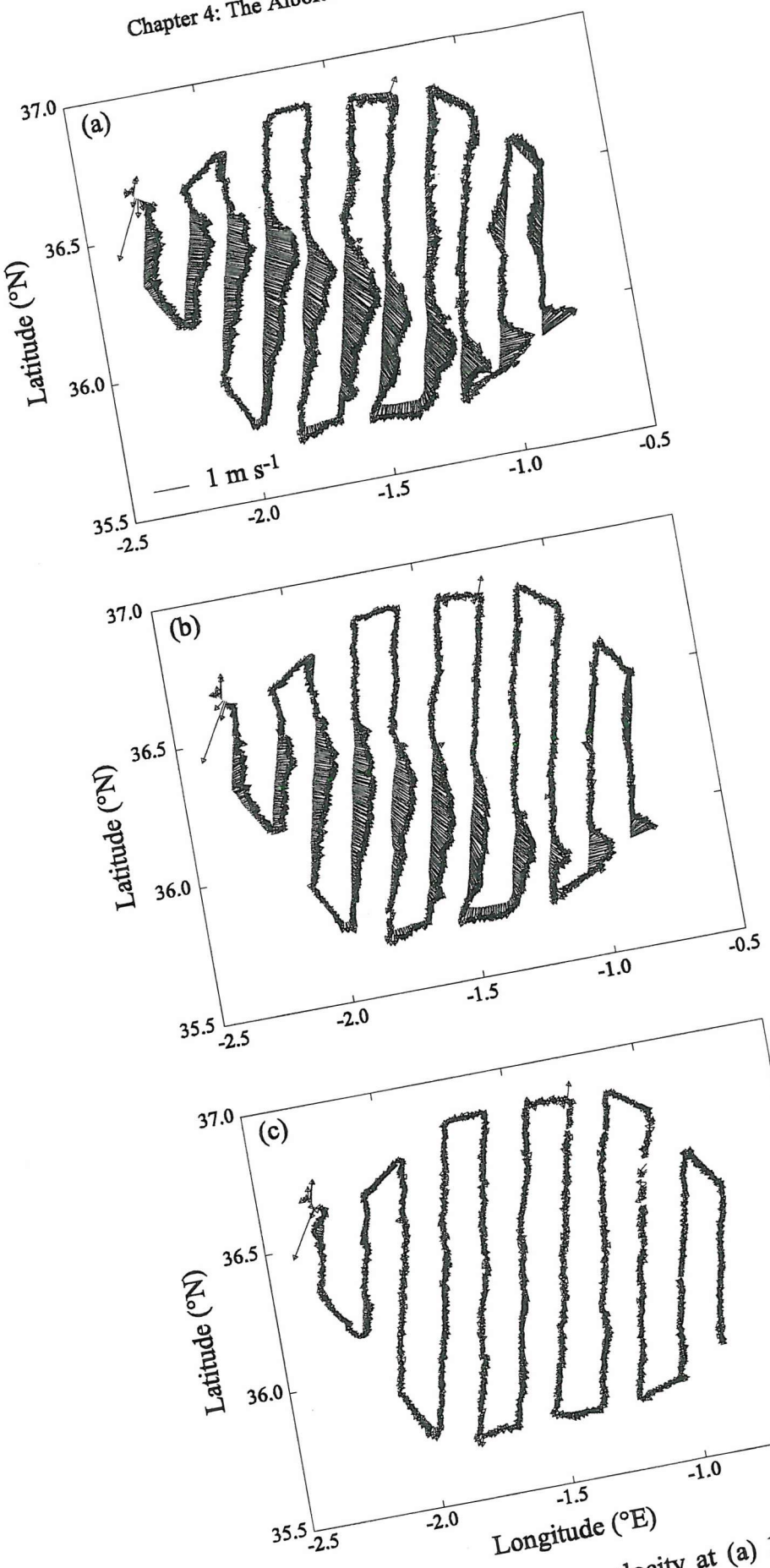

Figure 4.2.5. Maps of VM-ADCP derived current velocity at (a) 14 m, (b) 54 m and (c) 150 m depth for FSS1.

4.2.4 The vertical structure of the AOF

Vertical hydrographic sections, from SeaSoar CTD data, across the Almeria-Oran front (Figure 4.2.6) exhibit a temperature, salinity and density structure typical of the front, with a steep gradient in isotherms, isohalines and isopycnals sloping sharply upwards and breaking the surface. On the western side of the front the high temperature low salinity signature of (MAW), present in the Eastern Alboran Gyre (EAG), was observed down to depths of ~200 m. The mixed layer depth decreased from west to east across the front from ~150 m to ~ 50 m on the Mediterranean side. Below the surface waters was the TML and below that, the high salinity low temperature signature of LIW.

The slope of the density surfaces, across the front, changed with time and position along the front. Along Leg e the front moved south and steepened between FSS1 and FSS2, and then moved back northwards between FSS2 and FSS3. During FSS3 the front was shallower than FSS1 (Figure 4.2.7). For future reference, the 27.9 isopycnal surface has been chosen to represent the "path" of the front (depicted in yellow in Figure 4.2.7) separating the EAG from MSW and is typically the water referred to as AMIW.

4.2.5 Subduction at the AOF

Through the examination of θ/S envelopes from each of the FineScale Surveys (Figure 4.2.8), the presence of MSW within the survey area was found only in FSS 2 and 3. The appearance and distribution of MSW within the survey area can be followed by plotting salinity on the 27.9 σ_0 surface (Figure 4.2.9). During FSS2 MSW was observed at the surface off the coast of Spain, whereas during FSS3 MSW was clearly observed at the southern end (off the coast of Algeria) of three SeaSoar legs (*h*, *I*, and *j*) at depths of up to 150 m. As the duration of each SeaSoar survey was 4 days with 1 day between each survey, it implies that MSW was drawn down the front at mean vertical velocities of at least 25 m d^{-1}.

4.2.6 Discussion of the hydrography at the AOF

The AOF front forms where waters of Atlantic origin meet Mediterranean surface waters in the Alboran Sea, and its shape and position are variable on a time scale of days. In this study the AOF was found in its usual position as the eastern boundary of the eastern of two Alboran gyres, the Eastern Alboran Gyre (Tintore *et al.*, 1988; Folkard *et al.*, 1994; Prieur and Sournia, 1994). Within the Eastern Alboran Gyre, associated with the AOF, is a strong frontal jet with a speed of ~1 m s^{-1}. This frontal jet exits the Eastern Alboran Gyre off the North African Coast, forming the Algerian Current. The observations of the movement of the surface signature of the front south and back north, and the change in slope of the density surfaces across the front between the surveys are

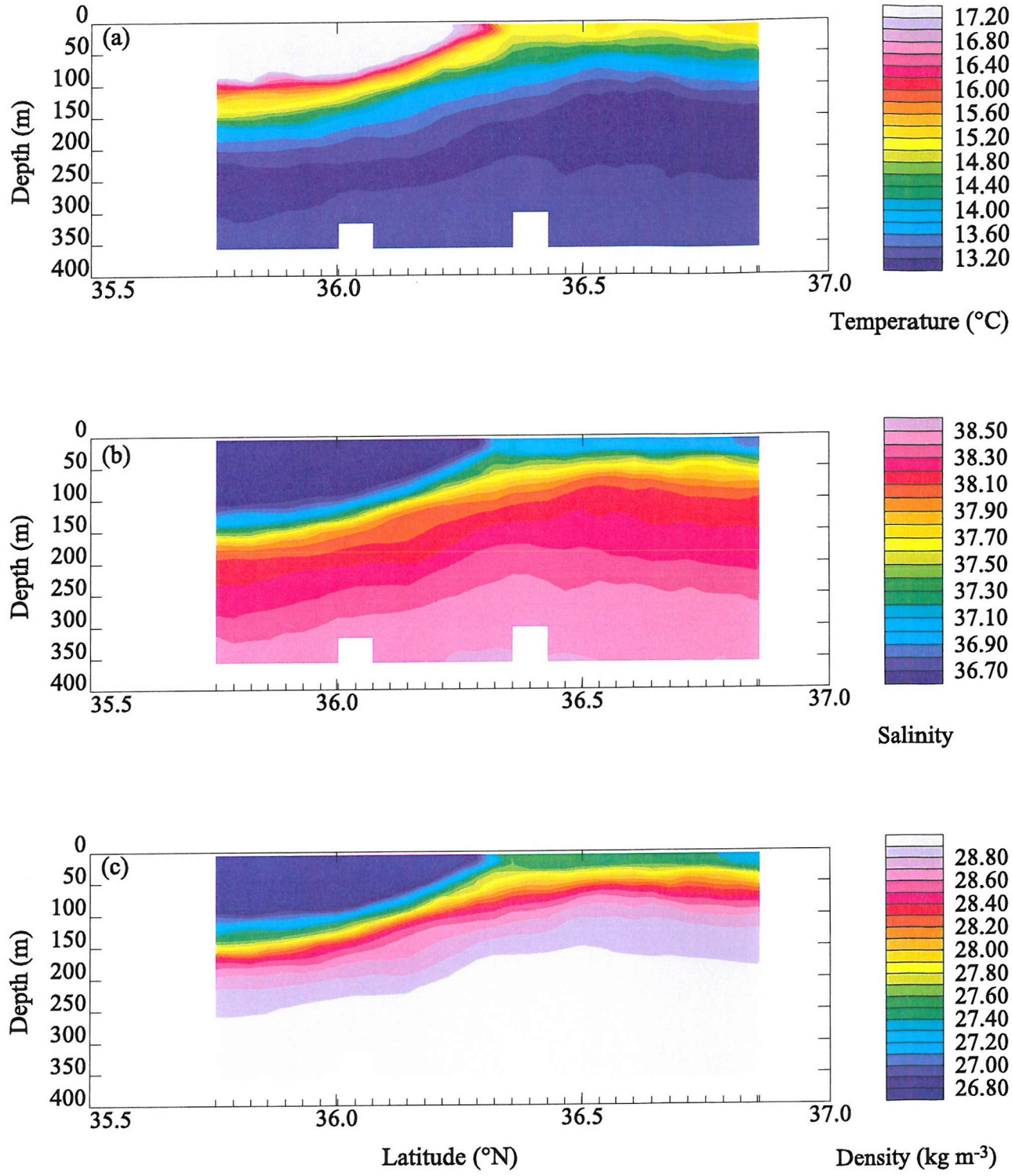

Figure 4.2.6. Contoured sections of (a) temperature, (b) salinity and (c) density for leg e of FSS1.

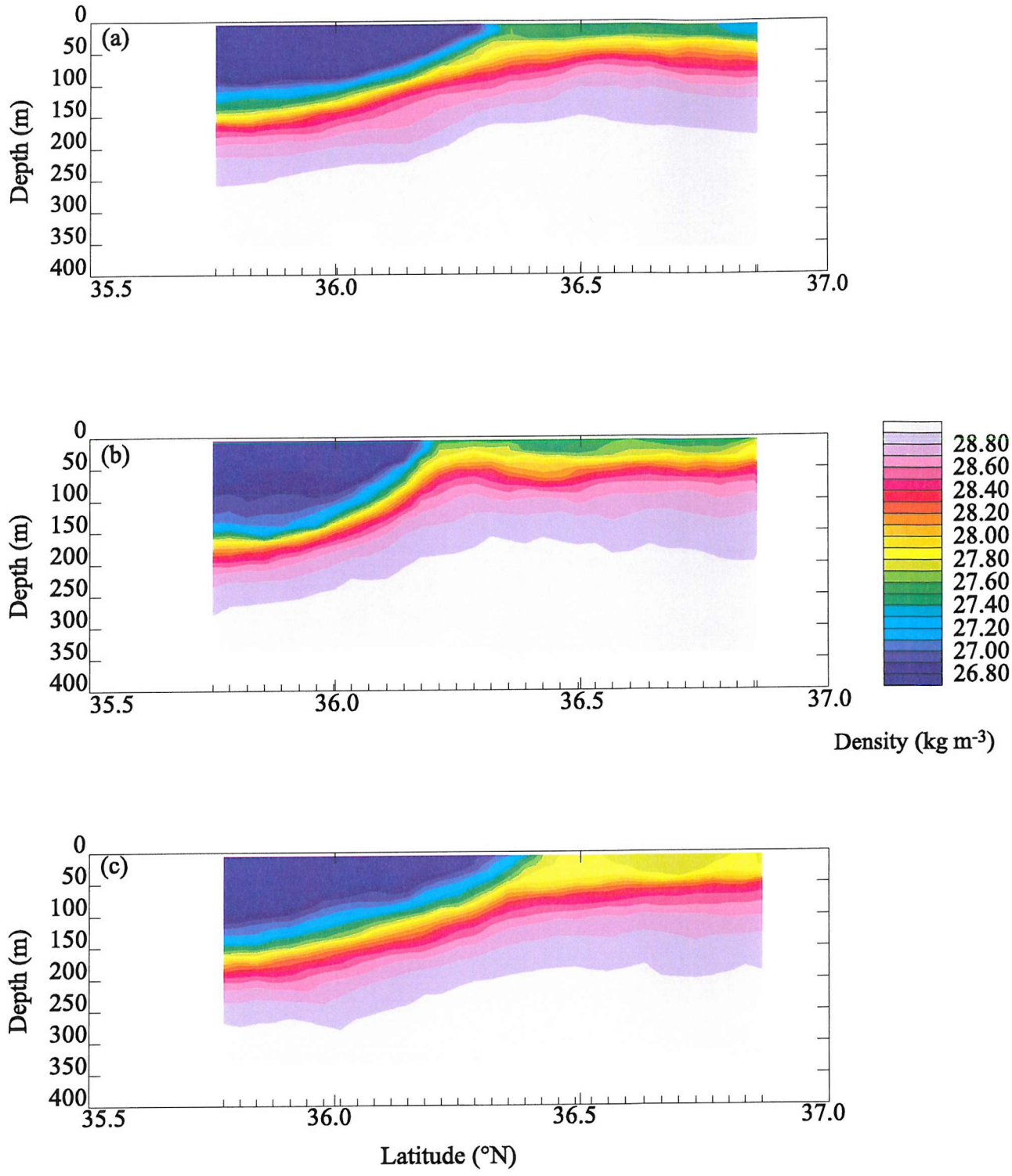

Figure 4.2.7. Contoured sections of density for leg e of (a) FSS1, (b) FSS2 and (c) FSS3.

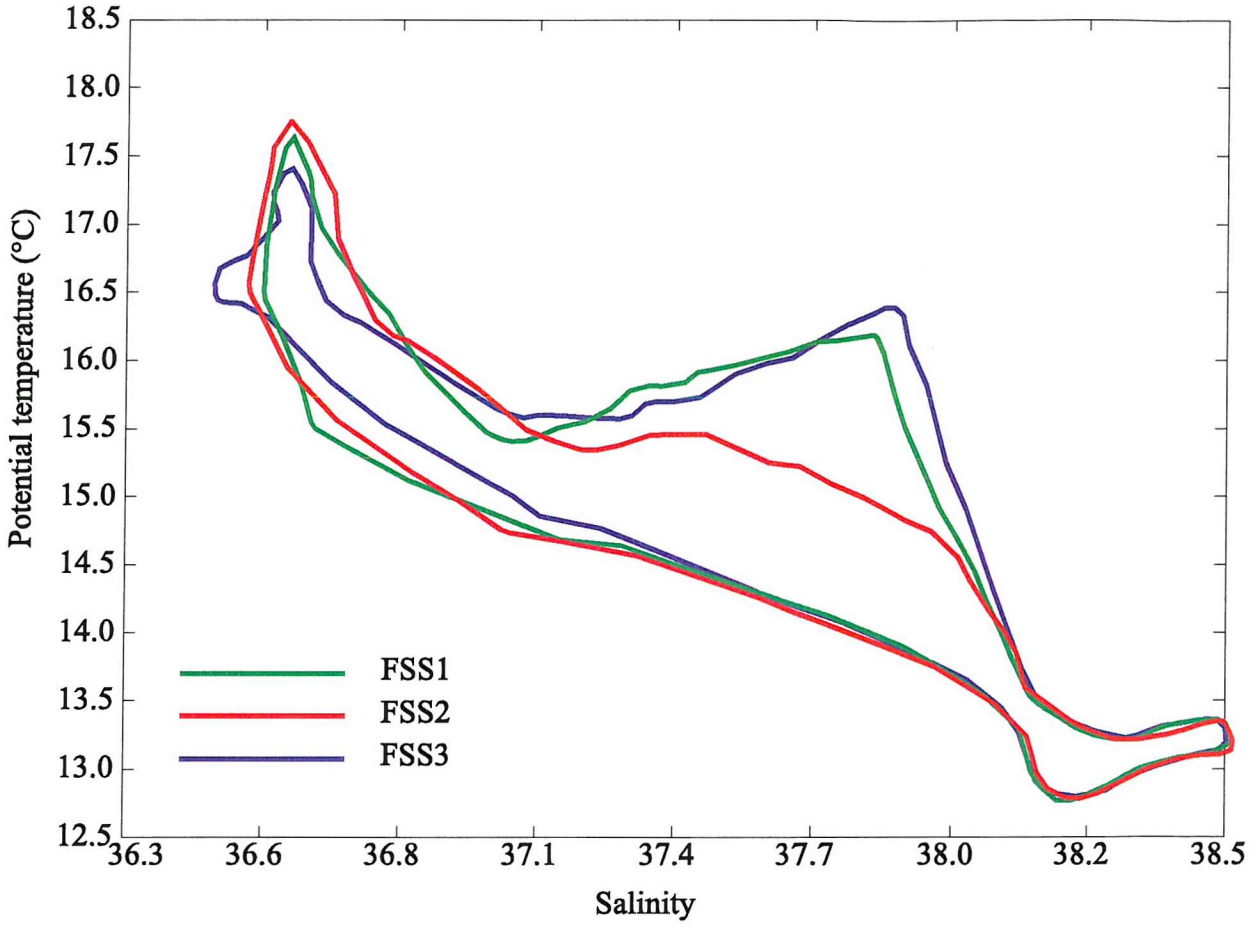

Figure 4.2.8. Envelopes of potential temperature as a function of salinity for FSS1, FSS2 and FSS3.

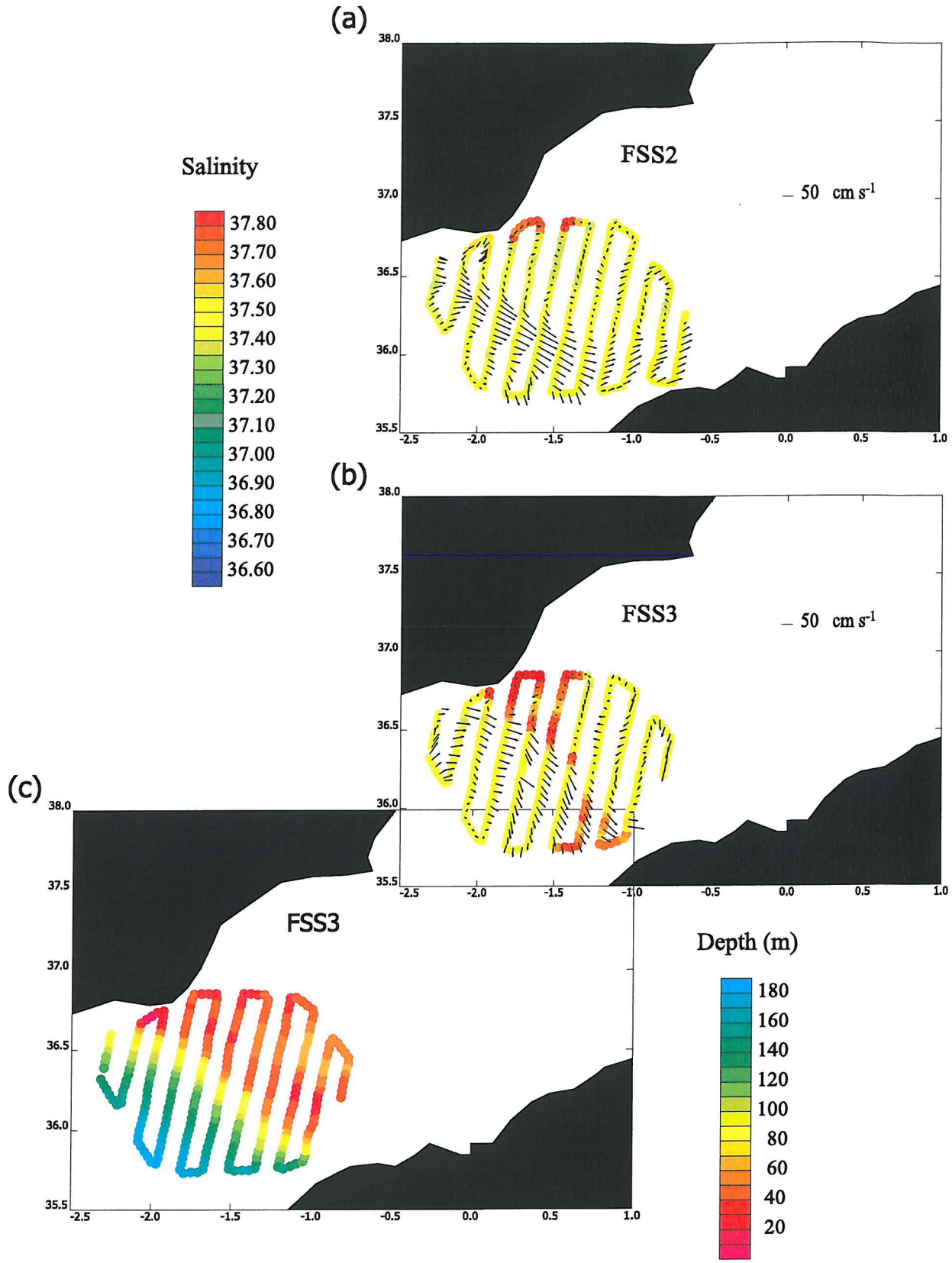

Figure 4.2.9 Salinity (coloured dots) on the density surface σ_0 = 27.9 and VM-ADCP derived current velocity vectors at 54 m depth for (a) FSS2 and (b) FSS3. The depth of the density surface σ_0 = 27.9 is identified in (c). From Allen *et al.*, 2001.

consistent with baroclinic instability and propogation of wavelike meanders across the front (Allen *et al.*, 2001). Hence as Prieur and Sournia (1994) surmised, the AOF has a primary geostrophic circulation with secondary ageostrophic components.

The analysis of temperature and salinity on density surfaces showed MSW advecting westwards along the Spanish Coast until it reached the AOF. At this point, MSW became entrained into the frontal jet and advected with MAW along the front. The repeat surveys showed that instability of the front caused subduction of water down and across the front at an observed subduction rate of ~25 m d^{-1}. This subduction is known to result from the significant baroclinic component to the instability of the frontal jet (Allen *et al.*, 2001). Previous authors have used a knowledge of the density fields and the Q-vector form of the omega equation to diagnose quantitatively the vertical transport resulting from the mesoscale ageostrophic circulation and found it to be similar (15 m d^{-1}, Viudez *et al.*, 1996; 20-25 m d^{-1}, Allen *et al.*, 2001). Vertical velocities of this magnitude associated with baroclinic instabilities are consistent with other studies (Pinot *et al.*, 1996; Nurser and Zhang, 2000).

4.3 The distribution of phytoplankton and nutrients at the AOF during cruise D224

4.3.1 The horizontal distribution of phytoplankton at the AOF

The surface distribution of chlorophyll *a* concentration (a proxy for phytoplankton biomass), measured from the underway water surface sampler, showed no obvious increase concurrent with the position of the surface of the AOF, throughout all three surveys (Figure 4.3.1). Highest surface chlorophyll concentrations (>4.10 mg m^{-3}) were recorded in FSS1 in the Northwest of the survey area. During FSS2 chlorophyll concentration had decreased and was near-uniformly distributed throughout the survey area. The lowest values of chlorophyll concentration (<1.7 mg m^{-3}) were observed at the northern edge of the survey area in FSS3, although chlorophyll concentration elsewhere was increasing compared with FSS2 but had not returned to the levels observed in FSS1.

Chlorophyll concentration plotted as a third variable on a θ/S diagram for each survey exhibits the difference in concentration between frontal and surrounding waters in FSS1 and FSS3 and indicates there is also a difference in FSS2 (Figure 4.3.2). With lower chlorophyll concentration within MAW (~2.90, 2.30 and ~2.30 mg m^{-3}), and higher concentration in the AMIW (~3.50, 3.10 and ~2.90 mg m^{-3}) in FSS1, FSS2 and FSS3 (values respectively). In all surveys the lowest salinity waters (typically LIW) also contain

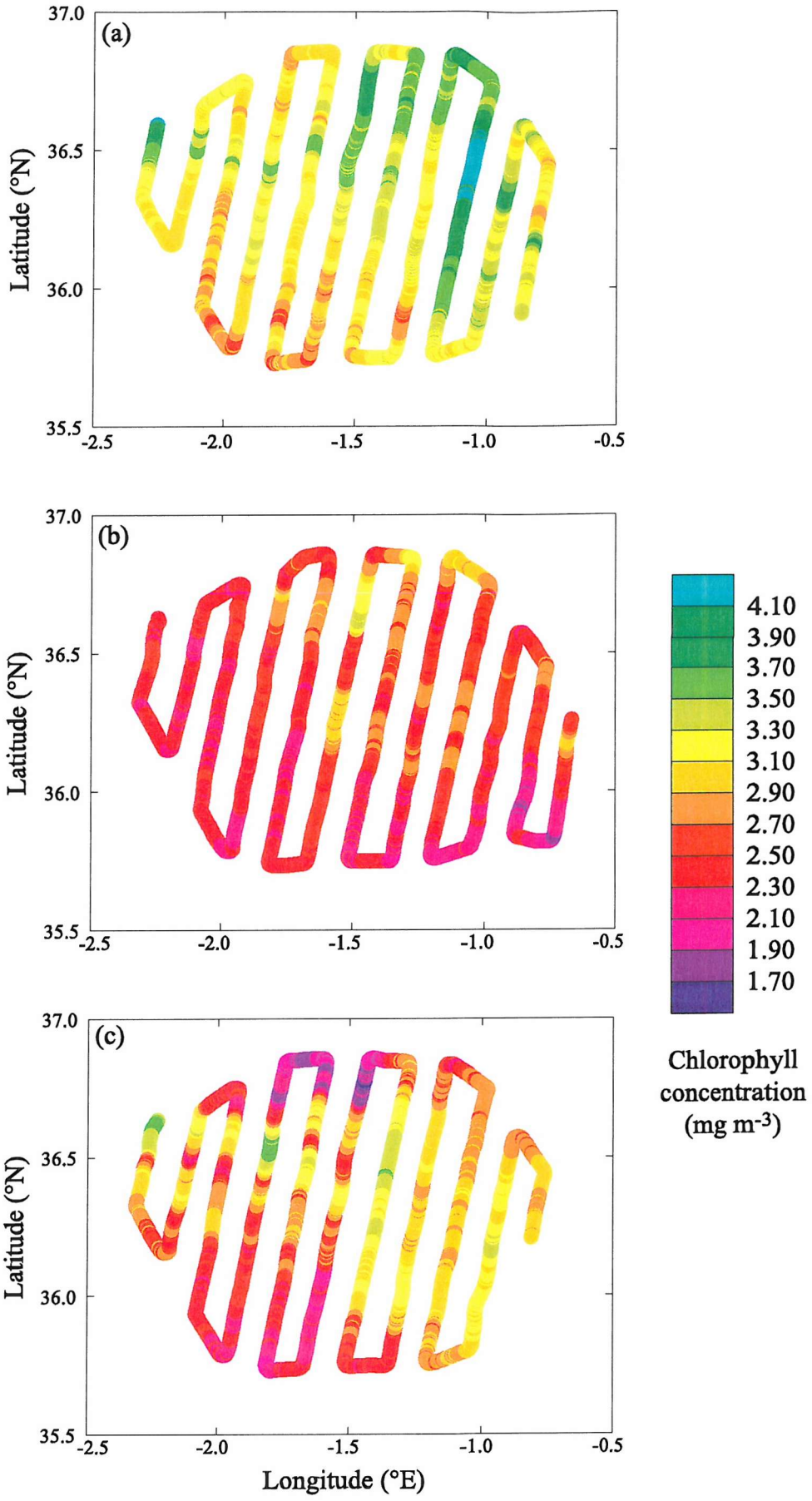

Figure 4.3.1. Maps of surface chlorophyll concentration (mg m^{-3}) for (a) FSS1, (b) FSS2 and (c) FSS3 measured from the underway water source.

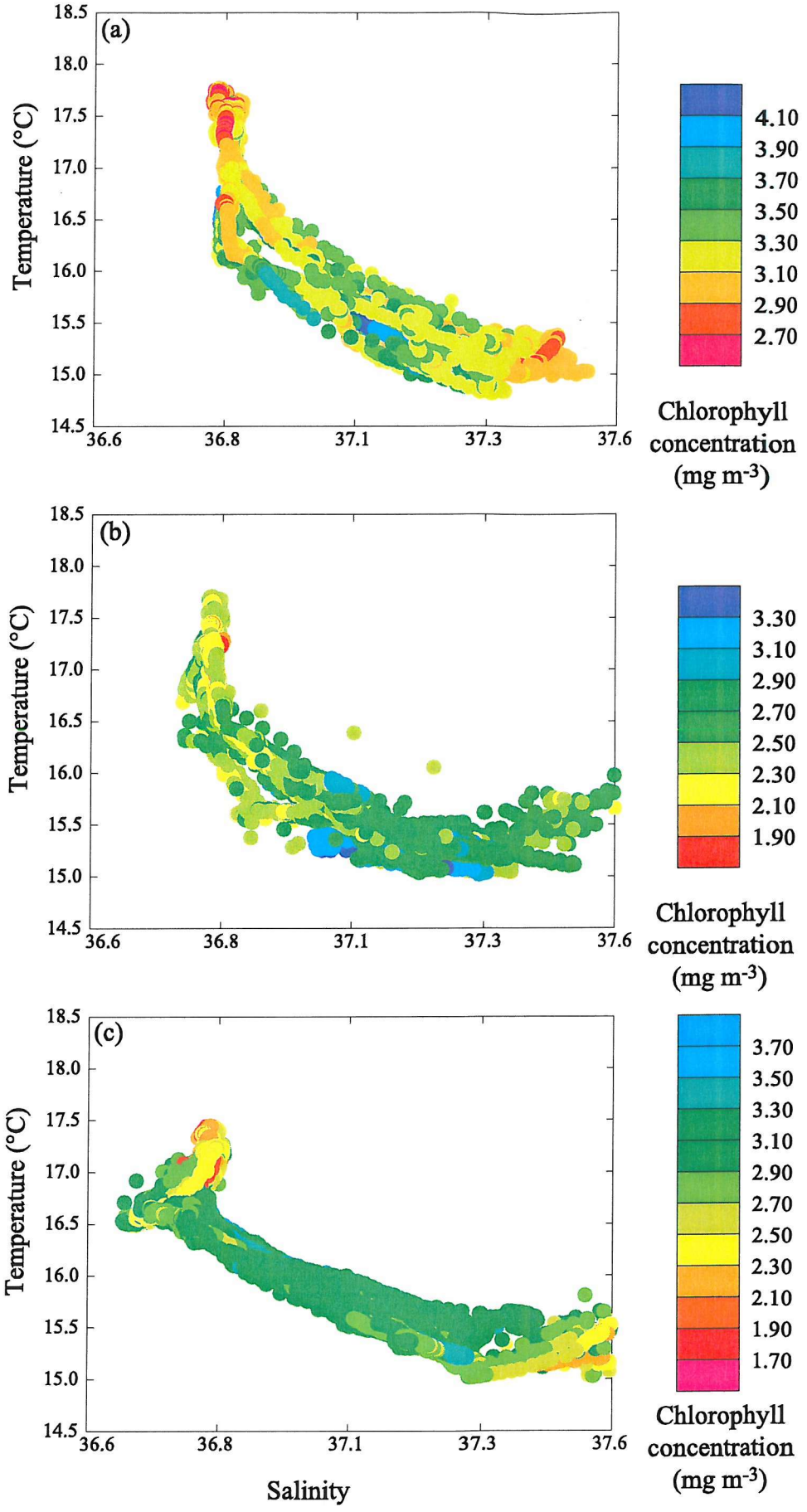

Figure 4.3.2. Potential temperature plotted as a function of salinity, colour-coded for the chlorophyll concentration of each sample for (a) FSS1, (b) FSS2 and (c) FSS3.

low chlorophyll concentration. Lower chlorophyll concentrations also occurred in waters with properties similar to MSW.

Integrated chlorophyll concentration (Σchl) was estimated from SeaSoar fluorescence measurements. ΣChl *a* was estimated to 50 (Σchl_{50}), 150 (Σchl_{150}) and 250 m (Σchl_{250}) for each of the three surveys (Figure 4.3.3). Fifty metres was chosen because it represented the depth of the mixed layer on the Mediterranean side of the front. The depth of 150 m was chosen because it represented the mixed layer depth within the EAG. In addition, it allowed the data to be compared with the ALMOFRONT-1 dataset (Prieur *et al.*, 1993; Videau *et al.*, 1994), and 250 m was identified as the depth below which chlorophyll was not observed.

In FSS1, high Σchl_{50} occurred only in the Northwest of the survey area, with surrounding water containing less than half the concentration (~75 and ~25 mg m^{-2} respectively). When chlorophyll concentration was integrated over 150 and 250 m, the front was clearly identified by higher chlorophyll values than surrounding waters (Figure 4.3.3d,h), with highest values occurring in the north-west of the survey area off the coast of Almeria. One area, in the Southeast of the survey area on the EAG side of the front, showed an increase in Σchl_{250} concentration not seen in Σchl_{50}. This region is close to the coast of Algeria, near Oran.

During FSS2 there was no coherent structure to the distribution of integrated chlorophyll concentration that could be related to the position of the AOF (Figure 4.3.3b,e,h). The most notable feature was that Σchl_{50} contained typically only a third of the chlorophyll concentration of the total water column (Σchl_{50} = 20 mg m^{-2} compared with Σchl_{250} 65 mg m^{-2}). Similar to the surface chlorophyll concentration (see above), the integrated chlorophyll concentration was uniformly distributed over the survey area.

Integrated chlorophyll concentration from FSS3 exhibits the lowest values throughout the 3 surveys (Figure 4.3.3c,f,i), with no coherent structure related to the AOF. Similar to FSS1 there was a high in Σchl_{250} off the coast of Algeria, in the Southeast of the survey area, which did not appear in Σchl_{50}, indicating phytoplankton were present below 50 m.

4.3.2 The vertical distribution of phytoplankton at the AOF

The vertical distribution of fluorescence plotted from leg e of each survey indicated that phytoplankton were present throughout the mixed layer, with no distinct sub-surface maximum (Figure 4.3.4). In FSS1 the vertical extent of the fluorescence was limited to within the euphotic zone (0.1 W m^2 isolume depth = ~100 m) on both sides of

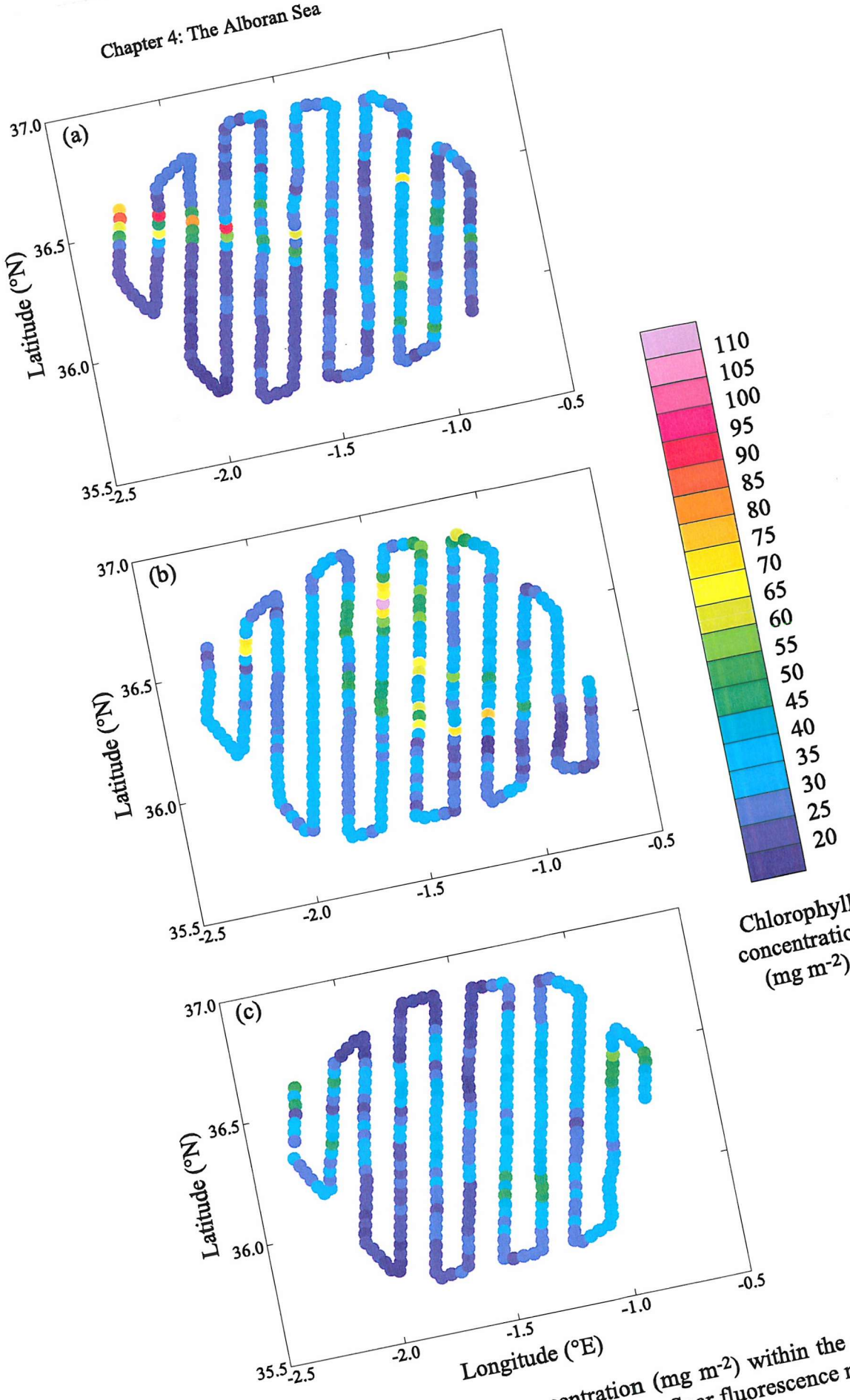

Figure 4.3.3a-c Maps of integrated chlorophyll concentration (mg m^{-2}) within the surface 50 m (Σchl_{50}) for (a) FSS1, (b) FSS2 and (c) FSS3 calculated from SeaSoar fluorescence measurements.

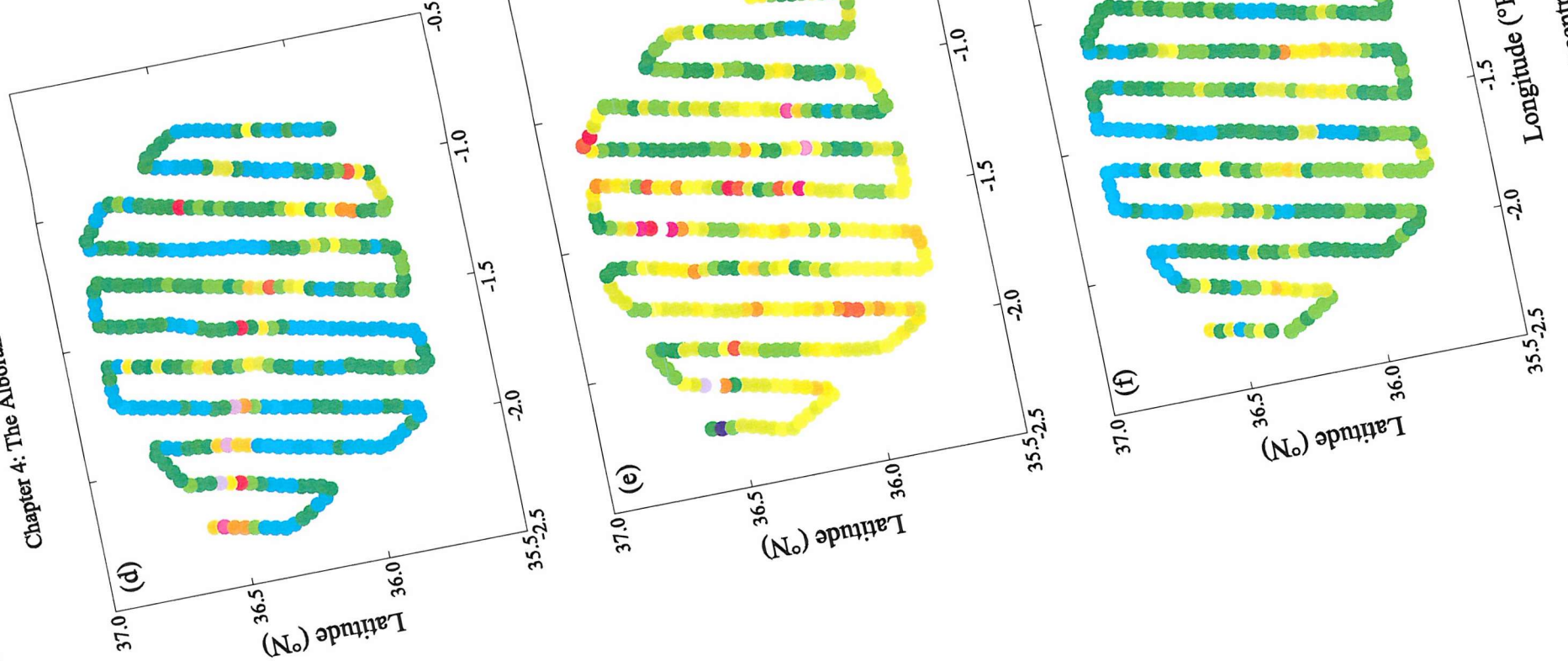

Figure 4.3.3d-f Maps of integrated chlorophyll concentration (mg m^{-2}) within the surface 150 m (Σchl_{150}) for (d) FSS1, (e) FSS2 and (f) FSS3 calculated from SeaSoar fluorescence measurements.

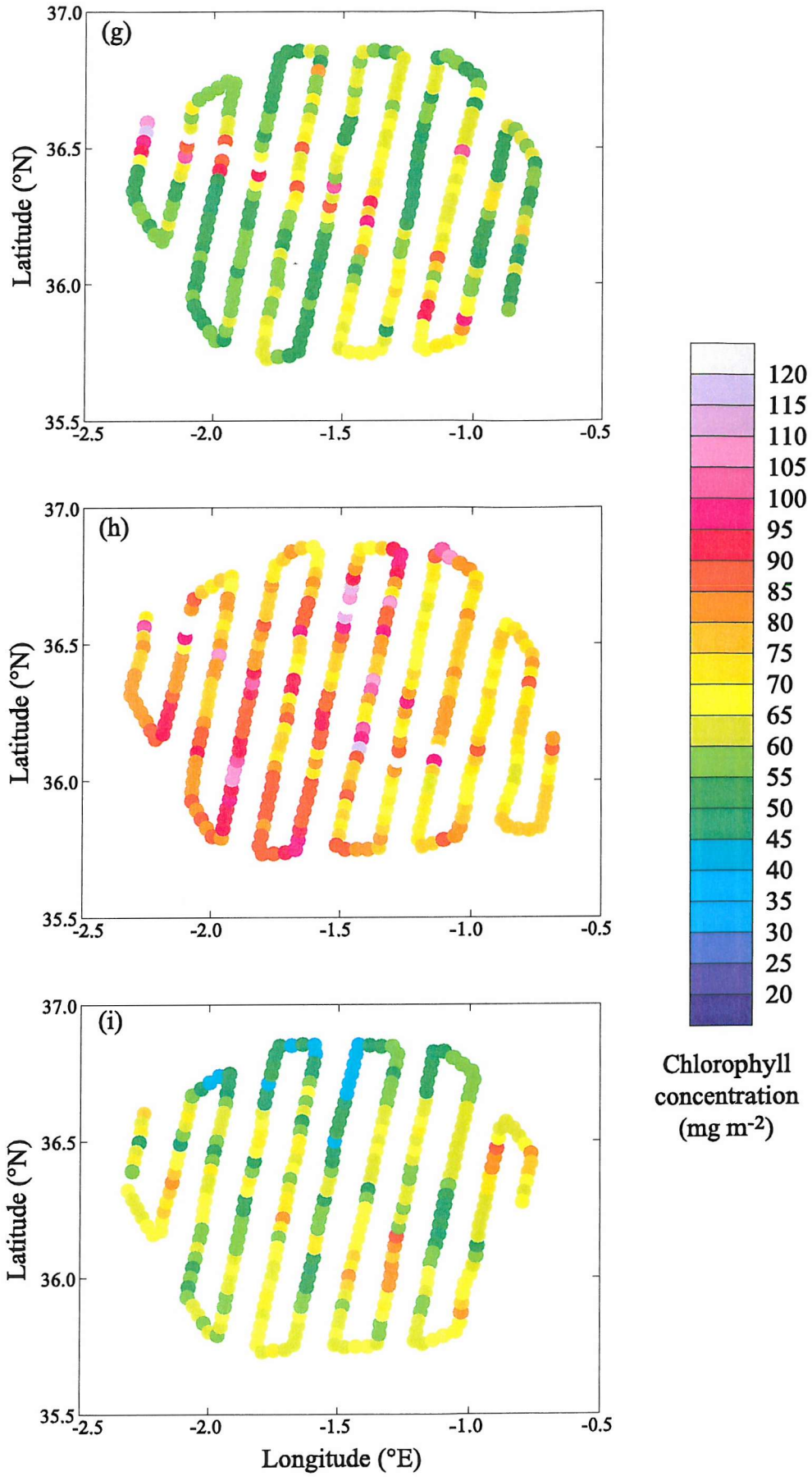

Figure 4.3.3g-i Maps of integrated chlorophyll concentration (mg m^{-2}) within the surface 250 m (Σchl_{250}) for (g) FSS1, (h) FSS2 and (i) FSS3 calculated from SeaSoar fluorescence measurements.

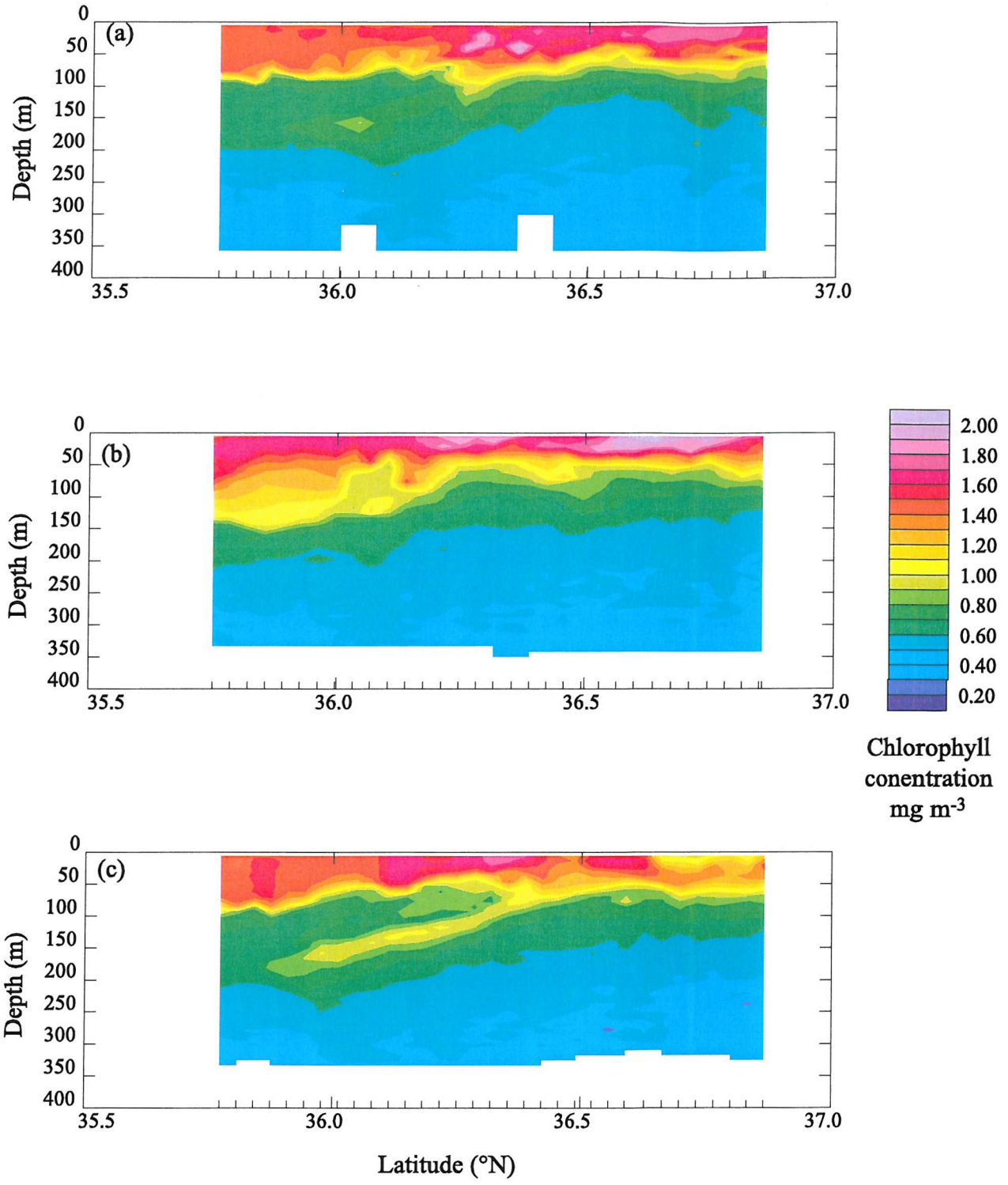

Figure 4.3.4 Contoured sections of chlorophyll a concentration for leg e of (a) FSS1, (b) FSS2 and (c) FSS3.

the front, with higher fluorescence values at and northeast of the surface front. Below the euphotic zone a small increase in fluorescence occurred along the frontal isopycnal (27.9 σ_0). In FSS2 the depth at which fluorescence was observed deepened to ~150 m within the EAG, whilst remaining within the euphotic zone east of the front. As with FSS1, there were higher fluorescence values east of the front. In leg e of FSS3 this situation had reversed, whilst high fluorescence values were still observed at the front, east of the front fluorescence values had decreased such that they were lower than within the EAG (which did not vary significantly between FSS1, 2 and 3). During FSS3 distinct tongues of fluorescence were observed lying between the 27.4 and 28.4 σ_0 isopycnals at the bottom of the thermocline, under the surface waters of the EAG and extending to depths of ~200 m (Figure 4.3.4c).

4.3.3 Finescale vertical structure of fluorescence and nutrients across the AOF

Five CTD stations across the AOF, taken between FSS1 and FSS2, were used to examine the finescale vertical distribution of fluorescence and nutrients. Station 13038 was within the EAG, whilst Station 13041 was on the eastern Mediterranean side of the front. An easterly shoaling of isotherms and isohalines was apparent, reflecting the position of the front, the depth of the thermocline increasing from ~100 m to ~50 m east of the front. The nitracline shelved from 50-100 m on the Alboran Gyre side of the front to 30-50 m on the Mediterranean side, following the change in mixed layer depth. Surface values of nitrate were typically ~1 μmol l^{-1}: below the nitracline, at 300 m depth, the nitrate concentration increased to ~8 μmol l^{-1} (Figure 4.3.5). Silicate and phosphate profiles showed similar distributions, with surface values of ~0.8 and 0.05 μmol l^{-1} and concentrations of ~7.9 and 0.41 μmol l^{-1} at ~400 m. The profile of phosphate at Station 13039 showed an erratic distribution with depth that was not reflected in the nitrate and silicate profiles. This may have resulted from analysis error or contamination of the phosphate samples; problems associated with the phosphate sensor of the autoanalyser were documented in the cruise report (Allen and Guymer, 1997).

Vertical profiles of fluorescence yield from 5 CTD stations, carried out across the front between FSS1 and FSS2 showed that phytoplankton were typically uniformly distributed above the nitracline, which was at a similar depth to the thermocline (Figure 4.3.5). Surface values of fluorescence were comparable at each of the five CTD stations, although fluorescence yield indicates that chlorophyll was present to greater depths at CTD station 13037 than at more easterly stations.

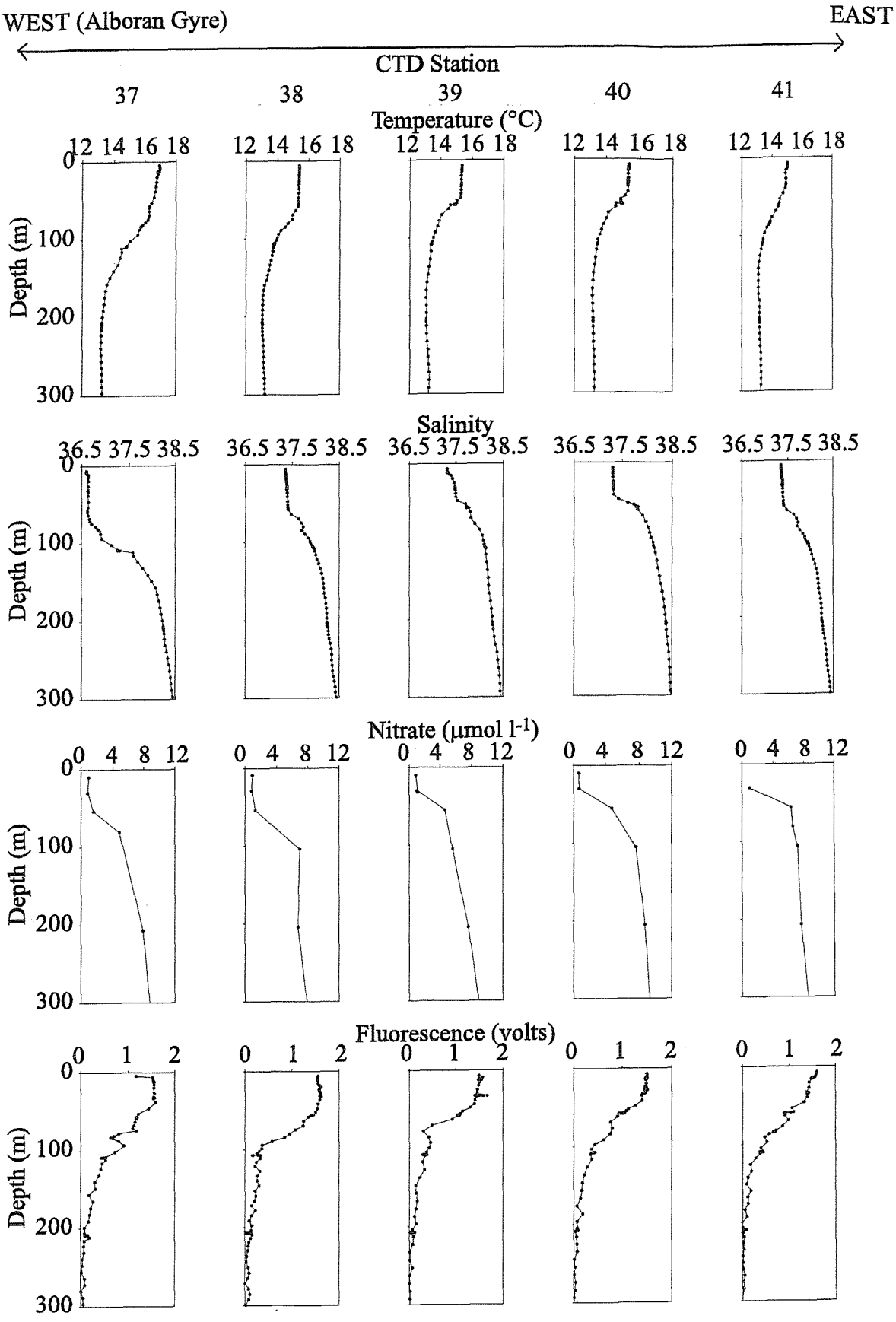

Figure 4.3.5 The vertical distribution of temperature (top), salinity (middle top), nitrate concentration (bottom middle) and fluorescence yield (bottom) from CTD stations 13037 - 13041 across the Almeria-Oran front (from west to east).

4.3.4 Discussion of the distribution of phytoplankton and nutrients at the AOF

Concurrent measurements of chlorophyll concentration (a proxy for phytoplankton biomass) and hydrography indicate that the AOF influenced the distribution and biomass of phytoplankton during OMEGA. These observations showed that: on occasion the front appeared to act as a barrier between Mediterranean waters that contained high surface phytoplankton biomass and the EAG that contained lower biomass; the horizontal distribution of surface and integrated phytoplankton biomass provided evidence to suggest frontal enhancement of phytoplankton biomass at the AOF; phytoplankton were observed periodically in a layer along the frontal isopycnal to depths of 200 m; and ultimately that, similar to the physics, the surface and integrated phytoplankton distributions were variable on a time scale of days. These findings will be discussed individually in greater detail below, but should not be deemed mutually exclusive. In fact, the observation of frontal enhancement of phytoplankton biomass is possibly the most important result, but is not discussed first because it draws on the conclusions of the other observations.

i) A gradient in phytoplankton biomass was observed crossing the front from west to east

The idea that fronts separate different water masses, and hence different plankton populations is well established (Sournia, 1994). In this case, the horizontal maps show that the surface chlorophyll concentration was up to 1 mg m^{-3} higher in the waters of Mediterranean origin, north east of the front, than in Atlantic waters within the EAG. From these surface maps, especially during FSS1 and FSS2, the AOF seemed to present a barrier between the surprisingly more productive Mediterranean waters (typically classified as oligotrophic, e.g. Estrada *et al.*, 1999) and the waters of Atlantic origin. From FSS1 to FSS2 the chlorophyll concentration at the surface reduced by up to a half. This was most likely a result of a storm-induced mixing event (Figure 4.3.6) that took place towards the end of FSS1, removing phytoplankton from the surface layer. During FSS3 surface chlorophyll concentration was highest within the frontal region, up to twice as high as within the EAG, implying a form of frontal enhancement.

ii) Enhanced phytoplankton biomass was observed at the front

Higher surface phytoplankton standing stocks within fronts compared with surrounding water has been widely reported (Savidge, 1976; Pingree *et al.*, 1978; Simpson *et al.*, 1979; Beardall *et al.*, 1982), leading to the notion of frontal enhancement (Le Fevre, 1986; Olson 2002). Whilst implied for FSS3, the surface chlorophyll values from each finescale survey (Figure 4.3.1) did not provide conclusive evidence of frontal enhancement of phytoplankton biomass. However Pingree *et al.* (1978) found subsurface high phytoplankton biomass at fronts, associated with the thermocline.

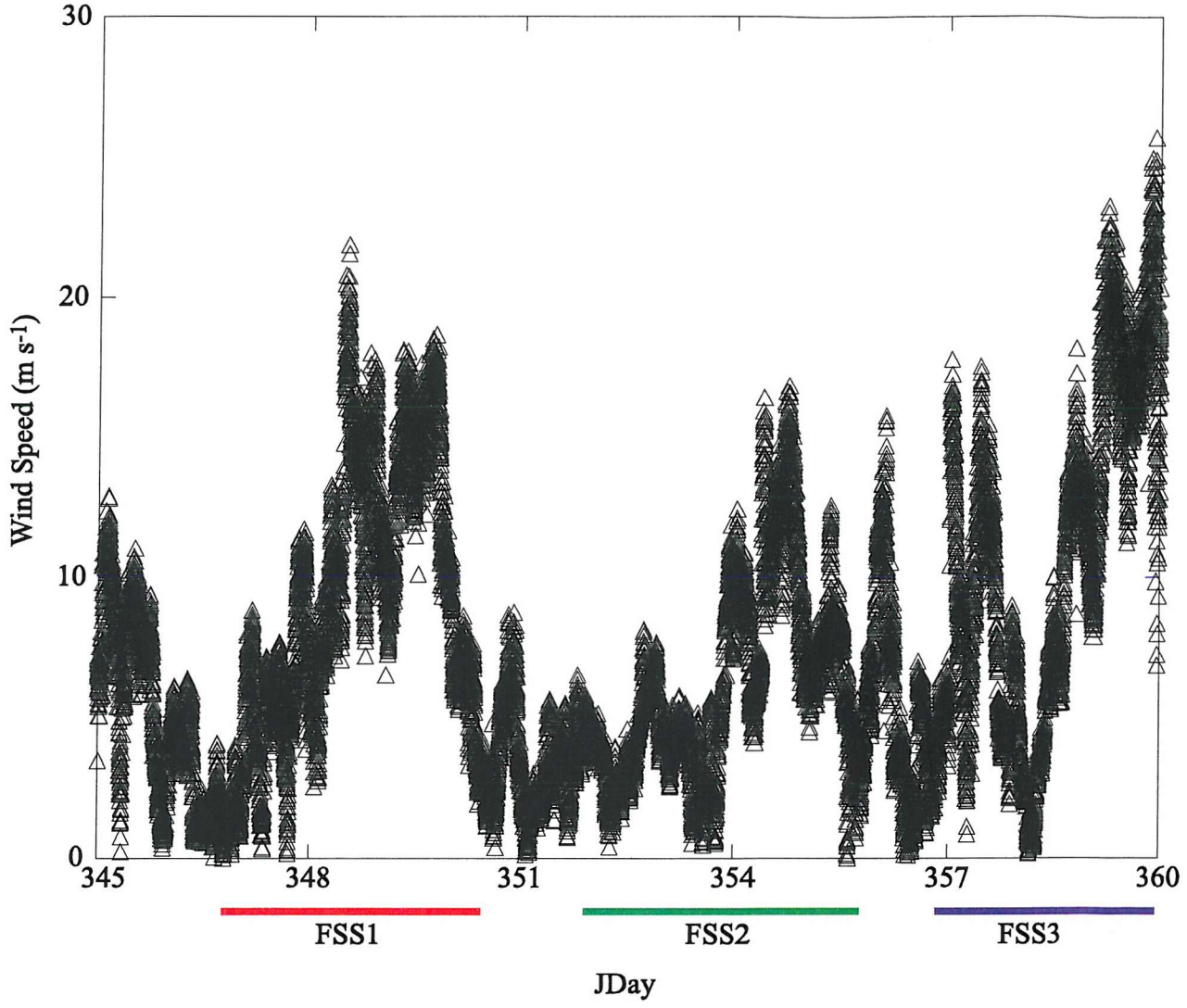

Figure 4.3.6 Wind speed during the three finescale surveys. The duration and timing of each finescale survey is identified.

On examination of the integrated chlorophyll concentrations at Σchl_{50}, Σchl_{150} and Σchl_{250} the surface position of the front could be easily identified by an increase in chlorophyll concentration compared with surrounding waters in FSS1. This distribution was similar to that observed by Prieur *et al.* (1993) and values of Σchl_{150} were comparable (60 - 100 mg m^{-2}, Prieur *et al.*, 1993; 60 - 120 mg m^{-2}, this study). For Σchl_{50} this higher chlorophyll concentration was only noticeable in the north west of the survey area. When integration was extended to 250 m this extended to the south east (Figure 4.3.3d,g). These observations suggest that there was a Subsurface Chlorophyll Maximum (SCM) or that phytoplankton were present at depth. Contour plots of the SeaSoar legs and the greater detail CTD stations do not exhibit an obvious SCM, although a shadow of higher fluorescence concurrent with the path of the front can be seen on Figure 4.3.4a. This pattern of frontal enhancement of integrated phytoplankton biomass was not observed in FSS2 or FSS3. The storm event mentioned previously is presumed to have increased mixing, disrupting the signal in FSS2 (Figure 4.3.5). This would also account for the general increase in chlorophyll concentration observed throughout the survey region in FSS2 (Figure 4.3.3) and within the mixed layer (Figure 4.3.4), where mixing would bring nutrients to the surface.

However, the lack of a high frontal productivity signal in FSS3 is perhaps more surprising. An obvious layer of enhanced phytoplankton biomass was observed in vertical contours of fluorescence data in FSS3 (Figure 4.3.4c), that may have been responsible for the signal of frontal enhancement in FSS1. It could be proposed that measurements of Σchl_{250} should also have exhibited a higher chlorophyll concentration along the front in FSS3, perhaps diluted by the significant across-front subduction (see below). The mechanisms and processes that control the origin and position of the SCM and typical frontal enhancement patterns are similar; either accumulation (Franks, 1992), or *in situ* activated population growth through increased nutrient availability and suitable light conditions (Simpson *et al.*, 1979; Le Fevre, 1986). Without investigations into the photoadaptive ability of the phytoplankton or speciation, that would indicate the origin of the phytoplankton (e.g. Latasa *et al.*, 1998), neither of these mechanisms can be discarded as the formation process governing the observed frontal enhancement in FSS1. The ALMOFRONT-1 study indicated the occurrence of frontal enrichment with subsequent downwelling within the Almeria-Oran front region (Fiala *et al.*, 1994; Thibault *et al.*, 1994; Videau *et al.*, 1994). However the lack of observed frontal enhancement in FSS3 and the speed of the frontal jet, which is fast enough to transport phytoplankton through the survey region in ~3 days (Allen *et al.*, 2001; Fielding *et al.*, 2001), may, in this case,

indicate a third mechanism for the integrated chlorophyll distribution observed in FSS1. Where a patch of high phytoplankton biomass, possibly originating from a productive coastal upwelling region north east of the survey area (Tintore *et al.*, 1991) could be entrained into the fast-flowing jet associated with both the EAG and the front, and advected through the survey region. Overlaying the map of VM-ADCP derived current velocity at 14 m depth on the map of Σchl_{150} shows that the highest values of Σchl_{150} lie within the fast frontal jet (Figure 4.3.7) supporting this supposition.

The vertical distribution of phytoplankton plays a major role in understanding the differences between the surface and integrated chlorophyll concentrations reported above. Fluorescence signals indicate that phytoplankton were present throughout the mixed layer in the survey area with no distinct subsurface chlorophyll maximum. This contrasts with previous work, including the ALMOFRONT-1 study, where a distinct chlorophyll maximum was identified at the depth of the nitracline (DePalma *et al.*, 1987; Videau *et al.*, 1994). In the present study the nitracline coincided with the thermocline at the bottom of the mixed layer, but the surface values of ~ 1 $\mu mol\ l^{-1}$ do not indicate severe nitrogen depletion. The nitrate concentrations reported in this study agreed with previously reported values (Bianchi *et al.*, 1994). In both the OMEGA and ALMOFRONT studies the nitracline shoaled across the AOF from Atlantic waters to Mediterranean waters, although its depth was shallower during the ALMOFRONT-1 study (18-30 m at the front, Videau *et al.*, 1994 compared with 30-50 m, this study). The deeper nitracline and more depth-independent fluorescence signal in the surface layers may be a seasonally dependent observation resulting from the entrainment of deeper waters through enhanced winter overturning.

iii) Phytoplankton was subducted down frontal isopycnals to a depth of ~200 m

In a significant number of the FSS3 legs distinct signatures of phytoplankton biomass below the euphotic zone, lying concurrent with the frontal isopycnal, were observed. High fluorescence was observed in layers coincident with the density surfaces ~27.4 - 28.4 extending to depths of up to 200 m, below the nitracline, euphotic zone and overlying Modified Atlantic Waters (MAW). This deep fluorescence maximum occurred coincidentally with the period of subduction of Mediterranean Surface Waters (MSW) discussed in Section 4.2. Phytoplankton will be rapidly advected along the front by the frontal jet (up to 1 $m\ s^{-1}$). Ageostrophic cross-front and vertical motion associated with periodic mesoscale instability of the front will result in a downward and cross-front secondary transport of phytoplankton. Lohrenz *et al.*, (1988) previously observed chlorophyll maxima occurring along isopycnals on the Mediterranean side of the front.

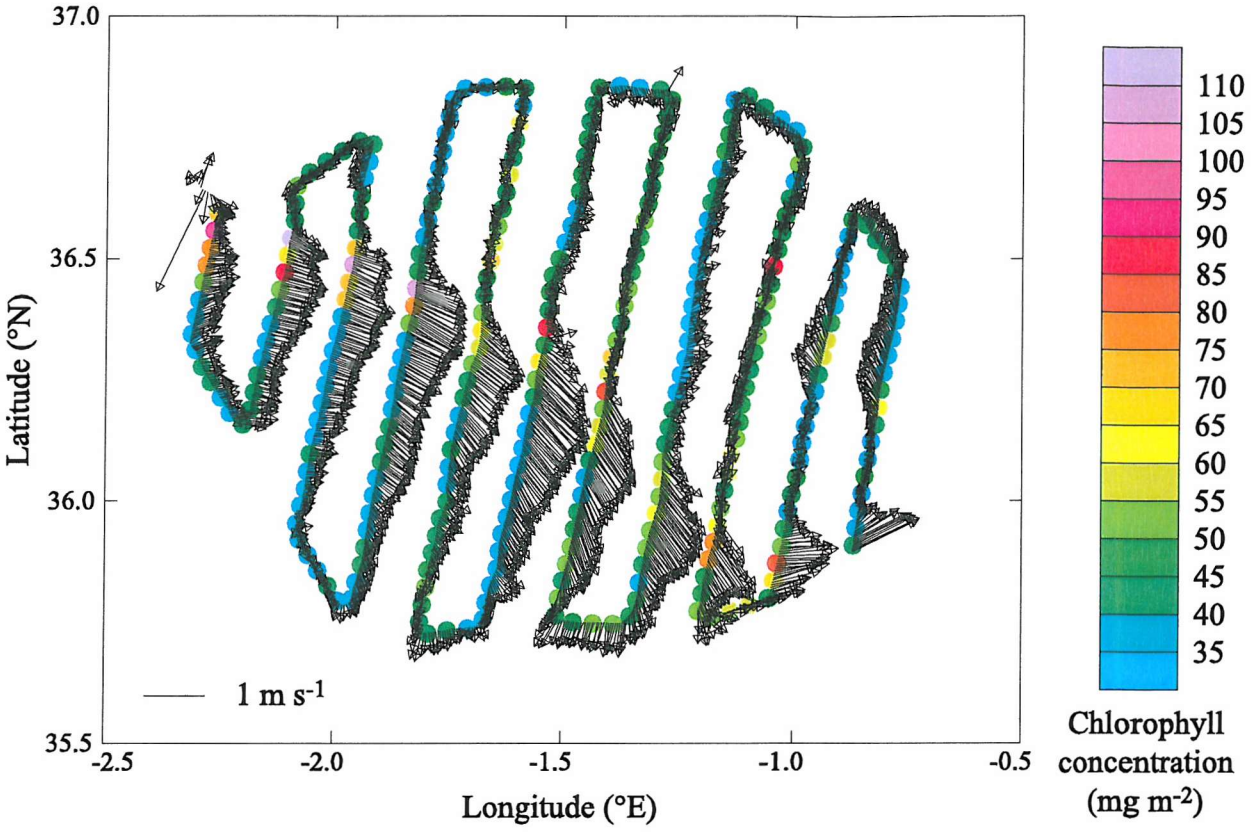

Figure 4.3.7 VM-ADCP derived current velocity at 14 m over laid on chlorophyll concentration integrated over 150 m.

However, this was attributed to the accumulation of cells in a particular zone of density stratification (as hypothesised by Hobson and Lorenzen, 1972). The present observations of layers of fluorescence coincident with the subducted MSW and the depth attained suggest that at least some phytoplankton were drawn down and along the isopycnals. Boucher *et al.* (1987), Dewey *et al.* (1991) and Hood *et al.* (1991) made similar observations of downward and oblique transport of phytoplankton along isopycnals. The subduction of phytoplankton at the Almeria-Oran front has been commented on previously, resulting in a virtual south-north transect of chlorophyll concentration (Figure 8 in Videau *et al.*, 1994) analogous to the in-situ fluorescence transects presented here (Figure 4.3.4). Using estimates of vertical displacement rates, Videau *et al.* (1994) calculated isopycnal descent rates to be 35 m d^{-1}, not dissimilar to the subduction rate of 25 m d^{-1} calculated and observed during this study (Section 4.2; Allen *et al.*, 2001).

This observation of the subduction of Mediterranean Surface Water and an associated phytoplankton population may explain why frontal enhancement of phytoplankton biomass was not evident in FSS3 in the Σchl_{250} data. Since the phytoplankton which were subducted down and across the front originated from the Mediterranean waters (which were advected along the coast of Spain, Allen *et al.*, 2001; Fielding *et al.*, 2001) in FSS3, rather than from within the frontal region as postulated for FSS1.

4.4 The distribution of zooplankton at the AOF during cruise D224

Longhurst-Hardy Plankton Recorder (LHPR) net samples and acoustic backscatter data from the VM-ADCP and SIMRAD EK500 echosounder were used to investigate the distribution of zooplankton at the AOF.

4.4.1 Data collected with a Longhurst Hardy Plankton Recorder (LHPR)

4.4.1.1 Hydrographic conditions during the LHPR stations

Both LHPR stations were undertaken in the southwest corner of the survey region at the starting point of the SeaSoar surveys, six days apart (Figure 4.4.1). LHPR station 13036, taken on the 15th of December 1439 - 1715, was prior to FSS2, LHPR station 13048, taken on the 21st of December 0915 – 1149, occurred after FSS2 and before FSS3. In each case the LHPR was deployed on the Mediterranean side of the AOF, and towed in a v-shaped profile across the front. Retrieval was in Atlantic waters within the Alboran Gyre. As a result in the shift in water masses across the tow, the down and up part of each tow is displayed and discussed separately.

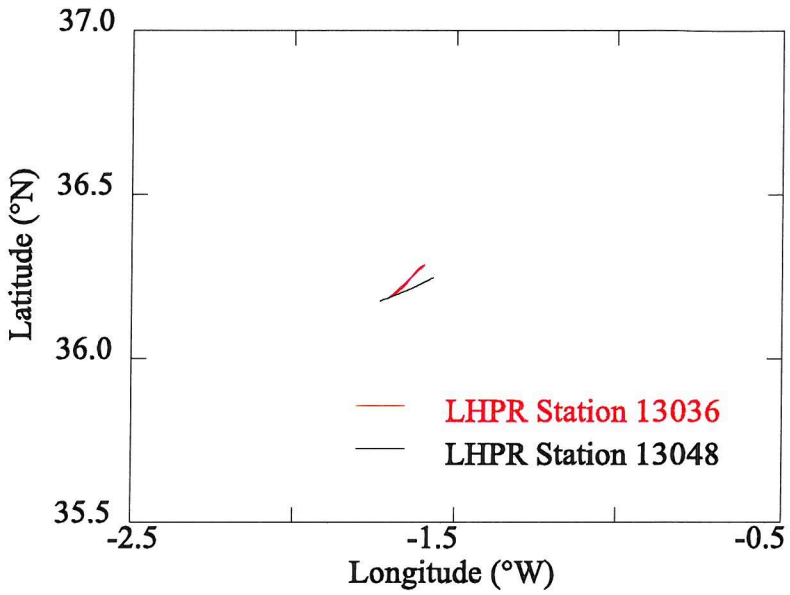

Figure 4.4.1 The cruise track of RRS *Discovery* during LHPR station 13036 and 13048.

The surface waters of the downcast of station 13036 had a salinity (>37.5) and temperature (~14 °C) typical of Atlantic-Mediterranean Interface Water (AMIW), found predominantly in the frontal region (Figure 4.4.2a). The mixed layer depth was ~100 m, and below this the temperature (~13 °C) and salinity (>38) were more typical of deeper Mediterranean waters such as Levantine Intermediate Water (LIW). The surface waters of the upcast were warmer and fresher than those found at the surface during the downcast, the temperature (>15 °) and salinity (<37.5) indicative of Modified Atlantic Water (MAW) found within the Alboran Gyre (Figure 4.4.2b). As well as a difference in surface water mass the other major feature of note between the down and upcast was the deepening of the thermocline. During the upcast the mixed layer extended to ~130 m, below which were deeper Mediterranean waters identified by their increasing salinity.

The vertical profile of temperature and salinity from the downcast of LHPR station 13048 shows a similar pattern to station 13036. Cooler (respective to MAW) and saltier AMIW, representative of water in the frontal region, was present within the mixed layer which extended to ~100 m. A slight anomaly of warmer and saltier water was found at ~30 m (Figure 4.4.3a). This may have been present in station 13036, but was not measured because the LHPR had not switched on at this point (see Chapter 2 methods referring to logging mode of LHPR). The water below the mixed layer in both the down and upcast was cool and salty, indicative of the deep Mediterranean waters. Similar to station 13036 the upcast mixed layer depth was deeper than the downcasts. In this case the mixed layer extended further, to ~150 m, and was represented by a steeper change in temperature and salinity than during station 13036 (Figure 4.4.3b). The surface waters of the upcast of station 13048 were warm and fresh showing that the LHPR surfaced into MAW within the Alboran Gyre. Above the thermocline, during the upcast a temperature anomaly was observed at ~75 m that did not have an associated change in salinity, neither was it observed in station 13036.

The deepening of the thermocline between station 13036 and 13048 may have been a result of "where" in the Alboran Gyre the LHPR surfaced rather than an "actual" deepening of the mixed layer. This can be concluded from the consistent depth of the mixed layer within the Alboran Gyre (~150 m) shown in the SeaSoar density plots of FSS1, 2 and 3 (Figure 4.2.7). Since the front moved southwest during or prior to FSS2, even though the start and end positions of the LHPR stations were similar (Figure 4.4.1), station 13036 may not have extended as far in to the Alboran Gyre as station 13048, which occurred when the front had returned to a more northeasterly position.

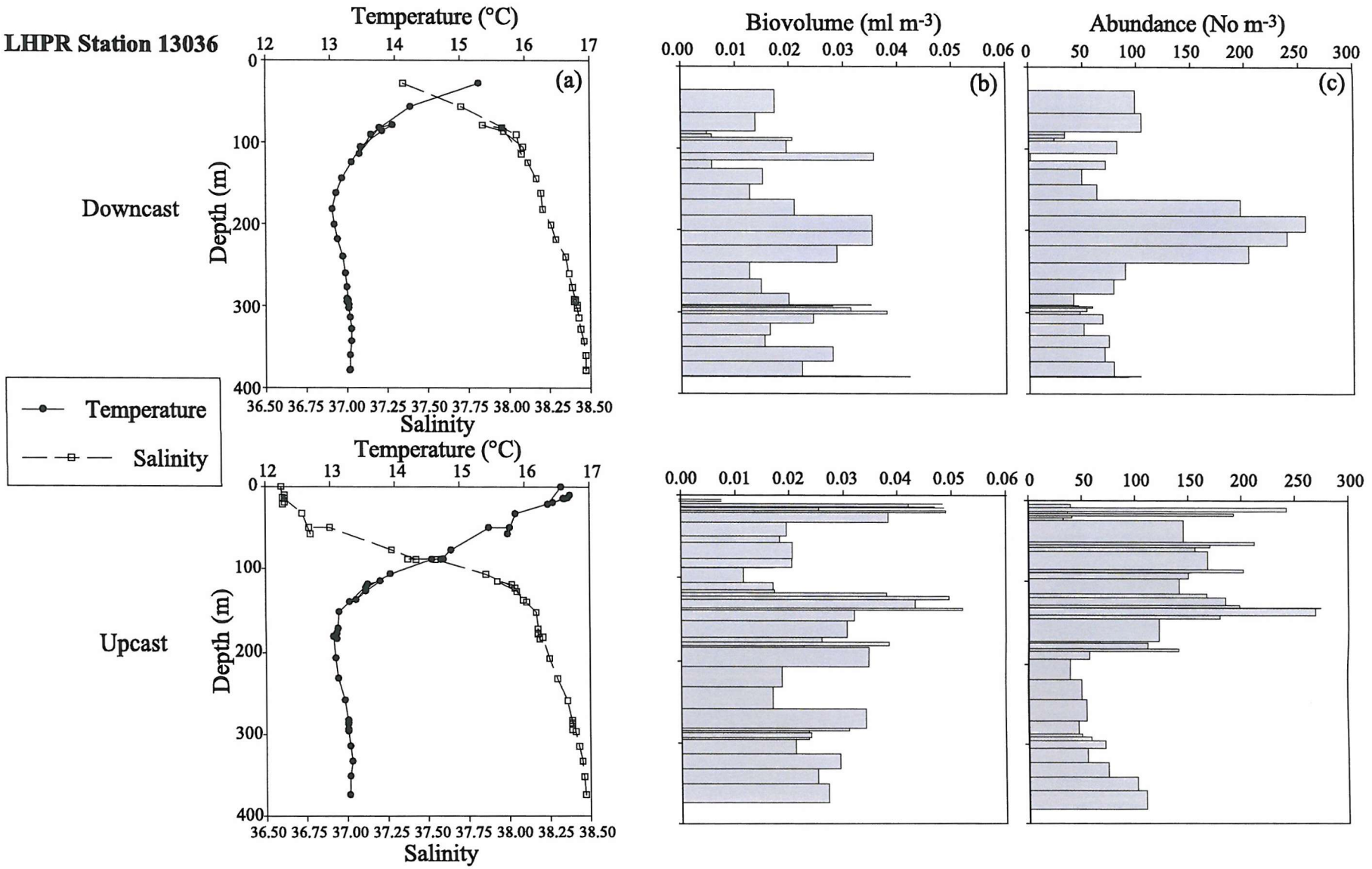

Figure 4.4.2 Vertical profiles of (a) temperature and salinity, (b) total zooplankton biovolume and (c) total zooplankton abundance for LHPR station 13036. The top three graphs represent the downcast and the bottom three the upcast.

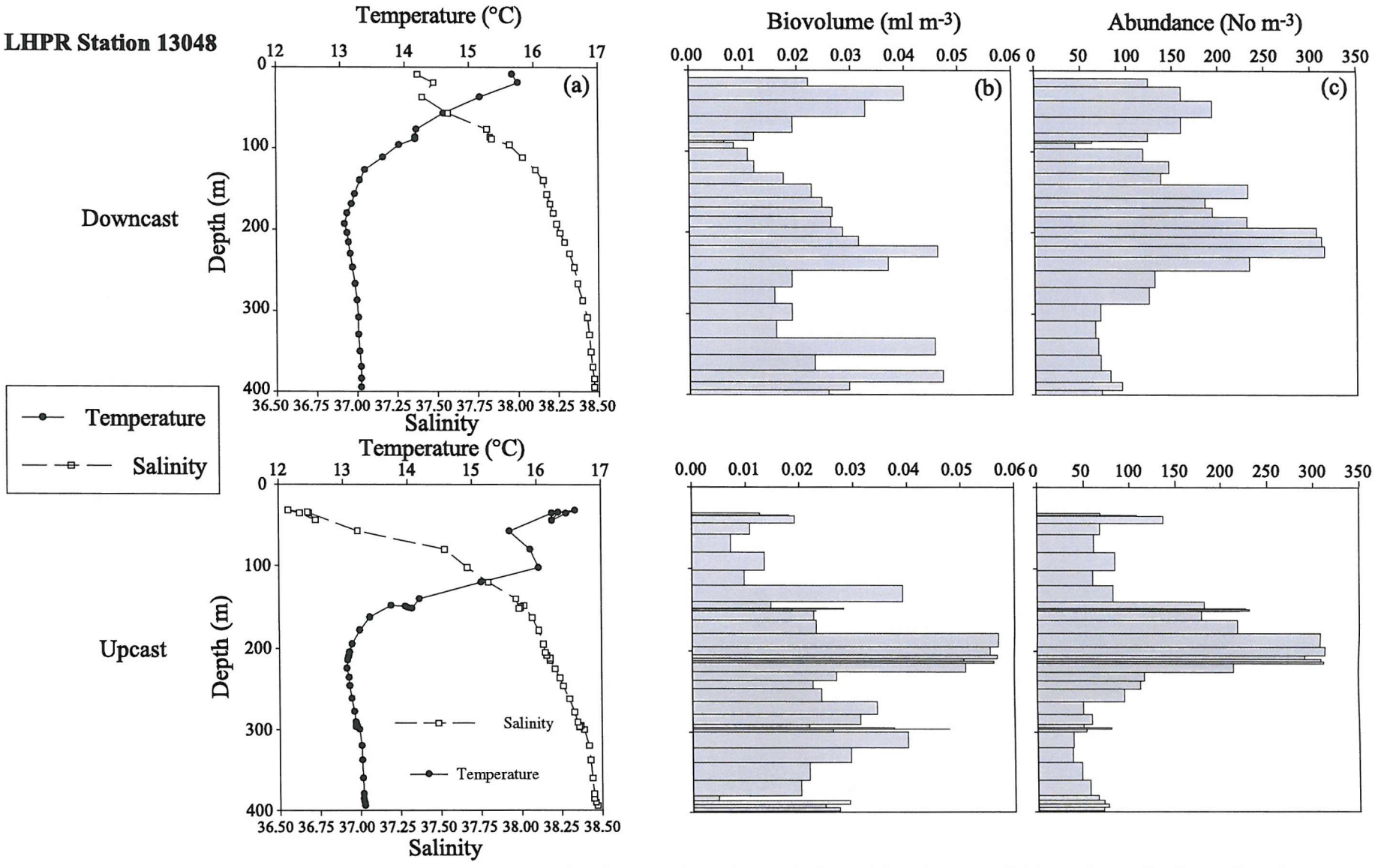

Figure 4.4.3 Vertical profiles of (a) temperature and salinity, (b) total zooplankton biovolume and (c) total zooplankton abundance at LHPR station 13048. The top three graphs represent the downcast and the bottom three the upcast.

4.4.1.2 The distribution of zooplankton biovolume at LHPR station 13036

The vertical distribution of biovolume at station 13036 showed differences between the down and upcast (Figure 4.4.2). During the downcast biovolume was low (~0.02 ml m^{-3}) in the AMIW within the mixed layer (Figure 4.4.2a). Below this four maxima (~0.04 ml m^{-3}) occurred. These were at the mixed layer depth (~100 m), at 200 m, 300 m and the bottom of the cast (~400 m). Between these depths biovolume remained relatively constant ranging from 0.01 to 0.02 ml m^{-3}. The maxima, occurring at 200 m, corresponded to the depth at which the lowest temperature was observed, and was just below the depth at which density became constant on the Mediterranean side of the front as observed in the SeaSoar data (Figure 4.2.7). The maxima at 300 m does not correspond to a respective change in temperature or salinity recorded by the LHPR, but can be associated with the boundary below which density remains constant (Figure 4.2.7).

During the upcast, as with the downcast, four maxima were observed, although their depths and vertical extent were different. The surface values, within the Alboran Gyre were consistently high (~0.05 ml m^{-3}), over double that observed on the Mediterranean side of the front within AMIW. Although this difference could also be attributed to the true surface waters not being sampled on the downcast, as below ~50 m values of biovolume decrease to ~0.02 ml m^{-3} similar to values observed in the downcast. The second maxima occurred at ~130 m, coincident with the mixed layer depth. This same feature was observed in the downcast at the bottom of its shallower mixed layer. The third maxima occurred slightly above 200 m, which corresponded to a depth just below the greatest density contrast. The fourth maxima occurred below 275 m, where biovolume was consistently high between 0.02 and 0.03 ml m^{-3} in the bottom 100 m of the cast (300 to 400 m depth).

4.4.1.3 The distribution of zooplankton abundance at LHPR station 13036

The vertical distribution of zooplankton abundance at station 13036 was different on the down and upcast. During the downcast maximum zooplankton abundance occurred in an approximately 60 m thick layer between 170 and 230 m (Figure 4.4.2). This layer coincides with one of the maxima in biovolume, and is coincident with the depth of greatest density gradient. Throughout the rest of the sampled water column, abundance remained comparatively constant (between 50 to 100 m^{-3}), except for two minima of <50 m^{-3} that occurred at ~95 m and ~290 m (Figure 4.4.2a). These two minima coincide with two maxima in biovolume. It can be hypothesised that there may have been either a few large organisms within the sample or that the mean size of the zooplankton caught at

this depth was greater than surrounding water. Copepods accounted for >80 % of total zooplankton abundance at all depths except between 75 and 100 m and at ~130 m (Figure 4.4.4a), and below 170 m contributed between 90 and 96 % to the total abundance. Between 75 and 100 m, the first minimum in total zooplankton abundance, the percentage of copepods reduced to ~62 %. However a similar reduction did not occur in the second total zooplankton abundance minimum. The second most common group were ostracods, characteristically accounting for 5 – 10 % of total abundance. This increased to a maximum of 37 % coincident with the reduction in copepod contribution. This shift in percentage contribution resulted from not only a decrease in the number of copepods within the samples (half the number ~50 No. m^{-3} of surrounding waters), but also an increase in the number of ostracods present (Figure 4.4.5d,f). Chaetognatha were the third highest contributors to total abundance, occurring with greater dominance in the surface ~130 m, typically at ~2 %. Euphausiids were relatively important contributors to abundance only at certain depths; 40 m and 135 to 170 m, which corresponded with depths where an increase in their abundance was observed (Figure 4.4.5a) rather than a decrease in the abundance of other taxa. The remaining plankton was composed of Amphipoda, Appendicularia, Decapoda, Fish, Polychaeta, Pteropoda and other groups (see Figure 4.4.4a). Some taxa were only represented by one or two individuals in the whole sample (e.g. Cephalopods, Heteropods, *Pyrosoma*).

The upcast showed a similar total zooplankton abundance distribution to the downcast below the mixed layer depth, with copepods dominating the samples numerically (Figure 4.4.4b). Above this, within the MAW total zooplankton abundance was high (150 - 250 No. m^{-2}). Two maxima in total abundance occurred during the upcast; at ~130 m the bottom of the mixed layer, and at ~15 m, at the surface. Copepods were the most abundant group in all the upcast samples, contributing > 60 % of total abundance in all samples, and in the deep maxima of total abundance this contribution increased > 90 %. The second most common group were ostracods. Within the surface MAW the percentage contribution from euphausiids increased towards the surface with a maximum occurring at ~50 m (~5 %).

4.4.1.4 The vertical distribution and size of main taxonomic groups at LHPR station 13036

Figure 4.4.5 shows the vertical distribution of abundance of each taxonomic group, the downcast presented on the left of each graph (filled in white) and the upcast on the right (filled in grey). Two features are evident, (1) the abundance of each group below

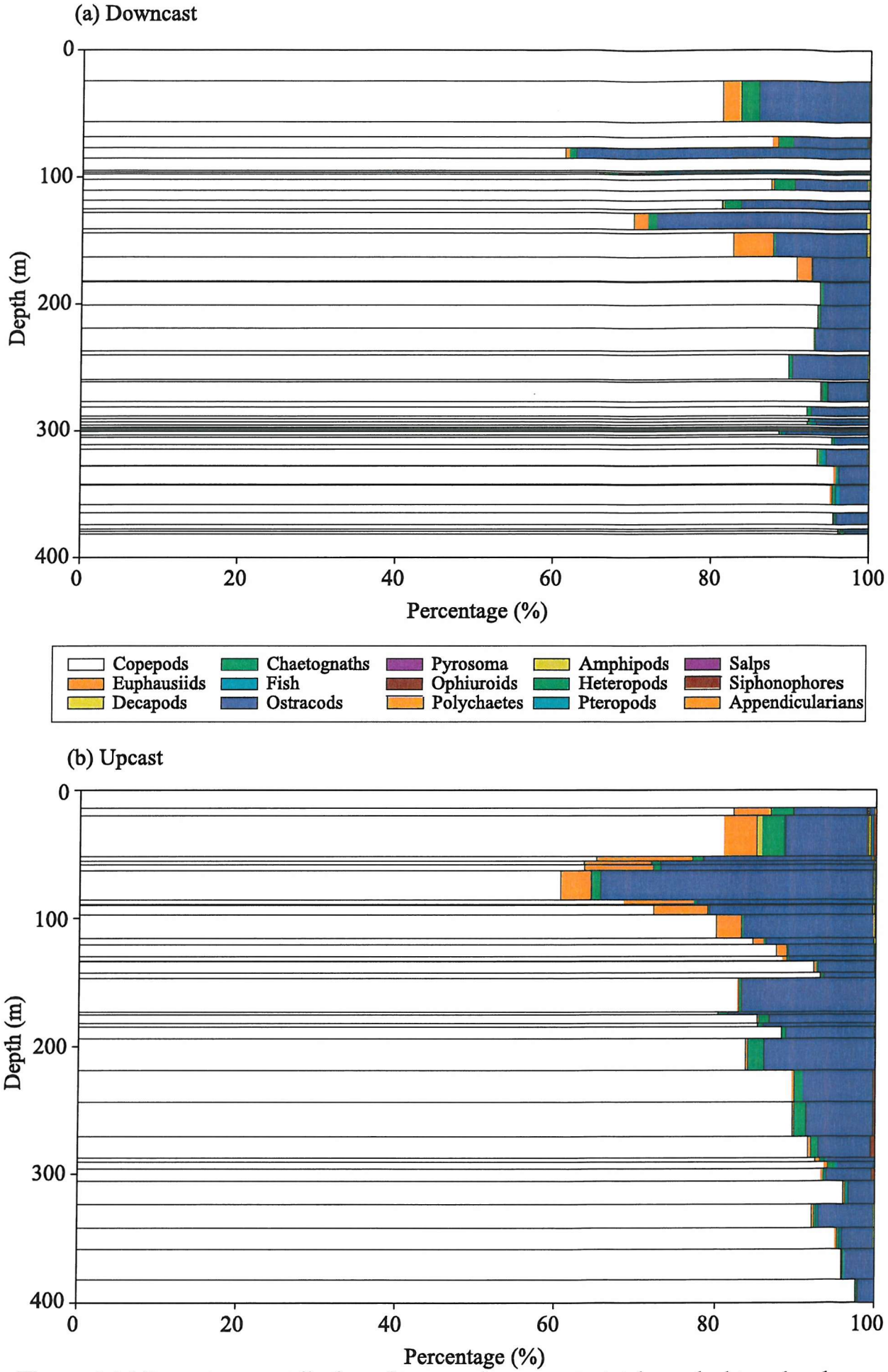

Figure 4.4.4 Percentage contribution of taxonomic groups to total zooplankton abundance during (a) the downcast and (b) the upcast at LHPR station 13036.

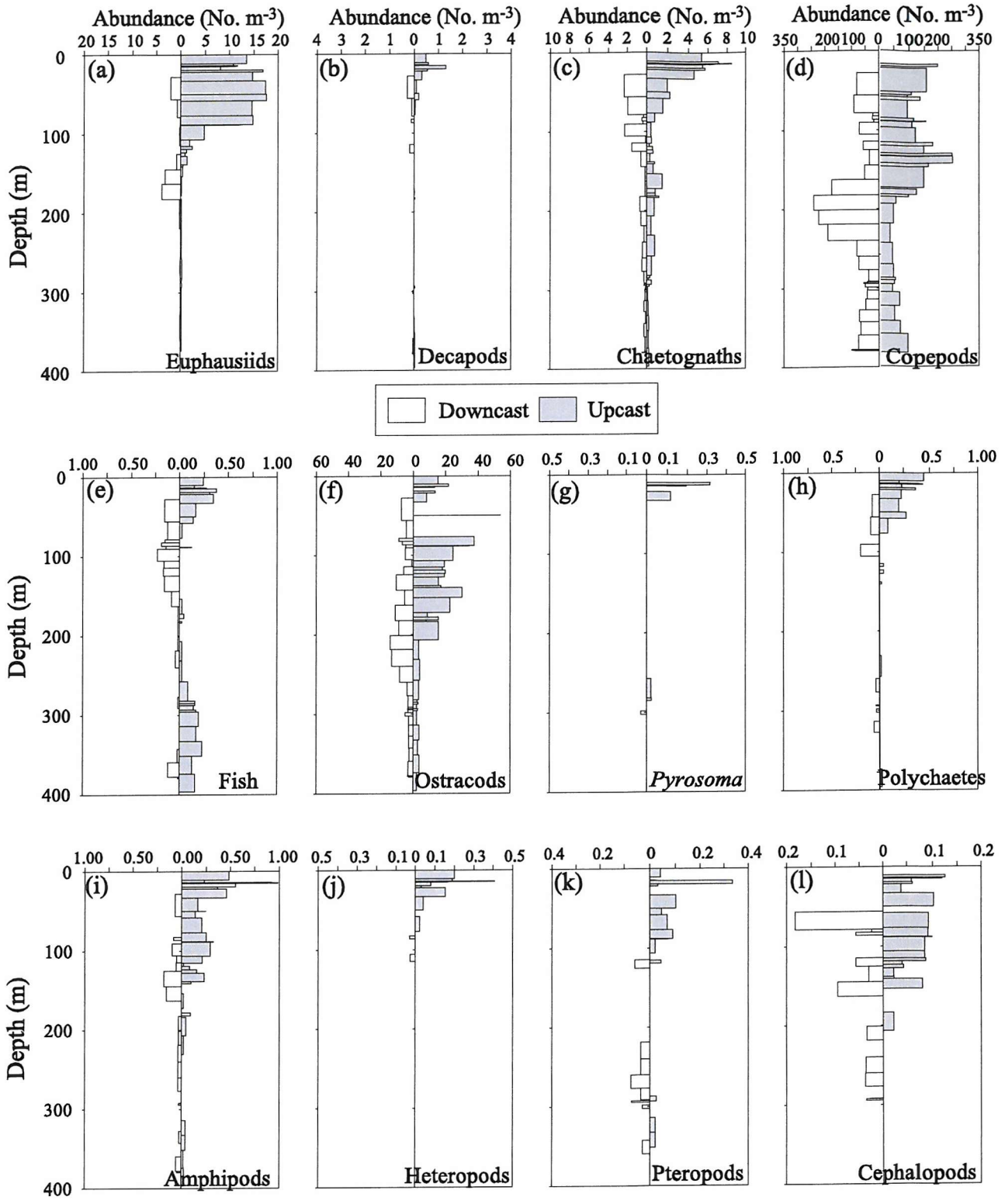

Figure 4.4.5 Vertical profiles of (a) Euphausiids, (b) Decapods, (c) Chaetognaths, (d) Copepods, (e) Fish, (f) Ostracods, (g) *Pyrosoma*, (h) Polychaetes, (i) Amphipods, (j) Heteropods, (k) Pteropods and (l) Cephalopods at LHPR station 13036.

~200 m is typically the same between the down and upcast, (2) there is a marked difference between the abundances caught towards the surface, in AMIW (on the downcast) and MAW (on the upcast), with greater abundances occurring in MAW. More specifically, the groups Copepoda, Euphausicea, Decapoda, Chaetognatha, Polychaeta, Amphipoda, Heteropoda and Pteropoda all show up to a five-fold increase in abundance within the MAW. In each case these greater abundances occur within the mixed layer depth, above ~150 m. Below the mixed layer their numbers are reduced dramatically, and are less than the smaller numbers found in AMIW. The Pteropod group are an exception. Their distribution was relatively constant throughout the water column except within AMIW, where they were absent (Figure 4.4.5k). Fish also show a different distribution to the other taxa, with similar and high abundance above the mixed layer depth in both AMIW and MAW and high abundance at depth, below ~300 m. It is expected that the analogous distributions of Doliolids, Salps and Siphonophores are a result of sampling inaccuracies caused by the inherent difficulties in identifying and counting gelatinous organisms in squashed zooplankton samples caught in a fast-towed LHPR (see Chapter 2). Notably, in each of these cases the total abundance of each taxa within a sample was small (<1 m^{-3}).

As well as variation in the distribution of different taxonomic groups, there were distinct variations in the mean size of organisms within some taxonomic group with depth (Figure 4.4.6). For euphausiids and fish, larger specimens occurred below ~200 m. These variations in size with depth appeared to be caused by variations in the life stage caught. The surface samples consisted of larval stages of euphausiids and fish, as well as juvenile stages of a bi-lobed eye euphausiid. The deeper samples (>200 m) contained adult stages of *Stylocheiron* sp. *Nematocelis* sp. and *Euphausia krohni*. The greater size, as well as the increase in abundance, of fish below 300 m was probably responsible for the total biovolume maxima observed at depth in both the down and upcast (section 4.4.1.2). The surface larval fish species were not identified, but the fish caught at depth were of the genera *Cyclothone* and *Argyropelecus* and the myctophid genera *Benthosema* and *Hygophum*. In general *Cyclothone* were the most abundant fish followed by the myctophids. The hatchet fish *Argyropelecus* sp. was caught infrequently. The pteropods caught possessed an external shell and were *Diaria* sp. and *Eulio* sp.. Although occurring in low abundance throughout the survey region, two features dominated the distribution of Pteropods. Their relative absence from the EAG and a marked increase in mean length with depth.

The mean length of chaetognaths shows a different distribution to the other groups measured. Their mean length remained relatively constant (~5-10 mm) throughout the water column (Figure 4.4.6b), except for two maxima occurring at ~100 m during the downcast, and between 100 and 130 m during the upcast. These depths are at the base of the mixed layer on either side of the front.

4.4.1.5 The distribution of zooplankton biovolume at LHPR station 13048

Similar to station 13036, the vertical distribution of zooplankton biovolume at station 13048 showed differences between the down and upcast (Figure 4.4.3). The downcast shows, in contrast to station 13036, high biovolume (up to ~0.04 ml m^{-3}) within the AMIW. This may be a result of the LHPR sampling from the surface on this occasion. As well as a surface maximum, two subsurface maxima in biovolume were observed at ~220 m and from ~340 m to the bottom of the cast (Figure 4.4.3a). The maximum at 220 m was the largest (~0.045 ml m^{-3}) and coincided with the depth at which the lowest temperature was observed. Between these maxima, biovolume varied between 0.01 and 0.02 ml m^{-3}, similar to the values observed at station 13036. Interestingly, the downcast biovolume maxima observed at ~100 m and ~300 m during station 13036 were represented by minima in station 13048 of ~0.01 and ~0.015 ml m^{-3} respectively.

During the upcast the maximum value of biovolume (0.055 ml m^{-3}) was observed in a layer ~40 m thick between 180 and 220 m, just below the depth of greatest temperature gradient (Figure 4.4.3b). Below this, in the deep Mediterranean waters, biovolume was relatively high (0.02 to 0.03 ml m^{-3}), except for an anomalous sample of 0.05 ml m^{-3} at ~390 m. Contrary to station 13036, biovolume was low within the Alboran Gyre MAW (0.005 – 0.02 ml m^{-3}) except for one sample at ~120 m that was the upper boundary of the thermocline.

4.4.1.6 The distribution of zooplankton abundance at LHPR station 13048

The vertical distribution of zooplankton abundance at station 13048 was relatively similar on the down and upcast, with greatest abundance (>300 m^{-3}) occurring between 200 and 230 m on the downcast and, slightly shallower, between 190 and 220 m on the upcast (Figure 4.4.3). In both cases, this maxima in abundance was surrounded by water of relatively high abundance (>150 m^{-3}) persisting from ~150 m to ~250 m during the downcast and to ~225 m during the upcast. These maxima in abundance coincided with the depth of greatest biovolume.

Above the mixed layer depth abundance was greater on the Mediterranean side of the front (typically >100 m^{-3} within AMIW) compared with the Alboran Gyre side

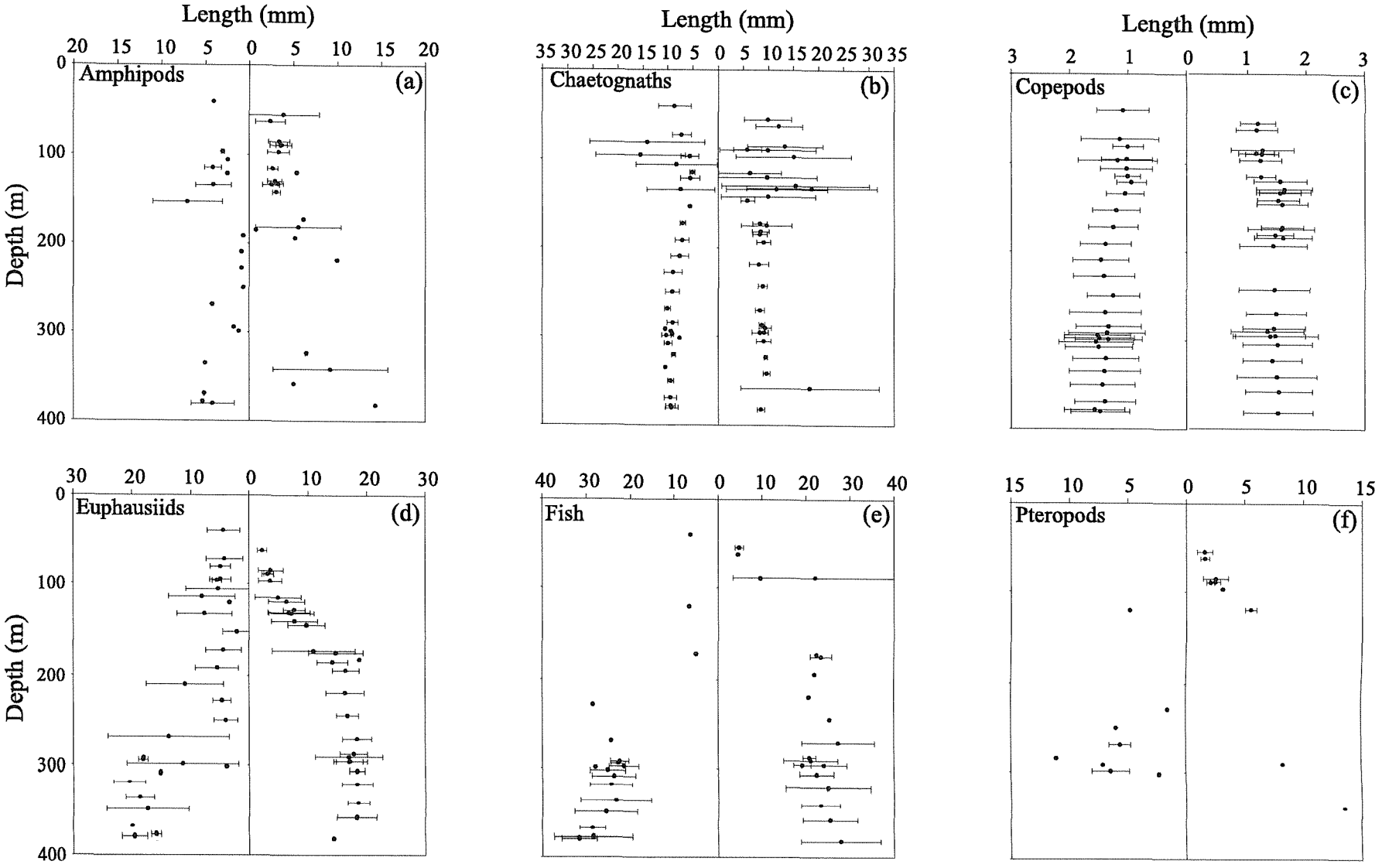

Figure 4.4.6 Vertical profiles of the mean length of (a) Amphipods, (b) Chaetognaths, (c) Copepods, (d) Euphausiids, (e) Fish and (f) Pteropods during LHPR station 13036. The downcast data are the left graphs and the upcast are the right.

(typically <100 m^{-3} within MAW). Total abundance within AMIW was ~ 50 % greater in station 13048 than in station 13036, the maximum occurring just above the thermocline.

At all depths except 174 m on the downcast and 33 m on the upcast copepods contributed >80 % to the total abundance (Figure 4.4.7). At these two exceptions copepods were still the dominant taxa but their contribution had reduced to 75 % and 71 % respectively. This lower dominance was not associated with a distinct reduction in copepod abundance (Figure 4.4.8). Below ~190 m the contribution from copepods to total zooplankton increased to >90 %, similar to station 13036 and this may have been related to reduced numbers of euphausiids and chaetognaths. The second most important group were ostracods, that contributed typically ~4 % of total abundance but this increased to ~16 % where the copepod contributions decreased. As with station 13036 Chaetognatha and Euphausiacea were the next most dominant groups, occurring above ~190 m as up to 8 % of total zooplankton. In both cases this probably resulted from an increase in their abundance compared with deeper waters rather than a change in the numbers of other groups (Figure 4.4.8a,c). The other taxa caught at this station are shown in Figure 4.4.7.

4.4.1.7 The vertical distribution and size of main taxonomic groups at LHPR station 13048

The vertical distribution of abundance of each taxonomic group identified during station 13048 is presented in Figure 4.4.8, the downcast shown on the left side of each graph (filled in white) and the upcast on the right (filled in grey). Three patterns can be identified: (1) as with station 13036, the abundance of each group below ~200 m is comparable between the down and upcast; (2) there are marked differences between the abundances caught towards the surface in AMIW (on the downcast) and MAW (on the upcast), with (in contrast to station 13036) greater abundances occurring in AMIW; and (3) several groups show maximum abundances between 180 and 200 m (Figure 4.4.8a,d,f). The increased abundances of euphausiids, chaetognaths, polychaetes, amphipods, doliolids, salps, siphonophores and appendicularians occurred in AMIW above ~100 m (Figure 4.4.8). Only in the euphausiids did this not represent the maximum abundance found throughout the cast. Copepods and ostracods show similar distributions, with maximum abundances occurring just below and just above ~200 m respectively. At similar depths a second and larger maxima in euphausiid abundance occurred on the Atlantic side of the front.

Three groups deviated from these distribution patterns. Fish (Figure 4.4.8e), as at station 13036, showed two peaks in abundance.

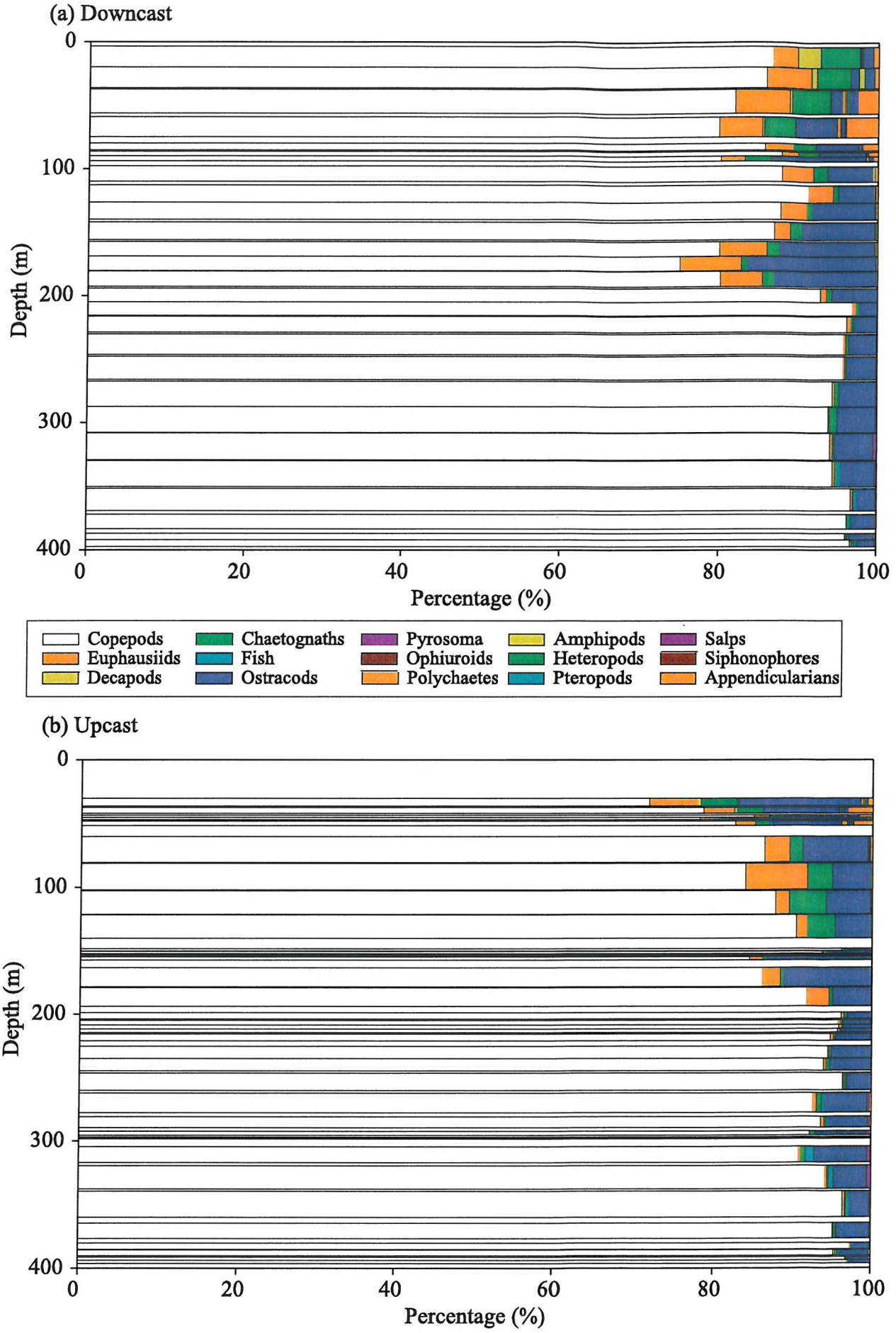

Figure 4.4.7 Percentage contribution of taxonomic groups to total zooplankton abundance during (a) the downcast and (b) the upcast at LHPR station 13048.

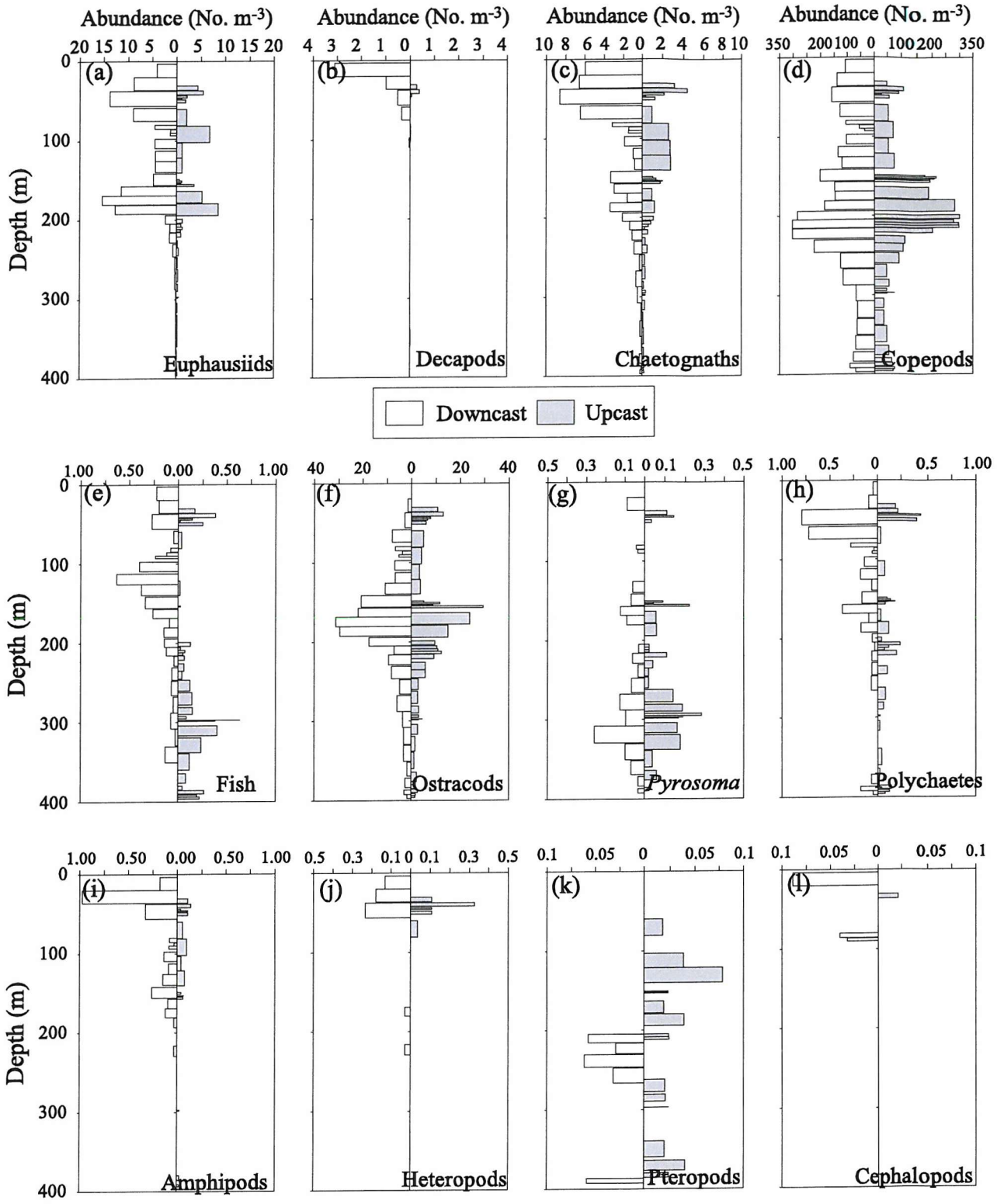

Figure 4.4.8 Vertical profiles of (a) Euphausiids, (b) Decapods, (c) Chaetognaths, (d) Copepods, (e) Fish, (f) Ostracods, (g) *Pyrosoma*, (h) Polychaetes, (i) Amphipods, (j) Heteropods, (k) Pteropods and (l) Cephalopods at LHPR station 13048.

The first within the surface 50 m (0.25 – 0.5 m^{-3}), comprised small fish ~5 mm long, and the second below 200 m (0.25 – 0.5 m^{-3}), comprised of larger individuals, 20 to 30 mm long (Figure 4.4.9e). During the downcast there was also an increase in fish abundance (>0.5 m^{-3}) just below the mixed layer depth. *Pyrosoma* shows a distribution independent of water mass, with maximum abundances (up to 0.3 m^{-3}) occurring at depth (~300 m). Pteropods occurred throughout the water column, the dominating feature of their distribution being their absence from AMIW, this was also observed at station 13036.

Variations in the mean length of other taxa with depth were similar to those observed at station 13036, the mean size of copepods, euphausiids and pteropods increasing with depth (Figure 4.4.9c,d,e,f) and amphipod size remaining constant independent of depth (Figure 4.4.9a). A maxima in mean length (>10 mm) for the euphausiid group also occurred at a shallower depth of ~140 m during the upcast, coinciding with the bottom of the mixed layer.

The maxima in mean length of chaetognaths (~110 m depth during the downcast and ~150 m during the upcast) occurred at the base of the mixed layer, comparable with the distribution observed at station 13036.

4.4.1.8 An analysis of zooplankton abundance and biovolume with water mass

The two LHPR stations provide contrasting and "conflicting" results, in terms of zooplankton abundance and biovolume either side of the front. In station 13036 higher biovolume was observed east of the front compared with within the Alboran Gyre, whilst station 13048 indicated that higher biovolume existed within the Alboran Gyre compared with east of the front. As a result of this ambiguity a more detailed examination of the exact water masses the LHPR sampled and their corresponding zooplankton abundance and biovolume was undertaken. Depth, a down or upcast identifier, zooplankton biovolume and zooplankton total abundance were plotted as a third coloured variable on a θ/S diagram (Figure 4.4.10). Figure 4.4.10a,b shows that LHPR station 13036 did not sample in MSW (east of the front) but within AMIW, continuing into the temperature minimum layer and LIW before returning through AMIW (a) and surfacing into MAW. The high biovolume observed within the surface waters of the downcast is therefore more indicative of frontal waters, often reported to support greater zooplankton biomass (Le Fevre, 1986). LHPR station 13048 also did not start within MSW. It should be noted, however, that the water masses sampled during the downcast were not the same as station 13036 (Figure 4.4.10c,d), and were more similar to waters sampled during the upcast of station 13036 that contained similar zooplankton biovolumes and abundances

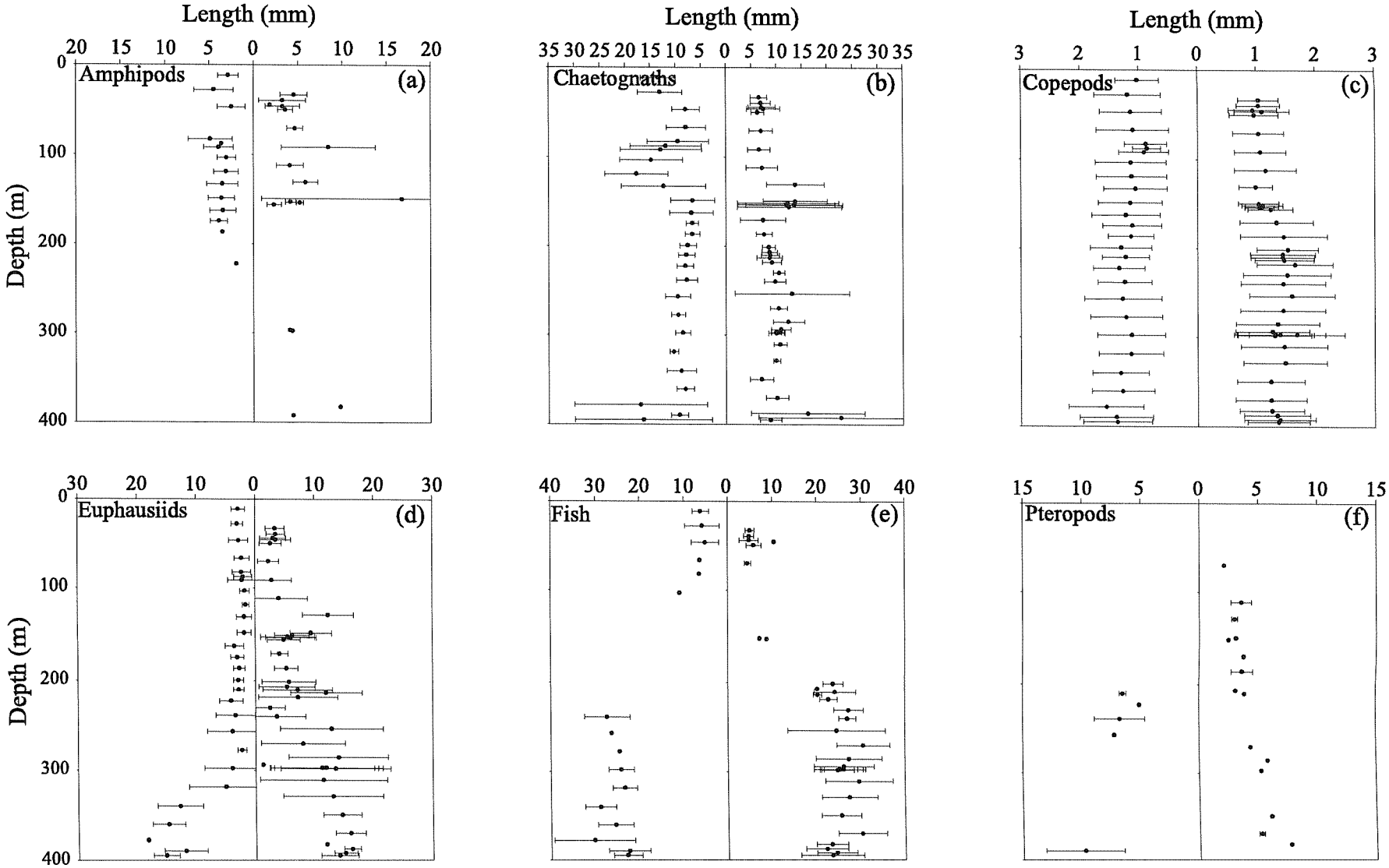

Figure 4.4.9 Vertical profiles of the mean length of (a) Amphipods, (b) Chaetognaths, (c) Copepods, (d) Euphausiids, (e) Fish and (f) Pteropods during LHPR station 13048. The downcast data are the left graphs and the upcast are the right.

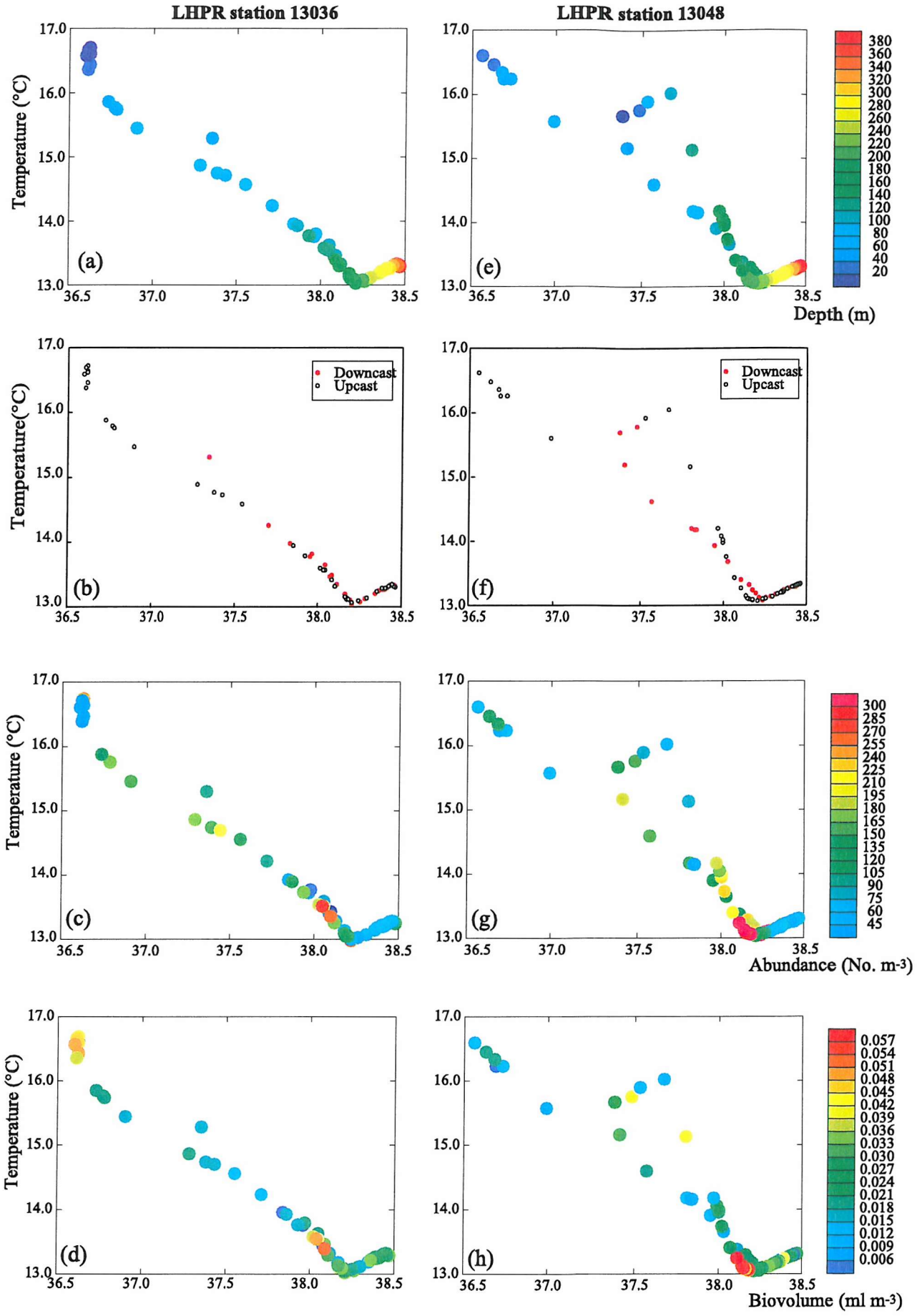

Figure 4.4.10 Temperature/Salinity diagrams with (a,e) depth, (b,f) a down or upcast identifier, (c,g) total zooplankton abundance and (d,h) total zooplankton biovolume plotted as a third coloured variable. Diagrams referring to LHPR station 13036 are on the left and LHPR station 13048 on the right.

(Figure 4.4.10e,f,g,h). The values of zooplankton biovolume and abundance found within the Temperature Minimum Layer and LIW are comparable between the two stations.

A difference between the two LHPR stations is the sampling of MAW, which occurred only at station 13036, and MSW, which occurred only at LHPR station 13048. The surface water mass of the upcast of station 13036 are clearly identifiable as MAW (Figure 4.2.2), compared with those sampled during station 13048. Distinct differences in the biovolume sampled at each station are evident in this warm and relatively fresh water.

During station 13048 MSW was sampled, not at the surface (as would be expected), but at depth (120-140 m) and during the upcast. The very warm and salty "true" MSW contained low biovolume and abundance as would be expected of an oligotrophic sea (Estrada *et al.*, 1999), greater zooplankton abundance and biovolume occurring where MSW mixed with AMIW (Figure 4.4.10f,h). This indicates that station 13048 was possibly undertaken during the period when phytoplankton was being subducted to ~200 m as observed in the fluorescence data from SeaSoar (section 4.3), and this water was associated with elevated values of zooplankton abundance and biovolume.

4.4.1.9 Acoustic backscatter data at LHPR stations 13036 and 13048

Acoustic backscatter data were collected concurrently with the LHPR casts using a 150 kHz VM-ADCP and a SIMRAD EK500. Only VM-ADCP data were collected at station 13036 as a result of the loss of the tail fin of the EK500 towed fish prior to FSS1. It was subsequently replaced after the LHPR station for use during FSS2. For ease of comparison with the previous temperature, salinity, density and fluorescence contoured plots of the AOF (section 4.2,4.3), VM-ADCP and EK500 acoustic backscatter collected during the LHPR stations have been plotted in reverse, crossing the front from West (within the Alboran Gyre) to East (the Mediterranean side). Figure 4.4.11 shows a contoured plot of acoustic backscatter collected using a VM-ADCP during station 13036 and LHPR sampled zooplankton biovolume. It is known (see Chapter 5) that there is not an exact relationship between acoustic backscatter and zooplankton biovolume, although some similar patterns are discernable. During the LHPR cast two "patches" of high acoustic backscatter were observed (-75 to -68 dB), labelled sound scattering layer 1 and 2 (SSL1 and SSL2) on Figure 4.4.11. Between these two patches was a layer of low acoustic backscatter (-84.5 to -80 dB). Comparison with the LHPR sampled biovolume show that; (1) high backscatter observed within the surface waters of the upcast of the LHPR (MAW) was associated with high zooplankton biovolume, (2) conversely in the surface waters of the downcast low zooplankton biovolume caught in the LHPR occurred coincidently with

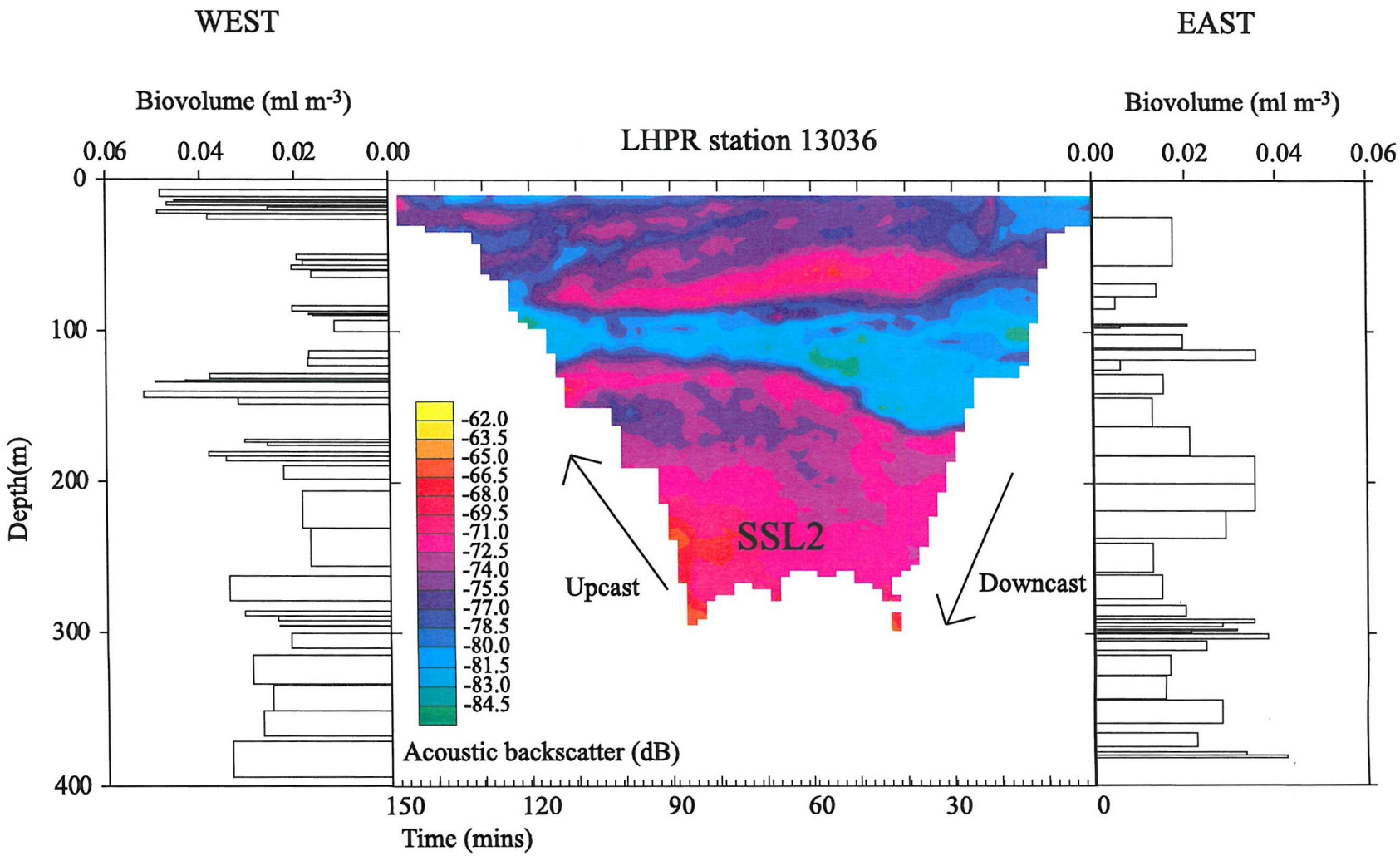

Figure 4.4.11 VM-ADCP acoustic backscatter during LHPR station 13036. On either side LHPR sampled total zooplankton biovolume. Note this station has been plotted in reverse.

low acoustic backscatter, (3) the layer of low acoustic backscatter was observed at depth where low zooplankton biovolume was observed, and (4) that below ~200 m, within SSL2 the picture is more confusing. The upper extent of SSL2 was defined by two peaks in zooplankton biovolume during the down and upcast. Below this level biovolume drops whilst acoustic backscatter remains high.

SSL2 was a common feature to both LHPR stations. The depth of SSL1 was more variable. Figure 4.4.12a-d shows the contour plots of acoustic backscatter collected using the VM-ADCP and the EK500 during LHPR station 13048. At this station two layers of low acoustic backscatter were observed, in addition to two patches of high acoustic backscatter. These separated SSL1 and SSL2, and, at the western end of the cast, SSL1 from the surface. SSL1 (-75.5 to -71 dB) extended from the surface, during the downcast, to ~130 m, during the upcast, and was associated with high values of zooplankton biovolume. The two layers of low acoustic backscatter (100 - 200 m during the downcast and 30 - 100 m during the upcast) similarly coincided with observations of relatively low zooplankton biovolume. As observed at station 13036, the upper extent of SSL2 was associated with high values of biovolume, below which acoustic backscatter increased whilst zooplankton biovolume decreased (Figure 4.4.12a).

Acoustic backscatter from the 200, 120 and 38 kHz frequencies (Figure 4.4.12b-d) shows similar scattering layers to the VM-ADCP, although both scattering layers are not evident at all frequencies. SSL1 was observed clearly in both the 200 and 120 kHz data (-83 and –79 dB respectively), whilst SSL2 was observed clearly only at 38 kHz. The absence of SSL2 from the data at 200 kHz and to some extent at 120 kHz is related to the increased attenuation of acoustic signal with depth at higher frequencies. Whilst SSL1 was not clearly observed at 38 kHz, acoustic backscatter values were higher within the surface 200 m during the downcast than the upcast. The presence of SSL1 in 200 and 120 kHz data and its absence from the 38 kHz data implies that SSL1 could have been composed of zooplankton smaller than the individual target size of the 38 kHz frequency (~4 cm).

4.4.2 Data collected with a VM-ADCP and an EK500 echosounder

4.4.2.1 Underway acoustic backscatter observations during FSS1-3

Acoustic backscatter data were collected from both the VM-ADCP and the EK500 throughout cruise D224 (except during FSS1 when the EK500 was under repair) and are used here to describe the distribution of zooplankton larger than a few millimetres in length, using the assumption that an increase in backscatter is related to an increase in zooplankton biomass (following Holliday and Pieper, 1995; Heywood, 1996; Roe *et al.*,

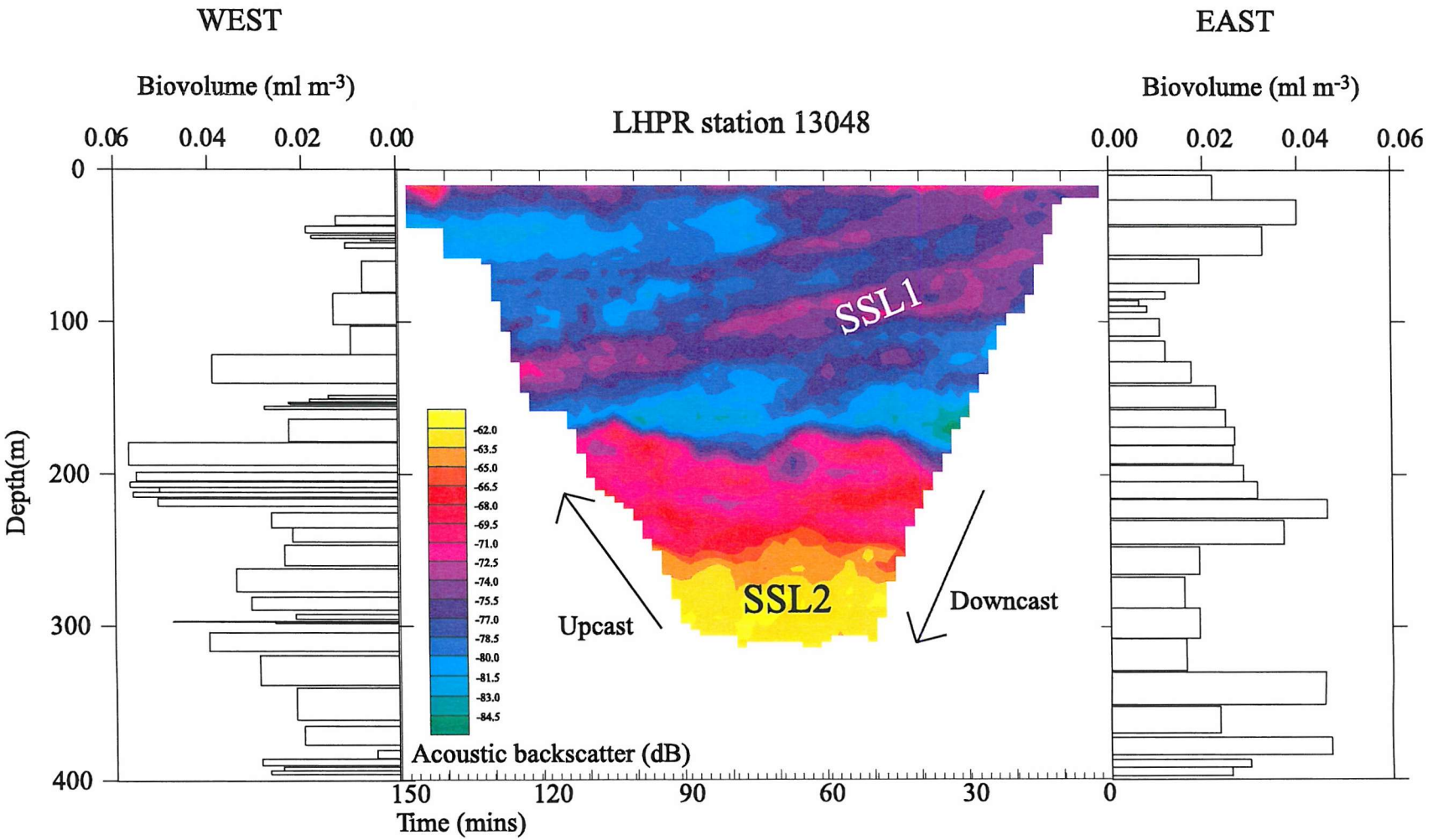

Figure 4.4.12a VM-ADCP acoustic backscatter during LHPR station 13048. On either side LHPR sampled total zooplankton biovolume. Two Sound Scattering Layers are identified. SSL1, a layer of higher backscatter concurrent with the 27.9 σ_0 isopycnal along the front, and SSL2, a permanent feature occurring between ~200 and >300 m. Note this station has been plotted in reverse.

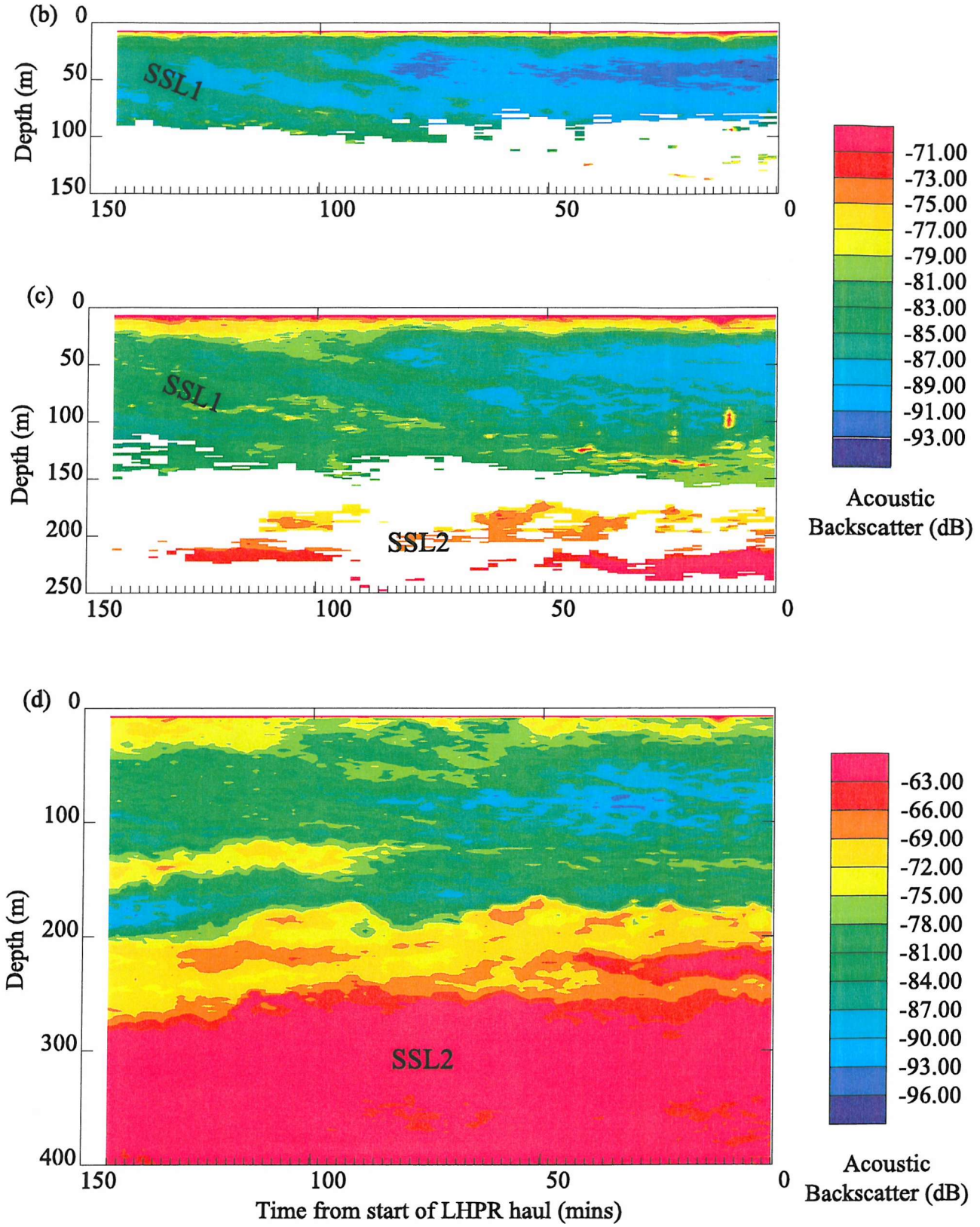

Figure 4.4.12b-d EK500 (b) 200 kHz, (c) 120 kHz and (d) 38 kHz acoustic backscatter during LHPR Station 13048 (note different scales). Two Sound Scattering Layers are identified. SSL1, a layer of higher backscatter concurrent with the 27.9 σ_t isopycnal along the front, and SSL2, a permanent feature occurring between ~250 and >600 m. Note this station has been plotted in reverse.

1996). The backscatter data for each frequency from each of the three finescale surveys was colour-contour plotted. The VM-ADCP data are presented in Figure 4.4.13 and the EK500 data for FSS2 in Figure 4.4.14 and for FSS3 in Figure 4.4.15. Acoustic backscatter data for the duration of the cruise can be found in two data reports (Allen *et al.*, 1997; Crisp *et al.*, 1998).

In Figure 4.4.13 (VM-ADCP acoustic backscatter) two separate patches of high backscatter can be clearly identified. These have been classified as Sound Scattering Layer two and three (SSL2 and SSL3), although it is recognised that "layer" may not be the most appropriate term.

SSL2 is represented by a permanent layer of high acoustic backscatter below ~200 m. At the lower limit of the VM-ADCP 150 kHz frequency range it represented the greatest intensities observed (~-58.5 dB). The upper depth limit of SSL2 was variable, ranging from ~200 m on the third day of FSS1 to ~250 m on the second day of FSS3, and was often clearly seen by stark contrast with targetless waters above it.

SSL3 does not refer specifically to a discrete layer, but is used here to describe a diurnal signal. Above SSL2, nighttime data are distinguished by high acoustic backscatter within the surface 200 m of the water column. These values were up to 20 dB higher than daytime values that varied between –90 and –70 dB.

SSL2 and SSL3 were also prominent features in the EK500 data (FSS2, Figure 4.4.14; FSS3, Figure 4.4.15). SSL2 was only observed in the 38 kHz frequency data, since the acoustic penetration of the 200 and 120 kHz frequencies was not sufficient to resolve below ~100 and ~200 m respectively. The 38 kHz data (Figure 4.4.14c; 4.5.15c) indicate that the SSL2 observed in the VM-ADCP data may be a separate layer or the upper limit of a large permanent deep scattering layer present between 200 m and > 600 m, that has its greatest intensities of ~-57 dB at 400 m. It is noticeable that this layer shows little diurnal variation in intensity or depth. This layer is coincident with the depths at which fish were more abundant in the LHPR samples, and at which the non-migratory *Cyclothone* spp. were observed by Baussant *et al.* (1993).

SSL3 was a consistent feature at all three EK500 frequencies, with nighttime surface intensities ~20 dB greater than daytime values, occurring within the surface 50-100 m. At all frequencies, smaller and less persistent discrete layers of high backscatter are identifiable.

Individual twenty-four-hour periods of VM-ADCP acoustic backscatter data (Figure 4.4.16), from each of the finescale surveys (jday 348, 353, 358), and EK500 data,

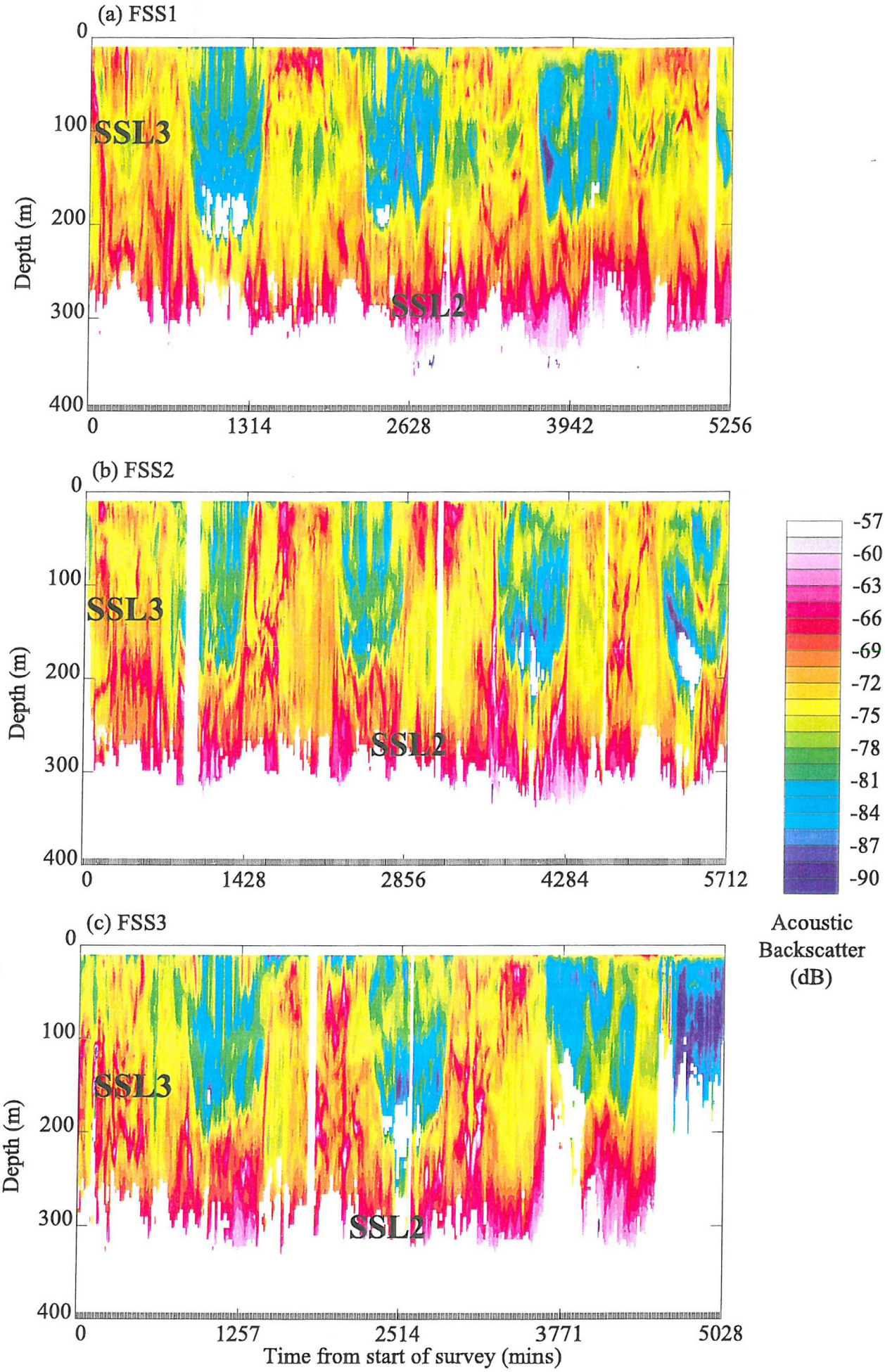

Figure 4.4.13 VM-ADCP acoustic backscatter during (a) FSS1, (b) FSS2 and (c) FSS3. Sound Scattering Layers 2 and 3 (SSL2 and SSL3) are identified.

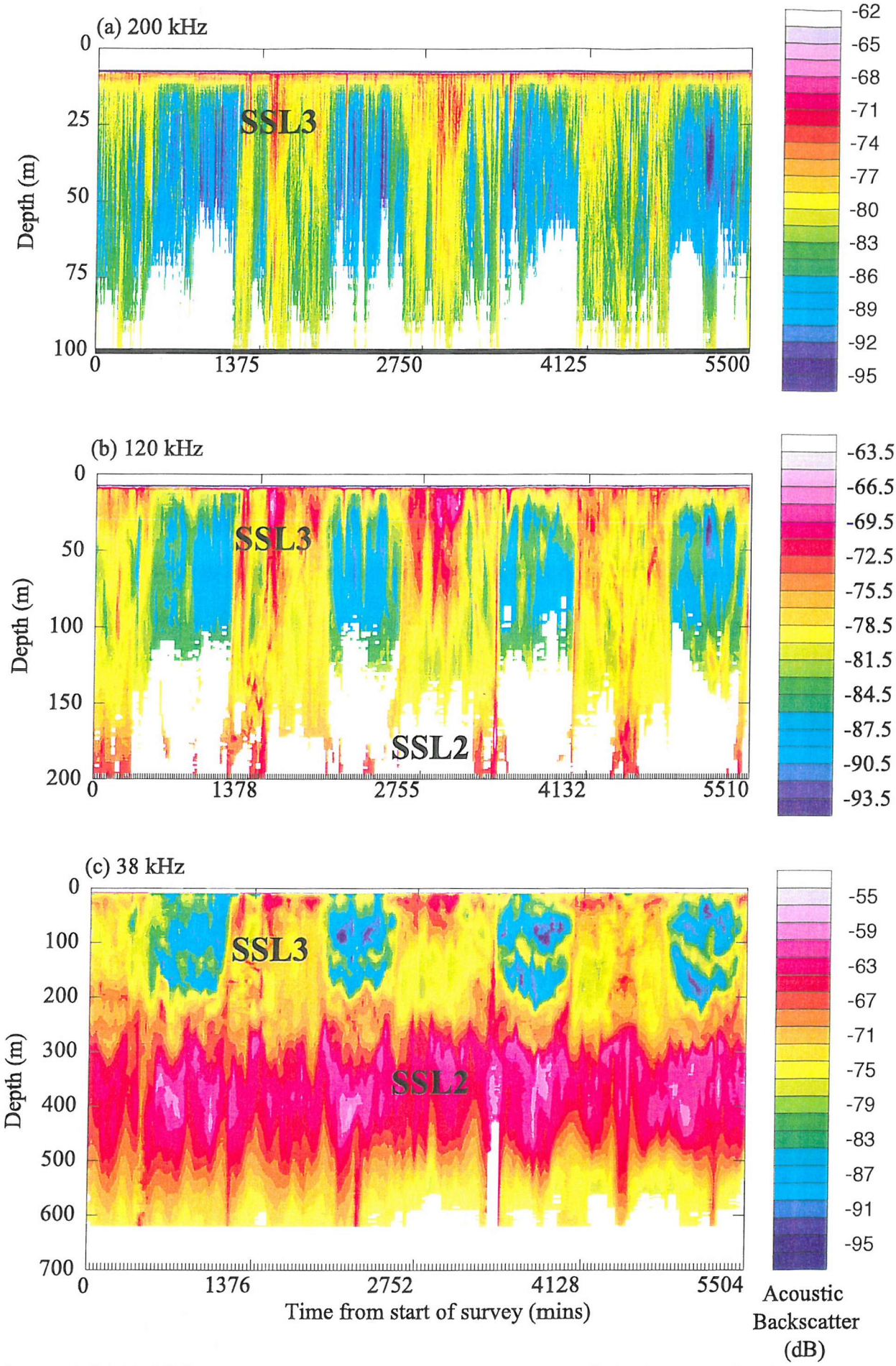

Figure 4.4.14 EK500 (a) 200, (b) 120 and (c) 38 kHz acoustic backscatter for FSS2. Sound Scattering Layers 2 and 3 (SSL2 and SSL3) are identified.

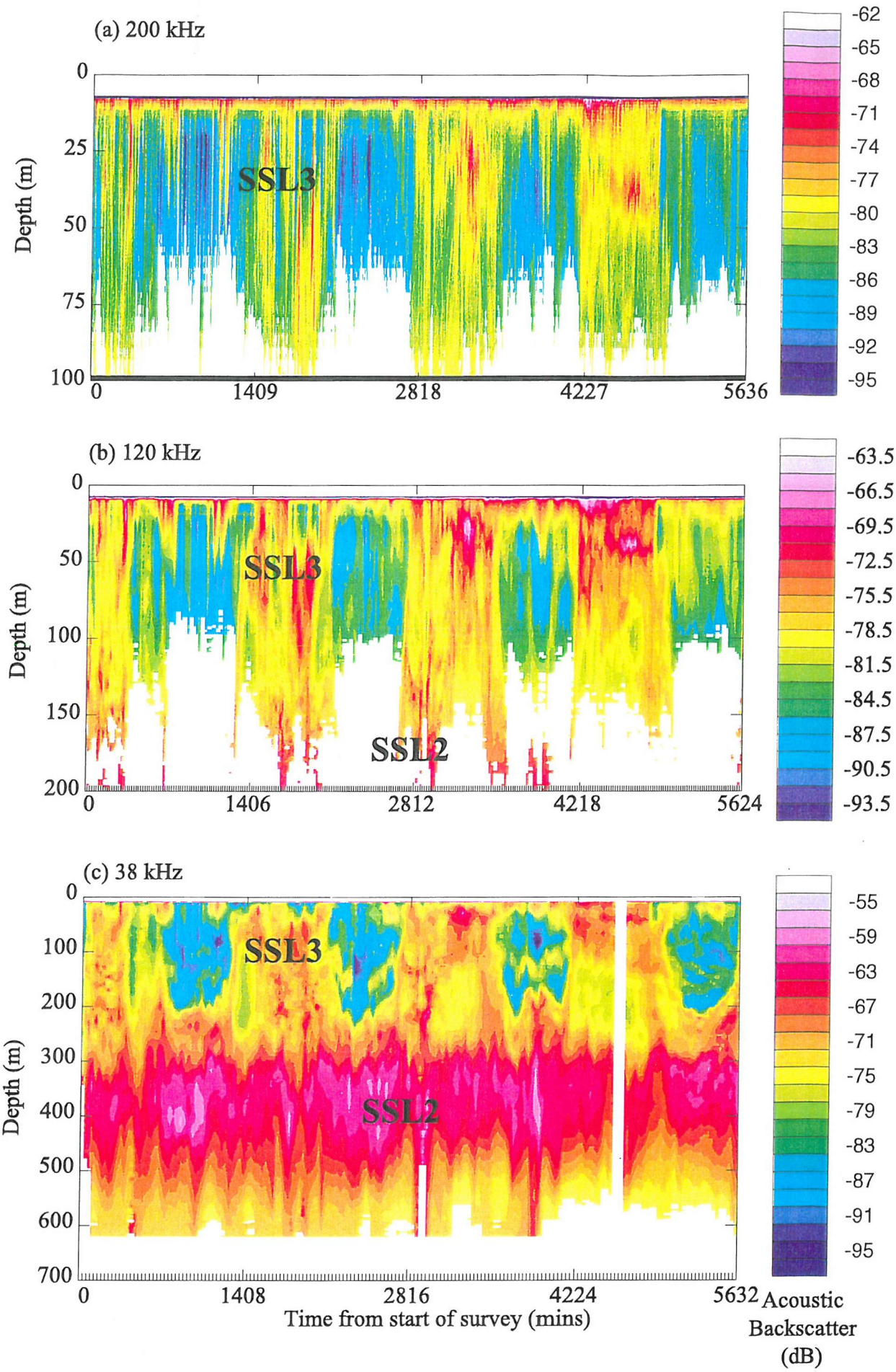

Figure 4.4.15 EK500 (a) 200, (b) 120 and (c) 38 kHz acoustic backscatter (Sv) for FSS3. Note different scales. Sound Scattering Layers 2 and 3 (SSL2 and SSL3) are identified.

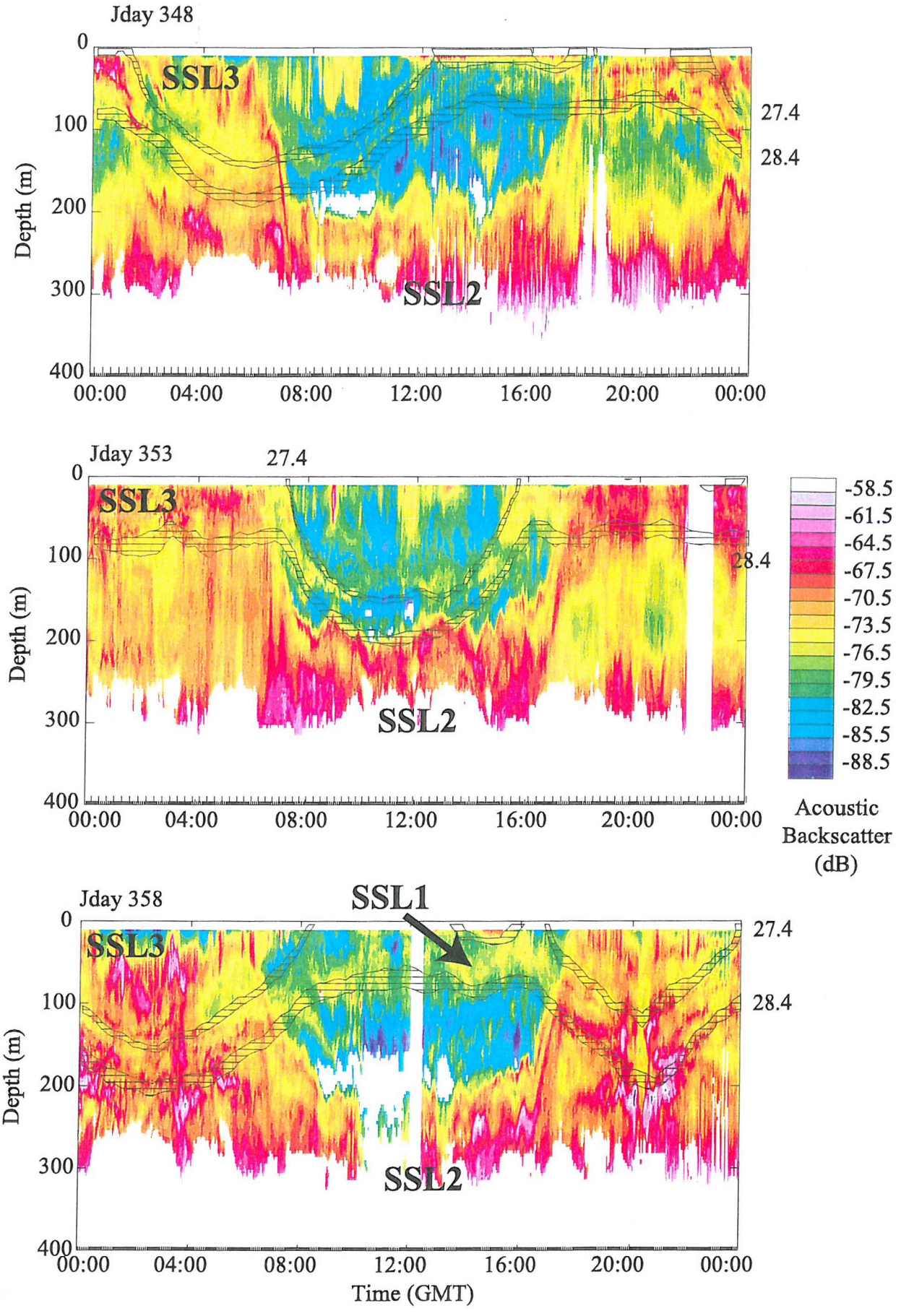

Figure 4.4.16 Twenty-four hour periods of VM-ADCP acoustic backscatter from jday 348 (top), 353 (middle) and 358 (bottom). Overlayed on each plot is the position of the 27.4 and 28.4 σ_0 isopycnal surfaces. Sound Scattering Layers 1-3 (SSL1, SSL2 and SSL3) are identified.

from jday 353 and 358 (Figure 4.4.17), show considerable detail and variety in acoustic patterns. Some of this variability can be attributed to the physical structure of the water column, and since the front was crossed at a different time each day the resulting pattern is complex (the position of the 27.4 and 28.4 σ_θ isopycnal surfaces are overlaid on Figures 4.5.16 and 4.5.17). This is particularly evident in the daytime data. During jday 348 (Figure 4.4.16a), VM-ADCP acoustic backscatter was relatively low (-90 to –81 dB) throughout the surface 200 m, except for a patch of high acoustic backscatter that occurred above the frontal isopycnal within the EAG. During jday 353 a distinct ~30 m thick layer of high backscatter occurred at ~150 m, above SSL2, coincident with the frontal isopycnal. This layer was present in the 38 kHz data and at the limit of the 120 kHz range (Figure 4.4.17ab). Dusk upward migration coincided with the crossing of the AOF on jday 353, although high backscatter in the surface 100 m within the EAG, similar to jday 348, was evident (at ~1500 hrs GMT) immediately prior to the vertical migration. The occurrence of high backscatter, indicating greater zooplankton biomass within the EAG close to the AOF is consistent with the observation of higher zooplankton abundance and biomass within surface waters on the EAG side of the AOF from LHPR station 13036.

The daytime pattern of acoustic backscatter on jday 358 was dominated by a ~70 m thick layer of high VM-ADCP acoustic backscatter (-78 to –66 dB) that surrounded the frontal isopycnal. This layer was at a similar depth and of similar thickness to SSL1 identified at LHPR station 13048. On jday 358 it rose from ~150 m at dawn to ~50 m at 1600 hrs GMT before deepening as the EAG was re-entered at dusk, contrary to more typical upward vertical migration of zooplankton at dusk. This layer persisted at the depth of the frontal isopycnal during and despite diurnal vertical migration. Concurrent fluorescence data, from the fluorometer mounted on SeaSoar, indicated that this layer was synchronous with the period at which phytoplankton was subducted down and along the front (Figure 4.4.18). According to LHPR station 13048 the depth of the SSL was coincident with higher net sampled biovolume which was composed of predominantly copepods, euphausiids and chaetognaths.

4.4.2.2 Diel vertical migration at the AOF

The observation of DVM in bioacoustic datasets has been widely reported (e.g Pleuddemann and Pinkel, 1989; Heywood, 1996; Roe *et al.*, 1996; Wade and Heywood, 2001). During D224 the acoustic data from all frequencies were characterised by a clear DVM signal of higher backscatter in surface waters at night (SSL3). Figure 4.4.19 presents the day and night vertical profiles of VM-ADCP data averaged for FSS1, FSS2

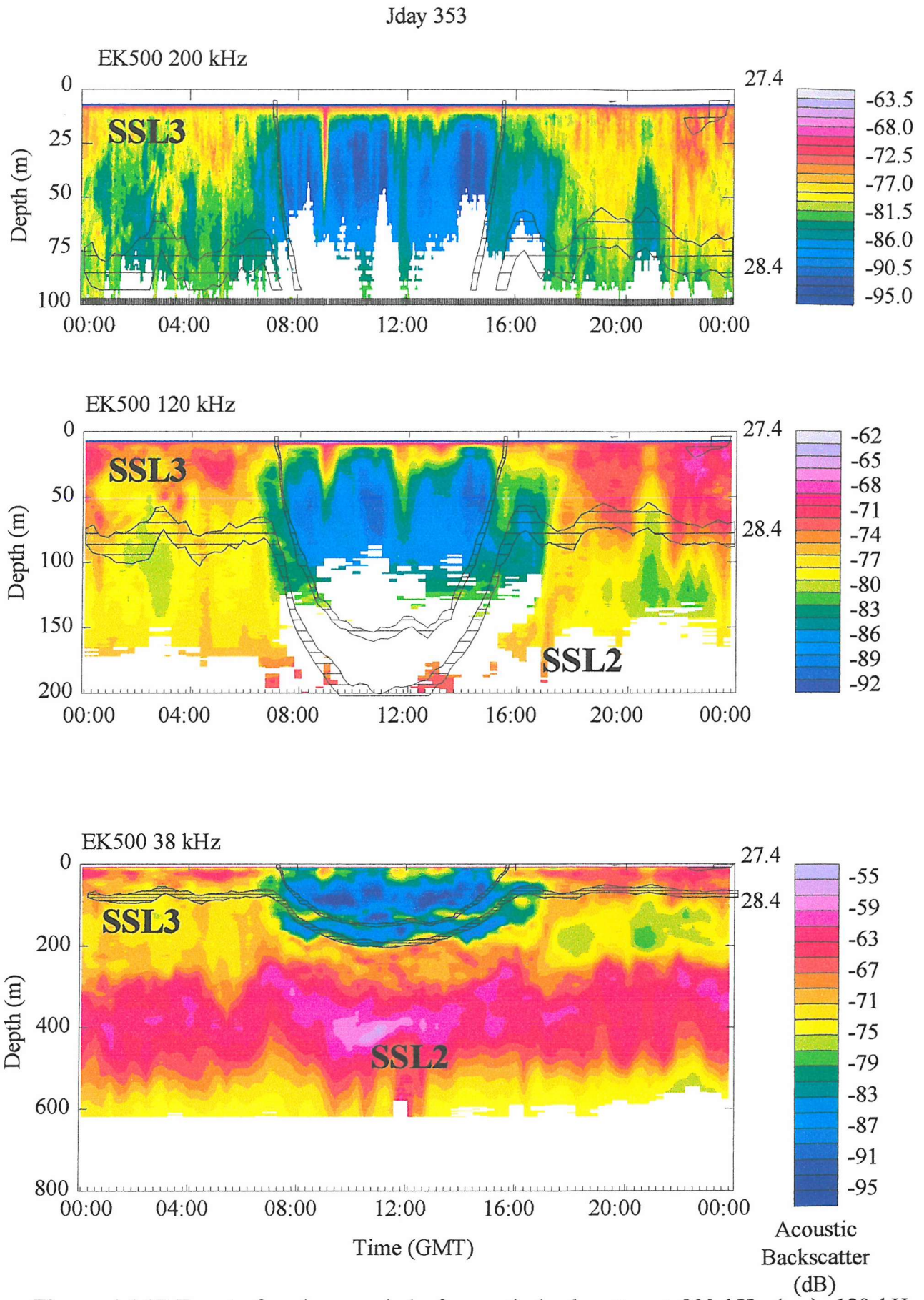

Figure 4.4.17 Twenty-four hour period of acoustic backscatter at 200 kHz (top), 120 kHz (middle) and 38 kHz (bottom) during jday 353. Overlayed on each plot is the position of the 27.4 and 28.4 σ_0 isopycnal surfaces. Sound Scattering Layers 2 and 3 (SSL2 and SSL3) are identified.

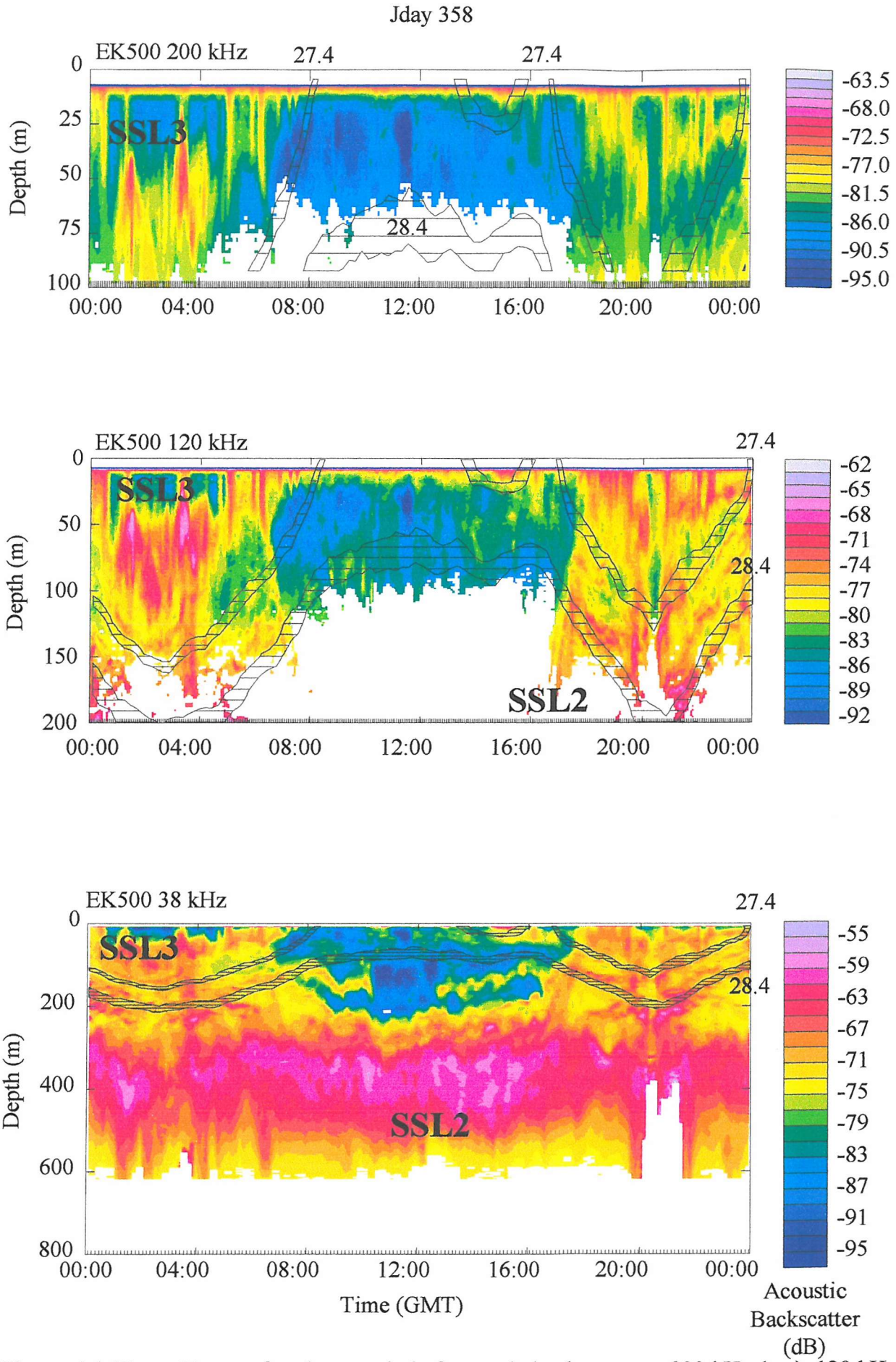

Figure 4.4.17cont Twenty-four hour period of acoustic backscatter at 200 kHz (top), 120 kHz (middle) and 38 kHz (bottom) during jday 358. Overlayed on each plot is the position of the 27.4 and 28.4 σ_0 isopycnal surfaces. Sound Scattering Layers 2 and 3 (SSL2 and SSL3) are identified.

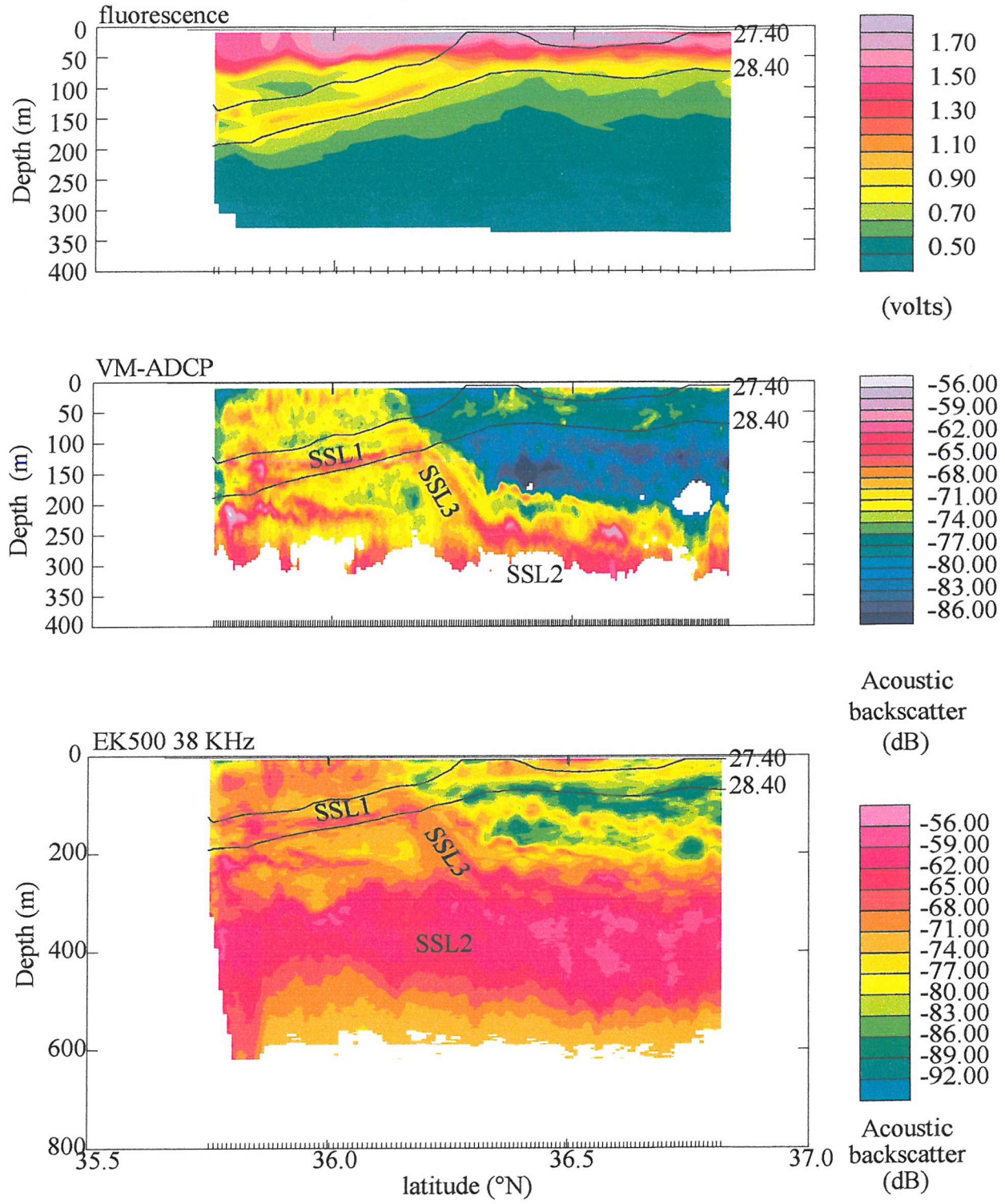

Figure 4.4.18 Contoured sections of fluorescence yield (instrument volts - top), VM-ADCP acoustic backscatter (middle) and EK500 38 kHz acoustic backscatter (bottom), across the Almeria-Oran front for leg g of FSS3. The 27.4 and 28.4 σ_0 isopycnals are over-layed for reference. The sound scattering layers discussed in the text are marked as SSL1-3.

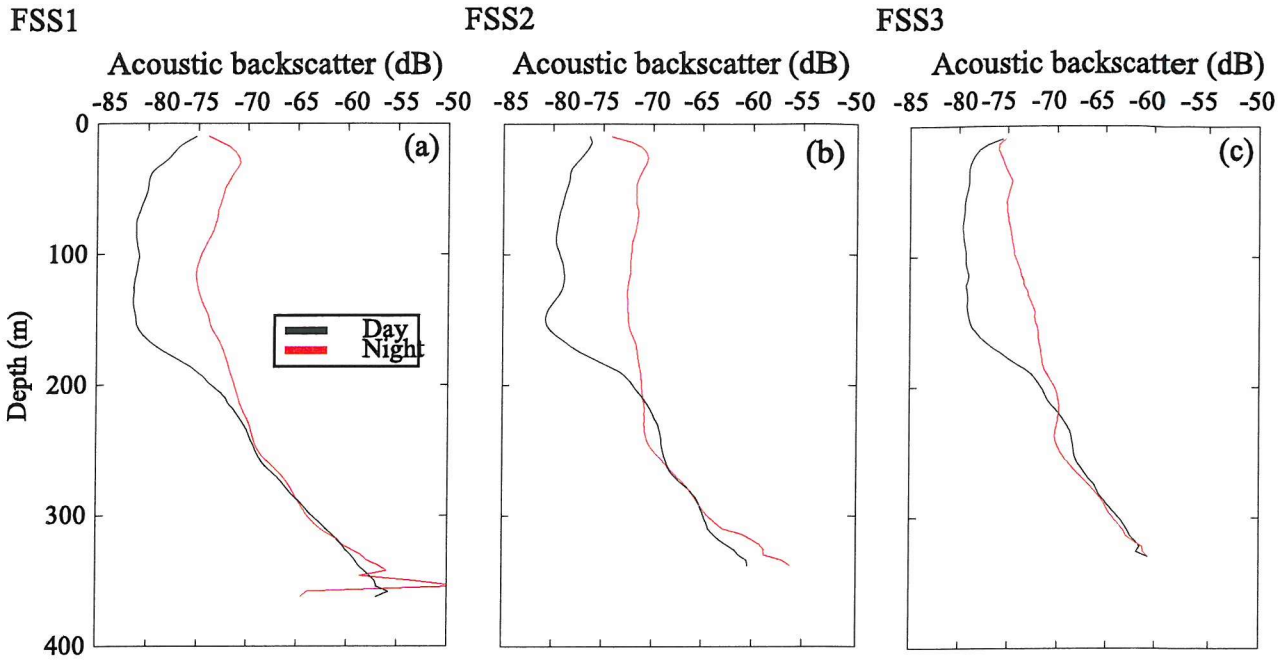

Figure 4.4.19 Vertical profiles of VM-ADCP acoustic backscatter data averaged for night and day during (a) FSS1, (b) FSS2 and (c) FSS3

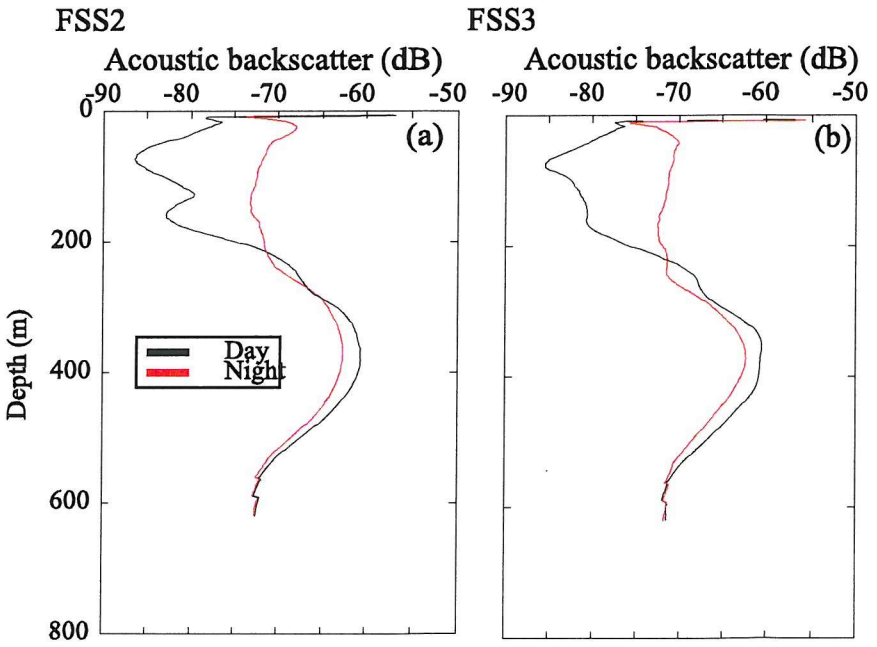

Figure 4.4.20 Vertical profiles of EK500 38 kHz acoustic backscatter data averaged for night and day during (a) FSS2 and (b) FSS3.

and FSS3. The data were split into night and day using light levels measured at 5 m (from the light sensor mounted on SeaSoar). All data where light = 0 W m^{-2} were deemed night, from approximately 17:30 to 06:47 GMT, and correspondingly data where light > 0 W m^{-2} were classed as day. An hour of data either side of these times (i.e. 16:30 – 18:30 and 05:47 – 07:47) was also removed as it was assumed that during this period zooplankton would be vertically migrating.

Figure 4.4.19 clearly shows a DVM signal above ~200 m, where at night acoustic backscatter throughout the surface 200 m was ~10 dB greater than daytime values. Below ~200 m the acoustic profiles were similar, indicating that the zooplankton migrating into the surface at night may have daytime depths below the range of the VM-ADCP.

Vertical profiles of 38 kHz acoustic backscatter show a distribution reinforcing the observation of two dominant scattering layers (SSL2 and SSL3). SSL2 is represented by a maximum in acoustic backscatter (~-60 dB) occurring around 400 m, its intensity only 5 dB less at night (Figure 4.4.20). Whereas above 200 m night-time values of acoustic backscatter are ~15 dB greater than daytime values. Therefore a proportion of the zooplankton and micronekton responsible for SSL2 are undertaking DVM into the surface 200 m at night.

RMT net samples, undertaken as part of leg 2 of cruise D224, indicated that siphonophores, heteropods, pteropods, cephalopods, amphipods, euphausiids, *Pyrosoma* and myctophid fish were undertaking DVM to varying depths (Powell, 1997), whilst *Cyclothone* fish presented no such behaviour. *Cyclothone* fish were the most abundant group of fish and maximum numbers occurred at ~400 m, coincident with the persistent SSL2.

The other facet of DVM behaviour that can be observed using acoustic methods is the speed of the migration. Many acoustic studies infer the vertical speeds of zooplankton through measuring the speed at which "backscattering bands" move up and down (e.g. Mauchline and Fisher, 1969; Mauchline, 1980). Using this method with the D224 dataset is complicated as discrete bands moving up or down were rarely identifiable. It was therefore decided to estimate the vertical speed of the leading edge of dawn and dusk migrations, where the slope of the leading edge would indicate the speed of the migration following:

$$c = \frac{\Delta Z}{\Delta t}$$

where c is the speed in cm s^{-1}, ΔZ is the change in depth of the band (cm) and Δt is the time (s) in which this change occurred.

Table 4.1 presents estimates of migrations speeds for jday 348, 353, 358 and the whole of the available data. Mean dusk upward migrations were faster than mean dawn downward migrations, although as shown for jday 358 dusk migrations were occasionally slower than dawn migrations. The migration speeds estimated here are not dissimilar to those reported by Tarling *et al.* (2001) of between 4 and 7 cm s^{-1} for the pteropod *Cavolinia inflexa*, and in excess of 11 cm s^{-1} for the euphausiid *Meganyctiphanes norvegica* in the Mediterranean Sea. In fact daily variations in estimated speeds may be a function of measuring different zooplankton populations migrating at different rates rather than a single population varying its rate of migration, since the data presented here is from a moving ship rather than an on-station study.

Jday	**Dawn** (cm s^{-1})	**Dusk** (cm s^{-1})
348	4.9	11.5
353	6.1	6.3
358	10.68	10.4
All available data	8.63 (±3.05)*	10.67 (±3.28)*

*Standard deviation

Table 4.1 Estimated speeds of dawn (upwards) and dusk (downwards) migration through examination of moving bands of high backscatter.

Pearre (1979) pointed out that these measurements represented the mean movement of the population, i.e. the vector sum of the mean velocities of all the individuals within a population moving in all directions at any time and that the vertical speed of individual zooplankton may greatly exceed that of the population. Pleuddemann and Pinkel (1989) and Roe and Griffiths (1993) noted that VM-ADCP-derived estimates of vertical motion resulted principally from the vertical migration of zooplankton. Roe and Griffiths (1993) and Tarling *et al.* (2001) propose that in using this estimate, vertical migration is being considered in terms of the vertical movement of individuals rather than the vertical movement of an entire band of backscatter, therefore bypassing Pearre's objections. The leading edge of the dawn downward migration on jday 348 had associated vertical velocities of ~3 cm s^{-1}, whilst the leading edge of the dusk upward migration had

maximum speeds of ~7 cm s^{-1}. The dawn and dusk migrations for jday 353 were 3 and 10 cm s^{-1} and for jday 358 were ~1.5 and ~8 cm s^{-1} respectively (Figure 4.4.21). It must be noted that VM-ADCP-derived vertical velocities include zooplankton movement plus water movement (Roe and Griffiths, 1993). The general background vertical speed of the water, away from the strong diel pattern, was of order 3 cm s^{-1} upwards. This background vertical velocity is likely to include instrumental bias as well as water movement. Subtracting this bias gives descent speeds between 4.5 and 6 cm s^{-1} and ascent speeds between 4 and 7 cm s^{-1}. These estimates of migration speeds are of the same magnitude as those calculated from the movement of backscatter bands and are far in excess of the downward 0.03 cm s^{-1} (25 m d^{-1}) associated with the ageostrophic nature of the AOF.

4.4.3 Discussion of the distribution of zooplankton at the AOF

4.4.3.1 The hydrography during the LHPR stations

From SeaSoar data, and previous studies (Tintore *et al.*, 1988; Prieur *et al.*, 1993; Allen *et al.*, 2001) it is known that the position and steepness of the AOF is highly variable on a time scale of days. LHPR station 13036 was undertaken prior to FSS2 when the AOF had steepened and moved southwest, whilst LHPR station 13048 occurred when the AOF had shallowed and returned to a more northeasterly positioned. This was reflected by the steeper density gradient observed at station 13036 compared with station 13048 (0.04 and 0.02 kg m^{-3} m^{-1} respectively).

4.4.3.2 The affect of the AOF on zooplankton distribution inferred from LHPR data

The distribution of zooplankton at the AOF was influenced by the physical structure of the water column. From the LHPR samples several features can be summarised: maximum zooplankton abundances occurred at ~200 m; maximum zooplankton biovolumes occurred at depths where there were variations in either density or temperature; the front appeared to have little influence on zooplankton distribution below ~200 m; pteropods were absent from the Mediterranean side of the front; enhanced zooplankton abundance was observed in frontal waters; larval stages were present in surface water, adult stages were present at depth; and an increase in zooplankton biomass occurred at the depth at which subducted phytoplankton was observed

Maximum zooplankton abundances at ~200 m

Maximum abundance of zooplankton occurred between 180 and 220 m. Specifically this resulted from an increase in the abundance of copepods and ostracods where numbers were two or three times greater than surface values and was represented by their near total dominance of the zooplankton taxa present (~99 %). Notably this maximum occurred on the down and upcast of both LHPR stations, significantly below

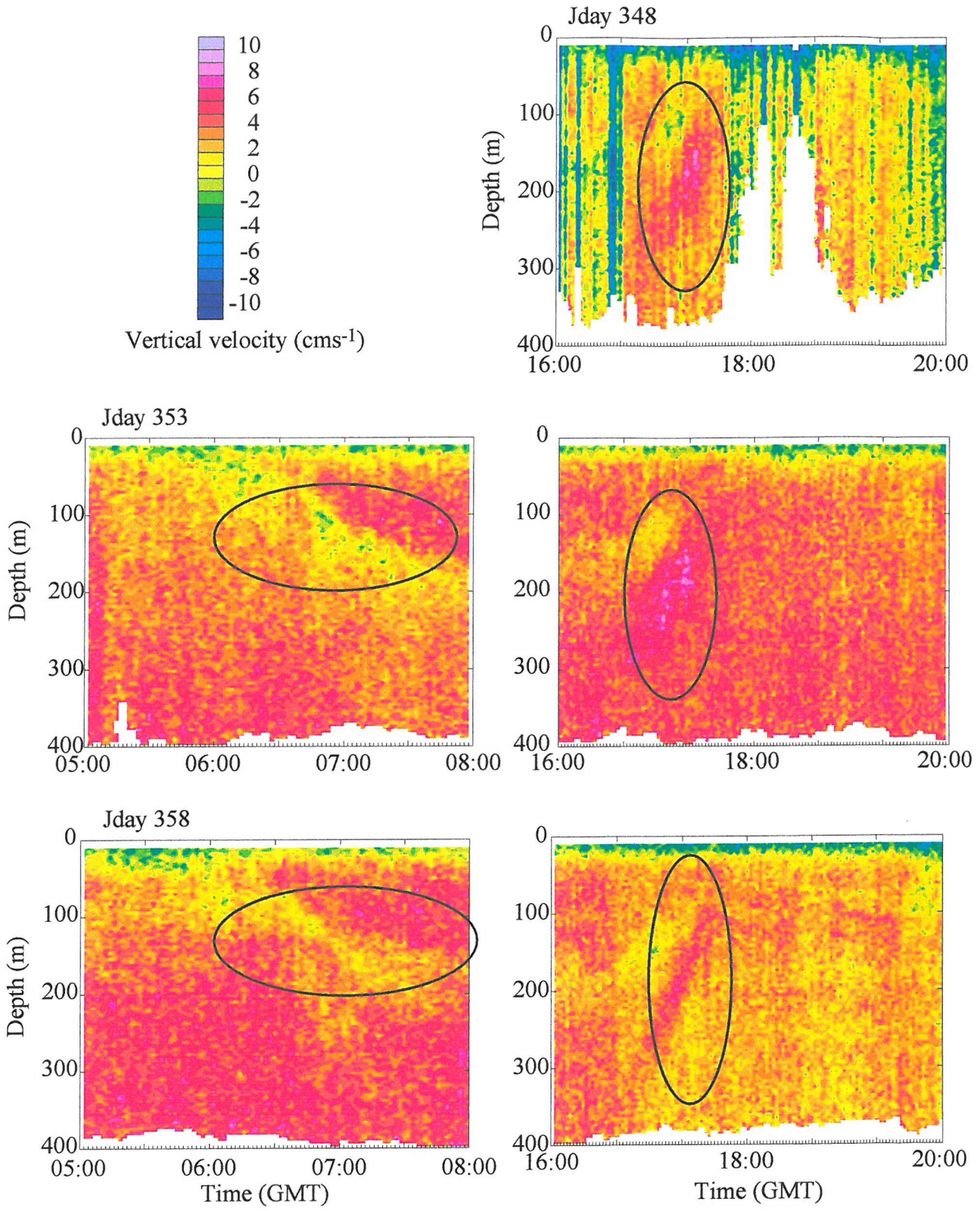

Figure 4.4.21 VM-ADCP derived vertical velocities for jday 348 (top), 353 (middle) and 358 (bottom). Periods of migration have been circled.

the pycnocline. Although not related to the water column structure at the LHPR stations this depth was coincident with the greatest depth of the MAW/LIW interface at the base of the middle of the EAG (as observed from SeaSoar data). It could therefore be speculated that the daytime distribution of copepods and ostracods was consistent with removal from MAW or to the depth of a density discontinuity. But without data from stations in the middle of the EAG the cause of this maximum is unknown. However it does have important implications for the conclusions drawn from previous studies. Thibault *et al.* (1994) and Youssara and Gaudy (2001) both used net hauls from only 0 to 200 m depth to examine the distribution of mesozooplankton, particularly copepods, based on the assumption that this was where most of the pelagic biomass and production is usually found. They cited day/night differences in total zooplankton to be not significant inferring that vertical migration, if present, occurred within the upper 200 m of the water column. In several cases, observed highest abundances in integrated vertical net hauls were during the day. These results, which Youssara and Gaudy (2001) refer to as ambiguous, may be caused by inconsistencies in "catching" the highest abundances of copepods at the vertical limit of their net hauls.

Maxima in biovolume were at depths consistent with density discontinuities

High values of both zooplankton abundance and biovolume were found at the base of the mixed layer on either side of the front and at the depth of the temperature minimum. This is consistent with observations by Murav'yev and Shirshov (1984), Ortner *et al* (1980; 1981) and Magnuson *et al.* (1981) of the orientation of zooplankton to density discontinuities and close association with thermal gradients. High values of biomass were also associated with depths just below or above the greatest change in density. This may have resulted from avoidance of large salinity or temperature gradients. For example, Harder (1968) observed pteropods actively avoiding large salinity gradients, and preferentially remaining with waters of smaller gradients.

Zooplankton distribution below ~200m

According to the LHPR samples the distribution of zooplankton below ~200 m was similar on both the down and upcast, the front presenting no obvious influence. Contrary to these results there is evidence that surface-enhanced productivity is exported to deep waters and the benthos below frontal zones enhancing deeper secondary productivity (Mann and Lazier, 1991; Gerin and Goutx, 1994). The greater spatial coverage attained using the RMT nets, during leg 2 of cruise D224, indicated that the biomass of fish, heteropods, euphausiids and possibly cephalopods were increased on waters sampled below the front compared with Mediterranean waters (Powell, 1997). The

lack of variations below ~200 m in the LHPR data is expected to be related to the small spatial distances covered by the LHPR (~15 km). The horizontal distance travelled by the LHPR below 200 m would be insufficient to sample below true MSW, frontal and MAW during the same cast.

Why were Pteropods were absent from the Mediterranean side of the AOF?

The distribution of pteropods at the AOF was notable by their presence in deep Mediterranean waters and the EAG, and their absence from the Mediterranean side of the front. Oceanic fronts acting as barriers to the distribution of fauna have long been recognised (Reid *et al.*, 1978; Backus, 1986). For example, Wiebe and Flierl (1983) observed a rapid cross-front transition in euphausiid species at a cold-core ring front. The temperate euphausiid *Nematoscelis megalops* was present in the ring core but was replaced by the subtropical euphausiid *Stylocheiron affine* in the surrounding Sargasso Sea waters.

The absence of pteropods from the Mediterranean side of the front was surprising, since species of pteropods present in Mediterranean waters have been observed previously (Sardou *et al.*, 1996). However Powell (1997) identified morphological differences in the pteropods present within Almeria-Oran frontal waters that were hypothesised by Van Der Spoel (pers. comm. refered to in Powell, 1997) to be indicative of environmental stress. This environmental stress being related, in this case, to encountering unfavourable temperature and salinity contrasts or values. It was hypothesised that these pteropods could have switched to asexual reproduction within the stressful frontal environment producing aberrant stages and therefore this could reduce the ability of the group to proliferate within the frontal region.

Increased zooplankton abundance within frontal water

High zooplankton abundance was observed on the EAG side of the front, within waters of a mix between AMIW and MAW. High zooplankton abundance and biomass often characterise frontal, compared with adjacent, waters (Gaudy *et al.*, 1996). Several mechanisms can explain this increase (see Chapter 1). For example the concentration of organisms through transportation towards a convergence zone (Herman *et al.*, 1981; Gaudy *et al.*, 1996). However the increased abundance observed in this study did not occur where the sloping isopycnals break the surface (which, incidentally, was not sampled because the LHPR was always at depth when the surface signature of the front was crossed) but occurred just within the EAG, in the region where the fast-flowing frontal jet was observed from SeaSoar and VM-ADCP data. High abundance of zooplankton, particularly copepods, within the frontal jet associated with the AOF has

been observed previously (Seguin *et al.*, 1993; Youssara and Gaudy, 2001). This high abundance could result from either accumulation of fauna transported in from the Atlantic, through the Strait of Gibraltar into the frontal current, or from a local increase in secondary production. Greze *et al.* (1985) observed high abundance of zooplankton to the east of the Strait of Gibraltar and attributed it to the permanent introduction of Atlantic fauna by the current entering the Mediterranean Sea. However, taxonomic identification of fauna within the AOF jet found only a small number, in low abundance, of species endemic to the Atlantic (Seguin *et al.*, 1993). The presence of larval stages in the present study and previous studies (Seguin *et al.*, 1994; Youssara and Gaudy, 2001) in these surface waters indicate that the high abundance in the frontal jet may be a consequence of local secondary production. Observations of primary and secondary productivity from the ALMOFRONT-1 study provide supporting evidence for this supposition. High abundance of diatoms, fuelled by the advection of nutrients into the euphotic zone by the secondary circulation, was observed at the AOF (Fiala *et al.*, 1994; Prieur *et al.*, 1993; Videau *et al.*, 1994). In accordance with the classic food chain concept (Cushing, 1989), where diatoms are considered the preferential food of copepods, maximum zooplankton grazing activity on phytoplankton was also observed at the front (Thibault *et al.*, 1994; Striby and Goutx, unpublished results cited in Youssara and Gaudy, 2001). Youssara and Gaudy (2001) postulate that since there is an isopycnal downwelling transfer of primary and secondary production from the Mediterranean to the Atlantic side of the front (Prieur *et al.*, 1993; Seguin *et al.*, 1994) and hence the jet, eggs produced at the front (the Mediterranean side of the jet) would develop during their cross frontal transport such that maximum numbers of nauplii would be present in the jet.

The continued observation of high zooplankton abundance within the frontal region, through subsequent studies (i.e. ALMOFRONT-1 and OMEGA), suggests the maintenance of favourable trophic conditions, responsible for reproductive success and larval growth. Zooplankton such as copepods require periods of 15-20 days for successful naupliar development (Landry, 1983; Hart, 1990) and since the AOF is a quasi-permanent structure in the Alboran Sea (Tintore *et al.*, 1988; Folkard *et al.*, 1994; Allen *et al.*, 2001), the minimum time for zooplankton growth is greatly exceeded. High zooplankton abundance at the AOF, having now been observed repeatedly at several periods of the year, may be a permanent feature of the Alboran Sea.

Ontogenetic variation in zooplankton with depth

Ontogenetic stratification of zooplankton is well documented (e.g. Roe, 1972). In the present study the mean length of euphausiids, fish and pteropods increased below

~200 m. Examination of the LHPR samples indicated that surface waters typically contained larval stages of euphausiids and fish. The partition of larval euphausiids within surface waters and adult euphausiids at depth has been observed previously at the AOF (Baussant *et al.*, 1993) and within the western Mediterranean (Anderson and Sardou, 1992). The vertical distribution of different-sized euphausiids within the water column may result from either a change in species or a change in life stage (ontogenetic behaviour). Anderson and Sardou (1992) indicate the presence of four abundant species of euphausiid; *Nematoscelis megalops, Stylocherion longicorne, Euphausia krohni* and *Thysanopoda aequalis* within the western Mediterranean Sea. According to Baker *et al.* (1990) the typical lengths of the four abundant species are 22-26 mm, 6-11 mm, 16 mm and 12-22 mm respectively. Therefore the change in mean length increasing with depth may indicate a vertical shift in species from *Stylocherion longicorne* at the surface to *Nematoscelis megalops* at depth. However Anderson and Sardou (1992) observed both these species occupying the same depth strata.

Alternatively, the increase of mean size with depth may indicate ontogenetic behaviour, i,e, the vertical separation of different life stages to prevent intra-specific competition. Ontogenetic behaviour has been observed and suggested for several euphausiids (Boysen and Buchholz, 1984; Trathan *et al.*, 1993; Tarling *et al.*, 1998). In the western Mediterranean the most abundant species found in the study by Anderson and Sardou was *Nematoscelis megalops*, which was observed to have a bimodal vertical distribution with a shallow maximum (75-150 m) of small individuals (<11 mm) and a deeper (350-550 m) layer of larger (>11 mm). Tarling *et al.* (1998) propose that variations in the depth and vertical migration of different life stages may be related to the energetic costs involved with maintaining a pelagic lifestyle. They calculated that a 25 mm krill would need to provide between 41 and 54 % of the ATP necessary for a 30 mm krill to maintain its pelagic lifestyle. Using this they hypothesised that it is energetically "understandable" that large individuals ascend less frequently than small ones.

The variation in mean length with depth observed in this study was related to the presence of a greater number of euphausiid larvae within the surface LHPR samples. Whilst an additional stratification of different euphausiid species may also have influenced the size structure, the numerical dominance of euphausiid larvae was such that the dominant mechanism controlling this distribution is proposed as being a result of ontogenetic stratification.

The similar pattern of increased mean fish length with depth was also a result of larval stages caught at the surface and juvenile and adult stages at depth. Taxonomic

identification of the fish larvae within the RMT net samples indicated that *Benthosema* sp. larvae were the most abundant at the surface, whilst *Cyclothone* sp. larvae and juveniles occurred at depth (Pugh, pers. comm.).

The final group to show a variation with depth in mean length were the pteropods. Whilst a degree of ontogenetic stratification may have caused this pattern (age was not identified) it is also possible that environmental stress, that was producing aberrant stages (Powell, 1997), may have stunted growth within the frontal waters.

Zooplankton were observed coincident with subducted phytoplankton

An increase in zooplankton biomass was observed at depths comparable with the frontal isopycnal. The orientation of zooplankton to density discontinuities is well documented (see above). However the increase in zooplankton at depths of the frontal isopycnal was not a consistent feature at both LHPR stations, but occurred only at station 13048 immediately prior to the period in which phytoplankton was observed to be subducted down the front in SeaSoar data during FSS3. The layer of zooplankton concurrent with the frontal isopycnal (also observed in the acoustic backscatter data) may result from either the subduction of zooplankton from surface waters, with the phytoplankton, or from some behaviourally-mediated concentration in the vicinity of a food source. Isopycnal downwelling of secondary production at the AOF has been suggested (Prieur *et al.*, 1993; Gerin and Goutx, 1994; Seguin *et al.*, 1994; Pedrotti and Fenaux, 1996) and cannot be discarded as the formative mechanism. However isopycnal downwelling, as part of the secondary circulation, is a consistent feature at the AOF, compared with only the periodic subduction of phytoplankton. Since the presence of a concurrent layer of zooplankton at the frontal isopycnal was also transient, coincident with the subducted phytoplankton, the author favours the theory that this layer of zooplankton was a consequence of behaviourally-mediated concentration.

Taxonomic identification of the LHPR samples indicated that this layer had increased abundances of larger (with respect to surrounding waters) chaetognaths and, during the upcast, of larger euphausiids. Euphausiids are omniverous, and as such may be concentrating at a food source, whilst chaetognaths are recognised to be voracious predators and the reason for the concentration of large specimens within this layer is unclear from the present data. Chaetognaths are a major predator of copepods (Sullivan, 1980; Feigenbaum and Maris, 1984) as well as feeding on fish larvae and micro- and meso-zooplankton (Feigenbaum, 1991). There was no dramatic decrease or increase in the abundance of copepods compared with surrounding waters, at depths of the frontal isopycnal, but it is possible that the concentration of herbivorous zooplankton at this depth

was attracting higher trophic level predators. The increase in mean size of the zooplankton within this layer may result from either the presence of adult specimens, remaining in surface food-rich waters rather than diel migration to deep waters during the day, or a shift in species present within the depth strata.

Both euphausiids and chaetognaths are able swimmers, capable of influencing their position within the water column and resisting transport through isopycnal downwelling of speeds observed at the AOF. Further evidence to suggest behavioural mediation of position rather than passive subduction was apparent in the acoustic backscatter data. The layer of high backscatter, coincident with the frontal isopycnal, was represented by greater intensities at night, possibly indicating that some zooplankton were interrupting their diel migratory behaviour to remain within a food rich region.

4.4.3.3 The affect of the AOF on zooplankton distribution inferred from acoustic backscatter data

Three scattering layers were identified in the acoustic backscatter data: a moving layer of high acoustic backscatter represented the diel migration of some zooplankton; The presence of a permanent deep scattering layer indicated that some zooplankton and/or micronekton were remaining at depth through both the day and night; and the presence of high backscatter coincident with the subducted phytoplankton indicated some zooplankton were interrupting their diel migration to accumulate at a source of food. In addition patches of high backscatter were observed within the fast flowing frontal jet.

Diel vertical migration at the AOF

Diel vertical migration of zooplankton was observed in the acoustic backscatter data from all frequencies. SSL3, the acoustic signal of DVM was typically identified by an increase in acoustic backscatter in the surface rather than a distinct layer migrating to the surface at dusk and down at dawn. Hydrographic changes along the cruise track resulted in variations of the depth of greatest acoustic backscatter within the surface 200 m, although where density gradients did not dominate highest backscatter was found in the surface 50 to 100 m. It is recognised that many zooplankton species do not migrate as compact populations, nor do they necessarily remain in surface waters throughout the night (Pearre, 1979; Roe, 1984a,b). Therefore highest biomasses may occur in surface waters throughout the night, with moderate biomasses occurring throughout the rest of the water column. If, for example, the model of vertical migration (Fig 3A, Pearre, 1979 and as suggested by Roe, 1984a,b) was correct (in which a vertically-migrating organism has a very short time spent in changing depth and long and equal times at the upper and lower ends of its range) it would represent a bimodal distribution of biomass (with maxima at the surface and

depth). Between these maxima was an intermediate biomass, similar to the observed pattern of night-time acoustic backscatter data.

Supplementary RMT (Rectangular Midwater Trawls) net samples showed that myctophid fish, decapods, euphausiids, pteropods and siphonophores were undertaking vertical migration at the front (Howell, pers. comm.). These animals represent dominant acoustic scattering groups, especially myctophid fish which have resonant gas bladders thereby augmenting their acoustic scattering (Johnson, 1977). Thibault *et al.* (1994) and Anderson and Sardou (1992) also observed the vertical migration of several groups of zooplankton (euphausiids, mysids, fish and decapods) over a depth range of 300-400 m.

Detailed examination of acoustic backscatter at dusk and dawn reveals various estimates of migratory speeds. With dawn, downward (5.4 cm s^{-1}), speeds being significantly slower than dusk, upwards (8.1 cm s^{-1}), motion ($P>0.05$, Students t-test). VM-ADCP-derived vertical velocity estimates were similar to those obtained from measuring the trajectories of backscattering bands over time, although upward velocities were slightly smaller. These estimates of migratory speeds are comparable with previous studies (Roe and Griffiths, 1993; Heywood, 1996; Tarling *et al.*, 1998; Wade and Heyward, 2001). Tarling *et al.* (1998) cite consistently lower VM-ADCP-derived speed estimates to be a result of methodological differences. It is expected that the discrepancy here is a result of the measured trajectory of a backscattering band estimating the speed of the population migration, whilst the VM-ADCP-derived vertical velocities measures the speed of individual zooplankton that may differ from the population. The estimated migratory speed deduced from the scattering layers may well be biased, high or low, as different portions of the population move at different rates. For example Roe *et al.* (1984) and Wiebe *et al.* (1992) noted that leading edge individuals of a copepod migration dropped back.

A permanent deep scattering layer was present at the AOF

A permanent deep scattering layer (SSL2) was observed in acoustic backscatter data from the VM-ADCP and 38 kHz echosounder, within the TML and LIW. The presence of a deep scattering layer is a common feature of bioacoustic surveys in the Mediterranean Sea (Baussant *et al.*, 1992; 1993) and has been attributed to the occurrence of mesopelagic fish, particularly *Cyclothone* and myctophid species. The pattern of 38 kHz sound scattering layers confirms this observation. The vertical distribution of fishes (Myctophid, *Cyclothone*) corresponds to the depth of SSL2. Myctophid fish, which contain a gas-filled swim bladder the size of which determines their acoustical properties (Marshall, 1970; Love, 1978), have been shown to be responsible for strong deep echo

signals (Barham, 1966; Aboussouan, 1971). They were observed in RMT net samples (Howell pers. comm.) to undertake DVM and were probably partly responsible for the DVM (SSL3) signal in the 38 kHz data. However, the most abundant group of fish present in this study (from both LHPR and RMT net samples) and in previous studies (Aboussouan, 1971; Laval *et al.*, 1989; Baussant *et al.*, 1993) were *Cyclothone* fish that did not undertake DVM. Since SSL2 showed little variation in depth or intensity through both the day and night it is probable that these fish were predominantly responsible for it. As the physical properties of the water mass below 200 m showed no significant variation, it is understandable that SSL2 remained at the same depth either side of the front. This is however contrary to the observation of a variation of 50 m in depth either side of the front (Baussant *et al.*, 1993).

Zooplankton occurred coincident with subducted phytoplankton

SSL1 was observed at LHPR station 13048 and found coincident with the layer of subducted phytoplankton during FSS3. LHPR samples identified an increase in biomass at corresponding depths and taxonomic identification revealed a maximum abundance of large euphausiids and chaetognaths. This observation of a scattering layer present in the frontal region at depths between 100 and 200 m is supported by observations of Baussant *et al.* (1993). These authors proposed that the observed scattering layer between 100 and 200 m in the frontal zone was a result of increased abundances of euphausiid larvae.

The layer of high backscatter (SSL1) at the front persisted despite and during the occurrence of diel migration. Sameoto (1976) observed deep chlorophyll maxima to be exploited by planktonic grazers, at least some of which would be expected to migrate to near-surface waters. More recently, Owen (1981) and Wishner and Allison (1986) observed zooplankton concentrating in convergence zones interrupting their diel migration. It is likely that the observations in this study indicate a similar occurrence, and thus the horizontal and vertical distribution of some of the zooplankton at the Almeria-Oran front are controlled by a combination of physical processes and animal behaviour.

Increases in zooplankton abundance and biomass within frontal waters, compared with adjacent waters, may be caused by physical processes (such as the drawing down of surface species by subduction) and/or behaviour (active accumulation of animals at a more abundant food source). The rate of subduction (25 m d^{-1} or 0.03 cm s^{-1}) is significantly less than the rate of vertical migration of some zooplankton (Heywood, 1996 Tarling *et al.*, 1998), and speeds observed in this study. In addition the coincident abundance of phytoplankton tends to suggest the increase in zooplankton abundance was a result of behaviourally-mediated concentration in the presence of convergence zones and increased

food abundance (as seen by Okubo, 1978; Gorsky *et al.*, 1991 and modelled by Franks, 1992; 1997). These observations support the hypothesis presented by Gorsky *et al.* (1991), that enhanced superficial production can influence the mesopelagic ecosystem.

High acoustic backscatter within the fast flowing frontal jet

In addition to the three identified scattering layers the acoustic data, a patch of high VM-ADCP, 120 and 200 kHz acoustic backscatter was consistently observed at the surface on the Atlantic side of the Almeria-Oran front, coincident with the strong frontal jet (1 m s^{-1}). LHPR station 13036 showed high abundance of small copepods and euphausiids at the surface within the EAG side of the front and Optical Plankton Counter data (not shown, Fielding *et al.*, 2001) also indicated the presence of a high abundance of particles sized between 0.65 - 1.35 and 1.35 - 2.75 mm ESD. High zooplankton biomass has been observed in strong jets by Nash *et al.* (1989) and at the Almeria-Oran front by Thibault *et al.* (1994) and Seguin *et al.* (1994). At the AOF that increase was dominated by copepods with approximate lengths of 1 mm. These copepods would be ideally sampled by the OPC in the size range 0.65 – 1.35 mm ESD (Herman, 1992; following particle length approximately 1.5 times ESD according to Beaulieu *et al.*, 1999) and are of similar size to the mean copepod length measured at LHPR station 13036. It is hypothesised that the increased abundance of small copepods within the frontal jet result from advection and concentration of localised secondary production as proposed by Thibault *et al.* (1994).

4.5 Summary

(1) The variability in the position and shape of the AOF and the strongly sheared velocity field indicate mesoscale frontal instability and the presence of ageostrophic flow. The observation of the entrainment of MSW into the frontal jet where it was drawn down and across the front permitted the estimation of a subduction rate of ~25 m d^{-1}.

(2) High phytoplankton biomass in the vicinity of the AOF was recorded and phytoplankton were also observed being drawn down the front to depths of ~200 m. The distribution of zooplankton appeared to be influenced by the AOF.

(3) This study shows that some organisms find a front to be a barrier (e.g. pteropods), whilst others find the front is an environment that promotes production or accumulation through either behaviourally or physically mediated processes (e.g. chaetognaths and euphausiids).

(4) It is likely that the observations in this study indicate that the horizontal and vertical distribution of larger zooplankton (e.g. > 5 mm in length) at the Almeria-Oran

front are controlled by a combination of physical processes, with downward vertical motion providing a vertically-displaced food source, and animal behaviour, with diel migration disturbed by food availability.

(5) The effects of mesoscale physical processes on zooplankton distribution/patchiness have similar temporal and spatial scales as some zooplankton behaviour (Haury, 1982), and as such can be difficult to differentiate in observations. Modern survey tools (SeaSoar, OPC, acoustics etc.) that determine physical and biological variables concurrently, and at the same high resolution time and space scales, permit a quasi-synoptic understanding of biological distributions about which previous investigators have had to speculate intuitively (Baussant *et al.*, 1993; Videau *et al.*, 1994).

(6) To identify ecosystem dynamics in the real ocean requires that relevant and complementary data are taken concurrently: the results of this study show convincingly that biological distributions in the vicinity of a front result from a combination of physical, chemical and biological factors.

Chapter 5

Biological validation of acoustic backscatter

5.1. Introduction

In this chapter the relationship between zooplankton net samples and observed acoustic backscatter is examined. In section 5.2 VM-ADCP acoustic backscatter is compared with LHPR sampled zooplankton from the Indian Ocean (*Discovery* cruise 209). The relationship is examined through direct comparison and through the use of acoustic models (see Chapter 1 and 2). In addition a direct relationship is examined using only groups classed as significant acoustic scatterers and included in the models. These are amphipods, chaetognaths, copepods, euphausiids (including decapods), fish and pteropods (Stanton *et al.*, 1994a). Even though siphonophores are significant acoustic scatterers (Warren, 2001), they could not be included in this study because, as with most net systems (Pugh, 1989), they are destroyed in the LHPR samples. The oxygen concentration of the water from which the LHPR sampled was categorized to identify whether the differences in zooplankton groups that occurred between the oxygenated and deoxygenated water was represented in the observed acoustic backscatter and the acoustic scattering models.

In section 5.3 the relationship between VM-ADCP acoustic backscatter data and LHPR zooplankton samples from the Mediterranean Sea (*Discovery* cruise 224) is examined. Concurrent acoustic backscatter data taken with a biological multifrequency echosounder (SIMRAD EK500) is analysed using the same method. Each frequency (153 kHz from the VM-ADCP and 200, 120 and 38 kHz from the EK500) is compared directly with the zooplankton samples and acoustic scattering models. The water mass (identified using the environmental sensors mounted on the net) from which the LHPR samples were taken is established and used to investigate whether changing zooplankton population size-structure affects observed and model-estimated acoustic backscatter.

Section 5.4 compares and contrasts the two studies and summarises the results and Section 5.5 lists relevant conclusions.

5.2 Comparison of observed acoustic backscatter (OAB) and zooplankton samples from the Arabian Sea

5.2.1. Description of concurrent acoustic backscatter and zooplankton samples

Figure 5.2.1 shows a contour plot of VM-ADCP acoustic backscatter over the period of the downcast of the LHPR Station 12664#1. Two sound scattering layers can be identified, Sound Scattering Layer One (SSL1) occurred between the surface and 70 m depth with intensities from –64 to –76 dB, with the greatest intensities occurring near the surface above 50 m. The second Sound Scattering Layer (SSL2) occurred below 250 m

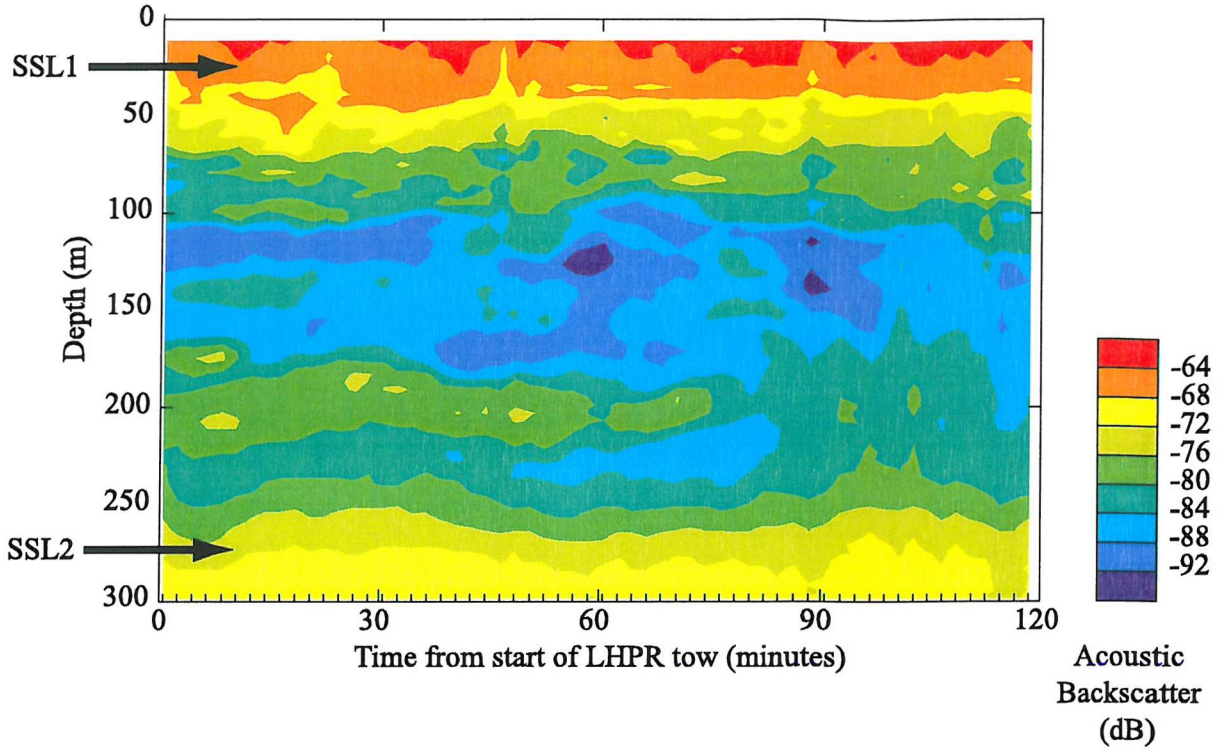

Figure 5.2.1 A contour plot of VM-ADCP acoustic backscatter during the LHPR Station 12664#1. Two Sound Scattering Layers (SSL) are identified. SSL1 in the surface 0 to 70 metres and SSL2 below 250 metres.

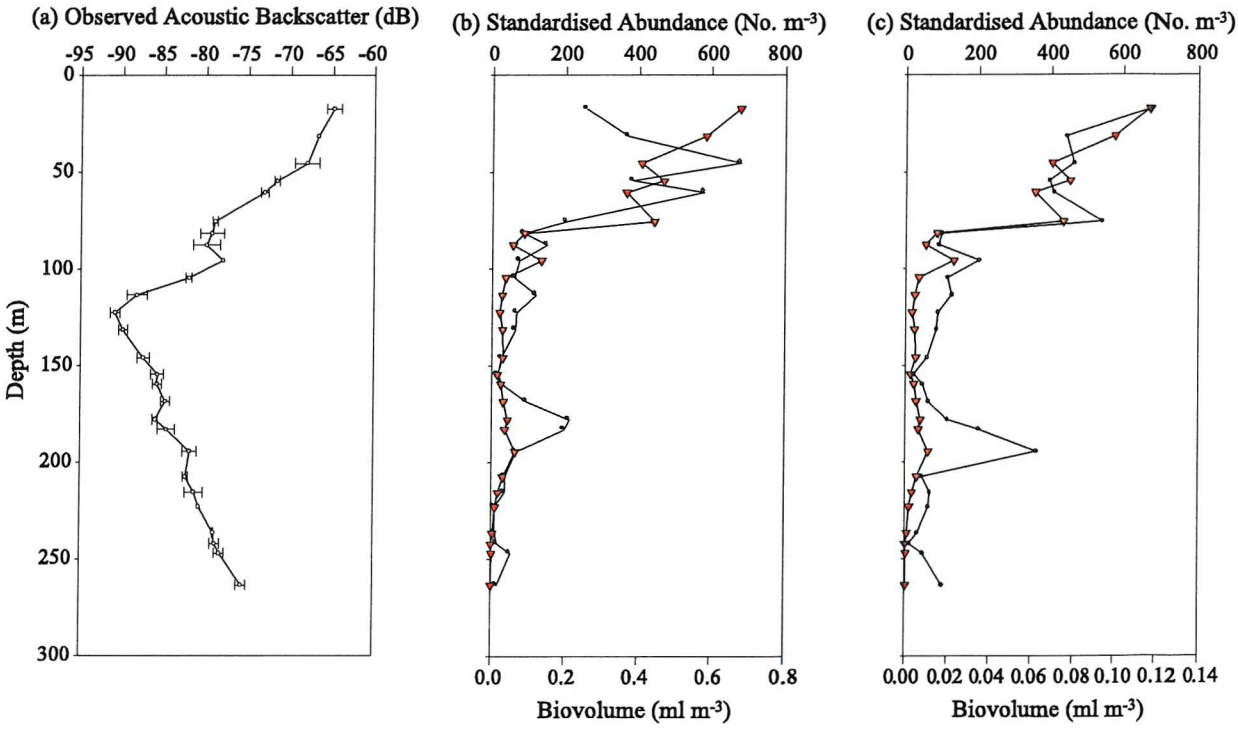

Figure 5.2.2 The distribution with depth of (a) observed VM-ADCP acoustic backscatter, (b) total LHPR sample biovolume (red) and total sample abundance (black), and (c) acoustic group biovolume (red) and acoustic group abundance (black).

and was ~-70 dB in intensity. Between these two scattering layers was a region of low acoustic backscatter, ranging between –94 and –80 dB, with the lowest values recorded between 100 and 175 metres.

Using the method outlined in Section 2.3.2.1, acoustic data in the vicinity of each two-minute LHPR sample were calculated. A summary of the acoustic volume backscattering statistics and the standardised biovolume and abundance for each sample is shown in Table 5.2.1. The standard deviation of the observed VM-ADCP acoustic backscatter was calculated in linear form before converting to decibels (dB). Values of the observed VM-ADCP acoustic backscatter range from –64.85 to –90.86 dB and the standard deviation varies between 0 and 1.64 dB. The final column indicates whether the sample was collected from water with high or low oxygen concentration (identified from the CTD prior to the LHPR cast, see chapter 3). Samples collected from the surface to 50 m were in oxic conditions (45 – 200 μmol l^{-1}), from 50 to 100 m were in dysoxic conditions (4.4 – 45 μmol l^{-1}) and below 100 m were in anoxic conditions (<4.5 μmol l^{-1}) (classified following Bernhard and Sen Gupta, 1999).

Figure 5.2.2 shows the distribution with depth of VM-ADCP Observed Acoustic Backscatter (OAB), total biovolume, total abundance, acoustic group biovolume and acoustic group abundance for each two-minute LHPR sample. OAB (Figure 5.2.2a) was strongest at the near-surface (-65 dB), dropping 15 dB between 50 and 70 metres to ~ -80 dB. A secondary maximum of approximately -77 dB occurred at 95 m. The lowest value of VM-ADCP acoustic backscatter (-90 dB) occurred around 122 m, below this depth VM-ADCP acoustic backscatter increased to a maximum of -75 dB at the bottom of the LHPR cast. This distribution was approximately constant throughout the LHPR haul.

The strongest backscatter, at the surface, was not concurrent with the highest zooplankton biovolume. The maximum total biovolume (0.68 ml m^{-3}) was found at ~50 m with a secondary maximum at ~70 m (Figure 5.2.2b). Total biovolume decreased dramatically below 70 m, coinciding with the first decrease in VM-ADCP OAB. From 70 m to the bottom of the LHPR cast total biovolume ranged between 0.01 and 0.2 ml m^{-3}, with four small maxima occurring at 87 (0.15 ml m^{-3}), 113 (0.13 ml m^{-3}), 180 (0.21 ml m^{-3}) and 247 m (0.05 ml m^{-3}). These maxima were predominantly caused by euphausiids in the sample. The lowest total biovolume of 0.01 ml m^{-3} was recorded at 223 m. In general although there was higher biovolume at the surface concurrent with the high acoustic backscatter, this relationship was not continued at depth i.e. the increase in acoustic

Sample Number	Mean Backscattering to 2 d.p. (dB)	Standard Deviation to 2 d.p. (dB)	LHPR Sample Biovolume to 2 d.p. (ml m^{-3})	LHPR Sample Abundance to 2 d.p. (No. m^{-3})	Oxygen Conditions*
10	-64.85	0.86	0.26	678.82	Oxic
11	-66.71	0	0.37	585	Oxic
12	-68.04	1.46	0.68	408.03	Oxic
14	-71.58	0.28	0.38	469.08	Dysoxic
16	-73.08	0.46	0.53	366.94	Dysoxic
18	-78.94	0.28	0.20	443.56	Dysoxic
21	-79.29	1.43	0.09	88.98	Dysoxic
22	-79.94	1.64	0.15	57.33	Dysoxic
23	-77.98	0	0.08	135.33	Dysoxic
25	-82.03	0.37	0.06	38.2	Anoxic
28	-88.25	1.22	0.12	28.71	Anoxic
30	-90.86	0.56	0.07	21.26	Anoxic
31	-89.93	0.56	0.07	29.85	Anoxic
33	-87.48	0.75	0.03	31.59	Anoxic
35	-85.79	0.81	0.02	16.17	Anoxic
37	-85.82	0.56	0.03	25.71	Anoxic
38	-84.81	0.51	0.10	33.30	Anoxic
39	-86.00	0.29	0.21	44.93	Anoxic
40	-84.68	1.07	0.20	37.50	Anoxic
43	-81.87	0.82	0.07	65.59	Anoxic
45	-82.33	0.30	0.04	32.13	Anoxic
46	-81.33	1.08	0.04	19.53	Anoxic
47	-80.72	0	0.01	11.72	Anoxic
49	-78.99	0.06	0.01	5.18	Anoxic
51	-78.81	0.59	0.02	0.64	Anoxic
53	-78.26	0.59	0.05	2.69	Anoxic
56	-75.65	0.58	0.02	1.44	Anoxic

* Oxic - 45-200μmol m^{-3}
Dysoxic - 4.4 - 45 μmol m^{-3}
Anoxic - <4.4μmol m^{-3} (Bernhard and Sen Gupta, 1999)

Table 5.2.1 Summary of acoustic backscattering statistics, zooplankton biovolumes and abundance for LHPR samples from Station 12664#1.

backscatter below 125 m was associated with a relatively small zooplankton biovolume (0.068 ml m^{-3}) (discussed in Chapter 3).

Total zooplankton abundance showed maximum values (≥400 m^{-3}) above ~80 m (Figure 5.2.2b). The major contributors were copepods. Below 80 m, concurrent with the decreasing acoustic backscatter, total abundance was at most one quarter of surface values. A small increase in total abundance occurred at 95 m coincident with an OAB maximum. Below 100 m total abundance typically remained below 50 m^{-3}.

The acoustic groups biovolume (Figure 5.2.2c) followed a similar distribution to the total biovolume, although in all cases the acoustic groups biovolume was at least an eighth of the total (note different scales). The only tangible difference was in the surface samples, where the acoustic groups' biovolume was at its maximum values concurrent with the maximum values of acoustic backscatter.

The acoustic groups' abundance mirrored the distribution of total abundance, and as copepods were the dominant contributors and are classified as a significant acoustic scatterer the abundances were of a similar magnitude.

5.2.2 Direct comparison

5.2.2.1 Direct comparison of zooplankton biovolume and observed acoustic backscatter

The correlation between acoustic backscattering values and LHPR biovolumes was examined using a predictive (following Flagg and Smith, 1989a and Heywood *et al.*, 1991) and a functional regression (following Wiebe *et al.*, 1996 and Greene *et al.*, 1998).

In Figure 5.2.3 the total VM-ADCP acoustic backscatter observed in the vicinity of each two-minute LHPR sample is plotted against total zooplankton biovolume for that sample. An exponential curve fit to the data yields the expression:

$$DV = a \exp (b \times OAB)$$

Where DV is total zooplankton biovolume (displacement volume) and OAB represents observed acoustic backscatter. The values of a and b are 178.3 and 0.09098 respectively.

The correlation coefficient is 0.67 (to 2.d.p.) (which is significant at the 99% level for 27 points) and 45% of the data fitted the regression line.

To compare the results with Flagg and Smith (1989a) (henceforth denoted FS1), Heywood *et al.* (1991) (henceforth denoted HSB) and Batchelder *et al* (1995) (henceforth

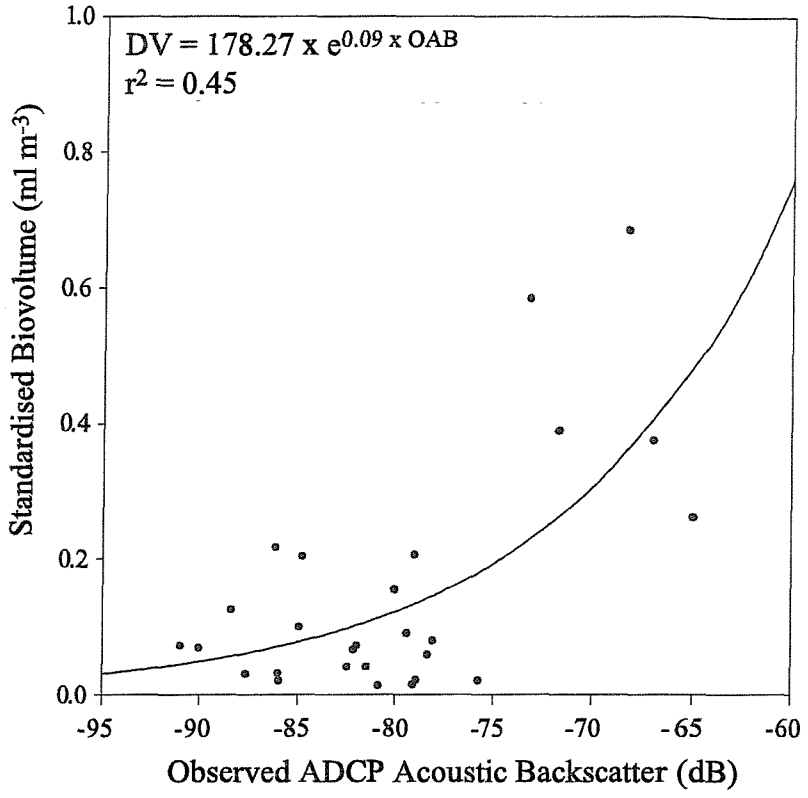

Figure 5.2.3 LHPR sample total standardised biovolume (DV) plotted against observed VM-ADCP acoustic backscatter (OAB).

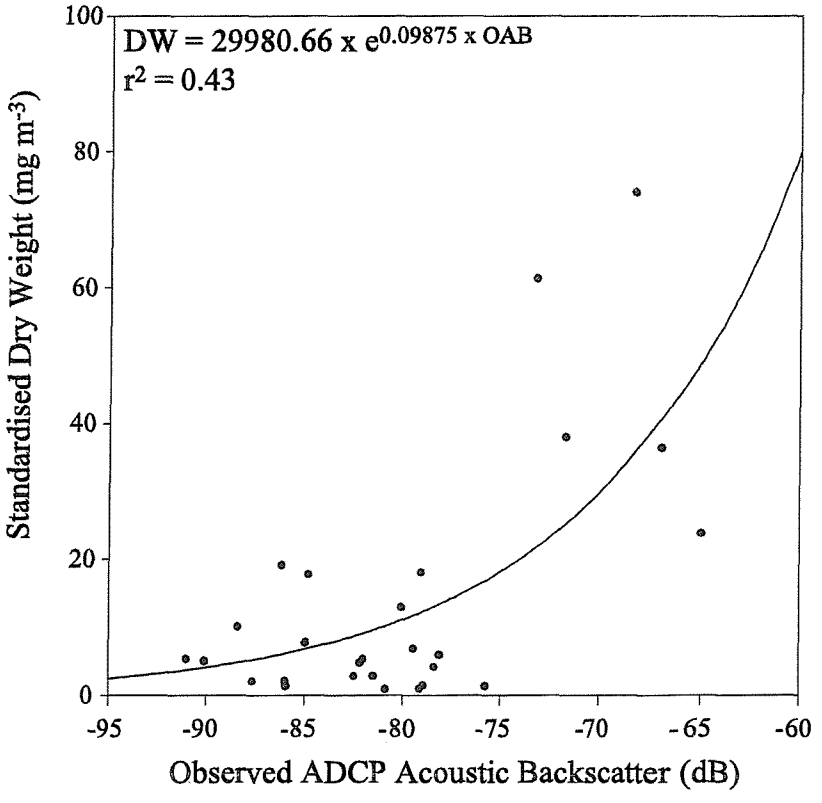

Figure 5.2.4 LHPR sample zooplankton dry weight (DW) plotted against observed VM-ADCP acoustic backscatter (OAB).

denoted BVVS), biovolume was converted to dry weight (mg m^{-3}) using Wiebe *et al.* (1975) conversion tables where:

$$LOG(DV) = -1.828 + 0.848LOG(DW) \qquad (\text{mg m}^{-3})$$

DV is displacement volume or total zooplankton biovolume and DW is dry weight. Flagg and Smith (1989b) (henceforth denoted FS2) found that the Wiebe *et al.* (1975) method over-estimated the dry weight and applied the following correction:

$$DW = 0.81DW_m \qquad (\text{mg m}^{-3})$$

where DW_m is the dry weight estimated by Wiebe *et al.* (1975).

Two comments should be made concerning this method: 1) the conversion tables detailed in Wiebe *et al.* (1975) were later corrected (Wiebe, 1988), and 2) it should be noted that it is not clear whether HSB converted displacement volume to carbon weight (mg C m^{-3}) or dry weight (mg m^{-3}) as both are referred to in the text (Heywood *et al.*, 1991). For comparative purposes the exact method outlined by FS2 was followed.

Zooplankton dry weight plotted against VM-ADCP OAB (Figure 5.2.4) yields an exponential relationship, where the values of a and b are 29980.66 and 0.09875 respectively, the correlation coefficient is 0.66 (to 2.d.p.), which is significant at the 99% level for 27 points and 43% of the data fitted the regression line. However these data and relationship use absolute backscatter and not relative backscatter as used in previous studies. To compare the relationship between zooplankton dry weight and VM-ADCP acoustic backscatter with previous data sets, dry weight was log-transformed so that the rate of change could be examined (i.e. $\Delta DW/\Delta AB$). Figure 5.2.5 shows the logarithm of dry weight divided by 4π plotted against acoustic backscatter. Dry weight was divided by 4π after the theory suggested by FS2. This follows the premise that since target strength (and therefore the backscattered signal) is equal to $\log(\sigma_s/4\pi)$, where σ_s is the acoustic cross section, and dry weight is approximately proportional to cross-sectional area (which should be proportional to acoustic cross section), it is logical to plot $\log(DW/4\pi)$ against the observed VM-ADCP acoustic backscatter.

A predictive linear regression line fitted to the data in Figure 5.2.5 yields the relationship:

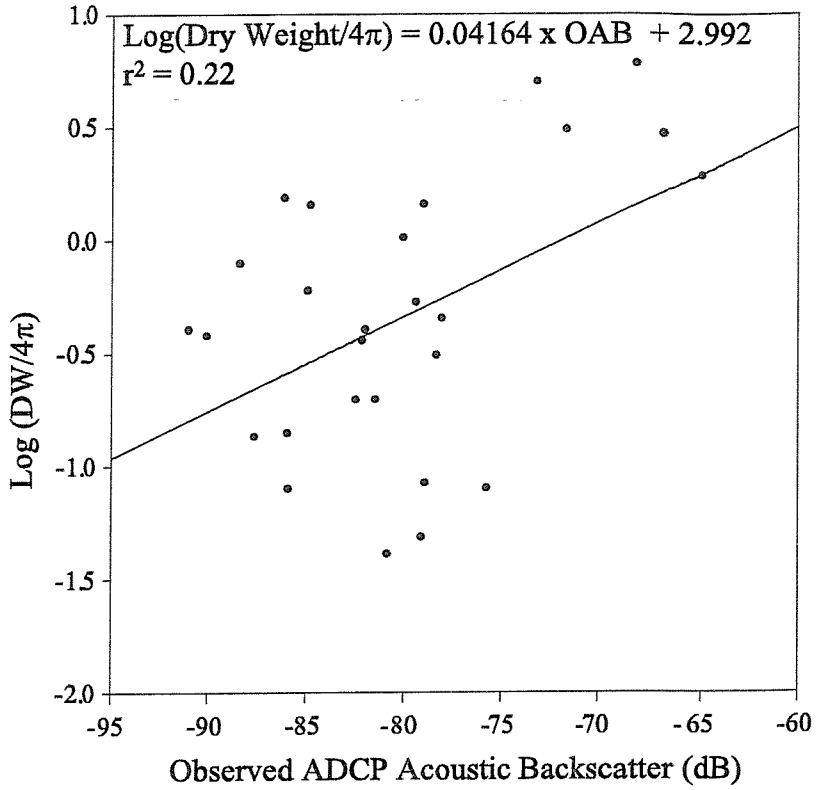

Figure 5.2.5 LHPR sample log(DW/4π) plotted against observed VM-ADCP acoustic backscatter (OAB).

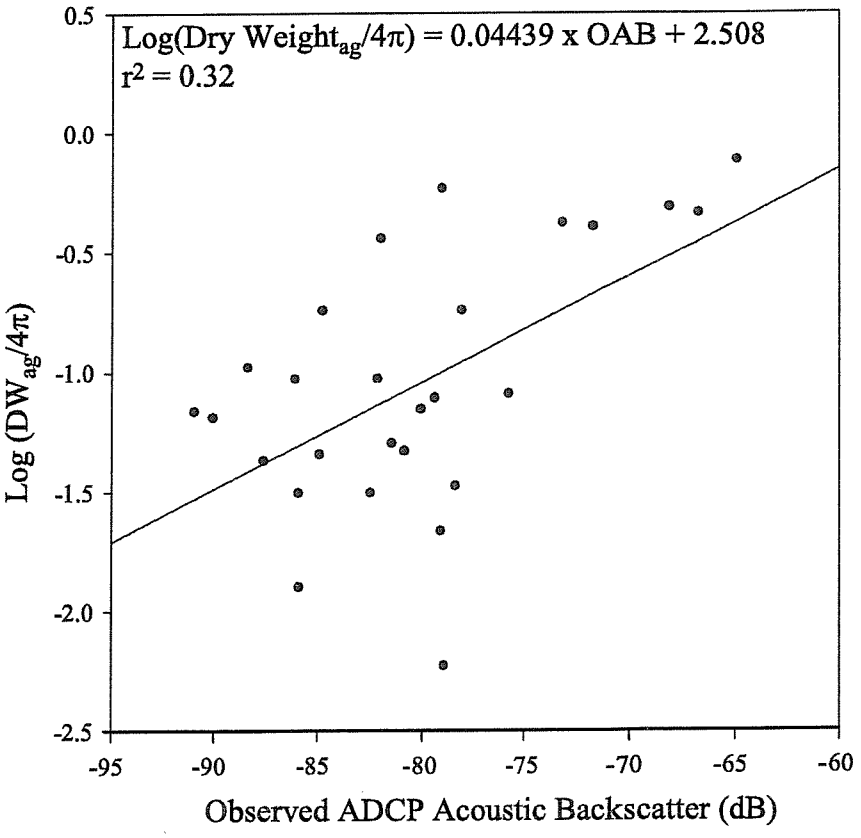

Figure 5.2.6 LHPR sample log(DW_{ag}/4π) of significant acoustic scattering groups plotted against observed VM-ADCP acoustic backscatter (OAB).

$$\log(DW/4\pi) = 0.04164 \text{ x } OAB + 2.992$$

The correlation coefficient is 0.47 (n = 27, P = 0.05) and 22% of the data fitted the line. The significant coefficient in this equation is the slope of the line (0.04164, S_v = 0.0158), which represents $\Delta DW/\Delta AB$. FS2 comment that the intercept (2.992) will be, at the least, instrument specific.

$\Delta DW/\Delta AB$ was compared with previous results (0.115, FS2; 0.056, HSB; and 0.055, BVVS) using a students t-test. The null hypothesis (H_0) was that $\Delta DW/\Delta AB$ was not significantly different from the slope of previous regression lines (i.e. 0.115, 0.056 and 0.055). The null hypothesis was accepted when $\Delta DW/\Delta AB$ was compared with HSB, BVVS, and rejected when compared with FS2 (Table 5.2.2).

(H_0) v =	**0.115 (Flagg and Smith, 1989b)**	**0.056 (Heywood *et al.*, 1991)**	**0.055 (Batchelder *et al.*, 1995)**
H_0 accepted at P = 0.01 ($\Delta DW/\Delta AB$ = 0.0416)[1]	YES	no	no
H_0 accepted at P = 0.01 ($\Delta DW/\Delta AB$ = 0.08769)[2]	no	no	no
H_0 accepted at P = 0.01 ($\Delta DW_{ag}/\Delta AB$ = 0.0444)[1]	YES	no	no
H_0 accepted at P = 0.01 ($\Delta DW_{ag}/\Delta AB$ = 0.07736)[2]	YES	no	no

[1] = calculated using a predictive regression.

[2] = calculated using a geometric mean estimate of the functional regression

Table 5.2.2 Examination of $\Delta DW/\Delta AB$ compared with previous studies

The above method was also applied to the biovolume data (DW_{ag}) of only the significant acoustic scattering groups (Figure 5.2.6). The resultant regression line has a correlation coefficient of 0.56 (n = 27, P = 0.05) and 32 % of the data fitted the line. The regression yielded the following relationship:

$$\log(DW_{ag}/4\pi) = 0.04439 \text{ x } OAB + 2.508$$

$\Delta DW_{ag}/\Delta AB$ (= 0.04439 with a standard error of 0.013) was compared with previous results (Table 5.2.2) and found to be significantly different from FS2 result but not from HSB and BVVS.

At this point it should be noted that the present author disagrees with the regression analysis outlined above. According to Wiebe *et al.* (1975), when examining a relationship between variables which are subject to both natural variability and measurement error and when the observations cannot be assumed to be a random sample from a bivariate normal population, the geometric mean estimate of the functional regression of Y on X (Ricker, 1973) is appropriate. In addition the correct algorithms for the conversion of biovolume (*DV*) to dry weight (*DW*) were used (Wiebe, 1988) where:

$$\log(DV) = -1.842 + 0.865\log(DW)$$

Recalculating equations for the regression lines of $\log(DW/4\pi)$ and $\log(DW_{ag}/4\pi)$ versus observed backscatter (Figures 5.2.5 and 5.2.6 respectively) gives:

$$\log(DW/4\pi) = 0.08769 \text{ x } OAB + 6.7743$$

and

$$\log(DW_{ag}/4\pi) = 0.07736 \text{ x } OAB + 5.2557$$

The correlation and regression coefficients remain the same values of 0.47 and 22 %, and 0.56 and 32 % respectively.

$\Delta DW/\Delta AB$ of the new regression equations were compared with previous work (Table 5.2.2). $\Delta DW/\Delta AB$ for $\log(DW/4\pi)$ was not found to be significantly different from previous work, and $\Delta DW_{ag}/\Delta AB$ for $\log(DW_{ag}/4\pi)$ was found to be only significantly different from the results of FS2.

5.2.2.2 Discussion of direct comparison

Zooplankton biovolume (*DV*) was found to be exponentially related to observed VM-ADCP acoustic backscatter (*OAB*). This was consistent with previous work and shows that acoustic backscatter can be used as a general proxy for the distribution of zooplankton (FS1, HSB).

As this, and other work, involves the use of "relative" acoustic backscatter and for statistical comparison with previous work, zooplankton volume (*DV*) was converted to dry weight, log-transformed and plotted against VM-ADCP acoustic backscatter. The resultant slope of a regression line ($\Delta DW/\Delta AB$) expresses the rate of change in biomass with a

change in acoustic backscatter and the intercept is instrument and experiment-specific. FS2 expected this to provide a linear dependence with a proportionality constant of 1/10 (i.e. $\Delta DW/\Delta AB = 0.1$), where the larger the slope the less sensitive the VM-ADCP would be to changes in zooplankton concentration.

The data presented in this study exhibit a poorer correlation between log(DW/4π) and VM-ADCP acoustic backscatter than that found by previous authors (FS1, FS2, HSB, BVVS). However, it should be noted that the study which had the greatest regression and correlation coefficient (by FS1 and FS2, $r^2 = 0.96$) was carried out in an area dominated by a single species of copepod, *Calanus finmarchicus* (Smith and Lane, 1988), i.e. a simplified "acoustic situation". Batchelder *et al.* attributed their and Heywood *et al.*'s "poorer" correlations to using depth integrated net hauls compared with vertically stratified net hauls.

$\Delta DW/\Delta AB$ in this study was 0.04164, lower than previous studies direct comparisons between VM-ADCP acoustic backscatter and net-sampled zooplankton. According to FS2 this implies that the VM-ADCP used in this study was the most sensitive or, alternatively that the zooplankton analysed were larger. The latter statement is certainly valid, because the mesh size of the net used in this study (333 μm) was larger than that used by FS2 and HSB. Therefore the mean length of zooplankton caught varied between 1 and 15 mm (see chapter 3), larger than the zooplankton sampled by HSB (where 50 % of the population < 1 mm). Additionally the wavelength of the acoustic signal of a 150 kHz VM-ADCP is ~ 10 mm, closer to zooplankton length in the present study than HSB's.

An alternative reason for variations in $\Delta DW/\Delta AB$ was proposed by HSB. They showed that the slope of the regression line ($\Delta DW/\Delta AB$), and the fit of the data to the line (r^2), varied if the value of the sound absorption coefficient (α), used in calculating acoustic backscatter, was changed. The value of α used to calculate acoustic backscatter in the present study was 0.44 dB m^{-1} (RD Instruments, 1990) compared with 0.46 and 0.4 used by HSB. The slope of their regression line varied from 0.056 to 0.052 with the change in α, not sufficient to account for the variation of 0.0144 (~25 %) between HSB's study and the one reported here. HSB also considered that the error caused by changes in α would be negligible compared with errors in the displacement method for measuring biovolume and patchiness in the zooplankton.

A comparison of the relationship between acoustic backscatter and zooplankton biomass found in the present study and previous ones is more complex than just

comparing the value of $\Delta DW/\Delta AB$. Each study occurred in a different area, the Western North Atlantic, Gulf Stream (FS1 and FS2), the southern Indian Ocean (HSB), the Eastern North Atlantic (BVVS) and the north Indian Ocean (this study), where different zooplankton populations and community structures will exist (Van der Spoel and Heyman, 1983). In addition, a different zooplankton net with different mesh sizes was used in each study. FS1 and FS2 used a MOCNESS with a 149 μm mesh, HSB used a WP2 with a 142 μm mesh, BVVS used a ring net with a 153 μm mesh and the present study used a LHPR with a 333 μm mesh. As we now know, acoustic backscatter is not related linearly to zooplankton biomass but is a complex function of zooplankton size, morphology and physiology (Stanton *et al.*, 1996; Chapter 1). Hence similar results should not be expected from the above comparison, as each study will be catching a different zooplankton population with a different size structure.

5.2.3 Model-estimated acoustic backscatter

5.2.3.1 Comparison of observed and model-estimated acoustic backscatter

The comparison of acoustic backscatter with net-sampled zooplankton has progressed from direct comparisons to the use of models (Zhou *et al.*, 1994; Wiebe *et al.*, 1996; Greene *et al.*, 1998). This uses a knowledge of the zooplankton population (the zooplankton net sample) combined with acoustic scattering models to predict acoustic backscatter.

The relative contribution of six "significant acoustic scattering" zooplankton groups, identified in the taxon-specific model equations given by Stanton *et al.* (1994a), were estimated and compared with the observed acoustic backscatter in the vicinity of the LHPR net sample. As is evident in Figure 5.2.7 the estimated pteropod contribution (Figure 5.2.7e) is larger than that of any other taxon in most of the samples. The contributions of all the groups except for the euphausiids are normally less than the observed value of acoustic backscatter, with the amphipod and chaetognath groups the smallest. The euphausiid group had the second highest estimated acoustic backscatter, and values from some samples are greater than the observed acoustic backscatter.

The percentage contribution of each group to the total model-estimated acoustic backscatter (TMEAB) was examined. In surface waters, above 70 m, pteropods had the largest model-estimated acoustic backscatter, comprising up to 69.5 % (Figure 5.2.8). Amphipods contributed the least, comprising only 0.3 % of the TMEAB. Below 70 m euphausiids had the greatest model-estimated acoustic backscatter, comprising up to 99.5 % of the total amount. Copepods were the second largest contributors, except below

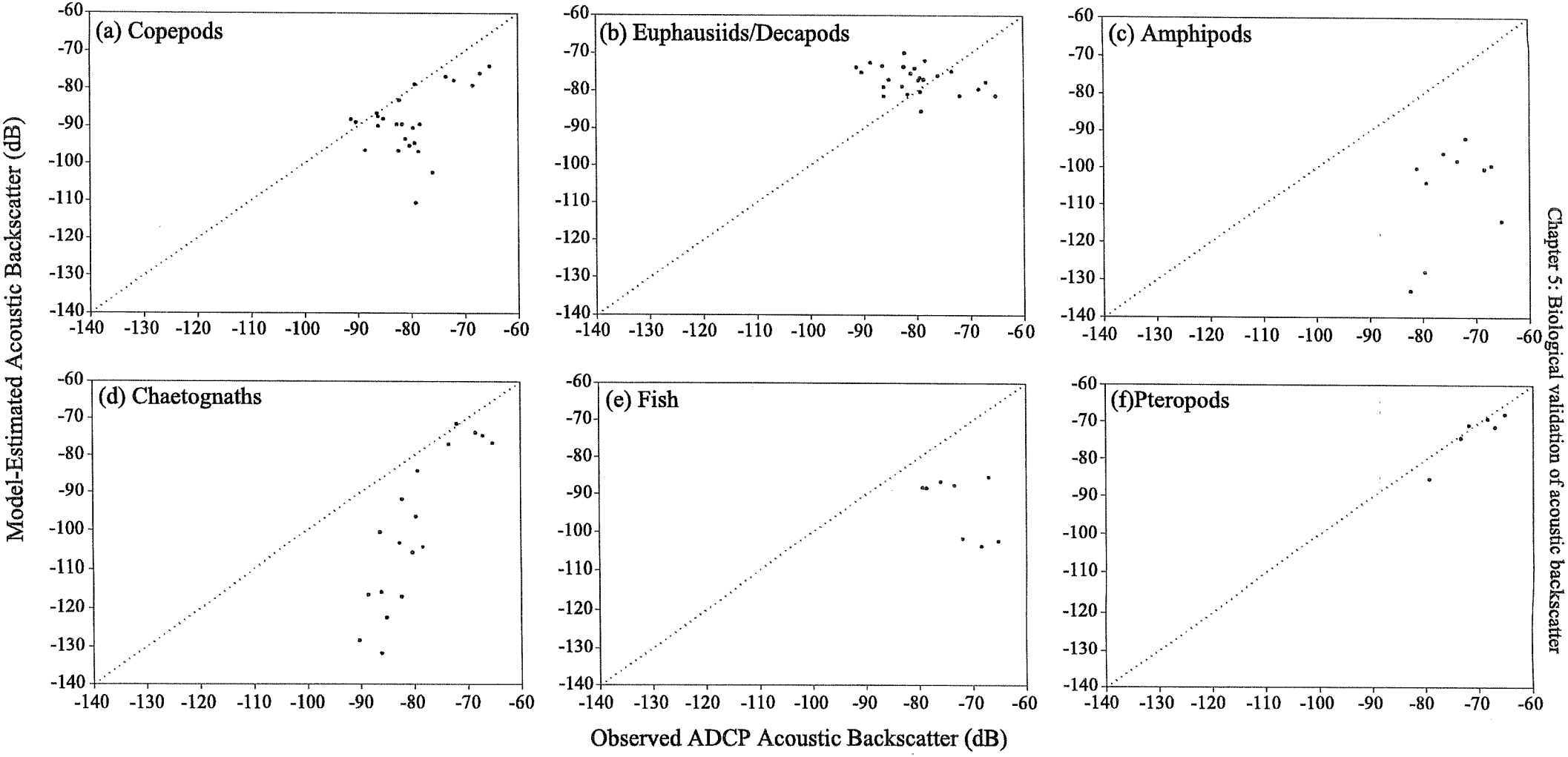

Figure 5.2.7 Model-estimated acoustic backscatter plotted against observed VM-ADCP acoustic backscatter for (a) Copepods, (b) Euphausiids and Decapods, (c) Amphipods, (d) Chaetognaths, (e) Fish and (f) Pteropods.

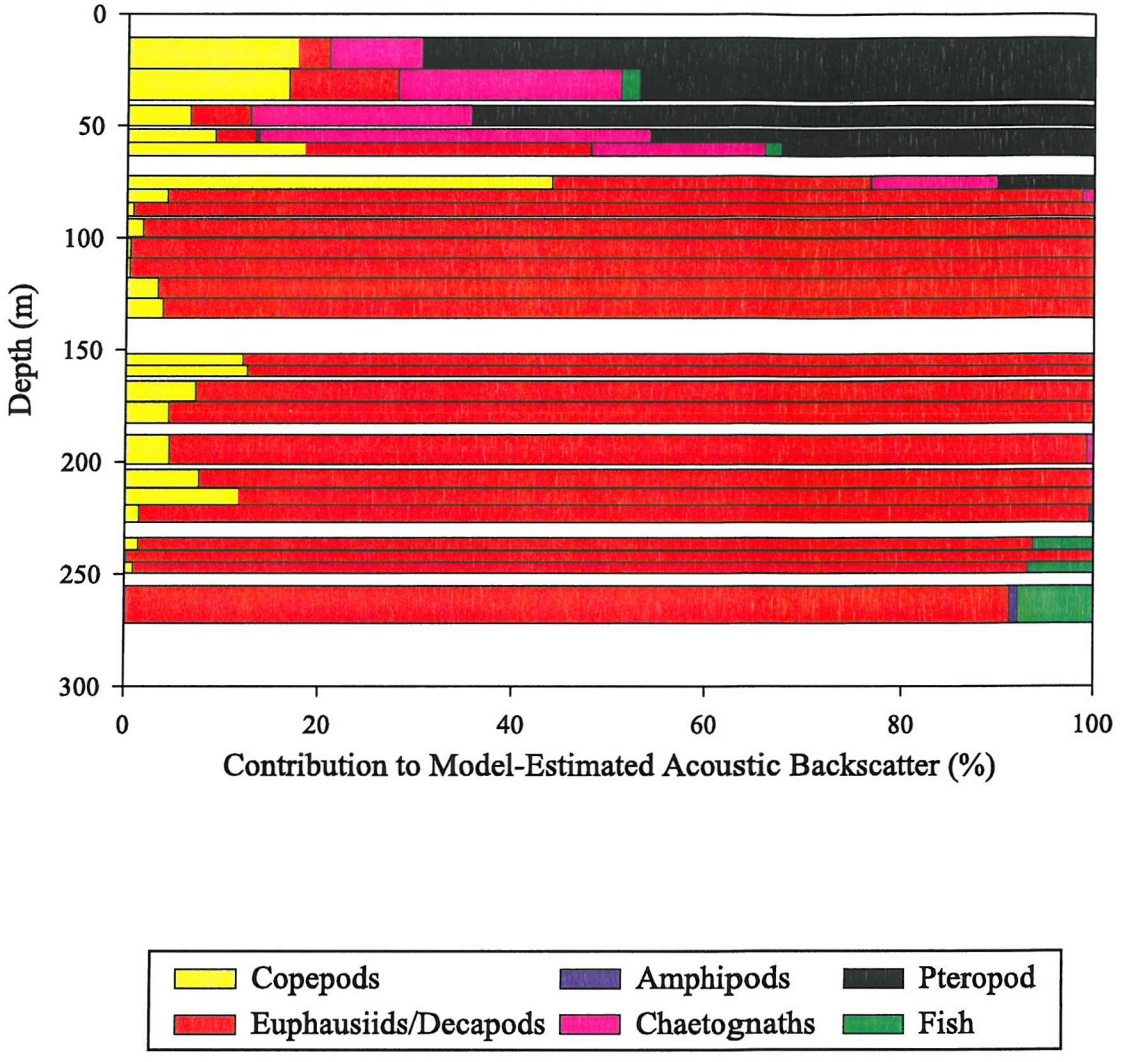

Figure 5.2.8 The percentage contribution of each significant acoustic scattering group to the total model-estimated acoustic backscatter.

230 m where they were replaced by fish. The contribution of each group to the TMEAB was not necessarily related to its abundance or biovolume. Figure 5.2.9 shows the contribution of each group to biovolume, abundance and TMEAB for three samples from 17.5, 159.5 and 242 metres depth. Sample 10 shows that whilst pteropods are numerically (0.1 %) and volumetrically (2.2 %) insignificant, they dominate the model-estimated acoustic signal (69.5 %). In deeper samples (where pteropods were not present) the abundance is dominated by copepods and the biovolume and TMEAB is dominated by euphausiids and decapods.

The TMEAB for each sample was compared with the observed acoustic backscatter (OAB) observed in the vicinity of the net-sampled volume (Figure 5.2.10). The functional regression line fit to the log-transformed data explained 29 % of the total variance of the data (r^2 = 0.29). The slope of the regression (0.67 to 2.d.p) was significantly different from the expected slope of one (t-test, n = 25, P>0.05). Colour coding the data according to the dominant acoustic scattering group indicates that when pteropods were present in the samples the TMEAB was comparable with the observed values. In deeper samples, where euphausiids and decapods were the largest contributors to the TMEAB it typically exceeded the observed value. This implies that the euphausiid and decapod model is incorrect. A possible cause of inaccuracy may be an orientation effect, which has both a biological and an instrumental origin (Griffiths *et al.*, 2002). Acoustic backscatter from an euphausiid-shaped animal is directional. Its dependence with angle has been studied by Stanton *et al.* (1993b), Macaulay (1994) and more recently in the laboratory by McGehee *et al.* (1998), in which variations of up to 25 dB were found. The models assume broadside incidence of the acoustic signal to the zooplankton. However, the orientation of an euphausiid within the water column is unknown and may vary (biological origin). In addition the VM-ADCP beams are inclined 30° from the vertical (instrumental origin). Therefore a –5 dB correction (applied to the euphausiid and decapod contribution) required to force agreement between the model-estimated and observed values is not inconsistent with the angular variation of backscatter between 0 and 30° reported by McGehee *et al.* (1998). A functional regression line fitted to the corrected log-transformed data (Figure 5.2.11) explained 44 % of the total variance of the data. The slope of the regression line (0.87 to 2.d.p) was not significantly different from the expected slope of one (t-test, n = 25, P>0.05).

The type of water the sample was drawn from was identified (Figure 5.2.11) and shows the model and observed acoustic data clusters depending on whether the source

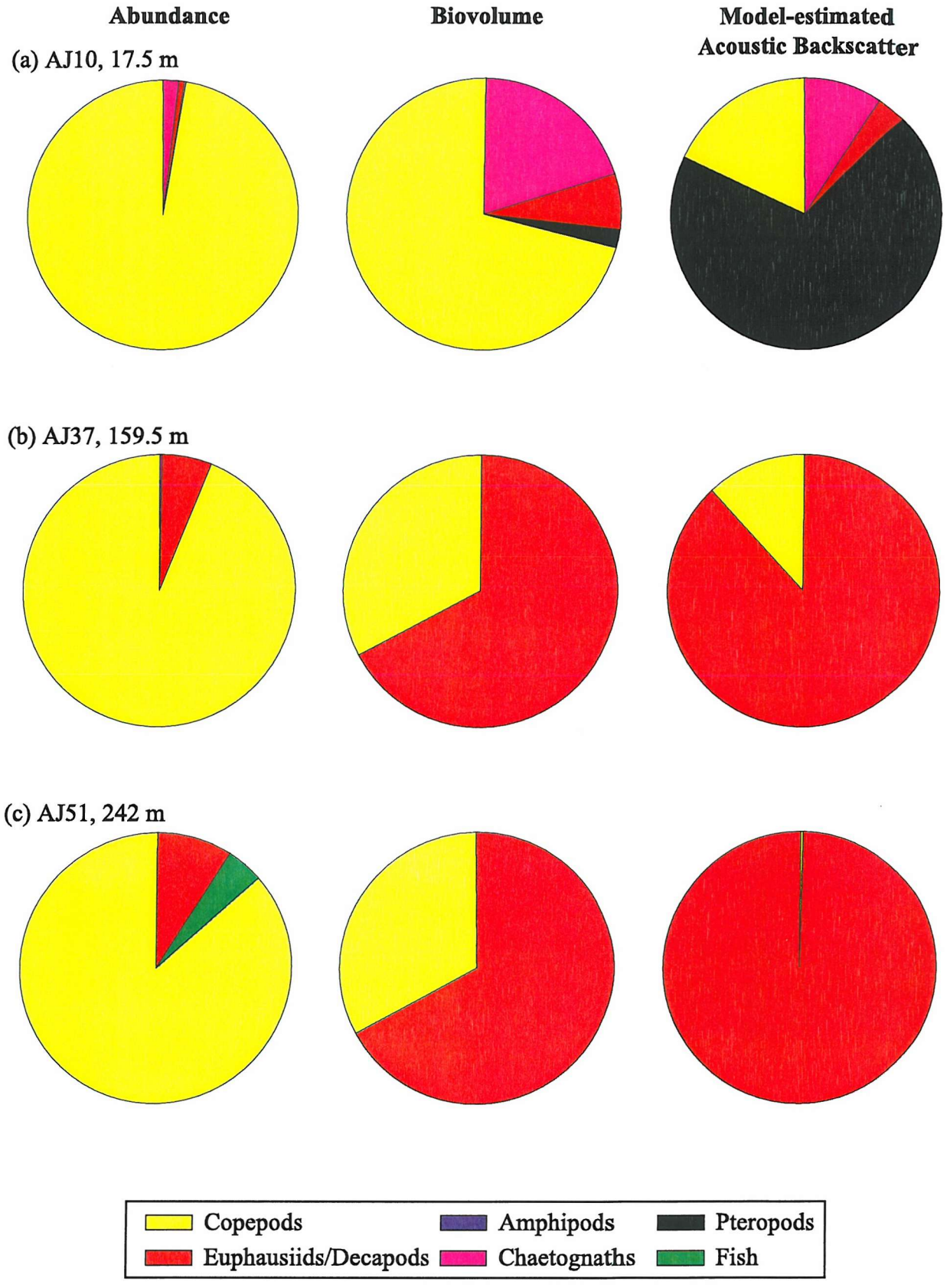

Figure 5.2.9 The contribution of each significant acoustic scattering group to abundance, biovolume and model-estimated acoustic backscatter at (a) 17.5 m, (b) 159.5 m and (c) 242 m.

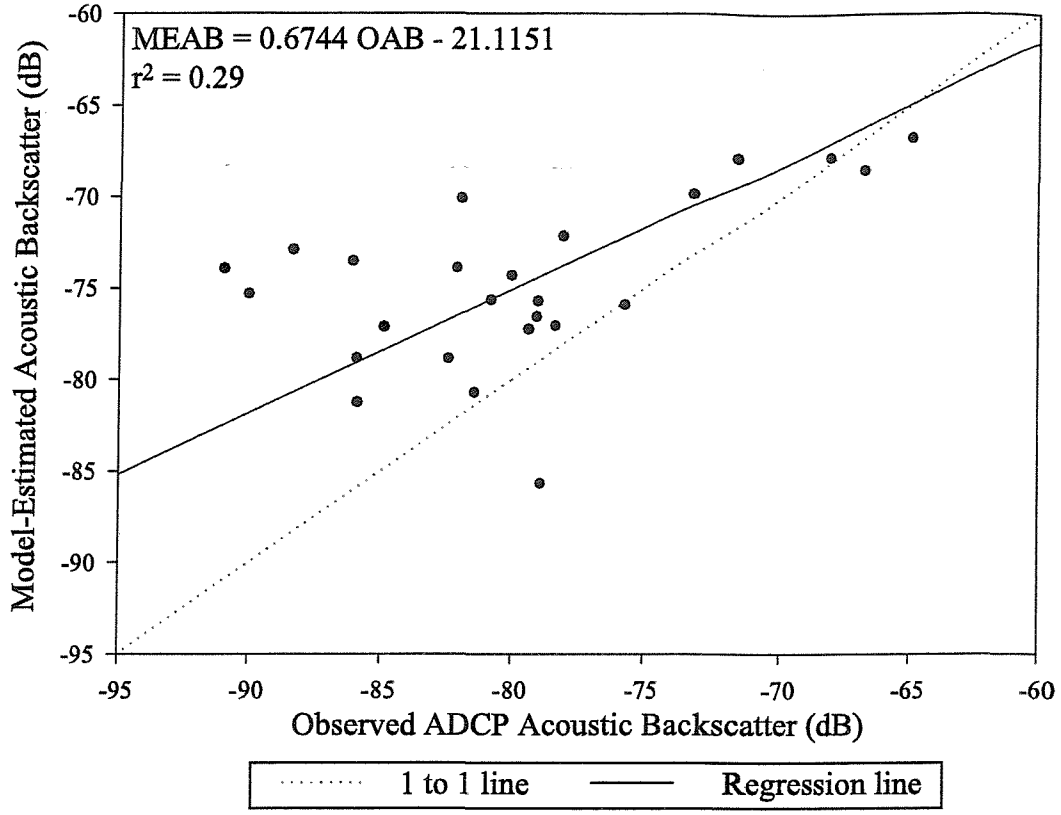

Figure 5.2.10 Model-estimated acoustic backscatter plotted against observed VM-ADCP acoustic backscatter.

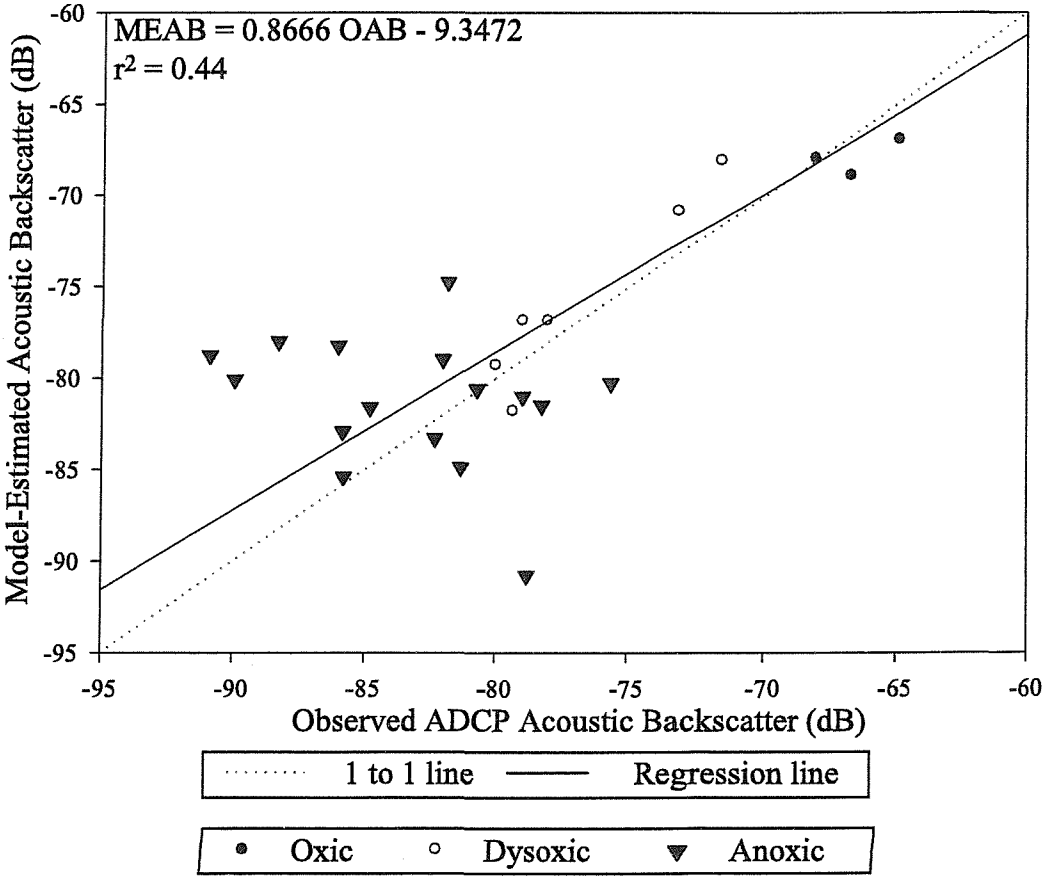

Figure 5.2.11 Model-estimated acoustic backscatter corrected for 30° orientation effect plotted against observed VM-ADCP acoustic backscatter. A description of the oxygen concentration of the water for each sample is provided.

water was oxic, dysoxic or anoxic. The model predictions work well for samples drawn from oxic and dysoxic water and not for samples drawn from anoxic water.

An alternate view is to analyse only the acoustic data that resulted from either "evenly" distributed, or frequent targets. This follows the conclusion of Brierley *et al.* (1998b) that VM-ADCP acoustic backscatter compared favourably with a calibrated echosounder only under these conditions. In this case all samples where the observed acoustic backscatter was greater than –80 dB were analysed and everything below –80 dB was discarded. This dynamic range was comparable with the datasets analysed by Wiebe *et al.* (1996) and Greene *et al.* (1998). The resultant regression line (Figure 5.2.12) fit to the log-transformed data explained 62 % of the variance of the data. The slope of the regression line (1.00 2.d.p) was not significantly different from the expected slope of one (t-test, n = 12, P>0.05).

5.2.3.2 Discussion of model estimations

The use of models to describe acoustic scattering has arisen because the echo return from a target is dependent not only on its size but also its composition (Stanton *et al.*, 1993a). The results presented here show that abundance, biomass and model-estimated acoustic scattering contributions of six zooplankton groups vary disproportionately. In particular, where a rare and small but strong acoustic scatterer such as a pteropod can contribute as little as 0.1 % to the total sample abundance, 0.1 % of the biovolume but represent 69.5 % of the TMEAB. These results indicate the necessity for caution when describing zooplankton abundance and biovolume from acoustic backscatter without concurrent net data to indicate the types of scatterers, and supports the need for accurate acoustic scattering models.

The results of this study provide a convincing demonstration that at high backscatter intensities the observed VM-ADCP acoustic backscatter data collected were consistent with the forward problem predictions. The relationship between observed VM-ADCP and TMEAB compared favourably with that found when using a well-calibrated biological echosounder (Wiebe *et al.*, 1996; Greene *et al.*, 1998), and like the study by Wiebe *et al.* the pteropod contribution was typically larger than the other taxa. However the results of this study also provide examples of situations in which inconsistencies between the observed and model-estimated acoustic backscatter indicate potential model, instrumental and methodological problems.

Model

When euphausiids and decapods were the dominant scattering group the TMEAB typically exceeded the observed values. Two potential sources of error affecting the model

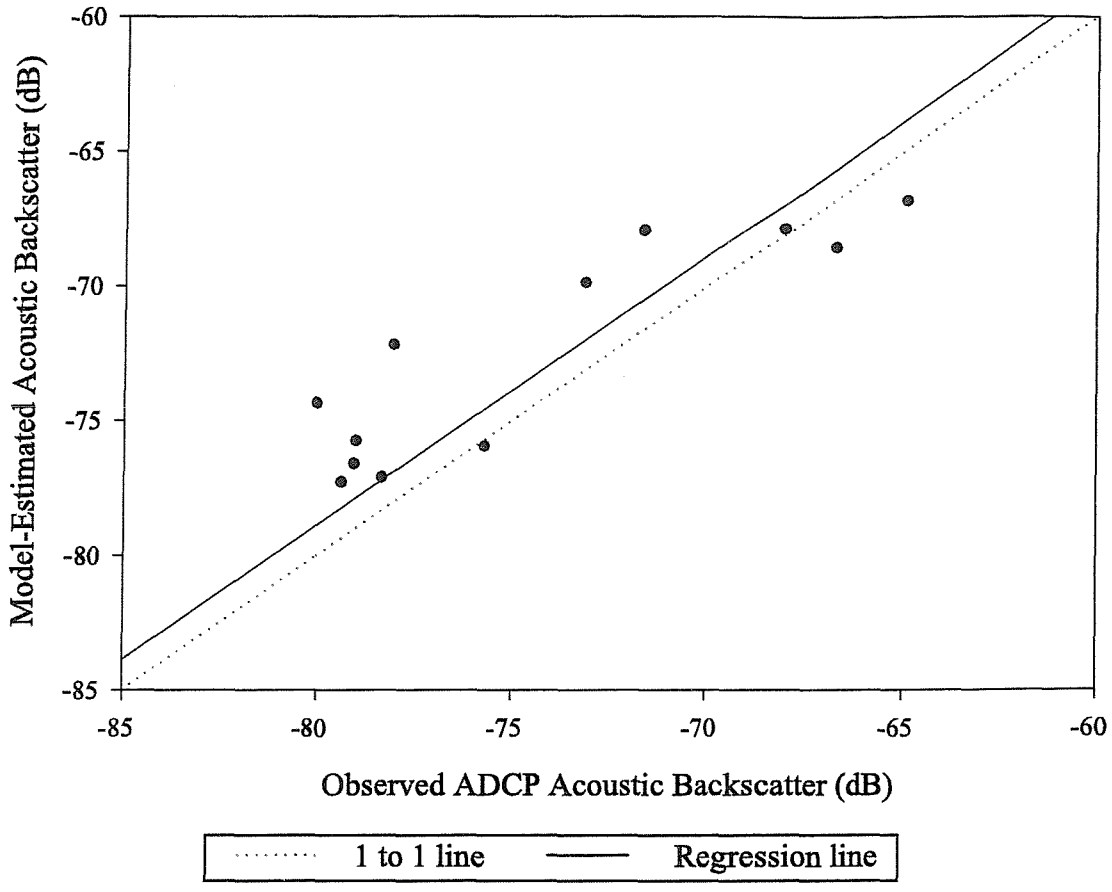

Figure 5.2.12 Model-estimated acoustic backscatter (in the same dynamic range as Wiebe *et al.*, 1996 and Greene *et al.*, 1998) plotted against observed VM-ADCP acoustic backscatter.

predictions for this group are an orientation effect and inadequate knowledge of the sound speed and density contrasts of the zooplankton. The orientation effect was allowed for in the results (see Figure 5.2.11), although it should be noted that if the animals in the ocean have a preferred orientation, the echo levels could easily differ by several decibels from the level averaged over all orientations (Wiebe *et al.*, 1996). The second error refers to the calculation of the reflection coefficient (see Chapter 1) used within the model. Euphausiids and decapods, which exist within the oxygen minimum layer of the Indian Ocean, have softer carapaces than their other ocean environment counterparts (Herring *et al.*, 1998). This would effect their density and hence their reflection coefficient. The value of the reflection coefficient used in Stanton *et al.* (1993a) and Greene *et al.* (1998) was R=0.058. Using an alternative value of R (R=0.031, given by Foote (1990)) would reduce the mean bias of the euphausiid and decapod dominated samples by 4.6 dB. Inadequate measurements of speed of sound and density contrasts, and the lack of knowledge regarding the orientation of euphausiids and decapods within the open ocean results in our inability to distinguish between these two errors. In fact a recent and novel proposal for the use of acoustic methods includes the ability to detect the orientation of zooplankton through repeated measurements of a zooplankton population at multiple angles (pers. comm. Stanton).

Instrumental

Brierley *et al.* (1998b) commented on the unreliability of acoustic measurements made with an VM-ADCP in regions of low or irregularly distributed targets. The results presented in this study show that at high backscatter intensities (which are related to many or evenly distributed targets) model-estimated and observed acoustic backscatter are comparable, the VM-ADCP behaving as well as a biological echosounder. However, at low backscatter intensities the model predictions become increasingly poor. This may be as a function of the VM-ADCP's method of averaging acoustic backscatter from four beams, instead of using just one as in a biological echosounder.

Methodological

Comparing model-estimated with observed acoustic backscatter assumes that the two instruments (in this case the VM-ADCP and the LHPR zooplankton net) are sampling the same zooplankton population. The first basic condition to be met is that both instruments are sampling similar size ranges. In this case the acoustic frequency used of 153 kHz, resolving single targets of ~10 mm and multiple targets of <10 mm, is comparable with the size of zooplankton caught by the LHPR (>~1 mm following Nichols and Thompson, 1991). The second condition should be that the two instruments have

comparable sampling volumes. Since the VM-ADCP has four conical beams (with a beamwidth of 2.5°) the volume of water insonified increases with depth, whereas the LHPR sample volume remains constant. Figure 5.2.13 shows the volume of water sampled by an VM-ADCP and the LHPR with depth during a two-minute period. At the surface the volumes sampled are similar, the VM-ADCP measuring from ~190 m^3 of water and the LHPR from ~40 m^3. At 300 m the VM-ADCP backscatter measurements are made from ~170000 m^3 of water, nearly four orders of magnitude greater than the LHPR. This divergence in the volume of water sampled affects the probability of each instrument in encountering strong but rare acoustic scatterers such as pteropods. Where, because of its larger sampling volume, the VM-ADCP is more likely to sample at least one pteropod than is the LHPR (Figure 5.2.14).

An additional problem resulting from spreading is singular to the VM-ADCP. An VM-ADCP has four beams, each angled 30° from vertical. This results in the fore and aft beams angled 60° from each other, so that at 10 m depth the centre of the beams are separated by 17 m and at 300 m depth by 520 metres. If a ship travels at 2 m s^{-1}, a sample taken at 10 m depth would contain zooplankton information over a distance of ~240 m (during a two-minute sample) whilst a sample taken at 300 m depth would cover a distance of ~750 metres. Hence zooplankton patches at depth could be smeared by the VM-ADCP.

A combination of these problems and the knowledge that when the LHPR is at 300 m depth it could be up to 850 m behind the ship (allowed for when calculating OAB, see chapter 2) creates a large margin for error.

5.3 Comparison of observed acoustic backscatter (OAB) and zooplankton samples from the Alboran Sea

5.3.1 Description of concurrent acoustic backscatter and zooplankton samples

Figure 5.3.1 presents a contour plot of VM-ADCP observed acoustic backscatter over the period of the LHPR station 13048. Two sound scattering layers are identified, Sound Scattering Layer 1 (SSL1) was a discrete layer that existed at the surface to 100 m at the beginning of the LHPR cast and deepened to a depth ~150 m during the upcast (following the ~28 σ_0 isopycnal, Chapter 4). The second Sound Scattering Layer (SSL2) occurred below ~250 m, in predominantly Levantine Intermediate Water (Chapter 4) with intensities of –65 dB and above. The SSL1 had lower backscattering intensities than

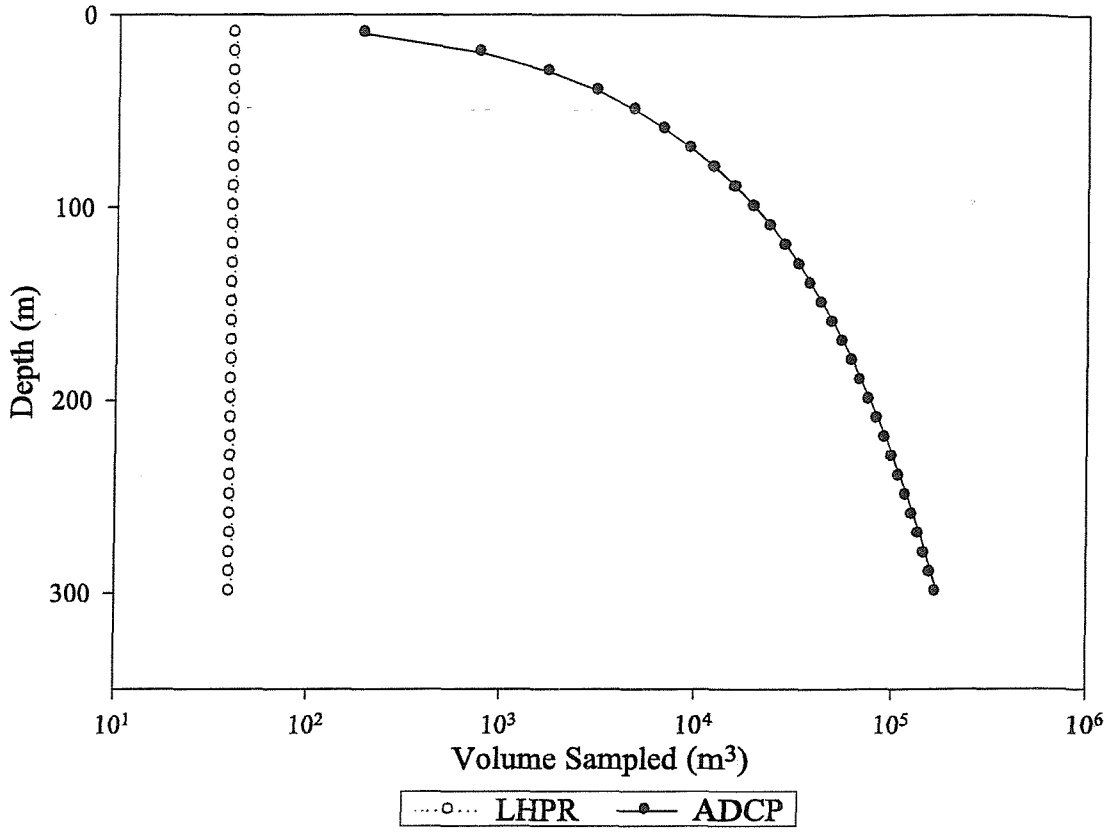

Figure 5.2.13 The volume of water sampled by the LHPR and the VM-ADCP as a function of depth.

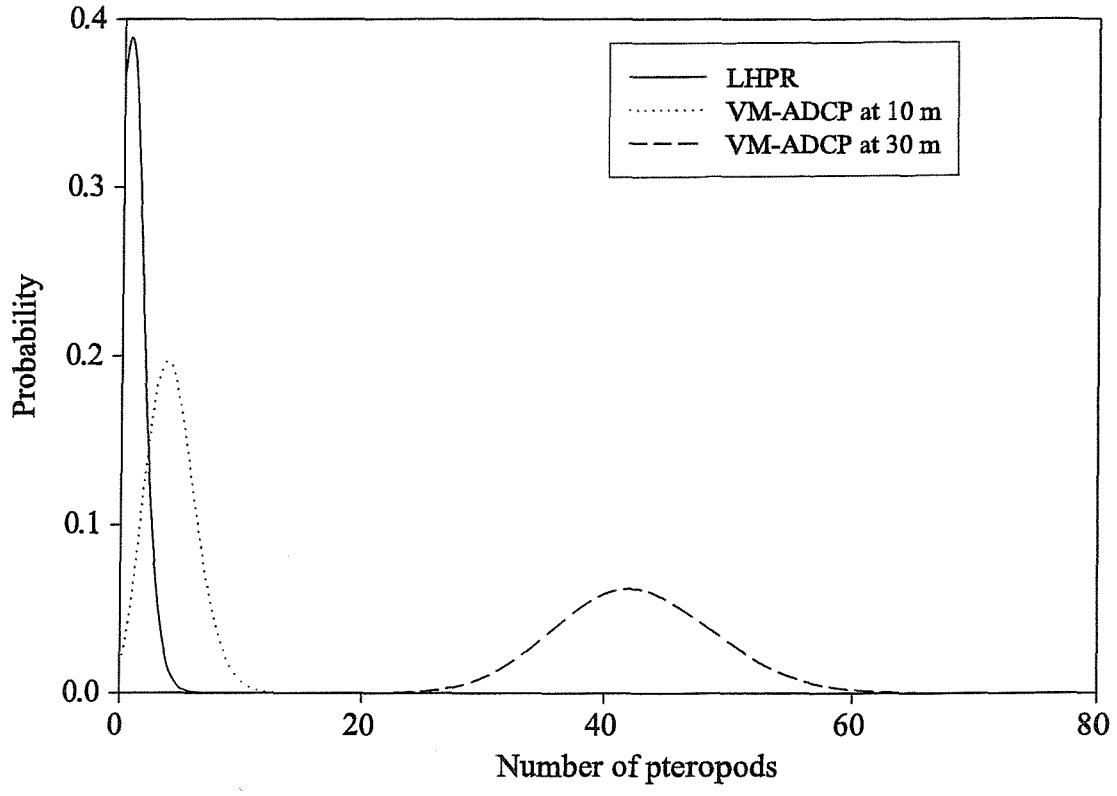

Figure 5.2.14 The probability distribution for the number of pteropods within a sample, given a probability of encountering one per m^3 of 0.025 (equivalent to catching 1 in a two-minute LHPR sample).

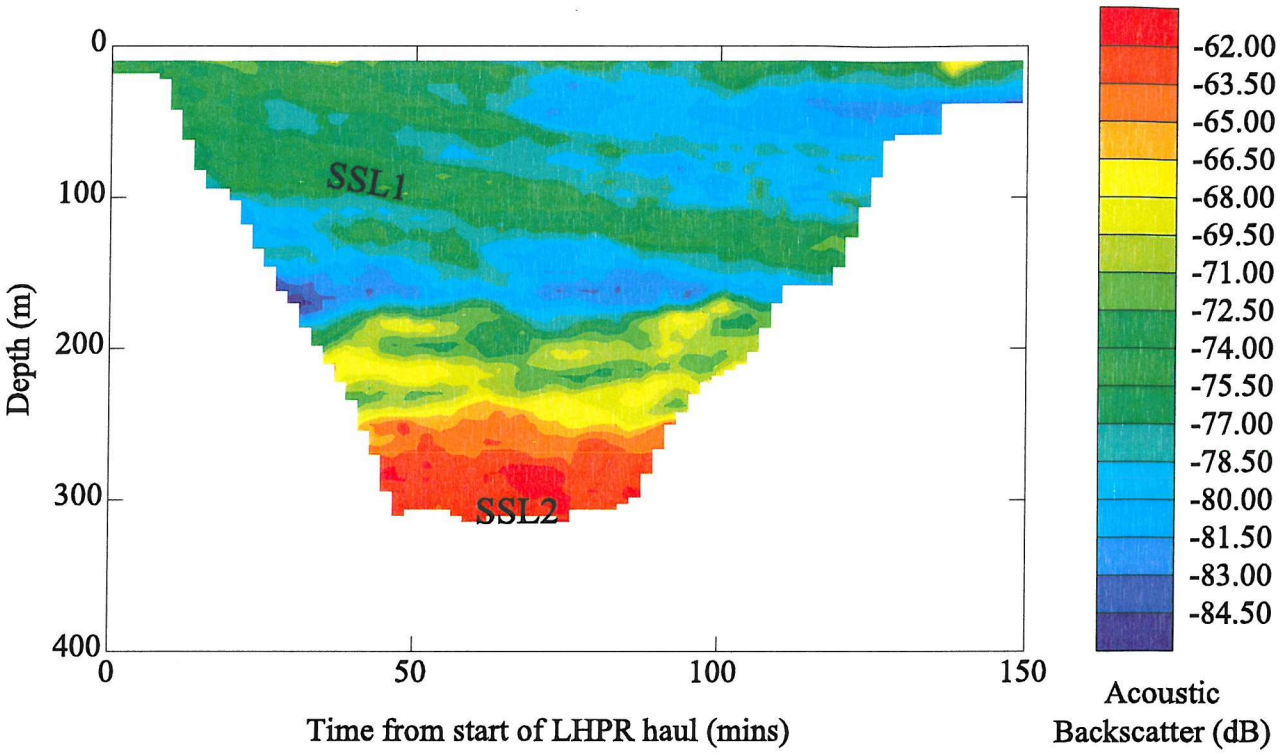

Figure 5.3.1 A contour plot of VM-ADCP observed acoustic backscatter during the LHPR Station 13048. Two Sound Scattering Layers are identified. SSL1, a layer of higher backscatter concurrent with the 27.9 σ_0 isopycnal along the front, and SSL2, a permanent feature occurring below ~250 m.

SSL2 of ~-75 dB. At ~200 m depth during the downcast the lowest values (~-85 dB) of acoustic backscatter were observed.

Observed acoustic backscatter from the EK500 for the three frequencies 200, 120 and 38 kHz during the LHPR haul is shown in Figure 5.3.2. The 200 kHz data show a thin layer of high backscatter in the surface 20 m and the beginning of SSL2 before it disappears below the acoustic penetration depth (Figure 5.3.2a). At 120 kHz the layer of high acoustic backscatter seen at the surface in 200 kHz data is thicker, extending ~25 m, and of similar intensities (Figure 5.3.2b). The greater depth resolution shows SSL2 in more detail and observed acoustic backscatter is higher at 150 m during the upcast than at the beginning of the downcast. The layer of highest backscatter (SSL1) at depth is seen occasionally, as it occurs at the greatest extent of the 120 kHz range. The SSL1 dominates the acoustic backscatter at 38 kHz (Figure 5.3.2c), it begins at ~200 m although the greatest intensities of >-65 dB are below 300 m. SSL2 is not obvious in the 38 kHz data, although there is higher acoustic backscatter in the surface 100 m during the downcast than during the upcast.

A summary of the acoustic volume backscattering statistics from the VM-ADCP and the standardised biovolume and abundance for each sample is shown in Table 5.3.1. Observed VM-ADCP acoustic backscatter values range between –61.20 and –84.44 dB and the standard deviation lies between 0 and 2.02 dB. The final column indicates from which water mass the sample was taken from. The water masses, identified using temperature and salinity data collected from the LHPR's environmental sensors, were separated into five groups: water of predominantly Atlantic origin (AOW); predominantly Mediterranean surface water origin (MOW), mixed Mediterranean and Atlantic water (MMAW), Temperature Minimum Layer water (TML) and Levantine Intermediate Water (LIW). The last two water masses were identified after Gascard and Richez (1985). The respective temperature and salinitys of each water mass are listed in Table 5.3.2.

The acoustic volume backscattering statistics for the three frequencies (38, 120 and 200 kHz) of the EK500 are presented in Table 5.3.3. The 38 kHz frequency data had the greatest dynamic range, with minimum and maximum values of –89 and –58 dB respectively and a standard deviation between 0.06 and 2.45 dB. The 120 kHz data ranged between –88.51 and –70.80 dB with a standard deviation of between 0 and 1.11 dB, and the 200 kHz data varied between –91.55 and –75.32 dB with a standard deviation between 0 and 1.92 dB. As in Table 5.3.1, the water mass from which the sample was taken has been identified in the final column.

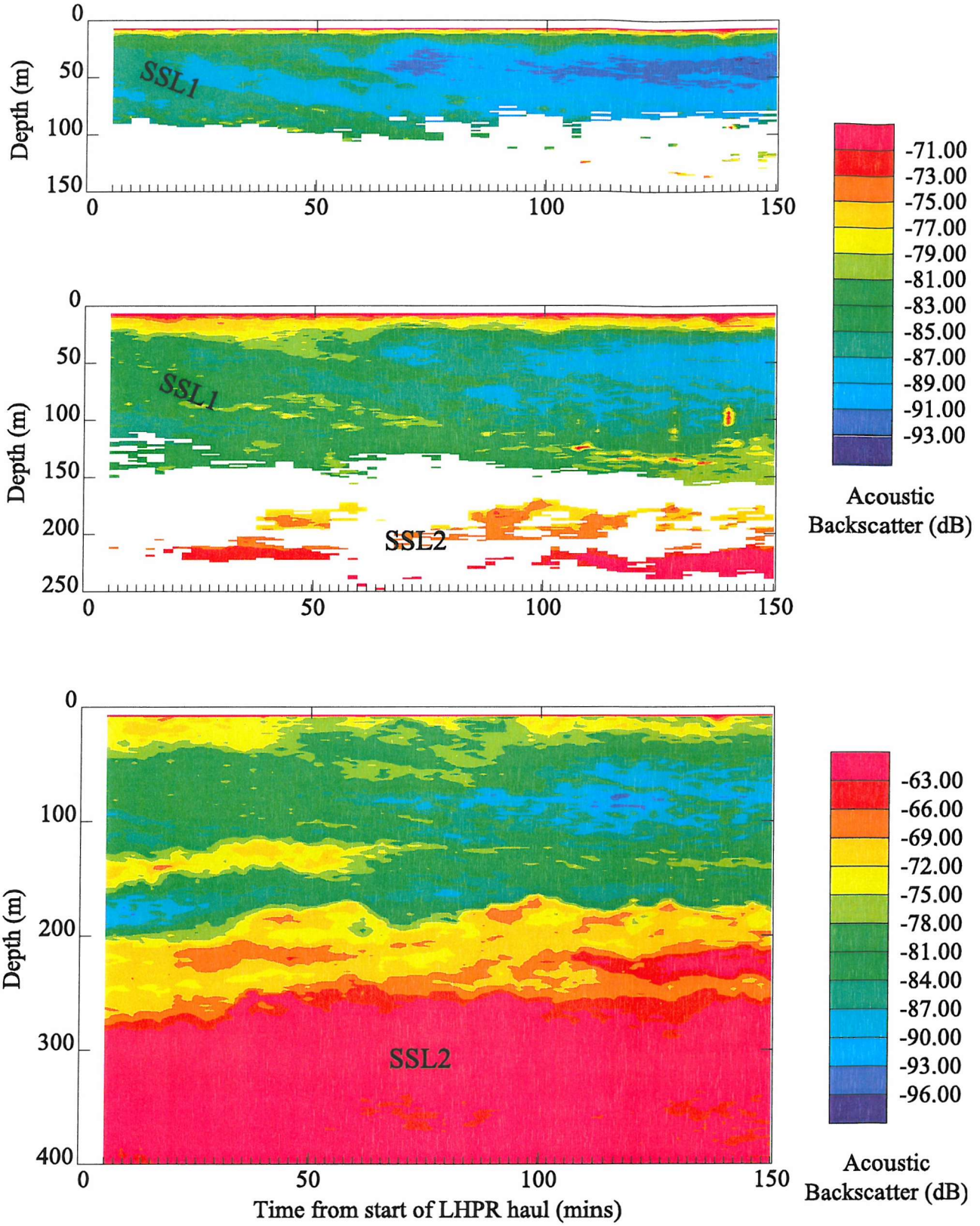

Figure 5.3.2 Contour plots of EK500 (a) 200 kHz, (b) 120 kHz and (c) 38 kHz observed acoustic backscatter during the LHPR Station 13048 (note different scales). Two Sound Scattering Layers are identified. SSL1, a layer of higher backscatter concurrent with the 27.9 σ_0 isopycnal along the front, and SSL2, a permanent feature occurring between ~250 and >600 m.

Table 5.3.1. Summary of ADCP acoustic backscattering statistics, zooplankton biovolumes and abundance for LHPR samples from Station 13048.

Sample Number	Mean Backscattering to 2 d.p. (dB)	Standard Deviation to 2 d.p. (dB)	LHPR Sample Biovolume to 2 d.p. (ml m^{-3})	LHPR Sample Abundance to 2 d.p. (No. m^{-3})	Water Mass*
1	-72.77	0.29	0.02	123.33	MOW
2	-75.47	0.34	0.04	159.28	MOW
3	-74.46	0.39	0.03	193.36	MOW
4	-75.98	0.29	0.02	159.20	MMAW
5	-76.32	0.56	0.01	122.81	MMAW
6	-77.16	0.88	0.01	62.26	MMAW
7	-76.02	1.29	0.01	44.25	MMAW
8	-79.78	0.64	0.01	118.01	MMAW
9	-80.70	0.39	0.01	146.10	MMAW
10	-78.60	0.57	0.02	137.28	TML
11	-81.22	0.46	0.02	231.58	TML
12	-84.33	0.59	0.02	185.07	TML
13	-84.45	0.00	0.03	193.19	LIW
14	-77.87	0.00	0.03	230.56	LIW
15	-74.34	0.85	0.03	306.16	LIW
16	-67.43	0.83	0.03	311.74	LIW
17	-67.41	0.01	0.05	314.92	LIW
18	-70.44	0.00	0.04	233.42	LIW
19	-66.40	0.89	0.02	130.49	LIW
20	-62.30	0.00	0.02	123.84	LIW
21	-62.28	0.00	0.02	71.58	LIW
35	-62.81	0.31	0.04	39.19	LIW
36	-61.91	0.30	0.04	79.97	LIW
37	-61.41	0.85	0.03	52.91	LIW
38	-61.20	0.58	0.05	56.84	LIW
39	-62.08	0.58	0.04	51.95	LIW
40	-62.03	0.31	0.02	49.65	LIW
41	-62.80	0.31	0.03	59.36	LIW
42	-62.86	0.57	0.03	49.58	LIW
43	-66.24	0.58	0.02	94.63	LIW
44	-68.99	0.78	0.02	112.65	LIW
45	-68.27	1.06	0.03	116.89	LIW
46	-69.01	0.01	0.05	213.75	TML
47	-70.74	0.29	0.06	312.17	TML
48	-72.06	0.01	0.05	309.17	TML
49	-71.19	0.30	0.06	291.36	TML
50	-70.99	0.29	0.06	313.19	TML
51	-72.85	0.30	0.06	307.81	TML
52	-74.39	2.02	0.02	217.65	MMAW
53	-79.69	0.63	0.03	226.73	MMAW
54	-78.62	0.25	0.02	230.69	MMAW
55	-78.99	0.29	0.02	220.15	MMAW
56	-78.75	0.58	0.02	178.41	MMAW
57	-76.71	0.30	0.01	181.24	MMAW

58	-71.79	1.06	0.04	82.07	MOW
59	-78.72	0.70	0.01	60.28	MOW
60	-79.21	0.34	0.01	84.49	MOW
61	-78.82	0.00	0.01	61.02	MOW
62	-81.58	0.29	0.01	37.15	AOW
63	-80.47	0.00	0.01	68.52	AOW
64	-81.83	0.61	0.02	137.28	AOW
65	-80.23	0.29	0.01	68.45	AOW
66	-81.76	0.27	0.02	108.39	AOW

* AOW – Atlantic Origin Waters
MOW – Mediterranean Origin Waters
MMAW – Mixed Mediterranean Atlantic Waters
TML – Temperature Minimum Layer Waters
LIW – Levantine Intermediate Waters

Table 5.3.2. Identification of Alboran Sea water masses

Water Mass	**Temperature (°C)**	**Salinity**
Atlantic Origin Water (MOW)	>16.2	<37
Mediterranean Origin Water (MOW)	>15.5	>37.5
Mixed Mediterranean Atlantic Water (MMAW)	13.5-15.5	37.5-38.1
Temperature Minimum Layer (TML)	<13.5	~38.2
Levantine Intermediate Water (LIW)		>38.2

Table 5.3.3. Summary of EK500 acoustic backscattering statistics for LHPR samples from Station 13048

Sample Number	38 kHz		120 kHz		200 kHz		Water Mass*
	Mean Backscatter (dB)	Standard Deviation (dB)	Mean Backscatter (dB)	Standard Deviation (dB)	Mean Backscatter (dB)	Standard Deviation (dB)	
1	-62.43	0.09	-76.28	0.56	-80.83	0.75	MOW
2	-73.69	0.17	-81.31	0.76	-85.40	0.29	MOW
3	-78.23	0.87	-81.48	0.47	-85.76	0.21	MOW
4	-80.24	1.16	-84.18	0.40	-87.69	0.10	MMAW
5	-81.08	0.78	-83.27	0.99	-84.95	1.92	MMAW
6	-81.96	1.25	-84.69	1.05	-87.02	0.00	MMAW
7	-81.80	0.15	-84.05	0.49	-86.04	0.91	MMAW
8	-82.65	0.61	-85.27	0.10			MMAW
9	-82.14	1.08	-85.15	0.01			MMAW
10	-73.63	1.54	-82.79	0.04			TML
11	-78.63	1.22					TML
12	-84.53	1.24					TML
13	-86.57	0.48					LIW
14	-79.84	1.67					LIW
15	-75.70	0.75					LIW
16	-68.51	1.16	-73.31	0.00			LIW
17	-67.01	0.45	-71.84	0.25			LIW
18	-72.16	0.13					LIW
19	-59.80	2.10					LIW
20	-60.01	0.64					LIW
21	-59.42	0.74					LIW
22	-61.29	0.46					LIW
23	-61.57	0.06					LIW
24	-61.31	0.54					LIW
25	-59.66	0.69					LIW
26	-58.88	0.61					LIW
27	-59.33	0.21					LIW
28	-58.63	0.67					LIW
29	-59.10	0.81					LIW
30	-58.81	0.07					LIW
31	-59.36	0.60					LIW
32	-61.95	0.38					LIW
33	-62.92	0.33					LIW
34	-60.75	0.12					LIW
35	-60.11	0.40					LIW
36	-58.89	0.55					LIW

37	-58.84	0.39					LIW
38	-59.21	0.41					LIW
39	-60.01	0.69					LIW
40	-60.70	0.06					LIW
41	-60.38	0.30					LIW
42	-60.64	0.53					LIW
43	-66.06	1.36					LIW
44	-69.44	0.91	-70.80	0.00			LIW
45	-68.40	1.21	-70.80	0.59			LIW
46	-69.60	0.98	-72.46	0.56			TML
47	-70.47	0.94					TML
48	-71.38	0.35	-73.65	0.00			TML
49	-71.11	0.41	-74.23	0.51			TML
50	-70.86	0.65	-74.70	0.15			TML
51	-72.86	0.66	-76.52	0.24			TML
52	-74.51	2.24	-78.03	0.91			MMAW
53	-83.54	0.27					MMAW
54	-81.55	0.25	-80.98	0.00			MMAW
55	-82.92	1.16	-81.55	0.00			MMAW
56	-83.20	0.71	-81.41	0.18			MMAW
57	-81.32	0.91	-81.38	0.20			MMAW
58	-80.64	0.67	-80.07	1.11	-75.32	1.59	MOW
59	-85.55	1.25	-85.53	0.35			MOW
60	-88.93	2.45	-86.90	0.55	-86.89	0.00	MOW
61	-86.59	1.57	-86.68	0.82	-88.68	0.62	MOW
62	-85.20	1.45	-88.51	0.76	-91.45	0.42	AOW
63	-79.30	0.98	-87.17	0.91	-90.95	0.90	AOW
64	-82.62	0.80	-88.41	0.09	-91.55	0.19	AOW
65	-83.85	1.45	-87.76	0.25	-90.72	0.25	AOW
66	-82.46	0.98	-87.99	0.15	-91.35	0.25	AOW

* AOW – Atlantic Origin Waters
MOW – Mediterranean Origin Waters
MMAW – Mixed Mediterranean Atlantic Waters
TML – Temperature Minimum Layer Waters
LIW – Levantine Intermediate Waters

In Figure 5.3.3 the distribution with depth of observed VM-ADCP acoustic backscatter, total biovolume, total abundance, acoustic group biovolume and acoustic group abundance for each two-minute LHPR sample is presented. In all variables there were differences between the up and downcasts of the LHPR haul, not surprisingly as the haul was conducted through several water masses and across a front. Values of observed VM-ADCP acoustic backscatter (Figure 5.3.3a), on the downcast, remained fairly constant around -75 dB to a depth of 100 m. Below this, acoustic backscatter decreased to its lowest values during the haul of ~-85 dB at 170 m, with a small maximum of –78 dB at 130 m depth. Below 170 m acoustic backscatter increased occurring with two maxima at 210 and 270 m depth. During the haul the highest acoustic backscatter was observed at 300 m depth (between –65 and –60 dB) and the acoustic backscatter values of both the up and downcast followed a similar distribution from the bottom of the VM-ADCP range to ~240 m. From 240 m to ~100 m acoustic backscatter was higher in the upcast than it had been in the downcast, although the distribution was comparable, with a maxima (-72 dB) at ~130 m. Above 100 m acoustic backscatter intensities remained around ~-81 dB, 6 dB less than on the downcast.

Whilst VM-ADCP acoustic backscatter remained constant from the surface to ~100 m, zooplankton biovolume (Figure 5.3.3b) had a subsurface maxima of ~0.04 ml m^{-3} at 40 m, this decreased to the lowest biovolume of the downcast (<0.01 ml m^{-3}) at 100 m. A second maximum occurred at ~240 m depth, coincident with a peak in acoustic backscatter. Below 240 m biovolume decreased, although two samples had elevated biovolumes as a result of large *Pyrosoma* being caught in the net. The abundance of zooplankton (Figure5.3.3b) followed a similar distribution to the biovolume on the downcast. The only discrepancies observed were caused by an increase in the abundance of copepods at 148 m and the occurrence of *Pyrosoma* below 300 m. The abundance of zooplankton showed similar distributions in both the up and downcast of the haul, except the minimum values of abundance were found at ~50 m on the upcast compared with at ~100 m on the down. Biovolume values of the upcast were more erratic than the downcast. The depth that the largest biovolume was found during the upcast (~200 m) was slightly shallower and occurring over a larger depth range than the downcast, and no subsurface maximum at ~50 m could be recognised. Like the VM-ADCP acoustic backscatter biovolume and abundance was smaller in the upcast than during the downcast. Biovolume and abundance data for only the significant acoustic scatterers (Figure 5.3.3c) followed a similar profile to those for the total zooplankton in both the up and downcast.

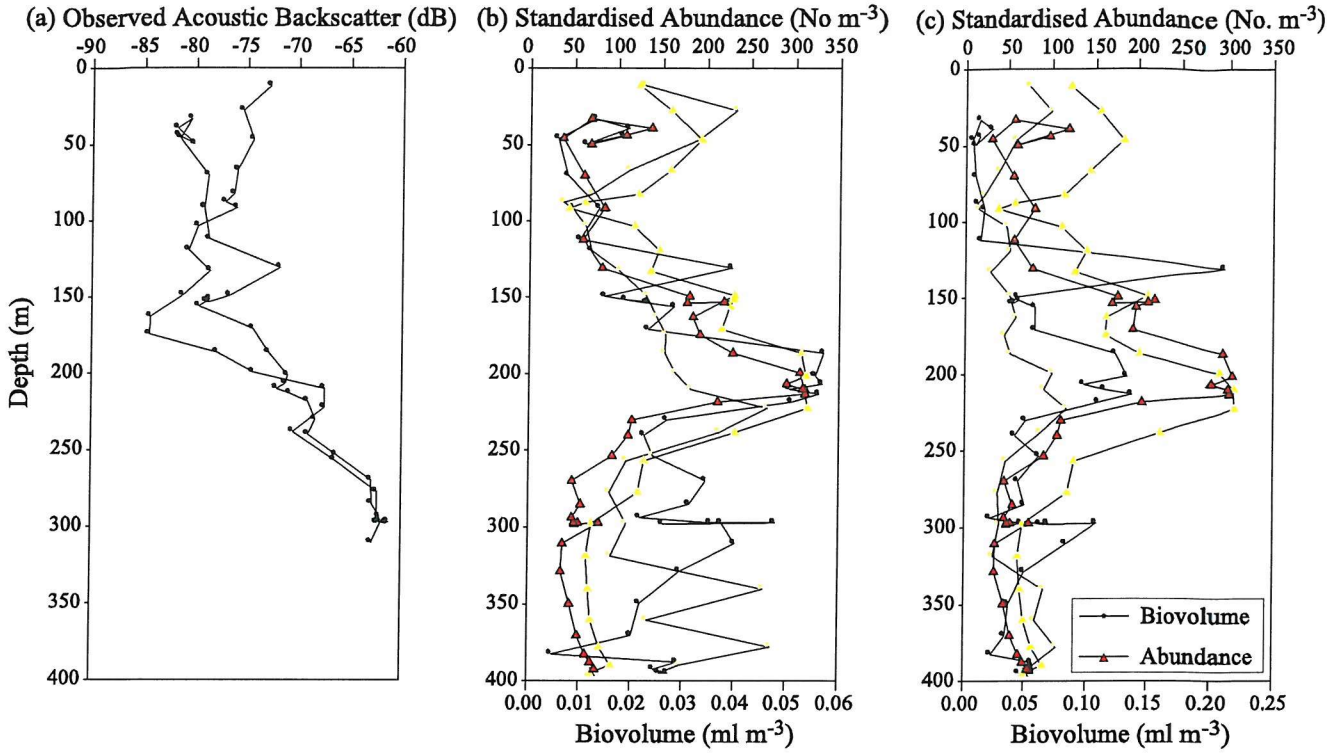

Figure 5.3.3 The distribution with depth of (a) observed VM-ADCP acoustic backscatter, (b) total LHPR sample biovolume and total sample abundance, and (c) acoustic group biovolume and acoustic group abundance. The downcast is in yellow, the upcast in red.

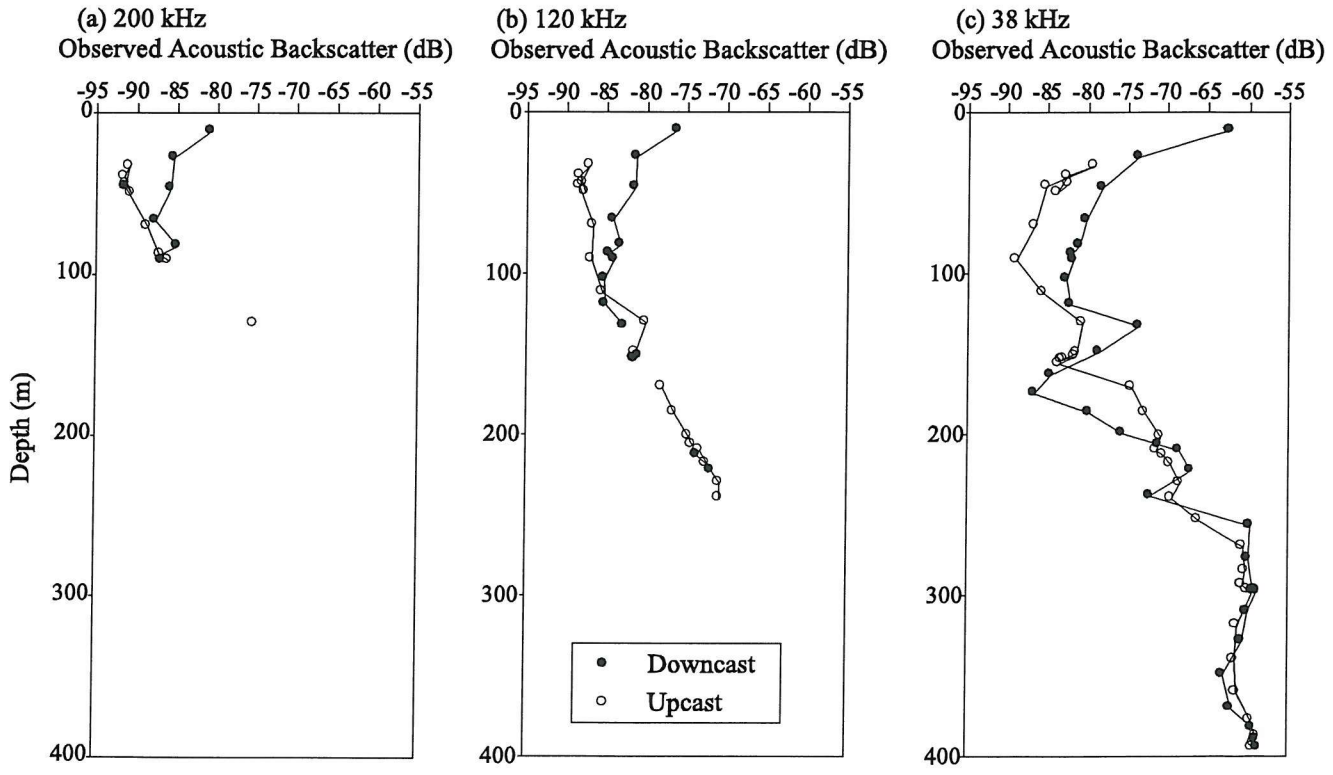

Figure 5.3.4 The distribution with depth of observed EK500 acoustic backscatter at (a) 200 kHz, (b) 120 kHz and (c) 38 kHz.

Resembling the VM-ADCP profile, the intensities of acoustic backscatter at depths above 100 m in the downcast of all three frequencies of the EK500 were greater than the upcast (Figure 5.3.4) with greatest intensities occurring at the surface. The difference in depth range attained with each frequency is shown in Figure 5.3.4, with the 200 kHz frequency producing values to ~100 m, the 120 kHz to ~240 m and the 38 kHz having the greatest depth range of ~800 m. The highest acoustic backscatter intensities at 120 and 38 kHz occurred at depth (-72 dB at 230 m and ~-60 dB below 250 m for each frequency respectively). Below 100 m in the 120 kHz data, acoustic backscatter intensities in both the up and downcast were of similar values (Figure 5.3.4b) except for a slight maximum of –80 dB at 130 m on the upcast. The 38 kHz data follows a similar profile to the VM-ADCP, with a maxima at ~130 m on both the up and downcast, a minima at ~170 m, which is lower and deeper on the downcast than the up (-86 at 170 m compared with –83 dB at 156 m) and a maxima (-67 dB) at 220 m on the downcast (Figure 5.3.4c). Acoustic backscatter intensities were fairly constant from 260 m to the bottom of the LHPR haul in both the up and downcast. The only similarity between the acoustic backscatter and zooplankton biovolume and abundance profiles is a maxima occurring between 200 and 230 m depth.

5.3.2 Direct comparison

5.3.2.1 Direct comparison of zooplankton biovolume and abundance and observed acoustic backscatter

Following the method outlined in section 5.2.2.1 the correlation between acoustic backscatter and LHPR-sampled zooplankton biovolumes was examined. In Figure 5.3.5 the total VM-ADCP and EK500 200, 120 and 38 kHz acoustic backscatter observed in the vicinity of the two-minute LHPR is plotted against zooplankton biovolume for that sample. Contrary to Section 5.2.2.1 an exponential curve was not fitted to the data. This procedure is thought to be slightly tenuous as both exponential and linear regression lines fitted to the data provide similar statistics (Table 5.3.4). However, it should be noted that, as with previous data (Section 5.2.2.1, FS1; FS2; HSB; etc.), a general trend of higher backscatter associated with larger biovolumes could be discerned at all frequencies. The best fit to the data was a linear regression line fit to the 120 kHz acoustic data, where 57 % of the data ($r^2 = 0.57$) fitted the regression line.

To compare the results with FS1, HSB, BVVS and section 5.2.2.1 (henceforth denoted S5) biovolume was converted to dry weight (DW, mg m^{-3}), using Wiebe's (1988) conversion tables, divided by 4π and logged (after FS2, see section 5.2.2.1). $\text{Log}(DW/4\pi)$

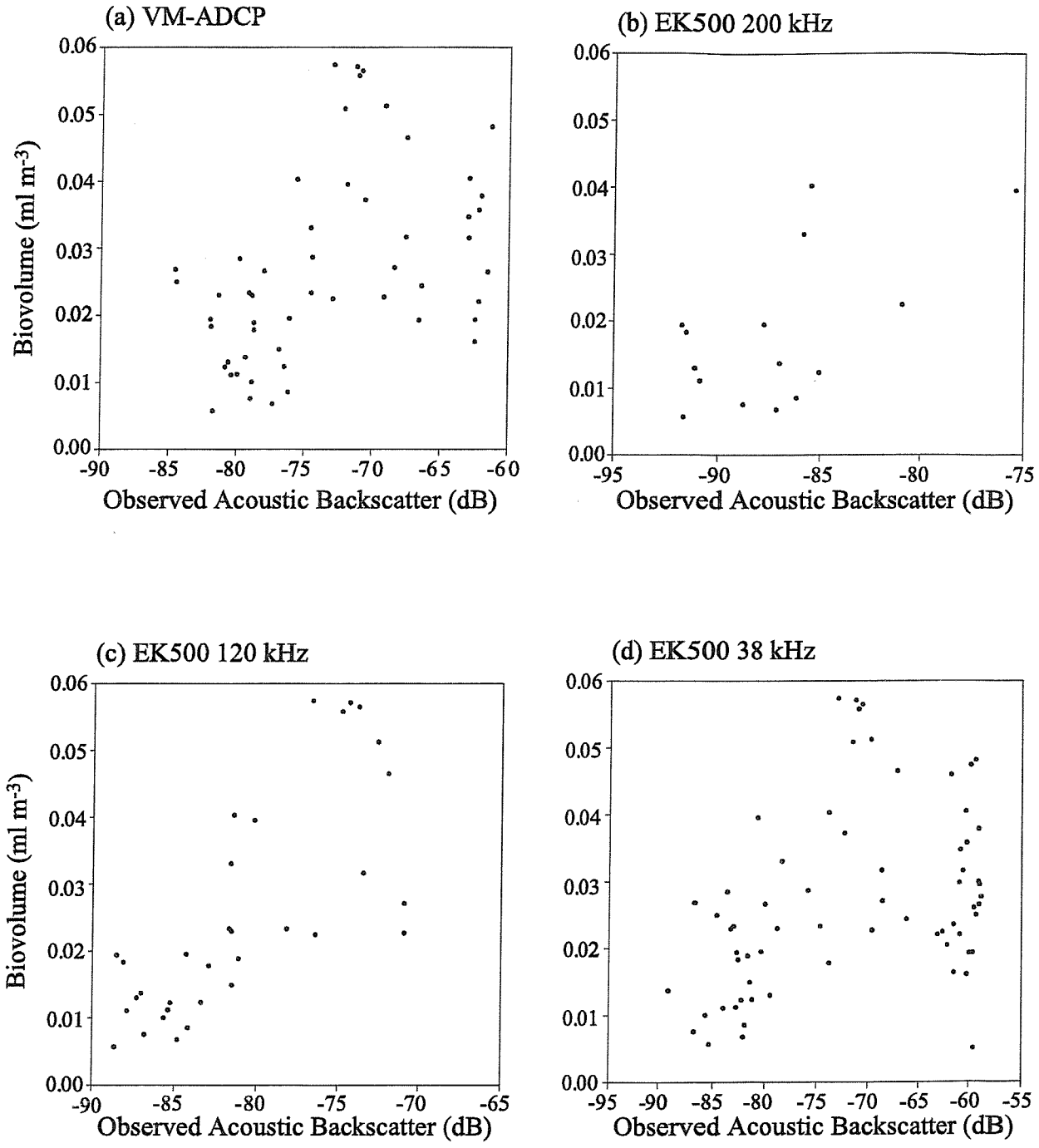

Figure 5.3.5 LHPR sample total standardised biovolume (DV) plotted against (a) observed VM-ADCP acoustic backscatter (OAB), (b) EK500 200 kHz acoustic backscatter, (c) EK500 120 kHz acoustic backscatter and (d) EK500 38 kHz acoustic backscatter.

Instrument and frequency	Equation	r^2
VM-ADCP linear	$DV = 0.09344+0.0009121OAB$	0.20
VM-ADCP exponential	$DV = 0.02192e^{0.02901OAB}$	0.18
EK500 200 kHz linear	$DV = 0.1505+0.001527OAB$	0.36
EK500 200 kHz exponential	$DV = 8.515e^{0.07159OAB}$	0.37
EK500 120 kHz linear	$DV = 0.1965+0.002122OAB$	0.54
EK500 120 kHz exponential	$DV = 6.942e^{0.07044OAB}$	0.49
EK500 38 kHz linear	$DV = 0.0606+0.0005OAB$	0.12
EK500 38 kHz exponential	$DV = 0.0804e^{0.0156OAB}$	0.11

Table 5.3.4 Equations and r^2 values for linear and exponential regression lines fit to zooplankton biovolume and observed VM-ADCP and EK500 acoustic backscatter.

was plotted against observed acoustic backscatter for each frequency (Figure 5.3.6) and $\Delta DW/\Delta AB$ was calculated using both a predictive and a functional regression for the VM-ADCP data. Values of $\Delta DW/\Delta AB$ were also investigated for acoustic data from the EK500 although, because they are not being compared with previous results, only a functional regression has been used in their calculation. The strongest correlation was again found in the 120 kHz data, where 57 % of the data fitted the regression line. This method was also used for the dry weight of solely the significant acoustic scattering groups and $\log(DW_{ag}/4\pi)$ was calculated and plotted against observed acoustic backscatter (Figure 5.3.7). The fit of the data to the regression line improved at all frequencies (r^2 = 0.22, 0.66, 0.61 and 0.19 compared with 0.23, 0.28, 0.57 and 0.16 for VM-ADCP, 200, 120 and 38 kHz respectively).

VM-ADCP $\Delta DW/\Delta AB$ was compared with previous results (0.115, FS2; 0.056, HSB; 0.055, BVVS; 0.0416 and 0.08769, S5) using a students t-test (Table 5.3.5). The null hypothesis (H_0) was that $\Delta DW/\Delta AB$ was not significantly different from the slope of previous regression lines (i.e. 0.115). This method was also applied to the biovolume data of only the significant acoustic scattering groups ($\Delta DW_{ag}/\Delta AB$).

The VM-ADCP $\Delta DW/\Delta AB$, calculated using a predictive regression, was the smallest value of all the studies and found to be statistically significantly different from that calculated by FS2, HSB and from the functional regression calculated value of $\Delta DW/\Delta AB$ from S5.

When calculated using a functional regression, VM-ADCP $\Delta DW/\Delta AB$ was still statistically different from FS2 and from the functional regression calculation of $\Delta DW/\Delta AB$ from S5. $\Delta DW_{ag}/\Delta AB$ was found not to be significantly different from $\Delta DW/\Delta AB$ (P=0.01), but were found to be significantly different from the results of FS2 and the functional regression calculated value from S5.

$\Delta DW/\Delta AB$ and $\Delta DW_{ag}/\Delta AB$ for each frequency of the EK500 were compared with each other (Table 5.3.6). No statistically significant difference was found between the two highest frequencies of 200 and 120 kHz. The only significant difference between the 200 and 38 kHz frequencies was between the 200 $\Delta DW_{ag}/\Delta AB$ and the 38 $\Delta DW/\Delta AB$. The insensitivity of the t-test could be a result of the large standard error and small sample size of the 200 kHz data set (S.E. = 0.0169, n = 15). For example, where the 38 kHz $\Delta DW/\Delta AB$ was compared with $\Delta DW_{ag}/\Delta AB$ (larger data sets, with smaller standard errors (n = 66, S.E. = 0.0033 and 0.004873 respectively) a significant difference is found, although the difference between values of $\Delta DW/\Delta AB$ is less.

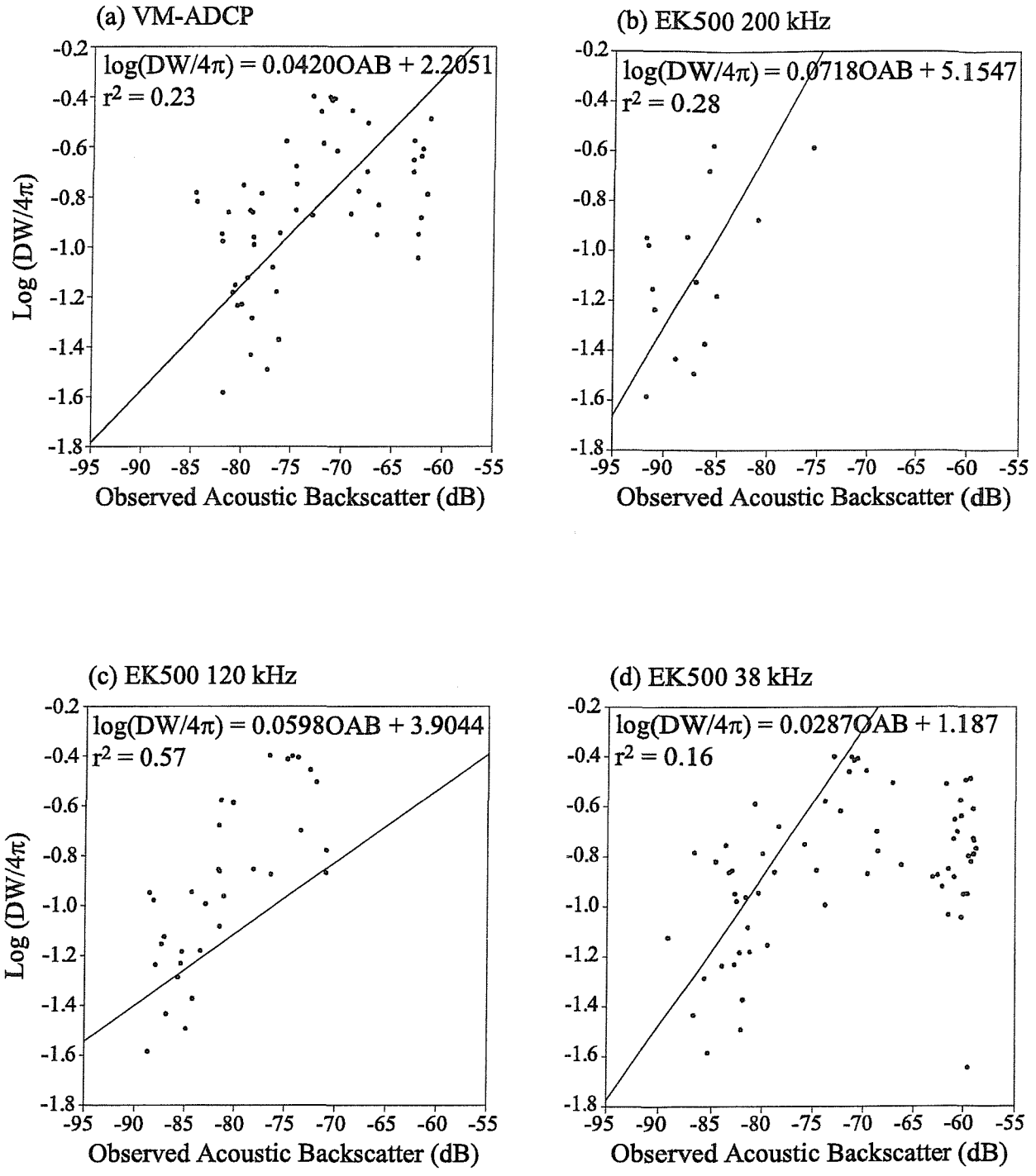

Figure 5.3.6 LHPR sample log(DW/4π) plotted against (a) observed VM-ADCP, (b) EK500 200 kHz, (c) EK500 120 kHz and (d) EK500 38 kHz acoustic backscatter (OAB).

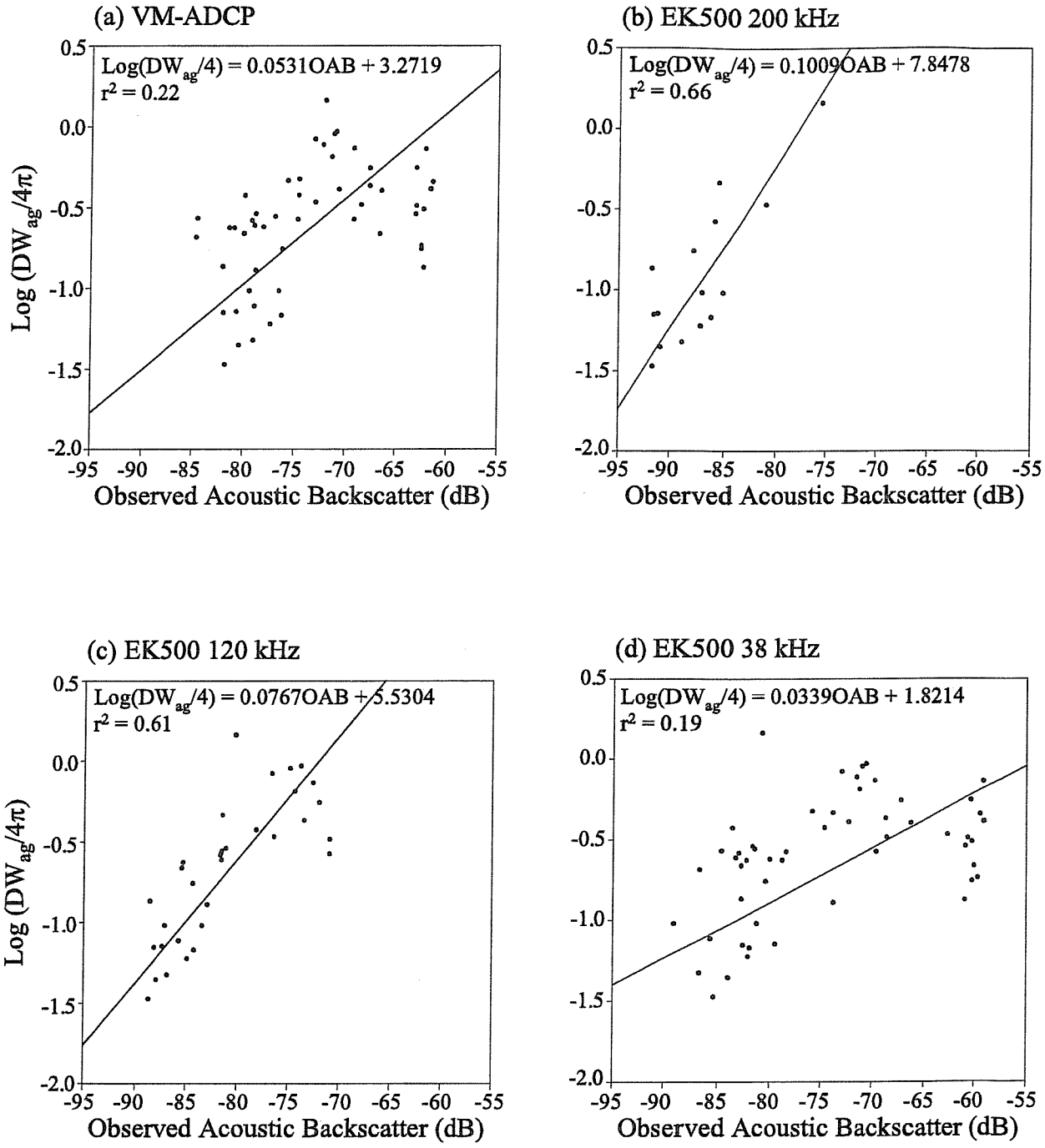

Figure 5.3.7 LHPR sample $\log(DW_{ag}/4\pi)$ of significant acoustic scattering groups plotted against (a) observed VM-ADCP, (b) EK500 200 kHz, (c) EK500 120 kHz and (d) EK500 38 kHz acoustic backscatter (OAB).

Table 5.3.5 Examination of VM-ADCP $\Delta DW/\Delta AB$ compared with previous studies

(H_0) v =	**0.115 (FS2)**	**0.056 (HSB)**	**0.055 (BVVS)**	**0.0416[1] (S5)**	**0.0877[2] (S5)**
Total sample					
H_0 accepted (P=0.01) ADCP$\Delta DW/\Delta AB$ = 0.0203[1]	YES	YES	no	no	YES
H_0 accepted (P=0.01) ADCP$\Delta DW/\Delta AB$ = 0.0420[2]	YES	no	no	no	YES
Acoustic groups only					
H_0 accepted (P=0.01) ADCP$\Delta DW_{ag}/\Delta AB$ = 0.0246[1]	YES	no	no	no	YES
H_0 accepted (P=0.01) ADCP$\Delta DW_{ag}/\Delta AB$ = 0.0531[1]	YES	no	no	no	no

[1] = calculated using a predictive regression

[2] = calculated using a geometric mean estimate of the functional regression

Table 5.3.6 Examination of EK500 $\Delta DW/\Delta AB$ between different acoustic frequencies

(H_0) v =	**200 kHz** $\Delta DW/\Delta AB$ = **0.0718**	**120 kHz** $\Delta DW/\Delta AB$ = **0.0598**	**38 kHz** $\Delta DW/\Delta AB$ = **0.0287**
Acoustic groups only			
H_0 accepted (P=0.01) 200kHz$\Delta DW/\Delta AB$ = 0.0718	X	no	no
H_0 accepted (P=0.01) 200kHz$\Delta DW_{ag}/\Delta AB$ = 0.1009	no	no	YES
H_0 accepted (P=0.01) 120kHz$\Delta DW/\Delta AB$ = 0.0598	no	X	YES
H_0 accepted (P=0.01) 120kHz$\Delta DW_{ag}/\Delta AB$ = 0.0767	no	no	YES
H_0 accepted (P=0.01) 38kHz$\Delta DW/\Delta AB$ = 0.0287	no	YES	X
H_0 accepted (P=0.01) 38kHz$\Delta DW_{ag}/\Delta AB$ = 0.0339	no	YES	No

5.3.2.2 Discussion of direct comparison

Zooplankton biovolume was not exponentially related to observed VM-ADCP or EK500 acoustic backscatter, contrary to the findings in Section 5.2. Although, agreeing with previous studies, a general trend of an increase in biovolume related to an increase in observed acoustic backscatter could be discerned (Table 5.3.4). The commercially built fisheries echosounder (the EK500) acoustic backscatter (at its higher frequencies) showed a better correlation with the zooplankton biomass than the VM-ADCP.

While the VM-ADCP acoustic data used in this study could be described as absolute (after Roe *et al.*, 1996), the inability to calibrate the instrument and for comparison with previous studies $\Delta DW/\Delta AB$ was calculated (see Section 5.2.2.1). A predictive regression produced the lowest value of $\Delta DW/\Delta AB$ (0.0203) compared with previous studies, and was significantly different from that of FS2 and HSB. The functional regression calculated $\Delta DW/\Delta AB$ was greater (0.0420), closer to the value of HSB, but still significantly different from FS2's and S5's. Again this indicates (according to FS2) that the VM-ADCP used in this study was the most sensitive to changes in zooplankton concentration. An interesting observation at this point is that the VM-ADCP used in this study was the same as that used in the Indian Ocean and the same type of net was used to catch the zooplankton (the Longhurst Hardy Plankton Recorder, although a modern version; see Chapter 2). Hence it is unlikely that the instruments could be "mechanically" more sensitive, therefore it is more likely the greater sensitivity could be attributed to differing zooplankton populations that live in the Indian Ocean and Mediterranean Sea. In this case the average mean length of the zooplankton caught in the Indian Ocean was larger than that in the Mediterranean Sea (7.23 and 6.7 mm respectively). Since the individual target size of the 150 kHz frequency is ~1 cm, it could be that the VM-ADCP was more sensitive to the target size (zooplankton) in the Indian Ocean than in the Mediterranean Sea.

As in Section 5.2.2.1, the data presented in this study exhibit a poorer correlation between log(DW/4π) and VM-ADCP acoustic backscatter than that found in previous studies (FS1, FS2, HSB and BVVS). Comparable with the data from Section 5.2.2.1, the poor regression and correlation coefficients are presumed to result from a sample set that is comprised of a complex size and composition structure resulting from a mixed species zooplankton population, rather than an environment dominated by a single species and cohort of *Calanus finmarchicus* (FS2).

This dataset, from a different area and environment, results in a different correlation from previous studies, although not statistically significantly different ($p>0.05$)

from BVVS or from S5. This is surprising as each study concerns different zooplankton populations with different size structures. This may have resulted from statistical error because of the small sample size and large scatter (BVVS, S5 and this study had the poorest correlation).

From Section 5.2.2.2 and above it could be concluded that the greatest effect on $\Delta DW/\Delta AB$ is the frequency of the acoustic instrument used and the size of zooplankton caught. This should show up in the value of $\Delta DW/\Delta AB$ that was calculated using multifrequency acoustic data from the EK500 and $\log(DW/4\pi)$. The frequency whose wavelength is comparable to the length of zooplankton caught ought to have the lowest value of $\Delta DW/\Delta AB$. The LHPR, using a 333 μm net, catches zooplankton of length >1.3 mm (Nichols and Thompson, 1991) and the average size of zooplankton caught in the Mediterranean Sea was ~6.7 mm, which is comparable with the wavelength of the 200 kHz frequency. However the 38 kHz had the lowest value of $\Delta DW/\Delta AB$, which would suggest the greatest sensitivity to the zooplankton present. But if we return to FS2's hypothesis that $\Delta DW/\Delta AB$ should be equal to 0.1, the best correlation occurs with acoustic data at 200 kHz (using only the significant acoustic scattering groups), agreeing with the supposition that the 200 kHz frequency target size (~7.5 mm) is comparable with the size of zooplankton caught.

Using this deduction, if we return to the VM-ADCP data we can conclude that the study with the best correlation was by either FS2 (using a predictive regression) using a 150 kHz VM-ADCP in the Gulf Stream or S5 (using a functional regression) using a 150 kHz in the Indian Ocean. Ambiguities in this study are related to FS2's original assumption where (working backwards):

$\text{Log}(DW/4\pi) \approx 0.1$ (1)

because:

$\text{TS} = 10\text{Log}(\sigma_{bs}/4\pi)$ (2)

where:

$\sigma_{bs} \propto \sigma_a$

and:

$\sigma_a \propto DW$

where TS is target strength or, in this case, acoustic backscatter, σ_{bs} is the backscattering cross section and σ_a is the cross-sectional area. Errors may arise based around assumptions

1 and 2. Table 5.3.7 provides a comparison of target strength (at 120 kHz), dry weight, cross-sectional area and the proportionality constant between σ_a and DW of seven zooplankton groups (after Table 1 in Griffiths *et al.*, 2002). σ_a/DW varied between 1.84 and 13 depending on zooplankton group and hence FS2's assumption of $\sigma_a \propto DW$ is questionable or may only be applicable in single zooplankton species studies. As such the value of the fit between observed acoustic backscatter and $\log(DW/4\pi)$ or $\Delta DW/\Delta AB$ becomes uncertain.

5.3.3 Model-estimated acoustic backscatter

5.3.3.1 Comparison of VM-ADCP observed and model estimated acoustic backscatter

To improve the relationship between acoustic backscatter and zooplankton, acoustic models must be used. The relative contribution of six "significant acoustic scattering" zooplankton groups, identified in the taxon-specific model equations given by Stanton *et al.* (1994a) are presented in Figure 5.3.8. The model estimates for all groups are less than the observed acoustic backscatter, with fish and amphipods having the lowest model-estimated values. As is evident in Figure 5.3.8f the estimated pteropod contribution to the total acoustic backscatter is larger than that of any other taxon in many of the samples i.e.≥-80 dB.

The percentage contribution of each group to the total model-estimated acoustic backscatter (TMEAB) was calculated (Figure 5.3.9). Whilst copepods contributed at least ~50 % to the TMEAB in most samples they did not dominate every sample. During the downcast, in waters of Mediterranean origin, chaetognaths contributed greatly to the TMEAB, especially in a twenty metre thick layer at 90 m where their contribution reached ~80 %. Below 160 m this contribution dropped to ≤ 10 % for the rest of the cast. Pteropods dominated the TMEAB in a fifty metre-thick layer from 200 m, where they contributed more than 70 % and up to 90 % of the TMEAB. This layer of pteropod dominated samples also occurred on the upcast, although in a thinner and deeper layer. During the upcast the euphausiid contribution to the TMEAB increased until they dominated up to 75 % of the TMEAB in samples above 50 m in waters of Atlantic origin. The fish group added little to the TMEAB, its greatest contributions (10-25%) occurring at depth (200-300 m) in Levantine Intermediate Water and between 50 and 100 m.

The model-estimated acoustic backscatter for each zooplankton group is summed (in linear form) to create TMEAB for each sample, which can be plotted against observed VM-ADCP acoustic backscatter to investigate the relationship between acoustic

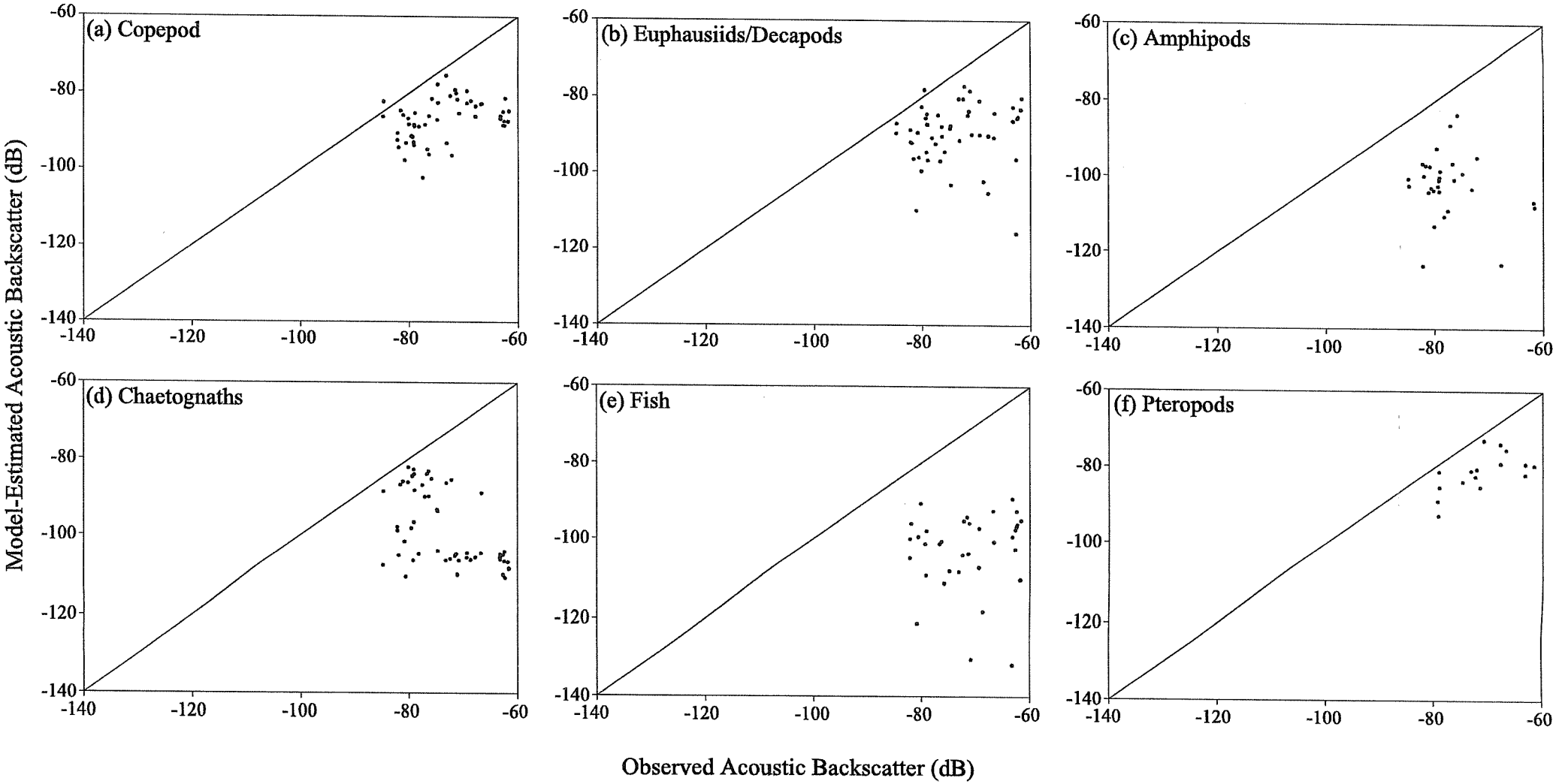

Figure 5.3.8 Model-estimated acoustic backscatter plotted against observed VM-ADCP acoustic backscatter for (a) Copepods, (b) Euphausiids and Decapods, (c) Amphipods, (d) Chaetognaths, (e) Fish and (f) Pteropods.

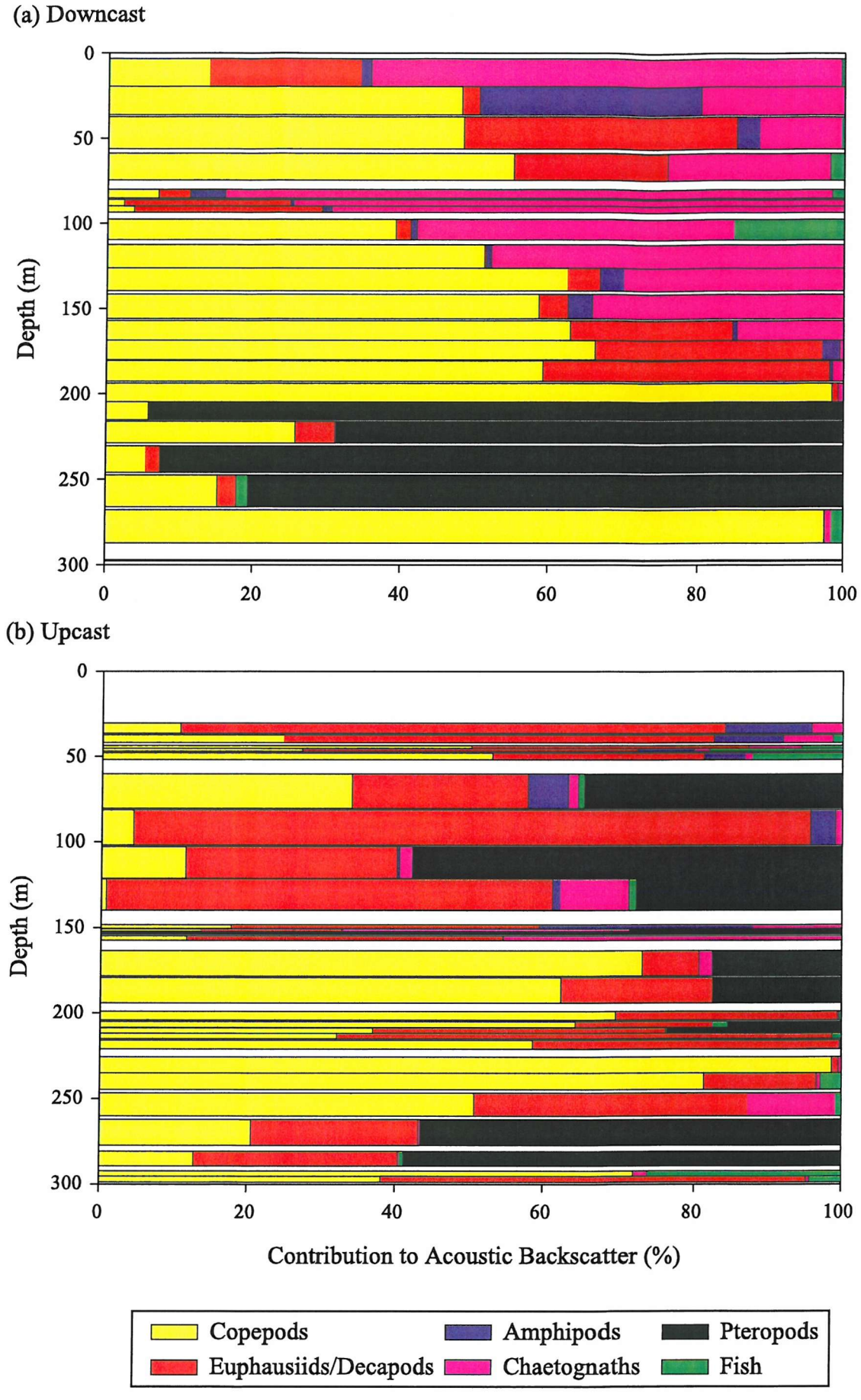

Figure 5.3.9 The percentage contribution of each significant acoustic scattering group to the total model-estimated VM-ADCP acoustic backscatter for the (a) downcast and (b) upcast of LHPR Station 13048.

Table 5.3.7 Target strength of single individuals from seven representative animal classes at a frequency of 120 kHz, together with estimates of dry weight, cross-sectional area, and σ_a/DW.

Zooplankton group	Target Strength, dB	Dry Weight (*DW*), mg	Area (σ_a), mm^2	σ_a/DW
Decapod	-72.3	87	160	1.84
Pteropod	-80.3	0.48	2	4.17
Fish	-103.3	25	200	8
Chaetognath	-106.7	0.26	1.43	5.5
Amphipod	-117.9	0.04	0.34	8.5
Large Copepod	-103.1	0.23	0.95	4.13
Small copepod	-124.3	0.01	0.13	13

Dry weights and areas were obtained from Stanton *et al.* (1994), Flagg and Smith (1989b), Foote (1990) and Davis and Wiebe (1985), either directly or by using the regression equations therein.

Table 5.3.8 Summary of the functional regression lines fit to EK500 data

Frequency	Equation of the line	r^2	t-test (p>0.05) significant
	Uncorrected model		
200 kHz	TMEAB = 0.8746OAB – 5.9187	0.65	no
120 kHz	TMEAB = 0.9497OAB – 6.5069	0.49	no
38 kHz	TMEAB = 0.7859OAB – 37.7310	0.48	YES
	Corrected model		
200 kHz	TMEAB = 0.7493OAB – 15.9922	0.64	no
120 kHz	TMEAB = 0.9687OAB – 5.1568	0.46	no
38 kHz	TMEAB = 0.9997OAB – 18.4659	0.70	no

backscatter and zooplankton (Figure 5.3.10a). The functional regression line fit to the log-transformed data explained 10% of the total variance of the data ($r^2 = 0.10$) and the slope of the line (0.61 to 2.d.p) was significantly different from the expected slope of one (t-test, n = 53, P>0.05). The relationship between TMEAB and observed VM-ADCP acoustic backscatter is poor; one inaccuracy may be the orientation effect referred to in Section 5.2.3. Ten samples, all with OAB values in excess of –65 dB were diminishing the relationship between OAB and TMEAB (identified in Figure 5.3.10a). When they were removed from the dataset the functional regression fit to the log-transformed data explained 37 % of the total variance of the data ($r^2 = 0.37$) and the slope of the line (0.87 to 2.d.p) was not significantly different from the expected slope of one (t-test, p>0.05) (Figure 5.3.10b). On examination of the LHPR haul it was noticed that all these samples were taken below 250 m in the *Cyclothone* and Myctophid rich Levantine Intermediate Water (LIW). Myctophid fish represent dominant acoustic scatterers that have resonant gas bladders, thereby augmenting their acoustic scattering (Johnson, 1977). However, the models used in this study represent fish as fluid filled spheres and therefore their acoustic backscatter is underestimated (see future work, Ben Reeder of WHOI running gas bladder models).

5.3.3.2 Comparison of EK500 observed and model-estimated acoustic backscatter

Concurrent with the VM-ADCP acoustic backscatter observations was the EK500. The EK500 is a multifrequency purpose-built biological echosounder and, as such, it is expected that the relationship between its acoustic backscatter and net-sampled zooplankton is superior to the VM-ADCP. The relative contributions of the significant acoustic scattering groups are presented in Figure 5.3.11. The disparity in the frequency used matched to the size of zooplankton caught is exhibited by the differences in the model-estimated acoustic backscatter. For example, using data at 200 kHz the model estimation is often greater than the observed value, whilst when using 38 kHz data the model estimation is always less than the observed value (Figure 5.3.11). Whilst the 38 kHz observed acoustic backscatter had the highest intensities, the model estimated values for all groups were the lowest except in the pteropod group. In general the model estimations calculated for the 200 and 120 kHz frequencies were similar, although the 120 kHz data was typically slightly lower.

The percentage contribution of each significant acoustic scattering group to the TMEAB for each frequency is shown in Figure 5.3.12a, b and c (note different depth axis). As with the VM-ADCP data, the dominant contributor to the TMEAB changes between the down and up cast of the LHPR haul. Analogous to all frequencies and the

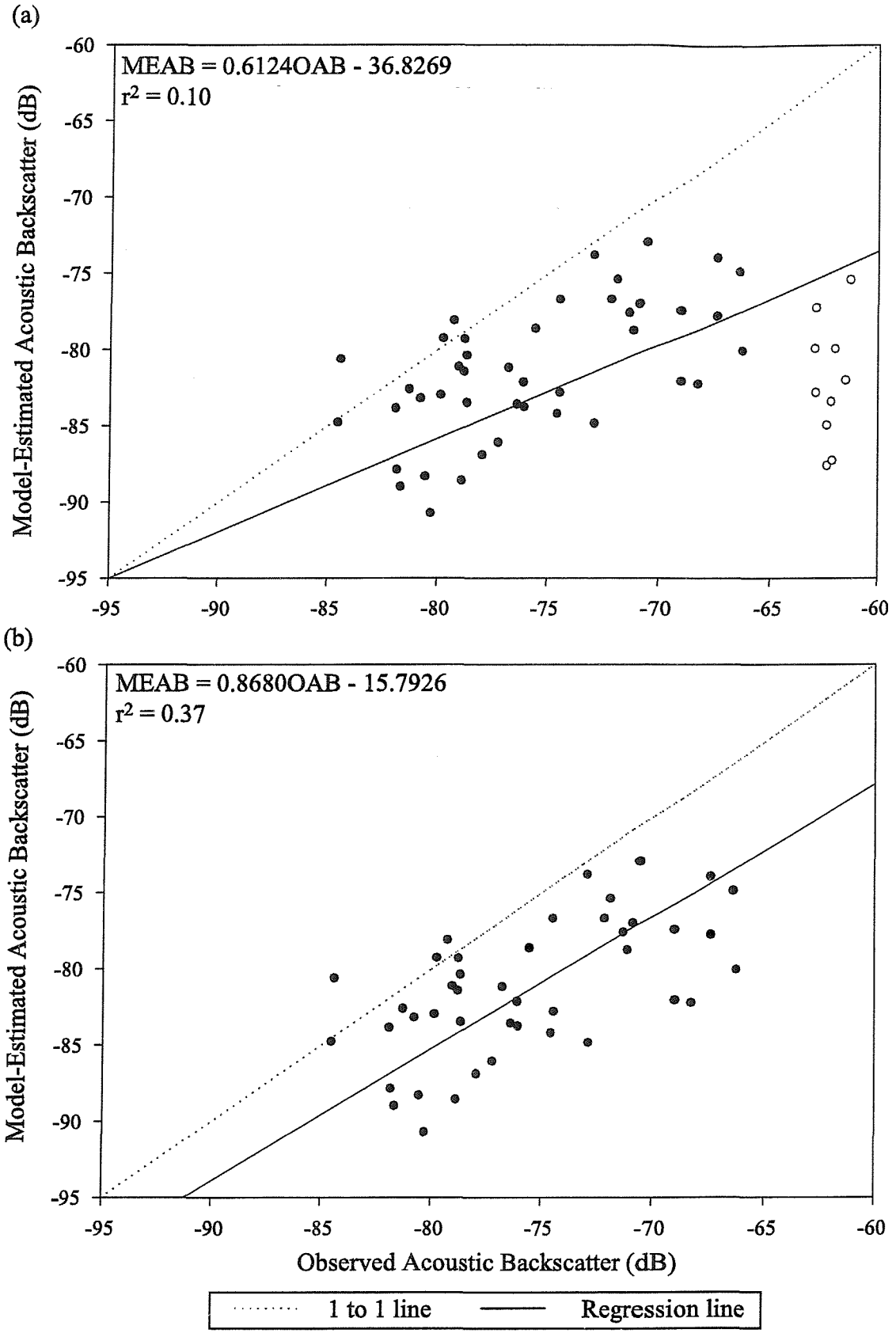

Figure 5.3.10 Model-estimated acoustic backscatter (MEAB) plotted against VM-ADCP observed acoustic backscatter, (a) all samples and (b) samples above 250 m. LHPR samples collected below 250 m are represented by the unfilled symbols.

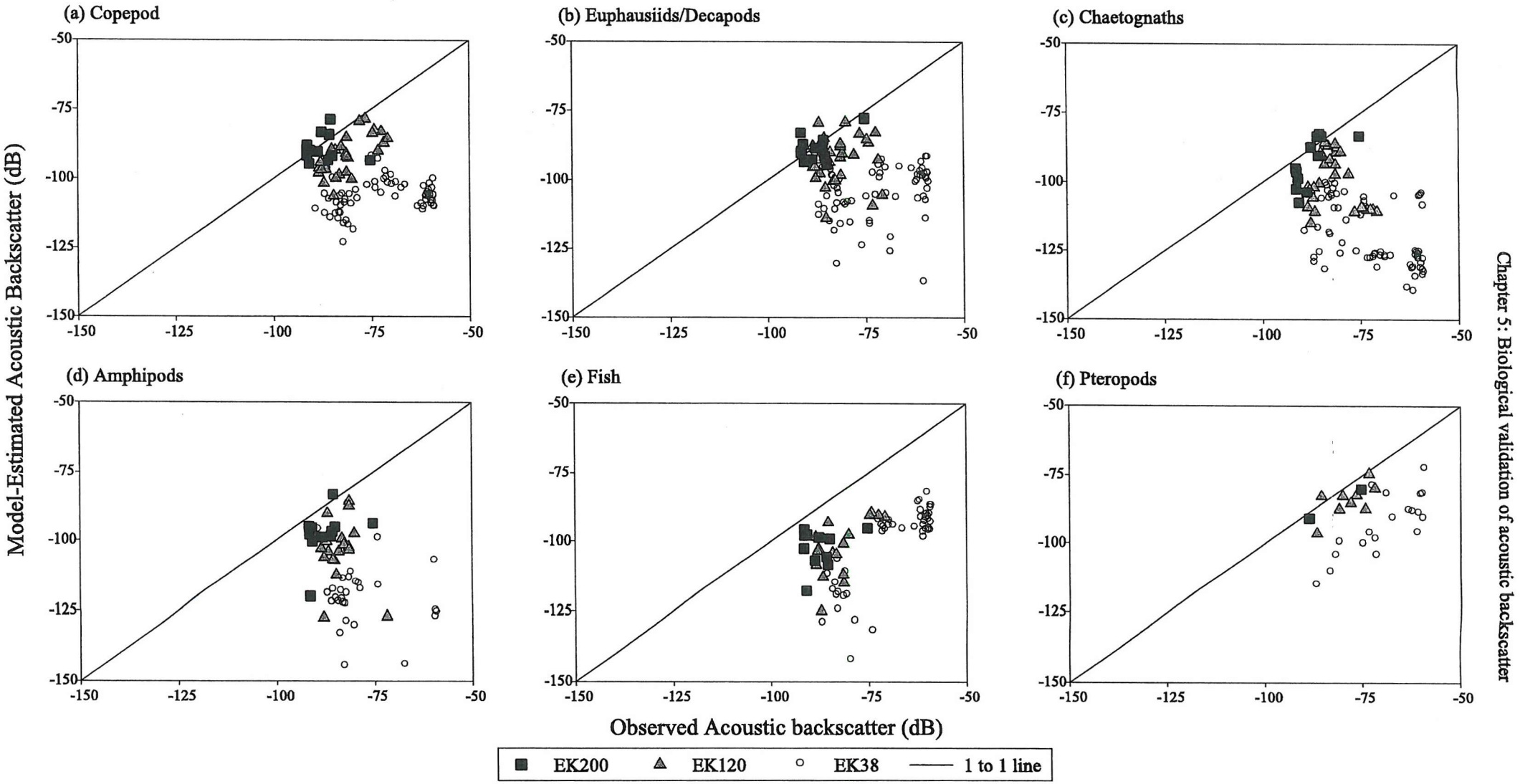

Figure 5.3.11 Model-estimated acoustic backscatter plotted against observed EK500 200, 120 and 38 kHz acoustic backscatter for (a) Copepods, (b) Euphausiids and Decapods, (c) Amphipods, (d) Chaetognaths, (e) Fish and (f) Pteropods.

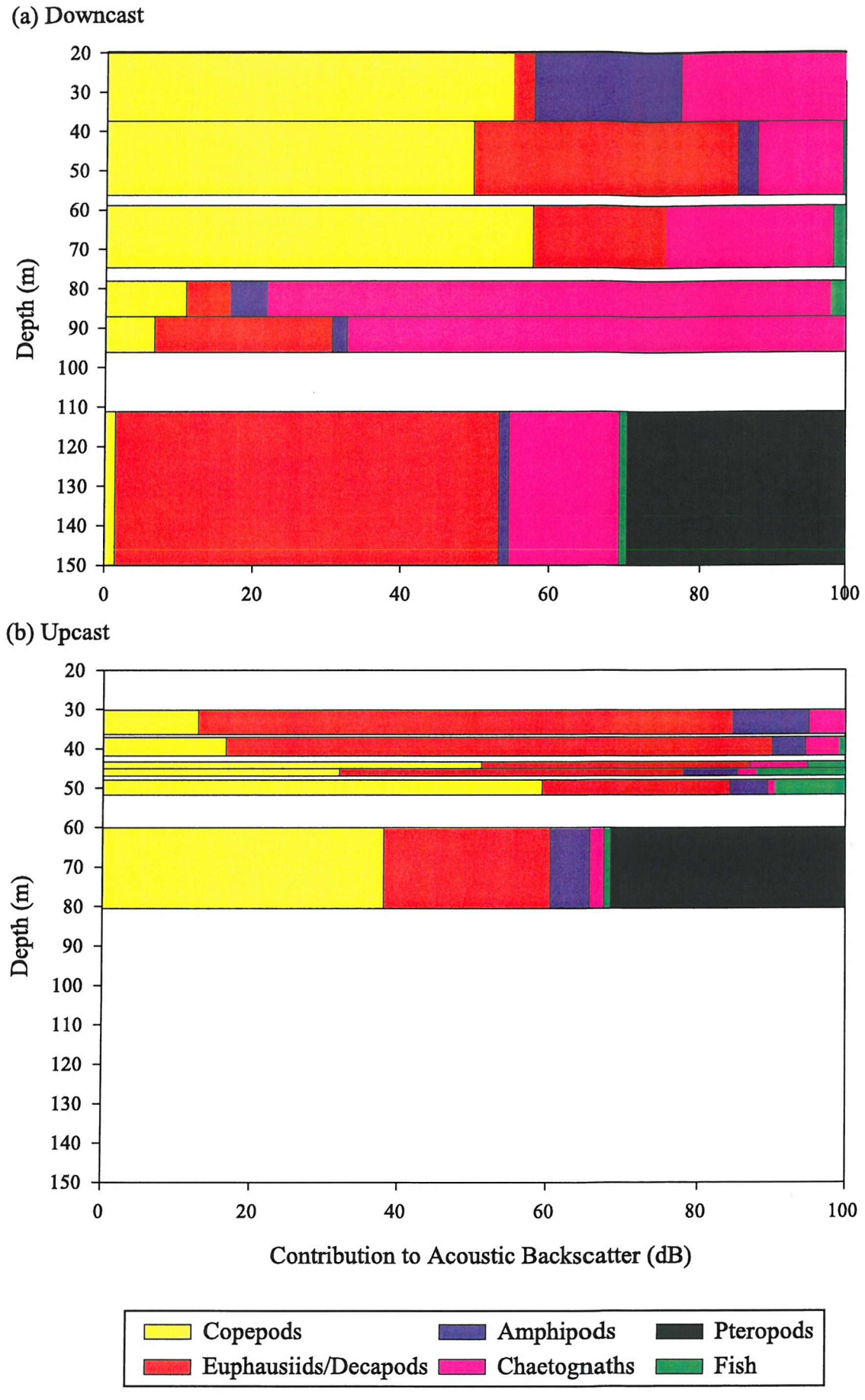

Figure 5.3.12a The percentage contribution of each significant acoustic scattering group to the total model-estimated 200 kHz acoustic backscatter for the (a) downcast and (b) upcast of LHPR Station 13048.

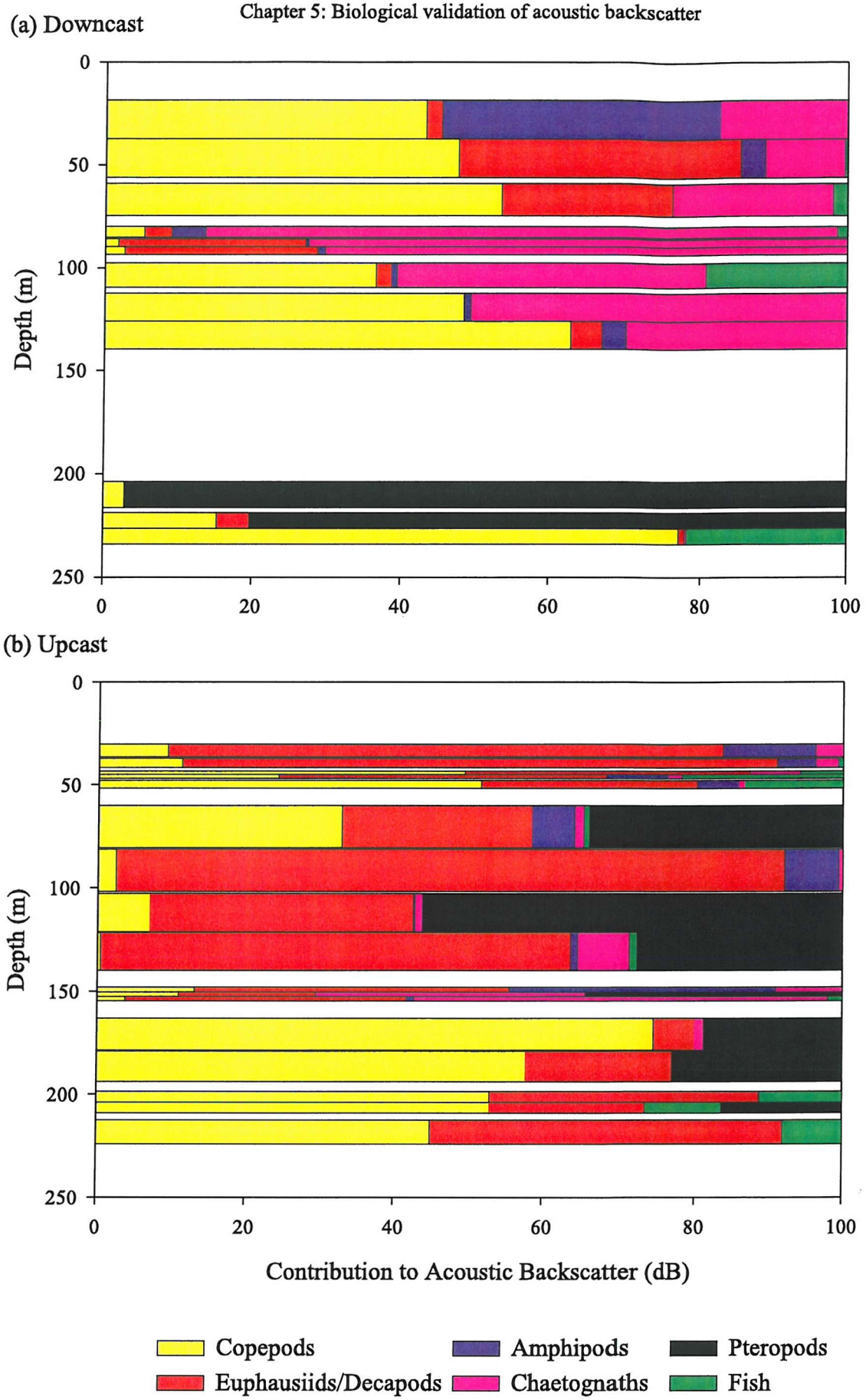

Figure 5.3.12b The percentage contribution of each significant acoustic scattering group to the total model-estimated 120 kHz acoustic backscatter for the (a) downcast and (b) upcast of LHPR Station 13048.

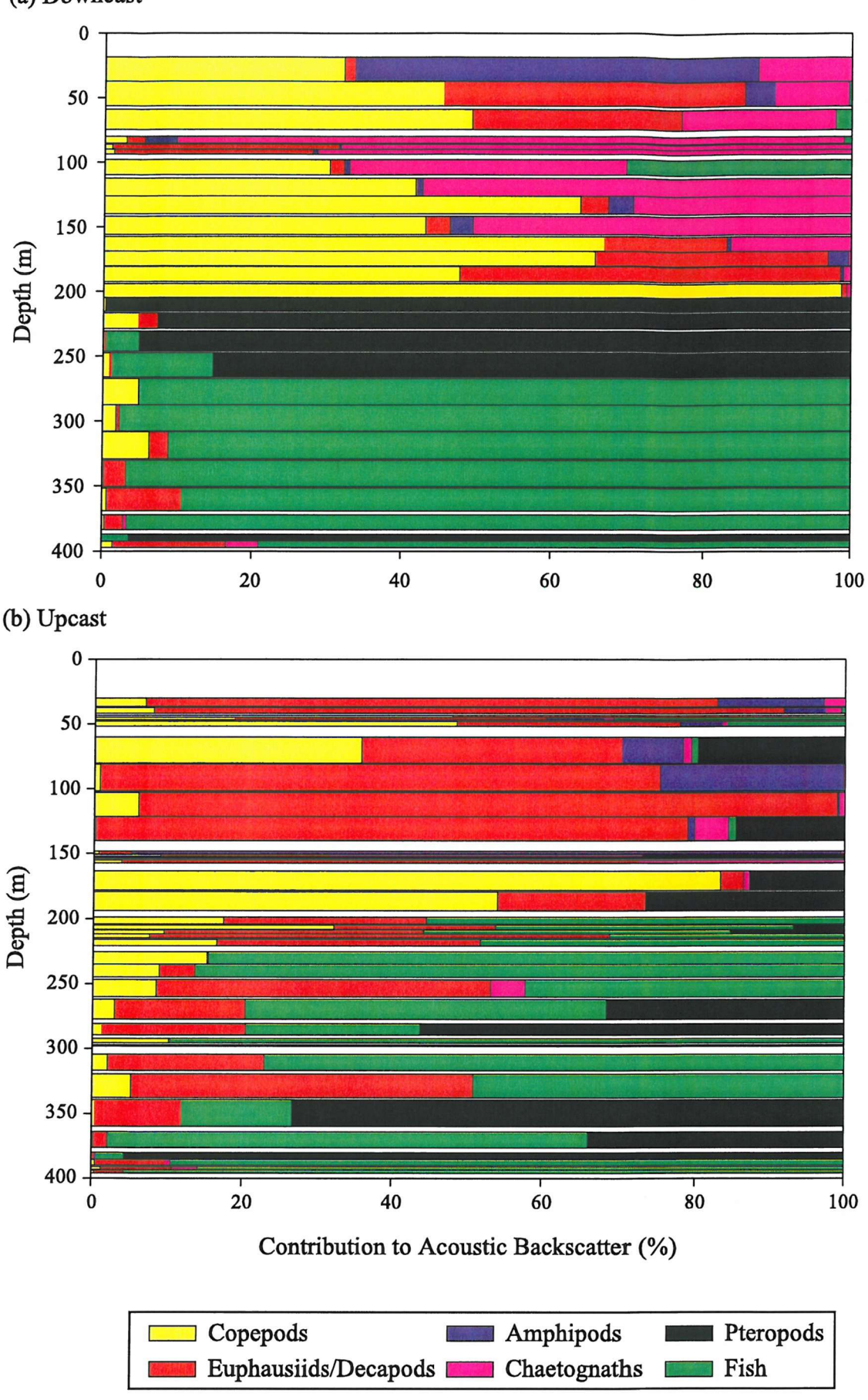

Figure 5.3.12c The percentage contribution of each significant acoustic scattering group to the total model-estimated 38 kHz acoustic backscatter for the (a) downcast and (b) upcast of LHPR Station 13048.

VM-ADCP, from 20-80 m depth the contribution from copepods dominated (~50 %) the TMEAB, below this it changed to a thin layer of chaetognath-dominated samples. From 100 m the percentage contributions of each group diversifies between the frequencies. At 200 kHz euphausiids (50 %) and pteropods (30 %) dominate the TMEAB, whereas at 120 and 38 kHz copepods (35-65 %) and chaetognaths (30-60 %) dominate. In a layer of ~50 m, just below 200 m depth, the TMEAB estimated at 150 (VM-ADCP), 120 and 38 kHz was dominated by pteropods. Below this, in Levantine Intermediate Water (LIW), fish became the main contributors to the TMEAB (note, only the 38 kHz frequency reached these depths). In the upcast, fish or pteropods dominated the TMEAB up to a depth of two hundred metres in the 38 kHz dataset. Whereas, comparable with the VM-ADCP data, copepods, euphausiids and pteropods played a major role in the 120 kHz TMEAB. Above 150 m, the percentage contributions of each significant acoustic scattering group at each frequency became similar again and from this depth to the surface, in waters of Atlantic origin (AOW), the TMEAB was comprised of euphausiids, copepods and pteropods. Amphipods also contributed noticeably to the TMEAB in the upcast, which was not seen in the downcast samples.

TMEAB plotted against observed acoustic backscatter for each frequency is presented in Figure 5.3.13. Following the pattern identified in Figure 5.3.11, the TMEAB calculated at 200 kHz was overestimated compared with the acoustic backscatter, the 120 kHz was typically within 5 dB and the 38 kHz was under estimated. The equations of the functional regression lines fit to the log-transformed data, the fit of the data to the line (r^2) and the result of the t-test testing whether the slope of the line differs from the expected slope of one are presented in Table 5.3.8. Data collected at 200 kHz showed the best correlation with observed acoustic backscatter ($r^2 = 0.65$) compared with the 120 and 38 kHz data ($r^2 = 0.49$ and 0.48 respectively). However, the 120 kHz data were closer to the expected relationship of one to one than the 200 kHz, though in both cases the slopes were not significantly different from the expected slope (t-test, $P>0.05$). The 38 kHz data exhibited the poorest correlation and the slope of the regression was significantly different from the expected (t-test, $P>0.05$).

The EK500 the transducers are vertically downward-looking, hence there is no reason to correct for angle of orientation errors as associated with the VM-ADCP data (e.g. the euphausiids contribution) However, as observed in Figure 5.3.12, fish are important contributors to the TMEAB (especially at depth). As commented earlier (Section 5.3.2.1), some of these fish have gas bladders that are not incorporated into the

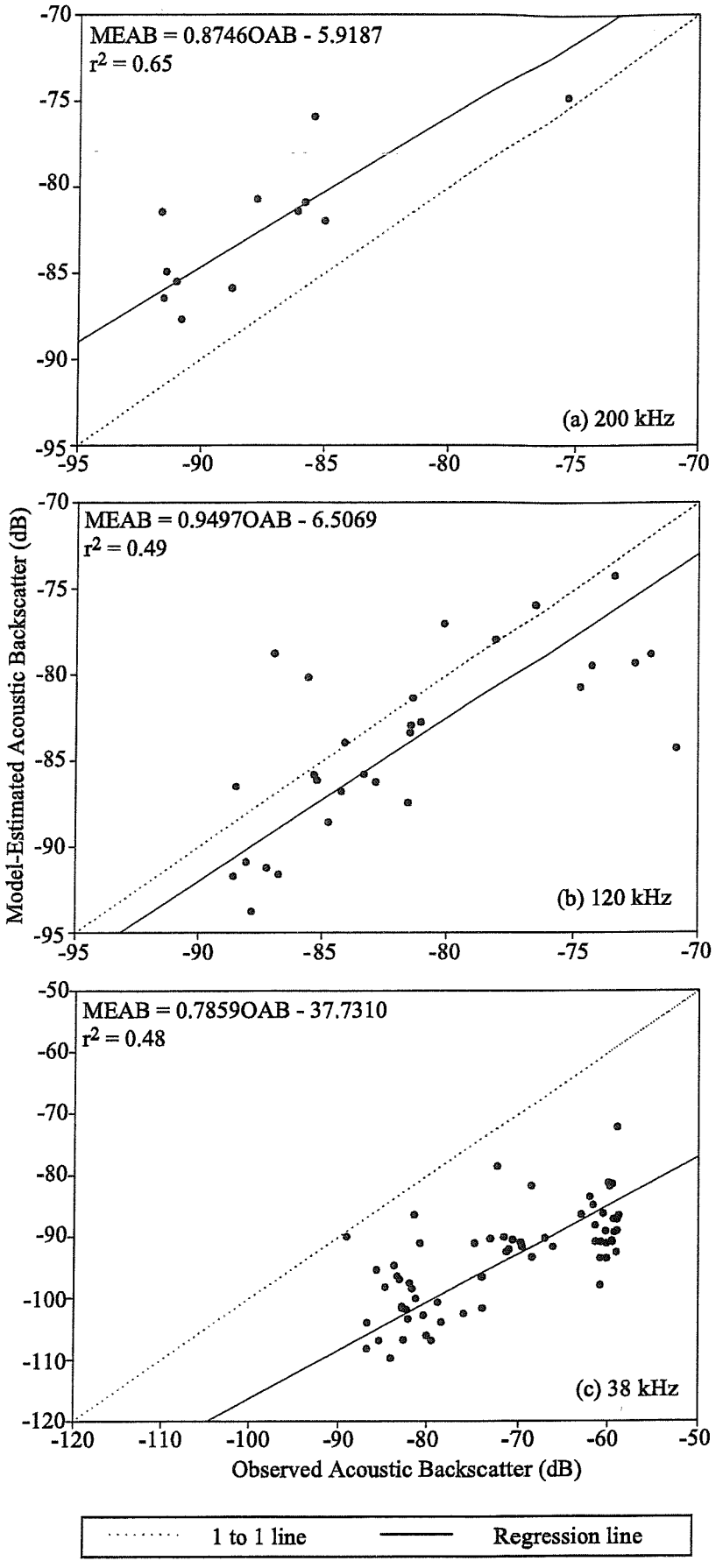

Figure 5.3.13 Model-estimated acoustic backscatter (MEAB) plotted against observed EK500 (a) 200 kHz, (b) 120 kHz and (c) 38 kHz acoustic backscatter (OAB).

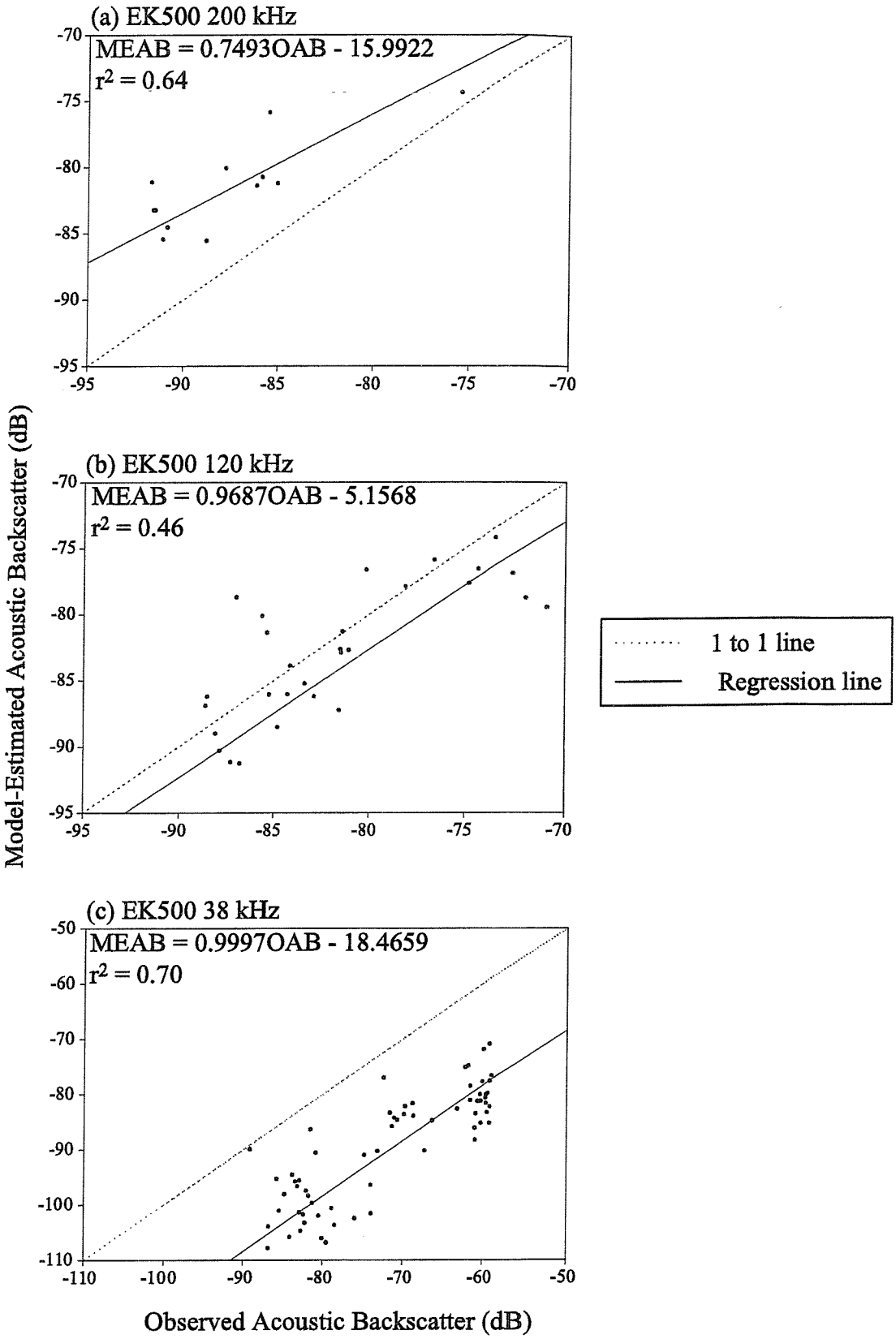

Figure 5.3.14 Model-estimated acoustic backscatter (MEAB) (corrected for omission of gas bladder) plotted against observed EK500 (a) 200 kHz, (b) 120 kHz and (c) 38 kHz acoustic backscatter (OAB)

acoustic models. This inaccuracy may cause the poor correlation identified in the 38 kHz data and was emphasised by the deeper transmission of the 38 kHz frequency which collected more samples in the fish rich LIW. Therefore a greater number of the samples at 38 kHz would have biased TMEAB caused by inaccuracies in the fish model. A correction of 10 dB was added to the model-estimated fish contribution and the relationship between model-estimated and observed acoustic backscatter re-examined (Figure 5.3.14). A summary of the functional regression lines fit to the log-transformed data is presented in Table 5.3.8. The correction reduced the relationship between TMEAB and OAB at 200 kHz, although the slope was still not significantly different from the expected. This is possibly because the sample size (n = 15) and the standard error of the regression line (S.E. = 0.1429) were too low to create a significant result. The relationship between TMEAB and OAB of the 38 and 120 kHz data was improved, with the slope of the regression line of the 38 kHz data no longer significantly different from the expected slope. In addition the correlation between TMEAB and OAB was notably improved from 48 % of the data fitting the regression line to 70 %.

Where the slope of the regression line is roughly equal to the expected ($v \approx 1$), the intercept provides an indication of the error of the models. For example, the error of the models at 120 kHz results in an offset of –5 dB, whilst TMEAB at 38 kHz has an intercept of –18 dB (Table 5.3.8). This provides an example of a situation where the statistical test implies that the models provide a suitable TMEAB, whereas the estimate is actually a factor of 6 different (remembering that an increase of 3 dB is equal to a doubling in the acoustic signal).

The water mass from which the LHPR sample was taken was identified. Figure 5.3.15 shows that the model and acoustic data cluster depending from which water mass the sample was drawn. Samples from Levantine Intermediate Water (LIW) typically had the highest OAB and in EK500 data the highest TMEAB. TML water had the second highest OAB and TMEAB, notably both these water masses had numerous samples containing myctophid fish. Water of Atlantic origin (AOW) characteristically had the lowest OAB and TMEAB. Between the AOW, TML and LIW clusters were samples from mixed Mediterranean and Atlantic water (MMAW) and water of Mediterranean origin (MOW), these water masses are typically found within the front (Chapter 4).

5.3.3.3 Discussion of model estimations

The results presented in this section show that the relationship between acoustic backscatter and zooplankton abundance/biomass is not simple. Through analysis of the

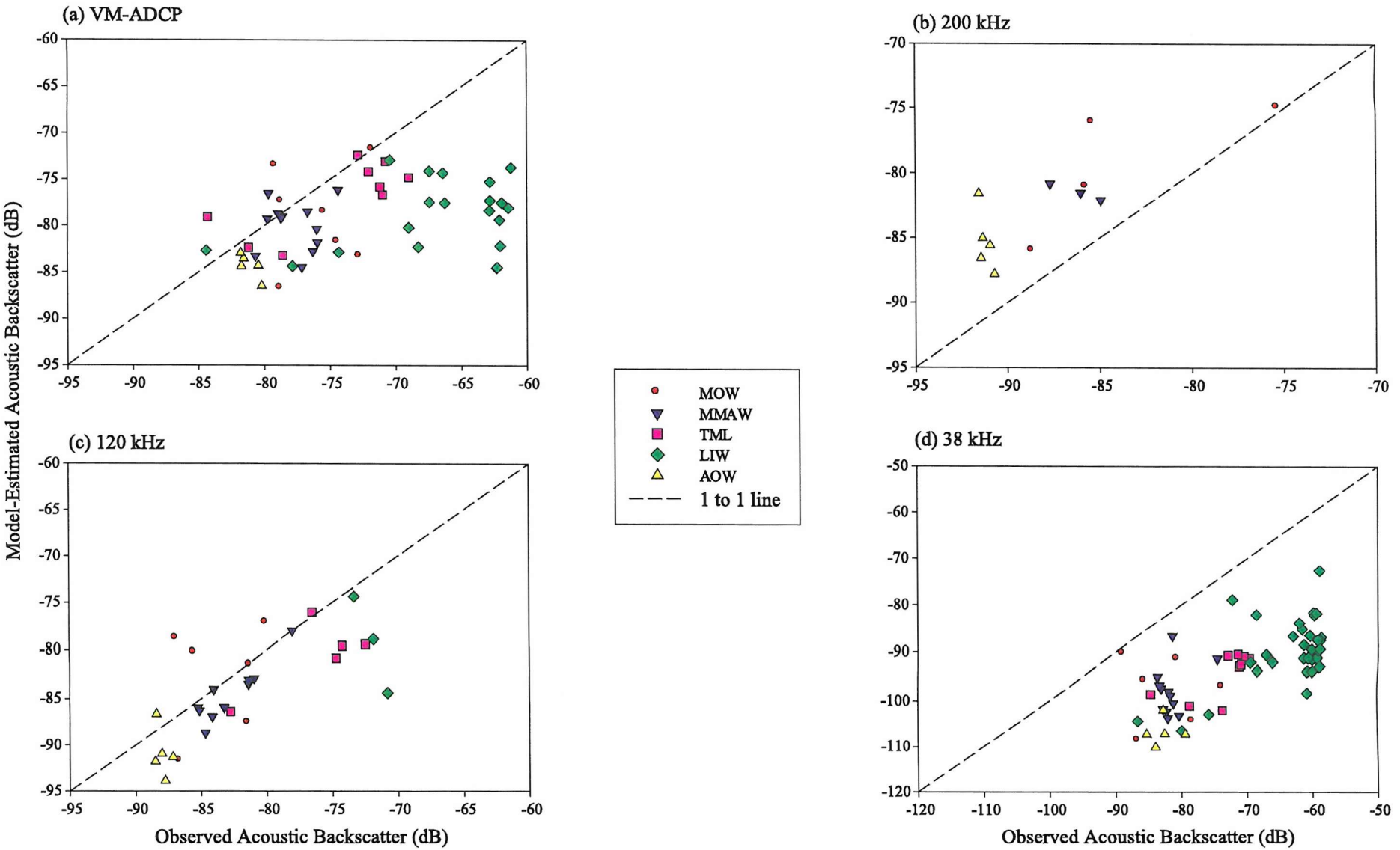

Figure 5.3.15 Model-estimated acoustic backscatter plotted against observed (a) VM-ADCP, (b) EK500 200 kHz, (c) EK500 120 kHz and (d) EK500 38 kHz acoustic backscatter. The water mass from which the LHPR sample was taken is identified.

percentage contributions of individual zooplankton taxa to the TMEAB it can be seen that within one region the dominant acoustic-scattering zooplankton group can vary both horizontally and vertically. Two features are evident from the acoustic scattering contribution. First, following previous studies when pteropods are present they typically dominate the TMEAB (Wiebe *et al.*, 1996), even though the numbers of pteropods encountered here are, on average, a factor of 10 less than those in the study by Wiebe *et al.*. This is not unexpected as pteropods have hard shells and, on a per-unit-biomass basis, are orders of magnitude stronger acoustic scatterers (at the frequencies used here) than other zooplankton types (See Table 1 in Stanton *et al.*, 1994a). Second, different zooplankton groups dominate the TMEAB at different frequencies. This is most likely a function of size, where smaller-sized zooplankton dominated the highest frequency but not the lower frequencies. For example, below 100 m the 200 kHz frequency TMEAB was dominated by euphausiids (of ~2 mm length), whereas the 120 and 38 kHz TMEAB were dominated by chaetognaths (of ~12 mm length). An aspect of this feature is also evident between the 150 kHz VM-ADCP and 38 kHz data. Where, below 250 m, copepods and euphausiids dominate the VM-ADCP TMEAB, whilst fish contribute the most to the TMEAB in 38 kHz data. This is very important with respect to the relationship between OAB and TMEAB at 38 kHz, because this frequency is particularly sensitive to resonant scattering from gas bladders (Medwin and Clay, 1998). Hence any underestimate in the scattering models will dominate the 38 kHz TMEAB, as was shown in the above dataset where a 10 dB correction applied to the fish model estimate significantly improved the relationship between OAB and TMEAB.

The data presented in this study show that under certain conditions acoustic scattering models can be used to explain the relationship between zooplankton and VM-ADCP OAB. In this case when samples from below 250 m (within the fish-rich LIW) were ignored the relationship between TMEAB and VM-ADCP OAB compared favourably with that found by Wiebe *et al.* (1996) and Greene *et al.* (1998). In fact the slope of the regression line (0.87 to 2.d.p) was closer to the expected slope of one compared with the study of Greene *et al.* (0.77; estimated from Figure 9, Greene *et al.*, 1998), although the correlation was poorer. This was contrary to Zhou *et al.* (1994) where, using a VM-ADCP and an acoustic scattering model to estimate acoustic backscatter from a single species population of *Euphausia superba*, they described a relationship significantly different from the expected ($v \neq 1$, $P>0.05$), but with good linear correlation ($r^2 = 0.77$).

The relationship between TMEAB and OAB is close to the expected when using a purpose-built biological echosounder. The results from this study show that the acoustic backscattering data collected with a SIMRAD EK500 are generally consistent with the forward-problem predictions when using an appropriate frequency. This is particularly true when using the 200 and 120 kHz frequency associated with 333 μm mesh LHPR collected zooplankton samples. As both the EK500 and VM-ADCP acoustic data were collected contemporaneously with the LHPR haul these results suggest that a commercial echosounder acoustic backscattering is better suited to ground-truthing than an VM-ADCP. However it should be noted that it was possible with a VM-ADCP.

The results from this study also provide situations in which inconsistencies between the observed and model estimated acoustic backscatter indicate potential model, instrumental and methodological problems.

Model

It is suspected that the model used to describe the acoustic scattering contribution from the fish group was inadequate. Specifically, data collected using the 38 kHz frequency suggests that the modelled acoustic backscatter contribution from fish was underestimated. Since it is known that gas bladders resonate at 38 kHz (Medwin and Clay, 1998) and that the presence of Myctophid fish (that bear gas bladders) at a depth comparable with SSL1 in the Mediterranean Sea is documented (Baussant *et al.*, 1993; Chapter 4). It is expected that results would significantly improve if a model capable of describing acoustic scattering from a fish containing a gas bladder was used (this is ongoing research with Ben Reeder of WHOI). Other inaccuracies within the models may be caused by variations in the variables used to calculate the reflection coefficient (see Section 5.2.3.2).

Instrumental

As in Section 5.2.3.2, the uncertainty of the reliability of acoustic measurements made with an VM-ADCP in regions of low or irregularly distributed targets should be considered. The VM-ADCP acoustic data from the Mediterranean were all > -85 dB, and as such could be deemed to be taken from a region of many or evenly distributed targets. On removal of data points assumed to have been modelled incorrectly the relationship between OAB and TMEAB was not significantly different from the expected of one to one (t-test, $P>0.05$). However the results presented in this study do show, through less scatter in the relationship of OAB with TMEAB in data from the EK500 than data from the VM-ADCP (r^2 = 0.65, 0.49, 0.48 compared with 0.1), that a greater correlation between zooplankton and acoustic backscatter exists with data collected with a biological

echosounder. As summarised in Section 5.2.3.2, the greater scatter associated with the VM-ADCP data may be attributed to averaging over four beams instead of using just the one and, agreeing with Brierley *et al.* (1998b) this problem is magnified with depth.

Methodological

The error associated with mismatching between the acoustic frequency used and the target size of zooplankton caught is demonstrated in the present study. The same zooplankton samples were used to compare TMEAB with acoustic backscatter data from frequencies with target sizes of ~0.75 mm (200 kHz), ~1 cm (120 kHz) and ~4 cm (38 kHz). Since the LHPR, with a net diameter of 45 cm, rarely catches zooplankton and fish greater than a few cms, it is tenuous to compare the zooplankton caught with acoustic data from the 38 kHz. Especially when considering that in the calculation of the models many of the zooplankton caught would fall into the size range corresponding to the Rayleigh scattering region, where target strength falls rapidly as a function of size (calculated through extrapolating from the target strength vs length relationships given by Greene *et al.* (1991) at different frequencies). Hence, the 38 kHz modelled acoustic backscatter was underestimated, whereas the better approximations at the 200 and 120 kHz frequencies resulted from having target sizes more comparable with the size of zooplankton caught (Section 5.3.2.2).

Continuing with the theme of matching sampling instruments, the discrepancy between the volume of water sampled by the acoustic instrument and the net has been commented on in Section 5.3.2.2. Acoustic backscatter data collected using an EK500 are not immune to these inaccuracies. The volume sampled by the EK500 is comparable with the VM-ADCP (as a result of its larger beam angle, 7° compared with 2.5°), and as such is approximately four orders of magnitude greater than that sampled by the LHPR. This problem may have caused the greater scatter observed in these data sets when compared with previous results. Both Wiebe *et al.* (1996) and Greene *et al.* (1998) present results from studies with shallow net hauls (0-80 m)

5.4 Conclusions

The results presented in this chapter are part of the on-going quest to define the relationship between acoustic backscatter and zooplankton. The methods covered include a direct comparison (following Flagg and Smith, 1989a; Heywood *et al.*, 1991), simple manipulation of the zooplankton data to resemble target strength (following Flagg and Smith, 1989b), through to the use of modern acoustic scattering models (Stanton *et al.*, 1998a,b,c).

Through comparing zooplankton biovolume and acoustic backscatter directly it is possible to conclude that they are related, although the relationship is more complex than simple increases in biovolume resulting in higher acoustic intensities. This has resulted in the investigation of what many authors have termed "the forward problem" (Holliday and Pieper, 1995; Griffiths *et al.*, 2002). The forward problem approach of comparing acoustic backscatter observed *in situ* with those predicted from a combination of net-sampled data and acoustic scattering models has been applied in zooplankton studies only recently and rarely (Zhou *et* al., 1994; Wiebe *et al.*, 1996; Greene *et al.*, 1998). This study presents the first results using VM-ADCP and multifrequency acoustic backscatter with model estimates using open ocean mixed zooplankton populations. It should be noted that solving the forward problem does not lead directly to the goal of acoustic determination of animal populations, rather resolution of it can provide valuable diagnostic information. These include: 1) determining the consistencies between observed acoustic backscatter and the net sampled data, assuming that the models are correct and the nets used are appropriate in terms of zooplankton size sampled; 2) determining the relative contributions of each "significant" acoustic scattering group to the TMEAB; 3) the potential to detect when the acoustic scattering models are inadequate and 4) permitting the detection of inadequate acoustic or net sampling.

However, it is necessary to remember that zooplankton are not the only particles within the open ocean from which we get an acoustic signal, and alternative sources such as turbulence (Stanton *et al.*, 1994b), bubbles (Thorpe and Hall, 1987) and non-living particles (Wiebe *et al.*, 1997) must be considered.

5.5. Summary

1) VM-ADCP observed acoustic backscatter was found to be related to net caught zooplankton biovolume, but the correlation was low leaving most of the variability in the acoustical data unaccounted for.
2) The calculation of model-estimated acoustic backscatter from several zooplankton groups showed that the contribution to total abundance, biovolume and TMEAB vary disproportionately.
3) Taxon-specific models can be used to improve the relationship between observed acoustic backscatter and known zooplankton distributions.
4) It is essential to match the acoustic frequency used to the size of zooplankton caught (and hence the net used).

5) More than one set of model parameter values are needed to predict volume backscattering accurately, and more information about the scattering properties of the zooplankton particular to the study region are needed to transform acoustic backscatter into meaningful biological variables.

Chapter 6

Summary, data limitations and future directions

6.1 Introduction

The data presented in this thesis provide observations on the distribution of zooplankton from two contrasting regions, the Arabian Sea (North Indian Ocean) and the Alboran Sea (western Mediterranean Sea). From analysis of acoustic backscatter data and net samples, coupled with concurrent hydrographic measurements, two major features were identified as dominant forcing mechanisms on distribution. In the Arabian Sea, the vertical distribution of zooplankton was predominantly controlled by the oxygen minimum zone, whilst in the Alboran Sea the frontal structure affected both the distribution and behaviour of zooplankton. This study demonstrates that acoustic methods for studying zooplankton, combined with ground-truthing net data and hydrographic data, provide a powerful tool for observing zooplankton distributions on time and space scales comparable with physical variability.

6.2 The Arabian Sea

6.2.1 Summary

The vertical structure of the water column at the Arabesque Reference Site in the Arabian Sea was dominated by a strong oxygen minimum zone that persisted from a depth of ~50 m to ~1100 m depth. This oxygen minimum layer appeared to be the most important factor influencing the vertical distribution of zooplankton.

A substantial proportion of the zooplankton residing in the upper 250 m of the water column occurred above the oxycline within the oxygenated, well-lit surface waters. VM-ADCP acoustic backscatter measurements and net data indicate that some zooplankton and some micronekton (euphausiids, decapods and fish) were undertaking diel vertical migration into and out-of the OMZ, between the surface and daytime depths of 300-400 m. Daytime acoustic backscatter returns from deep daytime layers were strong, and dawn-downward and dusk-upward movements were obvious. At night the biomass remaining below the oxycline was so low that no acoustic signal, as a result of insufficient targets, could be discerned.

Maximum biovolumes and a peak in the acoustic signal were observed at the depth of the thermocline. A dominant proportion of the zooplankton population, especially in surface waters were copepods, and their distribution appeared to be limited to depths above truly suboxic waters (oxygen concentration <0.5 μmol l^{-1}). Contrary to all other taxa observed, the distribution of polychaetes appeared to be independent of the oxygen minimum zone and it is suggested that, like benthic polychaetes, this group are possibly the best adapted to low oxygen environments.

6.2.2 Data limitations

The data presented in Chapter 3 show a limited snap-shot of the distribution of zooplankton in relation to the oxygen minimum during the SW monsoon in 1994. It is not necessarily representative of the distribution of zooplankton at other periods (i.e. the NE monsoon or other years), as inter-annual and seasonal variations in the abundance of zooplankton have been widely documented (e.g. Smith *et al.*, 1998). It does however provide evidence of a dominant feature affecting the distribution of zooplankton.

Oxygen concentration is not the only factor influencing the distribution of zooplankton in the Arabian Sea (see Chapter 3). The Arabian Sea is a site of intense upwelling and mesoscale activity that together have a large impact on the distribution of both phytoplankton and zooplankton (Flagg and Kim, 1998; Smith *et al.*, 1998; Barber *et al.*, 2001). The dataset presented in this thesis was limited to observations of oxygen concentration and zooplankton distribution at a single station. Nevertheless sufficient data were obtained to show the effects of oxygen on the distribution of the zooplankton in the area. A complete study would require considerably more data. For example, measurements of physical circulation, phytoplankton species, biomass and productivity and zooplankton species, biomass, feeding and productivity (e.g. Edwards *et al.*, 1999; Stelfox *et al.*, 1999; Roman *et al.*, 2000; Barber *et al.*, 2001).

Sampling limitations

The time delay between the two LHPR samples complicated the interpretation of diurnal variations in the distribution of zooplankton. During the six day period between the two casts it is highly likely that the zooplankton populations sampled in the first cast will have advected away from the Arabesque Reference site. Hence, although inferences of diurnal migrations can be made, a certain degree of caution is required in the interpretation of these results.

6.2.3 Future directions

There is now a considerable amount of data describing the affects of water column structure on zooplankton distributions in the Arabian Sea (e.g. Vinogradov and Vorinina, 1961; Herring *et al.*, 1998; Ashjian *et al.*, 2002). What is much less known is the physiological basis of the ability to remain within the oxygen minimum zone. The Indian Ocean offers great potential for the study of adaptations to life within low oxygen environments.

6.3 The Alboran Sea

6.3.1 Summary

The Almeria-Oran front forms where surface waters of Atlantic and Mediterranean origin meet at the eastern end of the Alboran Sea. This front affected the distribution of both phytoplankton and zooplankton.

Mediterranean Surface Waters were observed to be drawn down and along the Almeria-Oran front. Observations of a layer of fluorescence coincident with the subducted surface waters indicated that phytoplankton were also drawn down and along isopycnals, by cross-front ageostrophic motion, to depths of ~200 m. Periodic vertical velocities of ~20 m d^{-1}, associated with the propagation of wave-like meanders along the front, have a significant effect on the vertical distribution of zooplankton across the front despite their ability to migrate at greater speeds. From the study of sound scattering layers (SSL) identified in acoustic backscatter data and analysis of LHPR net samples, a layer of zooplankton (composed of increased numbers of chaetognaths and euphausiids) was found coincident with the drawn-down phytoplankton. This layer persisted during and despite diel vertical migration. Smaller zooplankton identified in high frequency acoustic data and from the LHPR net samples, which did not undertake diel vertical migration, remained concentrated near the surface in the fast-flowing frontal jet (Allen *et al.*, 2001; Fielding *et al.*, 2001).

6.3.2 Data limitations

The Alboran Sea dataset would have benefited from measurements of primary productivity and zooplankton growth and grazing rates. The Almeria-Oran front periodically presents itself as a feature with associated high levels of phytoplankton biomass (depending on whether you look at surface or integrated chlorophyll concentration). However as a result of the dynamic nature of the region, without primary productivity measurements, it is impossible to conclude whether the associated high phytoplankton biomass has been advected into the region or is localised enhancement as a result of upwelling of nutrients resulting from the ageostrophic nature of the front. Without measurements of zooplankton growth this question also applies to the elevated levels of zooplankton abundance associated with the fast flowing frontal jet, that are hypothesised to result from localised enhancement of secondary production.

Sampling limitations

The fundamental goal for the LHPR samples was to collect zooplankton samples for comparison with acoustic backscatter data. For that reason the LHPR was not towed in the ideal fashion for interpreting zooplankton distributions. The high speed (>4 knots) nature of the tows, in order to catch significant acoustic scatterers such as euphausiids, often squashed the zooplankton precluding identification beyond group level. Zooplankton

counts were often represented by the number of heads (particularly with respect to euphausiids and chaetognaths which often became entangled on the gauze).

In addition, in order to sample the surface 400 m of the water column, the LHPR was towed in a v-shaped profile across the front. As a result a large proportion of surface data across the front was absent. This lack of surface data across the front prevents a thorough understanding of the affect of the Almeria-Oran front on the distribution of zooplankton. For a repeat study of this region it is suggested that the LHPR be towed in a shallower profile across the front as well as the deep profile and to wider extremes within the Eastern Alboran Gyre and within Mediterranean waters.

6.3.3 Future directions

The observations presented in this investigation represent a quasi-synoptic survey of the Almeria-Oran front region during November-December 1996. But how representative is this one-time section of the Almeria-Oran front? Even within this study the physical and biological environment was observed to change on a time scale of days and space scales of kilometres. During the project ALMOFRONT 1 the Eastern Alboran Gyre was not even present, let alone presenting the Almeria-Oran Front at its eastern margin. The dynamic nature of this region, suggests that as well as ship-borne investigations it would benefit from long-term mooring systems, with the capacity to measure biological and physical features of the water column, and satellite remote sensing.

6.4 Biological validation of acoustic backscatter

6.4.1 Summary

A major goal for biological oceanographers is to understand the processes regulating the distribution and abundance of organisms within the sea. Significant in-roads to achieving this goal have been achieved with the development of acoustic sensing techniques (Holliday and Pieper, 1995; Horne, 1998; Foote and Stanton, 2000). Acoustic techniques require ground-truthing and development of appropriate models that can transform the acoustic data into biological information.

The study presented here describes an attempt to ground-truth acoustic data with net-sampled data. Following the method of Flagg and Smith (1989b) the data indicate that, as with previous studies (Costello *et al.*, 1989; Flagg and Smith, 1989b; Holliday *et al.*, 1989), acoustic backscatter is related to zooplankton abundance and biomass. However, the relationship is far more complex than that provided by basic manipulation and linear regression analysis. It is recommended that, without further manipulation and interpretation using validated acoustic scattering models, the acoustic data are used to

provide qualitative rather than quantitative comments on the distribution of zooplankton - as is indeed the case with most acoustic/zooplankton studies (e.g. Roe *et al.*, 1996).

The forward-problem approach used here, of comparing acoustic volume backscattering observed *in situ*, with acoustic backscatter estimated from net-sampled data using acoustic scattering models, has been applied in zooplankton studies only recently (Wiebe *et al.*, 1996; Greene *et al.*, 1998) and for the first time in the present study with a VM-ADCP on a multi-specific population. The results from this study provide a convincing demonstration that the observed *in situ* acoustic backscatter data collected are generally consistent with the forward-problem predictions.

6.4.2 Data limitations and future directions

Mismatch between the acoustic and net samples

Spatial and temporal differences in the position of the net relative to the ship (from which the acoustic data were collected) and the vast discrepancies between the sampling volumes under scrutiny potentially make fitting of the datasets unreliable. By mounting the acoustic instrument directly onto the zooplankton-sampling instrument (be it a net or video plankton recorder) these problems are by-passed. However, by deploying the sonar system on the zooplankton sampler (e.g. Greene *et al.*, 1998; Jaffe *et al.*, 1998) the key advantage of acoustic remote sensing – the ability to survey a relatively large area rapidly – is sacrificed. Therefore it is recommended that this *in situ* method be used to supplement ground-truthing of the acoustic data, but not as an instrument designed for rapid spatial coverage critical to acoustic survey work.

An additional concern when comparing acoustic and net data is the necessity to match the size of animal caught or "seen" with the respective instruments. An example of a mismatch between the size of zooplankton caught and the size of animal "seen" by the acoustic signal was given in this study. The LHPR was not an ideal instrument to catch zooplankton and micronekton of a size comparable with the target size of the EK500 38 kHz frequency, and as a result the relationship between the model estimated and observed acoustic backscatter was characterised by a large offset.

Orientation of zooplankton

As shown in previous laboratory analyses (Sameoto, 1980; Chu *et al.*, 1993; McGeehee *et al.*, 1998) and inferred from this study, the orientation of zooplankton plays an important part in the intensity of the acoustic return. Little information is available regarding the *in situ* orientation of zooplankton and therefore this unknown variable may cause inaccuracy in the model estimate. As the sophistication of video and still photography increases it is expected that more information on zooplankton orientation will

become available. Additionally, a combination of optical and acoustic sampling methods will provide complimentary information on the abundance and size distribution of zooplankton that will further attempts to ground-truth acoustic data.

It is also possible that acoustics may provide data on orientation. Repeated acoustic observations of a monospecific zooplankton population from several angles, combined with acoustic scattering models could be combined to provide inferences of orientation (Stanton, pers comm.).

Optimisation of the acoustic scattering models

Variables within the acoustic scattering models, particularly g and h (the density and speed of sound contrast between the target and the surrounding fluid) may cause error in calculating the model estimated acoustic backscatter. Both g and h have to be measured empirically and are known to vary not just inter-specifically but intra-specifically with changes in life stage and according to gender (Chu *et al.*, 2000). The Indian Ocean provided an extreme environment where both morphological and physiological changes have been suggested for the organisms living within the oxygen minimum layer. In the future it is recommended that the parameters g and h are more precisely quantified by empirical measurements of live specimens of the zooplankton from the survey region.

Further advances in the complexity of the acoustic scattering models are not discussed here as these are proceeding in concert with improvements in technology such as the Computed Tomography-Scan and computer processing power.

Whilst the sophistication of the acoustic models is increasing, and multi-frequency instruments are becoming more standard as survey tools with a greater range in frequencies (e.g. TUBA, Crisp and Harris, 2000), it is questionable as to whether the forward (and hence inverse) problem will ever be solved because of the complexity of multi-specific zooplankton populations and the way they change in time and space. Current studies (including this one) are still constraining the forward problem, yet the inverse problem of interpreting acoustic data in terms of taxonomic identification is still a long way off. A first step towards this was presented by Pieper *et al.* (2001) using the multifrequency instrument TAPS in combination with only one simple spherical acoustic model to describe the distribution of different-sized zooplankton in the Arabian Sea. They did not corroborate their findings with supplementary zooplankton data. The future of acoustic taxonomic identification may lie in analysing the "shape" of the acoustic return signal, as yet a process only undertaken in laboratory single animal conditions (Traykovski *et al.*, 1998).

References

Aboussouan, A. (1971). Contribution a l'etude des teleosteens recoltes au chalut pelagique en relation avec la D. S. L. durant la periode du 1er novembre 1967 au 31 decembre 1968. *Cahiers oceanographiques* **23**, 85-99.

Allen, J.T. and T.H. Guymer (1997). RRS *Discovery* Cruise 224, Leg 1 27 Nov - 29 Dec 1996. OMEGA Observations and Modelling of Eddy scale Geostrophic and Ageostrophic motion. Physical and biological observations in the eastern Alboran Sea (western Mediterranean). Cruise Report No. 14, Southampton Oceanography Centre, 92pp.

Allen, J.T., M.C. Hartman, D.A. Smeed, S.G. Alderson, H.M. Snaith and J. Smithers (1997). SeaSoar and ADCP acoustic backscatter observations during RRS *Discovery* Cruise 224, 27 Nov 1996 - 17 Jan 1997. Internal Document 24, Southampton Oceanogrphy Centre, 172pp.

Allen, J.T., D.A. Smeed, J. Tintore and S. Ruiz (2001). Mesoscale subduction at the Almeria-Oran front: Part 1. Ageostrophic flow. *Journal of Marine Systems* **2001**, 263-285.

Andersen, V. and J. Sardou (1992). The diel migrations and vertical distributions of zooplankton and micronekton in the Northwestern Mediterranean Sea. 1. Euphuasiids, mysids, decapods and fishes. *Journal of Plankton Research* **14**, 8: 1129-1154.

Anderson, N.R. and B.J. Zahuranec (1977). Oceanic Sound Scattering Prediction. New York, Plenum, 859 pp.

Anderson, V.C. (1950). Sound scattering from a fluid sphere. *Journal of the Acoustical Society of America* **22**, 426-431.

Angel, M.V. (1986). Vertical migrations in the oceanic realm: possible causes and probable effects. In: Migration mechanisms and adaptive significance. M. A. Rankin (ed.), Contributions in Marine Science, Supplement to volume 27, 45-70.

Angel, M.V. (1990). Life in the benthic boundary layer: connections to the mid-water and sea floor. *Philosophical Transactions of the Royal Society of London A* **331**, 1616: 15-28.

Angel, M.V. and M.J.R. Fasham (1983). Eddies and Biological processes. In: Eddies in Marine Science. A. R. Robinson (ed.), New York, Springer-Verlag,

Arnone, R.A. and P.E. La Violette (1986). Satellite definition of the bio-optical and thermal variation of coastal eddies associated with the African Current. *Journal of Geophysical Research* **91**, 2351-2364.

Arnone, R.A., D.A. Wiesenberg and K.D. Saunders (1990). The origin and characteristics of the Algerian Current. *Journal of Geophysical Research* **95**, 1587-1598.

Ashjian, C.J., S.L. Smith, C.N. Flagg and N. Idrisi (2002). Distribution, annual cycle, and vertical migration of acoustically derived biomass in the Arabian Sea during 1994- 1995. *Deep-Sea Research II* **49**, 12: 2377-2402.

Ashjian, C.J., S.L. Smith, C.N. Flagg, A.J. Mariano, W.J. Behrens and P.V.Z. Lane (1994). The Influence of a Gulf-Stream Meander on the Distribution of Zooplankton Biomass in the Slope Water, the Gulf-Stream, and the Sargasso Sea, Described Using a Shipboard Acoustic Doppler Current Profiler. *Deep-Sea Research I* **41**, 1: 23-50.

Ashjian, C.J. and K.F. Wishner (1993). Temporal persistence of copepod species group in the Gulf Stream. *Deep-Sea Research I* **40**, 483-516.

Azam, F., T. Fenchel, J.G. Field, J.S. Gray, L.A. Meyer Reil and F. Thingstad (1983). The ecological role of water column microbes in the sea. *Marine Ecology Progress Series* **10**, 257-263.

Backus, R.H. (1986). Biogeographic boundaries in the open ocean. *Pelagic biogeography, UNESCO Technical Marine Science* **49**, 9-13.

Bainbridge, R. (1957). The size, shape and density of marine phytoplankton concentrations. *Cambridge Philisophical Society Biological Review* **32**, 91-115.

Baird, R.C., D.F. Wilson and D.M. Milliken (1973). Observations on *Bregmaceros nectabanus* Whitley in the anoxic, sulphurous waters of the Cariaco Trench. *Deep-Sea Research I* **20**, 503-504.

Baker, A.d.C., B.P. Boden and E. Brinton (1990). A practical guide to the euphausiids of the world. Natural History Museum Publications, British Museum (Natural History), 96pp.

Baldacci, A., G. Corsini, M. Diani, O. Chic, J. Font, P. Cipollini, T. Forrester, T.H. Guymer and H.M. Snaith (1998). The OMEGA atlas of remotely sensed data. Pisa, Italy, Università degli Studi di Pisa, Dipartimento di Ingegneria dell'Informazione, Via Diotisalvi, 64pp.

Balls, R. (1948). Herring fishing with the echometer. *Journal du Conseil pour l'Exploration de la Mer* **15**, 193-206.

Banse, K. (1964). On the vertical distribution of zooplankton in the sea. *Progress in Oceanography* **2**, 53-125.

Banse, K. (1987). Seasonality of phytoplankton chlorophyll in the central and northern Arabian Sea. *Deep-Sea Research I* **34**, 713-723.

Banse, K. (1994). On the coupling of hydrography, phytoplankton, zooplankton and settling particles offshore in the Arabian Sea. In: Biogeochemistry of the Arabian Sea. D. Lal (ed.), Indian Academy of Sciences, 27-63.

Barber, R.T., J. Marra, R.C. Bidigare, L.A. Codispoti, D. Halpern, Z. Johnson, M. Latasa, R. Goericke and S.L. Smith (2001). Primary productivity and its regulation in the Arabian Sea during 1995. *Deep-Sea Research II* **48**, 6-7: 1127-1172.

Barham, E.G. (1966). Deep scattering layer migration and composition: Observations from a diving saucer. *Science* **140**, 826-828.

Batchelder, H.P., J.R. Vankeuren, R. Vaillancourt and E. Swift (1995). Spatial and Temporal Distributions of Acoustically Estimated Zooplankton Biomass near the Marine Light-Mixed Layers Station (59-Degrees-30'n, 21-Degrees-00'w) in the North-Atlantic in May-1991. *Journal of Geophysical Research-Oceans* **100**, C4: 6549-6563.

Bauer, S., G.L. Hitchcock and D.B. Olson (1991). Influence of monsoonally-forced Ekman dynamics upon surface layer depth and plankton biomass distribution in the Arabian Sea. *Deep-Sea Research I* **38**, 531-553.

Baussant, T., B. Gasser, G. Gorsky and A. Kantidakis (1993). Mesopelagic micronekton and macrozooplankton observed by echosounding, multiple-net sampling and video profiling across the Almeria-Oran front (W Mediterranean Sea). *Annales de l'Institut Oceanographique (Paris)* **69**, 1: 87-93.

Baussant, T., F. Ibanez, S. Dallot and M. Etienne (1992). Diurnal mesoscale patterns of 50 kHz scattering layers across the Ligurian Sea front (NW Mediterranean Sea). *Oceanologica Acta* **15**, 1: 3-12.

Beardall, J., P. Foster, D. Voltolina and G. Savidge (1982). Observations on the surface water characteristics in the western Irish Sea: July 1977. *Estuarine, Coastal and Shelf Science* **14**, 589-598.

Beaulieu, S.E., M.M. Mullin, V.T. Tang, S.M. Pyne, A.L. King and B.S. Twining (1999). Using an optical plankton counter to determine the size distributions of preserved zooplankton samples. *Journal of Plankton Research* **21**, 10: 1939-1956.

Beers, J.R. (1976). Determination of zooplankton biomass. In: Zooplankton fixation and preservation. H. F. Steedman (ed.), Paris, UNESCO Press, 35-84.

Benfield, M.C., C.S. Davis and S.M. Gallager (2000). Estimating the in-situ orientation of *Calanus finmarchicus* on Georges Bank using the Video Plankton Recorder. *Plankton Biology and Ecology* **47**, 1: 69-72.

Benfield, M.C., P.H. Wiebe, T.K. Stanton, C.S. Davis, S.M. Gallager and C.H. Greene (1998). Estimating the spatial distribution of zooplankton biomass by combining Video Plankton Recorder and single-frequecy acoustic data. *Deep-Sea Research II* **45**, 1175-1199.

Benzohra, M. and C. Millot (1995). Characteristics and circulation of the surface and intermediate water masses off Algeria. *Deep-Sea Research I* **42**, 10: 1803-1830.

Bernhard, J.M. and B.K. Sen Gupta (1999). Foraminifera of oxygen depleted environments. In: Modern Foraminifera. B. K. Sen Gupta (ed.), Dordrecht, Kluwer Academic Publishers, 201-216.

Bianchi, M., P. Morin and P. Lecorre (1994). Nitrification Rates, Nitrite and Nitrate Distribution in the Almeria-Oran Frontal Systems (Eastern Alboran Sea). *Journal of Marine Systems* **5**, 3-5: 327-342.

Bottger-Schnack, R. (1994). The microcopepod fauna in the Eastern Mediterranean and Arabian Seas: a comparison with Red Sea fauna. *Hydrobiologia* **292/293**, 271-282.

Bottger-Schnack, R. (1996). Vertical structure of small metazoan plankton, especially non-calanoid copepods. I. Deep Arabian Sea. *Journal of Plankton Research* **18**, 7: 1073-1101.

Boucher, J. (1984). Localization of zooplankton populations in the Ligurian marine front: role of ontogenic migration. *Deep-Sea Research I* **29**, 953-965.

Boucher, J., F. Ibanez and L. Prieur (1987). Daily and seasonal variations in the spatial distribution of zooplankton populations in relation to the physical structure in the Ligurian front. *Journal of Marine Research* **45**, 1: 133-173.

Bowman, M.J. and W.E. Esaias (1978). Oceanic fronts in coastal processes. Berlin, Springer, xii-114 pp.

Boyd, D.M., S.L. Smith and T.J. Cowles (1980). Grazing patterns of copepods in the upwelling system off Peru. *Limnology and Oceanography* **2**, 583-596.

Boysen, E. and F. Buchholz (1984). *Meganyctiphanes norvegica* in the Kattegat. *Marine Biology* **79**, 195-207.

Brierley, A.S., M.A. Brandon and J.L. Watkins (1998b). An assessment of the utility of an acoustic Doppler current profiler for biomass estimation. *Deep-Sea Research I* **45**, 9: 1555-1573.

Brierley, A.S., P. Ward, J.L. Watkins and C. Goss (1998a). Acoustic discrimination of Southern Ocean zooplankton. *Deep-Sea Research II* **45**, 1155-1173.

Brierley, A.S. and J.L. Watkins (1996). Acoustic targets at South Georgia and the South Orkney Islands during a season of krill scarcity. *Marine Ecology Progress Series* **138**, 51-61.

Brink, K.H., R. Arnone, P. Coble, C. Flagg, B.H. Jones, J. Kindle, C.M. Lee, D. Phinney, M. Wood, C. Yentsch and D. Young (1998). Monsoons boost biological productivity in Arabian Sea. *EOS, Transactions, American Geophysical Union* **79**, 168-169.

Brink, K.H., B.H. Jones, C.M. Lee and M. Wood (1996). A cool filament off Oman, June 1995; origins and fates of its water. *EOS, Transactions, American Geophysical Union* **77**, 46: F382.

Brinton, E. (1979). Parameters relating to the distributions of planktonic organisms, especially euphausiids in the eastern tropical Pacific. *Progress in Oceanography* **8**, 125-189.

Brock, J.C. and C.R. McClain (1992). Interannual variability in phytoplankton blooms observed in the northwestern Arabian Sea during the Southwest Monsoon. *Journal of Geophysical Research-Oceans* **97**, 733-750.

Bruce, J.G. (1974). Some details of upwelling off the Somali and Arabian coasts. *Journal of Marine Research* **32**, 419-432.

Buchholz, F., C. Buchholz, J. Reppin and J. Fischer (1995). Diel Vertical Migrations of *Meganyctiphanes norvegica* in the Kattegat - Comparison of Net Catches and Measurements with Acoustic Doppler Current Profilers. *Helgolander Meeresuntersuchungen* **49**, 1-4: 849-866.

Burczynski, J. (1973). Hydroacoustic research system of R. V. Professor Siedlecki. Gdynia, Polish-UNSF Highseas Fisheries Research Project, 33pp.

Carey, F.G. and B.H. Robison (1981). Daily patterns in the activities of swordfish, *Xiphias gladius*, observed by acoustic telemetry. *Fisheries Bulletin, U.S.* **79**, 277-292.

Chae, J. and S. Nishida (1995). Vertical distribution and diel migration in the iridescent copepods of the family Sapphirinidae: a unique example of reverse migration? *Marine Ecology Progress Series* **119**, 1/3: 111-124.

Charney, J.G. (1955). The Gulf Stream as an inertial boundary layer. *Proceedings of the National Academy of Science of the USA* **41**, 731-740.

Chen, Y.Q. (1986). The vertical distribution of some pelagic copepods in the eastern tropical Pacific. *CalCOFI Report Vol. 27* 205-227.

Childress, J.J. (1975). The respiratory rates of midwater crustaceans as a function of depth of occurrence and relation to the oxygen minimum layer off Southern California. *Comparative Biochemistry and Physiology* **50A**, 787-799.

Childress, J.J. and E.V. Thuesen (1992). Metabolic potential of deep-sea animals:regional and global scales. In: Deep-Sea food chains and the global carbon cycle. G. T. Rowe and V. Pariente (ed.), Dordrecht, Kluwer Academic, 217-236.

Chu, D., T.K. Stanton and P.H. Wiebe (1992). On the frequency dependence of sound backscattering from live zooplankton. *ICES Journal of Marine Science* **49**, 97-106.

Chu, D.Z., K.G. Foote and T.K. Stanton (1993). Further Analysis of Target Strength Measurements of Antarctic Krill at 38 and 120 Khz - Comparison with Deformed Cylinder Model and Inference of Orientation Distribution. *Journal of the Acoustical Society of America* **93**, 5: 2985-2988.

Chu, D.Z. and T.K. Stanton (1998). Application of pulse compression techniques to broadband acoustic scattering by live individual zooplankton. *Journal of the Acoustical Society of America* **104**, 1: 39-55.

Chu, D.Z., P. Wiebe and N. Copley (2000). Inference of material properties of zooplankton from acoustic and resistivity measurements. *ICES Journal of Marine Science* **57**, 4: 1128-1142.

Claustre, H., P. Kerherve, J.C. Marty and L. Prieur (1994). Phytoplankton photoadaptation related to some frontal physical processes. *Journal of Marine Systems* **5**, 251-265.

Clay, C.S. and H. Medwin (1977). Acoustical Oceanography: Principles and Applications. New York, Wiley-Interscience, pp.

Cochrane, N.A., D.D. Sameoto, A. Herman and A.W. Neilson (1991). Multiple-frequency acoustic backscattering and zooplankton aggregations in the inner Scotian Shelf Basins. *Canadian Journal of Fisheries and Aquatic Science* **48**, 340-355.

Codispoti, L.A. (1989). Phosphorus vs. nitrogen limitation of new and export production. In: Productivity in the ocean: present and past. W. H. Berger, V. S. Smetacek and G. Wefer (ed.), Chichester, Wiley-Interscience, 377-394.

Coombs, S.H., C.A. Fosh and M.A. Keen (1985). The buoyancy and vertical-distribution of eggs of sprat (*Sprattus-sprattus*) and pilchard (*Sardina-pilchardus*). *Journal of the Marine Biological Association of the United Kingdom* **65**, 2: 461-474.

Coombs, S.H., J.H. Nichols, D.V.P. Conway, S. Milligan and N.C. Halliday (1992). Food availability for sprat larvae in the Irish Sea. *Journal of the Marine Biological Association of the United Kingdom* **72**, 4: 821-834.

Costello, J.H., R.E. Pieper and D.V. Holliday (1989). Comparison of acoustic and pump sampling techniques for the analysis of zooplankton distributions. *Journal of Plankton Research* **11**, 703-709.

Craig, R.E. and S.T. Forbes (1969). Design of a sonar for fish counting. *Fiskeridrektoratets Skrifter, Serie Havundersokelser* **15**, 210-219.

Crisp, N. and A. Harris (2000). TUBA II - A compact multifrequency sonar suited to use in autonomous or towed platforms for the study of upper-ocean zooplankton distribution and abundance. IEEE Underwater Technology, 2000, Tokyo, Japan,

Crisp, N.A., P. Velez and J.T. Allen (1998). Underway observations of Mean Volume Backscatter Strengths (MVBS) from the SIMRAD EK500 echosounder during Discovery cruise 224, 27 Nov 1996 - 17 Jan 1997. Southampton, Southampton Oceanography Centre, 70pp.

Crowder, L.B. and J.J. Magnuson (1983). Thermal habitat shifts by fishes at the thermocline in Lake Michigan. *Canadian Journal of Fisheries and Aquatic Science* **39**, 7: 1046-1050.

Currie, R.I. (1992). Circulation and upwelling off the coast of South-East Arabia. *Oceanologica Acta* **15**, 43-60.

Cushing, D.H. (1951). The vertical migration of planktonic Crustacea. *Biological Reviews* **26**, 158-192.

Cushing, D.H. (1989). A difference in structure between ecosystems in strongly stratified waters and in those that are only weakly stratified. *Journal of Plankton Research* **11**, 1-13.

Cushman-Roison, B. (1984). On the maintenance of the subtropical front and its associated counter current. *Journal of Physical Oceanography* **14**, 1179-1190.

Cuvier, L.B. (1817). La regne animale 2. (poissons). *Paris (reference taken from Longhurst, 1976)* 532.

Dagg, M.J., B.W. Frost and J.A. Newton (1997). Vertical migration and feeding behaviour of *Calanus pacificus* females during a phytoplankton bloom in Dabob Bay, US. *Limnology and Oceanography* **42**, 5: 974-980.

Dalpadado, P. and J. Gjosaeter (1988). Feeding ecology of the lanternfish *Benthosema pterotum* from the Indian Ocean. *Marine Biology* **99**, 555-567.

Dawe, E.G. and J.K.T. Brodziak (1998). Trophic relationships, ecosystem variability and recruitment. In: Squid recruitment dynamics. (ed.), Rome, Food and Agriculture Organization, 125-156.

De Palma, I.P., D.A. Wiesenberg, S.E. Lohrenz and R.A. Arnone (1987). Cross-frontal variations in chlorophyll a distribution in the western Mediterranean Sea. *EOS: Transactions, American Geophysical Union* **68**, 50: 1725.

Demer, D.A. and R.P. Hewitt (1995). Bias in Acoustic Biomass Estimates of *Euphausia superba* Due to Diel Vertical Migration. *Deep-Sea Research I* **42**, 4: 455-475.

Denman, K.L. and T.M. Powell (1994). Effect of physical processes on planktonic ecosystems in the coastal ocean. *Oceanography and Marine Biology Annual Review* **22**, 125-168.

Dewey, R.K., J.N. Moum, V.A. Paulson, D.R. Caldwel and S.D. Piera (1991). Structures and dynamics of a coastal filament. *Journal of Geophysical Research* **96**, 14885-14907.

Dickey, T.D. (1991). The emergence of concurrent high-resolution physical and bio-optical measurements in the upper ocean and their applications. *Reviews of Geophysics* **29**, 383-413.

Duing, W. (1970). The monsoon regime of the currents in the Indian Ocean. *Contribution No. 330 from the Hawaii Institute of Geophysics, University of Hawaii* 68.

Eckert, R.O. (1983). Animal physiology : mechanisms and adaptations. San Francisco, pp.

Edwards, E.S., P.H. Burkill and C.E. Stelfox (1999). Zooplankton herbivory in the Arabian Sea during and after the SW monsoon, 1994. *Deep-Sea Research II* **46**, 843-863.

Ehrenberg, J.E. (1974). Two applications for a dual-beam transducer in hydroacoustic fish assessment systems. In: Oceans '74 IEEE International conference on Engineering in the Ocean Environment. (ed.), 152-155.

Ehrenberg, J.E. (1983). A review of in situ target strength estimation techniques. *FAO Fisheries Report* **300**, 90-95.

Ehrenberg, J.E. and D.W. Lytle (1972). Acoustic techniques for estimating fish abundance. *IEEE Transactions on Geosciences Electronics* **10**, 138-145.

Elliott, A.J. and G. Savidge (1990). Some Features of the Upwelling Off Oman. *Journal of Marine Research* **48**, 2: 319-333.

Endo, Y. (1993). Orientation of Antarctic krill in an aquarium. *Nippon Suisan Gakkaishi* **59**, 3: 465-468.

Eppley, R.W. and B.J. Peterson (1979). Particulate organic matter flux and planktonic new production in the deep ocean. *Nature* **282**, 677-680.

Estrada, M., R.A. Varela, J. Salat, A. Cruzado and E. Arias (1999). Spatio-temporal variability of the winter phytoplankton distribution across the Catalan and North Balearic fronts (NW Mediterranean). *Journal of Plankton Research* **21**, 1: 1-20.

Everson, I. (1982). Diurnal variations in mean volume backscattering strength of an Antarctic krill (*Euphausia superba*) patch. *Journal of Plankton Research* **4**, 155-162.

Everson, I., J.L. Watkins, D.G. Bone and K.G. Foote (1990). Implications of a new acoustic target strength for abundance estimates of Antarctic krill. *Nature* **345**, 338-340.

Fager, E.N. and J.A. McGowan (1963). Zooplankton species groups in the North Pacific. *Science* **140**, 453-460.

Farquhar, G.B. (1971). Proceedings of an International Symposium on Biological Sound Scattering in the Ocean (Maury Center for Ocean Science, Washington, DC). pp.

Fasham, M.J.R., M.V. Angel and H.S.J. Roe (1974). An investigation of the spatial pattern of zooplankton using the Longhurst Hardy Plankton Recorder. *Journal of Experimental Marine Biology and Ecology* **16**, 93-112.

Fedorov, K.N. and S.L. Meschanov (1988). Structure and Propagation of Red-Sea Waters in the Gulf of Aden. *Okeanologiya* **28**, 3: 357-363.

Feigenbaum, D. (1991). Food and feeding behaviour. In: The Biology of Chaetognaths. Q. Bone, H. Kapp and A. C. Pierrot-Bults (ed.), Oxford, Oxford University press, 45–54.

Feigenbaum, D. and R.C. Maris (1984). Feeding in the chaetognatha. *Oceanography and Marine Biology Annual Review* **22**, 343-392.

Fiala, M., A. Sournia, H. Claustre, J.C. Marty, L. Prieur and G. Vetion (1994). Gradients of Phytoplankton Abundance, Composition and Photosynthetic Pigments across the Almeria-Oran Front (Sw Mediterranean-Sea). *Journal of Marine Systems* **5**, 3-5: 223-233.

Fielding, S., N. Crisp, J.T. Allen, M.C. Hartman, B. Rabe and H.S.J. Roe (2001). Mesoscale subduction at the Almeria-Oran front Part 2. Biophysical interactions. *Journal of Marine Systems* **30**, 287-304.

Findlater, J. (1969). A major low-level air current near the Indian Ocean during the northern summer. *Quarterly Journal of the Royal Meteorological Society* **95**, 362-380.

Fischer, J. and V. Visbeck (1993). Seasonal variation of the daily zooplankton migration in the Greenland Sea. *Deep-Sea Research I* **40**, 8: 1547-1557.

Flagg, C.M. and S.L. Smith (1989a). On the use of the Acoustic Doppler Current Profiler to measure zooplankton abundance. *Deep-Sea Research I* **36**, 455-474.

Flagg, C.M., C.D. Wirick and S.L. Smith (1994). The interaction of phytoplankton, zooplankton and currents from 15 months of continuous data in the Mid-Atlantic Bight. *Deep-Sea Research II* **41**, 2/3: 411-435.

Flagg, C.N. and H.S. Kim (1998). Upper ocean currents in the northen Arabian Sea from shipboard ADCP measurements collected during the 1994-1996 U.S. JGOFS and ONR programs. *Deep-Sea Research II* **45**, 1917-1959.

Flagg, C.N. and S.L. Smith (1989b). Zooplankton abundance measurements from Acoustic Doppler Current Profilers. OCEAN '89, Marine Technology Society and I.E.E.E., Seattle, WA,

Flierl, G. and D.J. McGillicuddy (2002). Mesoscale and submesoscale physical-biological interactions. In: Biological-Physical interactions in the sea. A. R. Robinson, J. J. McCarthy and B. J. Rothschild (ed.), New York, John Wiley & Sons Inc., 113-186.

Folkard, A.M., P.A. Davies and L. Prieur (1994). The Surface-Temperature Field and Dynamical Structure of the Almeria-Oran Front from Simultaneous Shipboard and Satellite Data. *Journal of Marine Systems* **5**, 3-5: 205-222.

Folt, C.L. and C.W. Burns (1999). Biological drivers of zooplankton patchiness. *Tree* **14**, 8: 300-305.

Folt, C.L., P.C. Schulze and K. Baumgartner (1993). Characterizing a zooplankton neighbourhood: small-scale patterns of association and abundance. *Freshwater Biology* **30**, 289-300.

Foote, K.G. (1983). Maintaining Precision Calibrations with Optimal Copper Spheres. *Journal of the Acoustical Society of America* **73**, 3: 1054-1063.

Foote, K.G. (1990). Speed of sound in *Euphausia superba*. *Journal of the Acoustical Society of America* **87**, 1405-1408.

Foote, K.G. (1998). Broadband acoustic scattering signatures of fish and zooplankton (BASS). *Proceedings of the third European Marine Science and Technology Conference, Lisbon, May 23-27*

Foote, K.G., A. Aglen and O. Nakken (1986). Measurement of fish target strength with a split-beam echosounder. *Journal of the Acoustical Society of America* **80**, 2: 612-521.

Foote, K.G., I. Everson, J.L. Watkins and D.G. Bone (1990). Target strengths of Antarctic krill (*Euphausia superba*) at 38 and 120 kHz. *Journal of the Acoustical Society of America* **87**, 14-24.

Foote, K.G. and T.K. Stanton (2000). Acoustical methods. In: Zooplankton methodology manual. R. P. Harris, P. H. Wiebe, J. Lenz, H. R. Skjodal and M. Huntley (ed.), London, Academic Press, 223-258.

Foote, K.G. and G. Stefansson (1993). Definition of the problem of estimating fish abundance over an area from acoustic line-transect measurements of density. *ICES Journal of Marine Science* **50**, 369-381.

Forward, R.B. (1988). Diel vertical migration: zooplankton photobiology and behaviour. *Oceanography and Marine Biology Annual Review* **26**, 361-393.

Fowler, J. and L. Cohen (1990). Practical statistics for field biology. Chichester, John Wiley & Sons Ltd, 227 pp.

Francois, R.E. and G.R. Garrison (1982). Sound absorption based on ocean measurements. *Journal of the Acoustical Society of America* **72**, 1879-1890.

Franks, P.J.S. (1992). Sink or swim - accumulation of biomass at fronts. *Marine Ecology-Progress Series* **82**, 1-12.

Franks, P.J.S. (1997). New models for the exploration of biological processes at fronts. *ICES Journal of Marine Science* **54**, 161-167.

Gascard, J.C. and C. Richez (1985). Water masses and circulation in the Western Alboran Sea and in the Straits of Gibraltar. *Progress in Oceanography* **15**, 157-216.

Gaudy, R., M. Bianchi, M. Pagano and Y. Soto (1996). Cross frontal variability in hydrological and biological structures observed in a river plume area (Rhone mouth, NW Mediterranean Sea). *Hydrobiologia* **324**, 131-140.

Gerin, C. and M. Goutx (1994). Iatroscan-measured particulate and dissolved lipids in the Almeria-Oran frontal system (ALMOFRONT-1, May 1991). *Journal of Marine Systems* **5**, 343-360.

Gorsky, G., N. Lins Da Silva, S. Dallot, P. Laval, J.C. Braconnot and L. Prieur (1991). Midwater tunicates: are they related to the permanent front of the Ligurian Sea (NW Mediterranean Sea)? *Marine Ecology-Progress Series* **74**, 195-204:

Goswami, S.C., S.N. Gajbhiye and G. Padmavati (1992). Distribution of *Pleuromamma* (Copepoda: Metridiidae) along a north-southtransect in the Indian Ocean. In: Oceanography of the Indian Ocean. B. N. Desai (ed.), New Dehli, Oxford and IBH, 159-166.

Gould, R.W. and D.A. Wiesenberg (1990). Single species dominance in a subsurface phytoplankton concentration at a Mediterranean Sea front. *Limnology and Oceanography* **35**, 1: 211-220.

Govoni, J.J. and C.B. Grimes (1992). The surface accumulation of larval fishes by hydrodynamic convergence within the Mississippi River plume front. *Continental Shelf Research* **12**, 1265-1276.

Grant, S., P. Ward, E. Murphy, D. Bone and S. Abbott (2000). Field comparison of an LHPR net sampling system and an Optical Plankton Counter (OPC) in the Southern Ocean. *Journal of Plankton Research* **22**, 4: 619-638.

Greene, C.H., T.K. Stanton, P.H. Wiebe and S. McClatchie (1991). Acoustic estimates of Antarctic krill. *Nature* **349**, 110.

Greene, C.H. and P.H. Wiebe (1988). New developments in bioacoustical oceanography: Applications of the dual-beam technique to studies of zooplankton and micronekton ecology. *Sea Technology* **29**, 27-29.

Greene, C.H. and P.H. Wiebe (1990). Bioacoustical oceanography: New tools for zooplankton and micronekton research in the 1990s. *Oceanography* **3**, 12-17.

Greene, C.H., P.H. Wiebe and J. Burczynski (1989). Analyzing Zooplankton Size Distributions Using High-Frequency Sound. *Limnology and Oceanography* **34**, 1: 129-139.

Greene, C.H., P.H. Wiebe, J. Burczynski and M.J. Youngbluth (1988). Acoustical Detection of High-Density Krill Demersal Layers in the Submarine Canyons Off Georges Bank. *Science* **241**, 4863: 359-361.

Greene, C.H., P.H. Wiebe, A.J. Pershing, G. Gal, J.M. Popp, N.J. Copley, T.C. Austin, A.M. Bradley, R.G. Goldsborough, J. Dawson, R. Hendershott and S. Kaartvedt (1998). Assessing the distribution and abundance of zooplankton: a comparison of acoustic and net-sampling methods with D-BAD MOCNESS. *Deep-Sea Research II* **45**, 7: 1219-1237.

Greenlaw, C.F. (1977). Backscattering specra of preserved zooplankton. *Journal of the Acoustical Society of America* **62**, 44-52.

Greenlaw, C.F. (1979). Acoustic estimation of zooplankton populations. *Limnology and Oceanography* **24**, 226-242.

Greenlaw, C.F. and R.K. Johnson (1983). Multiple-frequency acoustical estimation. *Biological Oceanography* **2**, 227-252.

Greze, V.N., A.V. Kovalev, E.P. Baldina, O.K. Bileva and A.A. Shmemeva (1985). Zooplankton transfer through the Gibraltar Strait and peculiarities of its taxonomic composition and distribution in adjacent areas. *Investigacion Pesquera Barcelona* **49**, 1: 3-13.

Grice, G.D. and A.D. Hart (1962). The abundance, seasonal occurrence and distribution of the epizooplankton between New York and Bermuda. *Ecological Monographs* **32**, 287-309.

Griffiths, G. and J.I. Diaz (1996). Comparison of acoustic backscatter measurements from a ship-mounted Acoustic Doppler Current Profiler and an EK500 scientific echo-sounder. *ICES Journal of Marine Science* **53**, 2: 487-491.

Griffiths, G., S. Fielding and H.S.J. Roe (2001). Some observations of biophysical interactions in the ocean using high frequency acoustics. Proceedings of the Institute of Acoustics Conference on Acoustical Oceanography, Southampton, United Kingdom,

Griffiths, G., S. Fielding and H.S.J. Roe (2002). Biological-Physical-Acoustical Interactions. In: Biological-Physical interactions in the sea. A. R. Robinson, J. J. McCarthy and B. J. Rothschild (ed.), New York, John Wiley & Sons, Inc.,

Griffiths, G. and H.S.J. Roe (1993). Acoustic Doppler Current Profilers - a tool for both physical and biological oceanographers. IEEE Conference on acoustic Sensing and Imaging, 29-30 March 1993, London,

Guerin-Ancey, O. and P.M. David (1993). Use of a multibeam-multifrequency sounder to study the distribution of small zooplankton. *Deep-Sea Research I* **40**, 1: 119-128.

Guzman, O. (1983). Distribution and abundance of Antarctic krill (*Euphausia superba*) in the Bransfield Strait. *Berichte zur Polarforschung* **4**, 169-190.

Halpern, D. and P.M. Woiceshyn (1999). Onset of the Somali Jet in the Arabian Sea during June 1997. *Journal of Geophysical Research-Oceans* **104**, C8: 18041-18046.

Harder, W. (1968). Reactions of planktonic organisms to water stratification. *Limnology and Oceanography* **13**, 156-168.

Hardy, A.C. (1924). The herring in relation to its animate environment. I The food and feeding habits of the herring with special reference to the east coast of England. *Fisheries Investigations London Series* **2**, 7: 1-53.

Hart, R.C. (1990). Copepod post-embryonic durations: pattern, conformity, and predictibility. The realities of isochronal and equiproportional development, and trends in the copepod-naupliar duration ratio. *Hydrobiologia* **206**, 175-206:

Haury, L.R. (1973). Sampling bias of a Longhurst Hardy Plankton Recorder. *Limnology and Oceanography* **18**, 500-506.

Haury, L.R. (1982). Mesoscale processes: Some biological and physical connections. *EOS* **63**, 18: 267-269.

Haury, L.R., J.A. McGowan and P.H. Wiebe (1978). Patterns and processes in the timescales of plankton. In: NATO Conference series IV: Marine Sciences. J. Steele (ed.), Plenum Press, 277-327.

Haury, L.R. and P.H. Wiebe (1982). Fine-scale multi-species aggregations of oceanic zooplankton. *Deep-Sea Research I* **29**, 7: 915-921.

Haury, L.R., P.H. Wiebe and S.H. Boyd (1976). Longhurst-Hardy Plankton Recorders: their design and use to minimise bias. *Deep-Sea Research* **23**, 1217-1229.

Heburn, G.W. (1985). Effects of wind versus hydraulic forcing on the dynamics of the western Mediterranean Sea. *Rapports et Proces-Verbaux des Reunions Commission Internationale pour l'Exploration Scientifique de la Mer Mediterranee* **29**, 3: 65-67.

Heburn, G.W. (1987). The dynamics of the western Mediterranean Sea: A wind forced case study. *Annales Geophysicae* **5B**, 1: 61-74.

Heburn, G.W. (1994). The dynamics of the seasonal variability of the western Mediterranean circulation. *Coastal and Estuarine Studies* **46**, 249-285.

Heburn, G.W. and P.E. La Violette (1990). Variations in the structure of the anticyclonic gyres found in the Alboran Sea. *Journal of Geophysical Research* **95**, C2: 1599-1613.

Herman, A.W. (1992). Design and calibration of a new optical plankton counter capable of sizing small zooplankton. *Deep-Sea Research I* **39A**, 3/4: 395-415.

Herman, A.W., D.D. Sameoto and A.R. Longhurst (1981). Vertical and horizontal distribution patterns of copepods near the shelf break south of Nova-Scotia. *Canadian Journal of Fisheries and Aquatic Sciences* **38**, 9: 1065-1076.

Herring, P.J. (1994). RRS *Discovery* Cruise 209, 3 Aug - 22 Aug 1994: Biological and physical studies of the oxygen minimum and other hydrographic features of the Arabian Sea at 19°N 59°W during the south west monsoon. *IOS Cruise Report No. 224*

Herring, P.J., M.J.R. Fasham, A.R. Weeks, J.C.P. Hemmings, H.S.J. Roe, P.R. Pugh, S. Holley, N.A. Crisp and M.V. Angel (1998). Across-slope relations between the biological populations, the euphotic zone and the oxygen minimum layer off the coast of Oman during the southwest monsoon (August, 1994). *Progress in Oceanography* **41**, 69-109.

Herring, P.J. and P.M. Hargreaves (1998). The vertical distribution of biomass in the Arabian Sea near Oman (19 N, 59 E) during the southwest monsoon, and its relation to the oxygen minimum. Pelagic Biogeography ICoPBII: Proceedings of the 2nd International Conference. Final report of SCOR/IOC Working Group 93 'Pelagic Biogeography', 9 - 14 July, 1995, Nordwijkerhout, The Netherlands,

Hersey, J.R. and R.H. Backus (1954). Sound scattering by marine organisms. In: The Sea. Vol. 1. M. N. Hill (ed.), New York, Interscience,

Hewitt, R.P. and D.A. Demer (1991). Krill abundance. *Nature* **353**, 310.

Hewitt, R.P. and D.A. Demer (1996). Lateral target strength of Antarctic krill. *ICES Journal of Marine Science* **53**, 2: 297-302.

Heywood, K.J. (1996). Diel vertical migration of zooplankton in the Northeast Atlantic. *Journal of Plankton Research* **18**, 2: 163-184.

Heywood, K.J., S. Scropehowe and E.D. Barton (1991). Estimation of Zooplankton Abundance from Ship-Borne Adcp Backscatter. *Deep-Sea Research I* **38**, 6: 677-691.

Hobson, L.A. and C.J. Lorenzen (1972). Relationships of chlorophyll maxima to density structure in the Atlantic Ocean and Gulf of Mexico. *Deep-Sea Research I* **19**, 297-306.

Holliday, D.V. (1977). Extracting bio-physical information from the acoustic signatures of marine organisms. In: Oceanic sound scattering prediction. N. R. Anderson and B. J. Zahuranec (ed.), New York, Plenum Press, 619-624.

Holliday, D.V. (1992). Zooplankton acoustics. In: Oceanography of the Indian Ocean. B. N. Desai (ed.), New Dehli, Oxford and IBH Publishing Co, 733-741.

Holliday, D.V. and R.E. Pieper (1980). Volume scattering strengths and zooplankton distributions at acoustic frequencies between 0.5 and 3 MHz. *Journal of the Acoustical Society of America* **67**, 135-146.

Holliday, D.V. and R.E. Pieper (1995). Bioacoustical Oceanography at High-Frequencies. *ICES Journal of Marine Science* **52**, 3-4: 279-296.

Holliday, D.V., R.E. Pieper and G.S. Kleppel (1989). Determination of zooplankton size and distribution with multi-frequency acoustic technology. *Journal du Conseil pour l'Exploration de la Mer* **46**, 52-61.

Hood, R.R., M.R. Abbott and A. Huyer (1991). Phytoplankton and photosynthetic light response in the coastal transition zone off northern California in June 1987. *Journal of Geophysical Research* **96**, C8: 14769-14780.

Hood, R.R., H.V. Wang, J.E. Purcell, E.D. Houde and L.W. Harding Jr. (1999). Modelling particles and pelagic organisms in Chesapeake Bay: Convergent features control plankton distributions. *Journal of Geophysical Research* **104**, C1: 1223-1243.

Horne, J.K. (1998). Acoustic approaches to remote species identification. Remote species identification (RSID) workshop, Monteray Bay, USA,

Iida, K., T. Mukai and D. Hwang (1996). Relationship between acoustic backscattering strength and density of zooplankton in the sound-scattering layer. *ICES Journal of Marine Science* **53**, 507-512.

Jaffe, J.S., M.D. Ohman and A. De Robertis (1998). OASIS in the sea: measurement of the acoustic reflectivity of zooplankton with concurrent optical imaging. *Deep-Sea Research II* **45**, 7: 1239-1253.

JGOFS_protocol (1994). IOC Training Course on Ocean flux monitoring in the Indian Ocean. Training Course Reports No. 26, Intergovernmental Oceanographic Commission, 9pp.

Johnson, G.E. and W.B. Griffiths (1990). Hydroacoustic surveys of zooplankton biomass and distribution in the Beaufort Sea in 1985 and 1986. *Rapports et Proces-verbaux des Reunions, ICES* **189**, 345-352.

Johnson, R.K. (1977). Sound scattering from a fluid sphere revisited. *Journal of the Acoustical Society of America* **61**, 375-377.

Kalinowski, J. (1982). Distribution and stocks of krill in the Drake passage and the Bransfield Strait, during the BIOMASS-FIBEX expedition 1981. *Polish Polar Research* **3**, 243-251.

Kamykowski, D. and S.-J. Zentara (1990). Hypoxia in the world ocean as recorded in the historical data set. *Deep-Sea Research I* **37**, 1861-1874.

Kearns, E.J., S.R. Emmerson, D.B. Olson, G.E. Johnson and J.M. Morrison (1989). CTD and bottle data from RRS "Charles Darwin" MASAI 86-87, RSMAS-WHOI -NOVA. Leg I: 20 December 1986 - 18 January 1987. Leg II: 17 July 1987 - 15 August 1987. Miami, Rosenstiel School of Marine & Atmospheric Science, University of Miami and Woods Hole Oceanographic Institution, Variouspp.

Kikutchi, K. (1930). Diurnal migration of planktonic Crustacea. *Quarterly Review of Biology* **5**, 189-206.

Kils, U. (1981). The swimming behaviour, swimming performance and energy balance of Antarctic krill, *Euphausia superba*. BIOMASS Scientific Series, 122.

Kinzer, J., R. Bottger-Schnack and K. Schulz (1993). Aspects of the horizontal distribution and diet of myctophid fish in the Arabian Sea with reference to the deep water oxygen deficiency. *Deep-Sea Research I* **40**, 783-800.

Klindt, H. and F. Zwack (1984). A method for acoustic estimation of krill (*Euphausia superba* Dana) abundance applied to FIBEX data. *Archiv fur Fischereiwissenschaft* **34**, 121-144.

Kogler, J.W., S. Falk-Petersen, A. Kristensen, F. Pettersen and J. Dalen (1987). Density and sound speed contrasts in sub-arctic zooplankton. *Polar Biology* **7**, 231-235.

Kristensen, A. and J. Dalen (1986). Acoustic estimation of size distribution and abundance of zooplankton. *Journal of the Acoustical Society of America* **80**, 601-611.

Kumar, S.P. and T.G. Prasad (1999). Formation and spreading of Arabian Sea high-salinity water mass. *Journal of Geophysical Research-Oceans* **104**, C1: 1455-1464.

La Violette, P.E. (1990). The Western Mediterranean Circulation Experiment (WMCE): Introduction. *Journal of Geophysical Research* **95**, 1511-1514.

Lamont, P.A. and J.D. Gage (2000). Morphological responses of macrobenthic polychaetes to low oxygen on the Oman continental slope, NW Arabian Sea. *Deep-Sea Research II* **47**, 1-2: 9-24.

Landry, M.R. (1983). The development of marine calanoid copepods with comments on the isochronal rule. *Limnology and Oceanography* **28**, 614-624.

Larsson, P. and S. Dodson (1993). Chemical communication in planktonic animals. *Archiv fur Hydrobiologie* **129**, 2: 129-155.

Latasa, M. and R.C. Bidigare (1998). A comparison of phytoplankton populations of the Arabian Sea during the Spring Intermonsoon and Southwest Monsoon of 1995 as described by HPLC-analysed pigments. *Deep-Sea Research II* **45**, 2133-2170.

Laval, P., J.C. Braconnot, C. Carre, J. Goy, P. Morand and C.E. Mills (1989). Small-scale distribution of macroplankton and micronekton in the Ligurian Sea (Mediterranean Sea) as observed from the manned submersible *Cyana*. *Journal of Plankton Research* **11**, 665-685.

Lavery, A.C., T.K. Stanton, D. McGehee and D. Chu (2002). Three-dimensional modeling of acoustic backscattering from fluid-like zooplankton. *Journal of the Acoustical Society of America* **111**, 3: 1197-1210.

Laws, P. (1985). A future policy for the Antarctic. Interdisciplinary Science Reviews. *Interdisciplinary Science Reviews* **10**, 4: 336-348.

Le Fevre, J. (1986). Aspects of the biology of frontal systems. *Advances in Marine Biology* **23**, 163-299.

Lee, C.M., B.H. Jones, K.H. Brink and A.S. Fischer (2000). The upper-ocean response to monsoonal forcing in the Arabian Sea: seasonal and spatial variability. *Deep-Sea Research II* **47**, 7-8: 1177-1226.

Legendre, L., S. Demers and D. Lefaivre (1986). Biological production at marine ergoclines. In: Marine interfaces ecohydrodynamics. J. C. J. Nihoul (ed.), Amsterdam, Elsevier, 1-29.

Legendre, L., F. Rassoulzadegan and J. Michaud (1999). Identifying the dominant processes (physical versus biological) in pelagic marine ecosystems from field estimates of chlorophyll *a* and phytoplankton production. *Journal of Plankton Research* **21**, 9: 1643-1658.

Levin, L.A., J.D. Gage, C. Martin and P.A. Lamont (2000). Macrobenthic community structure within and beneath the oxygen minimum zone, NW Arabian Sea. *Deep-Sea Research II* **47**, 1-2: 189-226.

L'Helguen, S., C. Madec and P. Le Corre (1992). Flux d'azote dans la zone du front Almeria-Oran: absorption et regeneration (mesures par l'azote 15). Processus et bilans dans les fronts geostrophiques [Processes and budgets in geostrophic fronts]. *Workshop held October 20-22, 1992, Marsaille-Luminy, France. JGOFS-France, Rapport 13* 123pp.

L'Helguen, S., P. Morin, P. Le Corre, C. Salaun, J. Le Fevre, J.Y. Le Tareau and R. Maze (1993). Frontal ecosystems: Physical control of the C and N fluxes. *Annales de l'Institut Oceanographique (Paris)* **69**, 1: 95-105.

Lillibridge, J.L., G.L. Hitchcock, R. Rossby, E. Lessard, M. Mork and L. Golmen (1990). Entrainment and mixing of shelf/slope waters in the near-surface Gulf Stream. *Journal of Geophysical Research* **95**, 13065-13087.

Lillo, S., J. Cordova and A. Paillaman (1996). Target-strength measurements of hake and jack mackeral. *ICES Journal of Marine Science* **53**, 2: 267-271.

Lohrenz, S.E., D.A. Wiesenberg, I.P. De Palma, K.S. Jihnson and D.E. Gustafson (1988). Interrelationships among primary production, chlorophyll, and environmental conditions in frontal regions of the Western Mediterranean Sea. *Deep-Sea Research I* **35**, 5: 793-810.

Longhurst, A.R. (1967). Vertical distribution of zooplankton in relation to theeastern Pacific oxygen minimum. *Deep-Sea Research I* **14**, 51-63.

Longhurst, A.R., A.D. Reith, R.E. Bower and D.L.R. Seibert (1966). A new system for the collection of multiple serial plankton samples. *Deep-Sea Research* **13**, 212-222.

Love, R.H. (1978). Resonant acoustic scattering by swimbladder-bearing fish. *Journal of the Acoustical Society of America* **64**, 571-580.

Luo, J., P.B. Ortner, D. Forcucci and S.R. Cummings (2000). Diel vertical migration of zooplankton and mesopelagic fish in the Arabian Sea. *Deep-Sea Research II* **47**, 1451-1473.

Macaulay, M., K. Wishner and K.L. Daly (1995). Acoustic scattering from zooplankton and micronekton in relation to a whale feeding site near Georges Bank and Cape Cod. *Continental Shelf Research* **15**, 4/5: 509-537.

Macaulay, M.C. (1993). Measurements of sound scattering as a means of examining ecological interactions between marine organisms and their environment. IEEE Conference on acoustic Sensing and Imaging, 29-30 March 1993, London,

Macaulay, M.C. (1994). A generalised target strength model for euphausiids, with applications to other zooplankton. *Journal of the Acoustical Society of America* **95**, 2452-2466.

Madureira, L.S.P., I. Everson and E.J. Murphy (1993b). Interpretation of Acoustic Data at 2 Frequencies to Discriminate between Antarctic Krill (*Euphausia superba* Dana) and Other Scatterers. *Journal of Plankton Research* **15**, 7: 787-802.

Madureira, L.S.P., P. Ward and A. Atkinson (1993a). Differences in Backscattering Strength Determined at 120 and 38 Khz for 3 Species of Antarctic Macroplankton. *Marine Ecology-Progress Series* **93**, 1-2: 17-24.

Magnuson, J.J., C.L. Harrington and D.J.H. Stewart, G. N. (1981). Responses of macro fauna to short-term dynamics of a Gulf Stream front on the continental shelf. *Coastal and Estuarine Studies* **1**, 441-448.

Malanotte-Rizzoli, P., B.B. Manca, M. Ribera D'Alcala, A. Theocharis, S. Brenner, G. Budillon and E. Ozsoy (1999). The eastern Mediterranean in the 80s and in the 90s: the big transition in the intermediate and deep circulations. *Dynamics of Atmospheres and Oceans* **29**, 2/4: 365-395.

Mann, K.H. and J.R.N. Lazier (1991). Biological-Physical interactions in the Oceans. In: Dynamics of Marine Ecosystems. (ed.), London, Blackwell, 223-254.

Mantoura, R.F. (1995). Arabesque I: cruise report. Plymouth, Plymouth Marine Laboratory, 102pp.

Manuel, J.L., C.M. Pearce and R.K. O'Dor (1997). Vertical migration for horizontal transport while avoiding predators: evidence for the tidal/diel model from two populations of scallop (*Placopecten magellanicus*) veligers. *Journal of Plankton Research* **19**, 12: 1949-1973.

Marshall, N.B. (1970). Swimbladder development and the life of deep sea fishes. In: Proceedings of the international sympposium on biological scattering in the oceans. G. B. Farquhar (ed.), U.S. Government Printing Office, 69-73.

Martin, L.V., T.K. Stanton, P.H. Wiebe and J.F. Lynch (1996). Acoustic classification of zooplankton. *ICES Journal of Marine Science* **53**, 2: 217-224.

Mauchline, J. (1980). The biology of mysids and euphausiids. *Advances in Marine Biology* **18**, 1-681.

Mauchline, J. and L.R. Fisher (1969). The biology of euphausiids. *Advances in Marine Biology* **7**, 1-454.

McClain, C.R., J. Ishizaka and E.E. Hofman (1990). Estimation of the processes controlling variability in phytoplankton pigment distributions on the southeastern U.S. continental shelf. *Journal of Geophysical Research* **95**, 20213-20236.

McClatchie, S., C.H. Greene, M. Macaulay and D.R.M. Sturley (1994). Spatial and temporal variability of Antarctic krill: implications for stock assessment. *ICES Journal of Marine Science* **51**, 1: 11-18.

McCreary, J.P., K.E. Kohler, R.R. Hood and D.B. Olson (1996). A four-component ecosystem model of biological activity in the Arabian Sea. *Progress in Oceanography* **37**, 193-240.

McGehee, D., R.L. O'Driscoll and L.V.M. Traykovski (1998). Effects of orientation on acoustic scattering from Antarctic krill at 120 kHz. *Deep-Sea Research I* **45**, 1273-1294.

McGowan, J.A. and V.J. Fraundorf (1966). The relationship between size of net used and estimates of zooplankton diversity. *Limnology and Oceanography* **11**, 456-469.

Medwin, H. and C.S. Clay (1998). Fundamentals of Acoustic Oceanography. San Diego, California, Academic Press, pp.

Miller, D.G.M. and I. Hampton (1989). Biology and ecology of Antarctic krill (*Euphausia superba* Dana): a review. BIOMASS Scientific Series, 9pp.

Millot, C. (1991). Mesoscale and seasonal variabilities of the circulation in the Western Mediterranean. *Dynamics of Atmospheres and Oceans* **15**, 179-214.

Millot, C. (1999). Circulation in the Western Mediterranean Sea. *Journal of Marine Systems* **20**, 423-442.

Misund, O.A. (1997). Underwater acoustics in marine fisheries. *Reviews of Fish Biology and Fisheries* **7**, 1-34.

Mitson, R.B. (1983). Acoustic detection and estimation of fish near the sea-bed and surface. *FAO Fisheries Report* **300**, 82-91.

Mitson, R.B., Y. Simard and C. Goss (1996). Use of a two-frequency algorithm to determine size and abundance of plankton in three widely spaced locations. *ICES Journal of Marine Science* **53**, 2: 209-215.

Miyashita, K., I. Aoki and T. Inagaki (1996). Swimming behavior and target strength of isada krill (*Euphausia pacifica*). *ICES Journal of Marine Science* **53**, 303-308.

Morrison, J.M., L.A. Codispoti, S. Gaurin, B.H. Jones, V. Manghnani and Z. Zheng (1998). Seasonal variation of hydrographic and nutrient fields during the JGOFS Arabian Sea Process Study. *Deep-Sea Research II* **45**, 2053-2101.

Morrison, J.M., L.A. Codispoti, S.L. Smith, K. Wishner, C. Flagg, W.D. Gardner, S. Gaurin, S.W.A. Naqvi, V. Manghnani, L. Prosperie and J.S. Gundersen (1999). The oxygen minimum zone in the Arabian Sea during 1995. *Deep-Sea Research II* **46**, 8-9: 1903-1931.

Morse, P.M. and K.U. Ingard (1968). Theoretical Acoustics. Princeton, New Jersey, Princeton University Press, pp.

Murav'yev, S.S. and P.P. Shirshov (1984). Relation of structure of ocean deep-scattering layers and hydrophysical processes. *Okeanologiya* **24**, 251-257.

Murray, A.W.A. (1996). Comparison of geostatistical and random sample survey analyses of Antarctic krill acoustic data. *ICES Journal of Marine Science* **53**, 415-421.

Nair, R.R., V. Ittekot, V. Manghnani, V. Ramaswamy, S. Hakke, E. Degens, B.N. Desai and S. Honjo (1989). Increased particle flux to the deep ocean related to Monsoons. *Nature* **338**, 749-751.

Napp, J.M., P.B. Ortner, R.E. Pieper and D.V. Holliday (1993). Biovolume-size spectra of epipelagic zooplankton using a Multifrequency Acoustic Profiling System (MAPS). *Deep-Sea Research I* **40**, 445-459.

Nash, R.D.M., J.J. Magnuson, T.K. Stanton and C.S. Clay (1989). Distribution of peaks of 70kHz acoustic scattering in relation to depth and temperature during day and night at the edge of the Gulf Stream - Echofront 83. *Deep-Sea Research I* **36**, 4A: 587-596.

Newell, G.E. and R.C. Newell (1963). Marine Plankton: A practical guide. 207 pp.

Nichols, J.H. and A.B. Thompson (1991). Mesh selection of copepodite and nauplius stages of four calanoid copepod species. *Journal of Plankton Research* **13**, 3: 661-671.

Nival, P. (1990). Mise en evidence des structures spatiales en mer. *Oceanis* **16**, 75-89.

Nurser, A.J.G. and J.W. Zhang (2000). Eddy-induced mixed layer shallowing and mixed layer/thermocline exchange. *Journal of Geophysical Research* **105**, C9: 21851-21868.

O'Brian, D.P. (1988). Direct observations of clustering (schooling and swarming) behaviour in mysids (Crustacea: Mysidacea). *Marine Ecology Progress Series* **42**, 235-246.

Okubo, A. (1978). Advection-diffusion in the presence of surface convergence. In: Coastal processes. M. J. Bowman and W. E. Esaias (ed.), New York, Springer-Verlag, 23-28.

Olson, D.B. (1986). Lateral exchange within Gulf Stream ring surface layers. *Deep-Sea Research I* **33**, 1691-1704.

Olson, D.B. (1991). Rings in the ocean. *Annual Review of Earth Planet Science* **19**, 283-311.

Olson, D.B. (2002). Biophysical dynamics of ocean fronts. In: Biological-Physical interactions in the sea. A. R. Robinson, J. J. McCarthy and B. J. Rothschild (ed.), New York, John Wiley & Sons inc., 187-218.

Olson, D.B. and R.H. Backus (1985). The concentrating of organisms at fronts: a coldwater fish and a warm-core ring. *Journal of Marine Research* **43**, 113-137.

Olson, D.B., G.B. Hitchcock, R.A. Fine and B.A. Warren (1993). Maintenance of the low-oxygen layer in the central Arabian Sea. *Deep-Sea Research I* **40**, 673-685.

Olson, D.B., G.L. Hitchcock, A.J. Mariano, C.J. Ashjian, G. Peng, R.W. Nero and G.P. Podesta (1994). Life on the edge: Marine life and fronts. *Oceanography* 7, 2: 52-60.

Ona, E. and R.B. Mitson (1996). Acoustic sampling and signal processing near the seabed: the deadzone revisited. *ICES Journal of Marine Science* **53**, 677-690.

Orr, M.H. (1981). Remote acoustic detection of zooplankton response to fluid processes, oceanographic instrumentation and predators. *Canadian Journal of Fisheries and Aquatic Science* **38**, 1096-1105.

Ortner, P.B., L.C. Hill and H.E. Edgerton (1981). In-situ silhouette photography of Gulf Stream zooplankton. *Deep-Sea Research I* **28**, 1569-1576.

Ortner, P.B., P.H. Wiebe and J.L. Cox (1980). Relationships between oceanic epizooplankton distributions and the seasonal deep chlorophyll maximum in the Northwestern Atlantic Ocean. *Journal of Marine Research* **38**, 507.

Owen, R.W. (1981). Fronts and eddies in the sea: mechanisms, interactions and biological effects. In: The Analysis of Marine Ecosystems. A. L. Longhurst (ed.), London, Academic Press,

Partridge, C. and E.R. Smith (1995). Acoustic scattering from bodies: Range of validity of the deformed cylinder method. *Journal of the Acoustical Society of America* **97**, 784-795.

Pauly, T. and J.D. Penrose (1998). Laboratory target strength measurements of free-swimming Antarctic krill (*Euphausia superba*). *Journal of the Acoustical Society of America* **103**, 6: 3268-3280.

Pearre, S. (1979). Problems of detection and interpretation of vertical migration. *Journal of Plankton Research* **1**, 20-44.

Pedlosky, J. (1979). Geophysical fluid dynamics. New York, Springer-Verlag, pp.

Pedrotti, M.L. and L. Fenaux (1996). Distribution of echinoderm larval populations in the geostrophic frontal jet of the eastern Alboran Sea. *Oceanologica Acta* **19**, 385-395.

Pickard, G.L. and W.J. Emery (1982). Descriptive physical oceanography: an introduction. Oxford, Pergamon Press, 249 pp.

Pieper, R.E. (1979). Euphausiid distribution and biomass determined acoustically at 102 kHz. *Deep-Sea Research I* **26**, 687-702.

Pieper, R.E. and D.V. Holliday (1984). Acoustic measurements of zooplankton distributions in the sea. *Journal du Conseil pour l'Exploration de la Mer* **41**, 226-238.

Pieper, R.E., D.V. Holliday and G.S. Kleppel (1990). Quantitative Zooplankton Distributions from Multifrequency Acoustics. *Journal of Plankton Research* **12**, 2: 433-441.

Pieper, R.E., D. McGehee, C.F. Greenlaw and D.V. Holliday (2001). Acoustically measured seasonal patterns of Zooplankton in the Arabian Sea. *Deep-Sea Research II* **48**, 1325-1343.

Pierrot-Bults, A.C., S. Van der Spoel, B.J. Zahuranec and R.K. Johnson (1986). Pelagic biogeography. *UNESCO Technical paper in Marine Science* **49**, Proceedings of the International Conference, the Netherlands:

Pijanowska, J. and A. Kowalczewski (1997). Predators can induce swarming behaviour and locomotry responses in *Daphnia*. *Freshwater Biology* **37**, 649-656.

Pinel-Alloul, B. (1995). Spatial heterogeneity as a multiscale characteristic of a zooplankton community. *Hydrobiologia* **300/301**, 17-42.

Pingree, R.D. (1978). Mixing and stabilizing of phytoplankton distributions on the northwest European continental shelf. In: Spatial patterns in planktonic communitie. J. Steele (ed.), New York, Plenum Press, 181-220.

Pingree, R.D., P.M. Holligan and G.T. Mardall (1978). The effects of vertical stability on phytoplankton distributions in the summer on the northwest European shelf. *Deep-Sea Research I* **25**, 1011-1028.

Pinot, J.-M., J. Tintore and D.-P. Wang (1996). A study of the omega equation for diagnosing vertical motions at ocean fronts. *Journal of Marine Research* **54**, 239-259.

Pipe, R.K., S.H. Coombs and K.R. Clarke (1981). On the sample validity of the Longhurst Hardy Plankton Recorder for fish eggs and larvae. *Journal of Plankton Research* **3**, 675-683.

Plueddemann, A.J. and R. Pinkel (1989). Characterisation of the patterns of diel migration using a Doppler sonar. *Deep-Sea Research I* **36**, 509-530.

Podesta, G.P., J.A. Browder and J.J. Hoey (1993). Exploring the association between swordfish catch and thermal fronts on the U.S. longline grounds in the western North Atlantic. *Continental Shelf Research* **13**, 253-277.

Pollard, R. (1986). Frontal Surveys with a Towed Profiling Conductivity Temperature Depth Measurement Package (Seasoar). *Nature* **323**, 6087: 433-435.

Postel, L., H. Fock and W. Hagen (2000). Biomass and abundance. In: Zooplankton Methodology Manual. R. Harris, Wiebe, PH, Lenz, J, Skjoldal, HR and Huntley, M. (ed.), Academic Press, 83-192.

Powell, D.K. (1997). Horizontal distribution of pelagic fauna across the Almeria-Oran front, SW Mediterranean Sea. MSc., University of Southampton, 73pp.

Prasad, T.G., M. Ikeda and S.P. Kumar (2001). Seasonal spreading of the Persian Gulf Water mass in the Arabian Sea. *Journal of Geophysical Research-Oceans* **106**, C8: 17059-17071.

Preller, R.H. and H.E. Hurlburt (1982). A reduced gravity numerical model of circulation in the Alboran Sea. In: Hydrodynamics of semi-enclosed Sea. J. C. J. Nihoul (ed.), New York, Elsevier, 75-89.

Premchand, K. (1981). Spreading and mixing of the Persian Gulf Water in the northern Arabian Sea. *Indian Journal of Marine Science* **11**, 321-326.

Premchand, K., J.S. Sastry and C.S. Murty (1986). Watermass structure in the western Indian Ocean - Part II: The spreading and transformation of the Persian Gulf water. *Mausam* **37**, 2: 179-186.

Prieur, L., C. Copin-Montegut and H. Claustre (1993). Biophysical aspects of "Almofront", an intensive study of a geostrophic frontal jet. *Annales de l'Institut Oceanographique (Paris)* **69**, 2: 71-86.

Prieur, L. and A. Sournia (1994). Almofront-1 (April-May 1991) - an Interdisciplinary Study of the Almeria-Oran Geostrophic Front, Sw Mediterranean-Sea. *Journal of Marine Systems* **5**, 3-5: 187-203.

Pugh, P.R. (1989). Gelatinous zooplankton - the forgotten fauna. *Progress in Underwater Science* **14**, 67-78.

Pugh, P.R. (1997). RRS Discovery Cruise 224 Leg 2, 30 Dec 1996-17 Jan 1997, Biological and physical investigations in the region of the Almeira-Oran Front (western Mediterranean). Southampton, Southampton Oceanography Centre, 50pp.

Qazim, S.Z. (1982). Oceanography of the northern Arabian Sea. *Deep-Sea Research I* **29**, 1041-1068.

RDInstruments (1990). Calculating absolute backscatter. San Diego, California, RD Instruments, 24pp.

Reeder, B.D., T.K. Stanton and D. Chu (2000). Broadband acoustic backscattering from alewife fish: Experiment and analysis. *Journal of the Acoustical Society of America* **108**, 5: 2457.

Reeve, M.R. (1988). Zooplankton - the connecting link: a historical perspective. In: Towards a theory on biological-physical interactions in the World Ocean. B. J. Rothschild (ed.), Dordrecht, Boston, London, Kluwer Academic Publishers, 501-512.

Reid, J.L., A. Brinton, E.L. Fleminger, E.L. Venrick and J.A. McGowan (1978). Ocean circulation and marine life. In: Advances in Oceanography. H. Charnock and G. E. R. Deacon (ed.), New York, Plenum Press, 65-130.

Richards, S.A., H.P. Possingham and J. Noyle (1996). Diel vertical migration: modelling light-mediated mechanisms. *Journal of Plankton Research* **18**, 12: 2199-2222.

Richter, K.E. (1985). Acoustic scattering at 1.2 MHz from individual zooplankters and copepod populations. *Deep-Sea Research I* **32**, 149-161.

Ricker, W.E. (1973). Linear regressions in fishery research. *Journal Fisheries Research Boards of Canada* **30**, 3: 409-435.

Ricketts, C., J.L. Watkins, J. Priddle, D.J. Morris and F. Buchholz (1992). An assessment of the biological and acoustic characteristics of swarms of Antarctic krill. *Deep-Sea Research I* **39**, A2: 359-371.

Rippeth, T.P. and J.H. Simpson (1998). Diurnal signals in vertical motions on the Hebridean Shelf. *Limnology and Oceanography* **43**, 7: 1690-1696.

Robinson, A.R. (1983). Eddies in Marine Science. New York, Springer-Verlag, pp.

Robinson, M.K. (1966). Arabian Sea. In: Encyclopaedia of earth sciences, Volume 1: The encyclopaedia of Oceanography. R. W. Fairbridge (ed.), Stroudsburg, Pennsylvania, Dowden, Hutchinson and Ross, Inc, 40-44.

Rochford, D.J. (1964). Salinity maxima in the upper 1000 m of the north Indian Ocean. *Australian Journal of Marine and Freshwater Research* **15**, 1-24.

Roe, H.S.J. (1974). Observations on the diurnal vertical migrations of an oceanic animal community. *Marine Biology* **28**, 99-111.

Roe, H.S.J. (1982). New deep-sea photometer and its biological applications. Proceedings of SIRA seminar, Guildford, Surrey, 8-9 September 1981. Bellingham, Wash.: Society of Photo-Optical and Instrumentation Engineers. (SPIE Vol. 262),

Roe, H.S.J. (1984a). The diel migrations and distributions within a mesopelagic community in the North East Atlantic. 2. Vertical migrations and feeding of mysids and decapod crustacea. *Progress in Oceanography* **13**, 3/4: 269-318.

Roe, H.S.J. (1984b). The diel migrations and distributions within a mesopelagic community in the North East Atlantic. 4. The copepods. *Progress in Oceanography* **13**, 3/4: 353-388.

Roe, H.S.J., M.V. Angel, J. Badcock, P. Domanski, P.T. James, P.R. Pugh and M.H. Thurston (1984). The diel migrations and distributions within a mesopelagic community in the North East Atlantic. 1. Introduction and sampling procedures. *Progress in Oceanography* **13**, 3/4: 245-268.

Roe, H.S.J. and G. Griffiths (1993). Biological Information from an Acoustic Doppler Current Profiler. *Marine Biology* **115**, 2: 339-346.

Roe, H.S.J., G. Griffiths, M. Hartman and N. Crisp (1996). Variability in biological distributions and hydrography from concurrent Acoustic Doppler Current Profiler and SeaSoar surveys. *ICES Journal of Marine Science* **53**, 131-138.

Roe, H.S.J., G. Griffiths, M. Hartman and N. Lane (1994). Bioacoustics: a remote in situ measure of biological variability. Oceanology International '94, The Global Ocean. Vol. 2, 8-11 March 1994, Brighton, UK,

Roman, M., S.L. Smith, K. Wishner, X. Zhang and M. Gowing (2000). Mesozooplankton production and grazing in the Arabian Sea. *Deep-Sea Research II* **47**, 1423-1450.

Russell, F.S. (1927). The vertical distribution of plankton in the sea. *Biological Reviews* **2**, 213-262.

Saltzman, J. and K. Wishner (1997a). Zooplankton ecology in the eastern tropical Pacific oxygen minimum zone above a seamount: 1. General trends. *Deep-Sea Research I* **44**, 6: 907-930.

Saltzman, J. and K. Wishner (1997b). Zooplankton ecology in the eastern tropical Pacific oxygen minimum zone above a seamount: 2 Vertical distribution of copepods. *Deep-Sea Research I* **44**, 6: 931-954.

Sameoto, D., P.H. Wiebe, J. Runge, L. Postel, J. Dunn, C. Miller and S.H. Coombs (2000). Collecting zooplankton. In: Zooplankton Methodology Manual. R. Harris, Wiebe, PH, Lenz, J, Skjoldal, HR and Huntley, M. (ed.), Academic Press, 55-81.

Sameoto, D.D. (1976). Distribution of sound scattering layers caused by euphausiids and their relationship to chlorophyll a concentration in the Gulf of St. Lawrence estuary. *Journal of Fisheries Research Board Canada* **33**, 681-687.

Sameoto, D.D. (1980). Quantitative measurements of euphausiids using a 120 kHz sounder and their in situ orientation. *Canadian Journal of Fisheries and Aquatic Science* **37**, 693-702.

Sameoto, D.D. (1986). Influence of the biological and physical environment on the vertical distribution of mesozooplankton and micronekton in the eastern tropical Pacific. *Marine Biology* **93**, 263-279.

Sameoto, D.D., N.A. Cochrane and A. Herman (1990). Use of multiple frequency acoustics and other methods in estimating copepod and euphausiid abundance's. Abstracts of scientific papers presented at the 78th Statutory Meeting, Copenhagen, Denmark 4-12 October, 1990,

Sameoto, D.D., L. Guglielmo and M.K. Lewis (1987). Da/night vertical distribution of euphausiids in the eastern tropical Pacific. *Marine Biology* **96**, 235-245.

Sardou, J., M. Etienne and V. Andersen (1996). Seasonal abundance and vertical distributions of macroplankton and micronekton in the Northwestern Mediterranean Sea. *Oceanologica Acta* **19**, 6: 645-656.

Sastry, J.S. and R.S. DeSouza (1972). Upward mixing in the Arabian Sea. *Indian Journal of Marine Science* **1**, 17-27.

Savidge, G. (1976). A preliminary study of the distribution of chlorophyll a in the vicinity of fronts in the Celtic and western Irish Seas. *Estuarine and Coastal Marine Science* **4**, 617-625.

Schott, F. (1983). Monsoon response of the Somali current and associated upwelling. *Progress in Oceanography* **12**, 357-381.

Seguin, G., A. Errhif and S. Dallot (1994). Diversity and structure of pelagic copepod populations in the frontal zone of the eastern Alboran Sea. *Hydrobiologia* **292/293**, 369-377.

Seguin, G., R. Gaudy, A. Errhif and D. Thibault (1993). Observations sur l'abondance, la composition taxonomique et les affinities ecologiques des copepodes pelagiques recoltes dans la region du front Almeria-Oran. *Marine Life* **3**, 19-29.

Sen Gupta, R. and S.W.A. Naqvi (1984). Chemical oceanography in the Indian Ocean, north of the equator. *Deep-Sea Research I* **31**, 671-706.

Sewell, R.B.S. and L. Fage (1948). Minimum oxygen layer in the ocean. *Nature* **162**, 949-951.

Shalapyonok, A., R.J. Olson and L.S. Shalapyonok (2001). Arabian Sea phytoplankton during Southwest and Northeast monsoons 1995: composition, size structure and biomass from individual cell properties measured by flow cytometry. *Deep-Sea Research II* **48**, 6-7: 1231-1261.

Shapiro, G.I. and S.L. Meschanov (1991). Distribution and Spreading of Red-Sea Water and Salt Lens Formation in the Northwest Indian-Ocean. *Deep-Sea Research I* **38**, 1: 21-34.

Shetye, S.R., A.D. Gouveia and S.S.C. Shenoi (1994). Circulation and Water Masses of the Arabian Sea. *Proceedings of the Indian Academy of Sciences-Earth and Planetary Sciences* **103**, 2: 107-123.

Simpson, J.H., D.J. Edelstein, A. Edwards, N.C.G. Morris and P.B. Tett (1979). The Islay front: Physical structure and phytoplankton distribution. *Estuarine and Coastal Marine Science* **9**, 713-726.

Smith, P.E., M.D. Ohman and L.E. Eber (1989). Analysis of the patterns of distribution of zooplankton aggregations from an acoustic doppler current profiler. *California Cooperative Oceanic Fisheries Investigations Reports* **30**, 88-103.

Smith, S.L. and J.S. Bottero (1977). On upwelling in the Arabian Sea. In: A Voyage of Discovery. M. V. Angel (ed.), Pergamon Press, 291-304.

Smith, S.L. and P.V. Lane (1988). Grazing of the spring diatom bloom in the New York Bight by the calanoid copepods *Calanus finmarchicus*, *Metridia lucens*, and *Centropages typicus*. *Continental Shelf Research* **8**, 485-510.

Smith, S.L., R.E. Pieper, M.V. Moore, L.G. Rudstram, C.H. Greene, J.E. Zanon, C.M. Flagg and C.E. Williamson (1992). Acoustic techniques for the in situ observations of zooplankton. *Archiv fur Hydrobiologie Ergebnisse der Limnologie* **36**, 23-43.

Smith, S.L., M. Roman, I. Prusova, K. Wishner, M. Gowing, L.A. Codispoti, R.T. Barber, J. Marra and C. Flagg (1998). Seasonal response of zooplankton to monsoonal reversal in the Arabain Sea. *Deep-Sea Research II* **45**, 2369-2403.

Sournia, A. (1994). Pelagic biogeography and fronts. *Progress in Oceanography* **34**, 109-120.

Sparnocchia, S., G.M.R. Manzella and P.E. La Violette (1994). The interannual and seasonal variability of the MAW and LIW core properties in the western Mediterranean Sea. *Coastal and Estuarine Studies* **46**, 177-194.

Stanton, T.K. (1988a). Sound Scattering by Cylinders of Finite Length .1. Fluid Cylinders. *Journal of the Acoustical Society of America* **83**, 1: 55-63.

Stanton, T.K. (1988b). Sound Scattering by Cylinders of Finite Length .2. Elastic Cylinders. *Journal of the Acoustical Society of America* **83**, 1: 64-67.

Stanton, T.K. (1989). Sound scattering by cylinders of finite length. III. Deformed cylinders. *Journal of the Acoustical Society of America* **86**, 691-705.

Stanton, T.K. (1992). Sound scattering by rough elongated elastic objects: I. Means of a scattered field. *Journal of the Acoustical Society of America* **92**, 1641-1664.

Stanton, T.K. and D. Chu (2000). Review and recommendations for modeling of scattering by fluid-like elongated zooplankton: euphausiids and copepods. *ICES Journal of Marine Science* **57**, 793-807.

Stanton, T.K., D. Chu, P.H. Wiebe and C.S. Clay (1993b). Average echoes from randomly orientated random-length finite cylinders: zooplankton models. *Journal of the Acoustical Society of America* **94**, 3463-3472.

Stanton, T.K., D.Z. Chu and P.H. Wiebe (1996). Acoustic scattering characteristics of several zooplankton groups. *ICES Journal of Marine Science* **53**, 2: 289-295.

Stanton, T.K., D.Z. Chu and P.H. Wiebe (1998b). Sound scattering by several zooplankton groups. II. Scattering models. *Journal of the Acoustical Society of America* **103**, 1: 236-253.

Stanton, T.K., D.Z. Chu, P.H. Wiebe, R.L. Eastwood and J.D. Warren (2000). Acoustic scattering by benthic and planktonic shelled animals. *Journal of the Acoustical Society of America* **108**, 2: 535-550.

Stanton, T.K., D.Z. Chu, P.H. Wiebe, L.V. Martin and R.L. Eastwood (1998a). Sound scattering by several zooplankton groups. I. Experimental determination of dominant scattering mechanisms. *Journal of the Acoustical Society of America* **103**, 1: 225-235.

Stanton, T.K., C.S. Clay and D. Chu (1993a). Ray representation of sound scattering by weakly scattering deformed fluid cylinders: simple physics and application to zooplankton. *Journal of the Acoustical Society of America* **94**, 3454-3462.

Stanton, T.K., R.D.M. Nash, R.L. Eastwood and R.W. Nero (1987). A Field Examination of Acoustical Scattering from Marine Organisms at 70 Khz. *IEEE Journal of Oceanic Engineering* **12**, 2: 339-348.

Stanton, T.K., P.H. Wiebe and D. Chu (1998c). Differences between sound scattering by weakly scattering spheres and finite-length cylinders with application to sound scattering by zooplankton. *Journal of the Acoustical Society of America* **103**, 1: 254-264.

Stanton, T.K., P.H. Wiebe, D. Chu and L. Goodman (1994b). Acoustic characterization and discrimination of marine zooplankton and turbulence. *ICES Journal of Marine Science* **51**, 469-479.

Stanton, T.K., P.H. Wiebe, D.Z. Chu, M.C. Benfield, L. Scanlon, L. Martin and R.L. Eastwood (1994a). On Acoustic Estimates of Zooplankton Biomass. *ICES Journal of Marine Science* **51**, 4: 505-512.

Steedman, H.F. (1976). Zooplankton fixation and preservation. UNESCO Press, 350.

Stelfox, C.E., P.H. Burkill, E.S. Edwards, R.P. Harris and M.A. Sleigh (1999). The structure of zooplankton communities, in the 2 to 2000 lm size range, in the Arabian Sea during and after the SW monsoon, 1994. *Deep-Sea Research II* **46**, 815-842.

Strass, V.H. (1992). Chlorophyll patchiness caused by mesoscale upwelling at fronts. *Deep-Sea Research I* **39**, 75-96.

Sullivan, B.K. (1980). In situ feeding behaviour of Sagitta elegans and Eukrohnia hamata (chaetognatha) in relation to the vertical distribution and abundance of prey at Ocean Station 'P'. *Limnology and Oceanography* **25**, 317-326.

Sund, O. (1935). Echo sounding in fishery research. *Nature* **135**, 953.

Swallow, J.C. (1984). Some aspects of the physical oceanography of the Indian Ocean. *Deep-Sea Research I* **31**, 639-650.

Szczucka, J. and Z. Klusek (1996). Migration patterns of acoustic scatterers in the southern Baltic Sea. *Oceanologia* **38**, 1: 61-79.

Tarling, G.A., J.B.L. Matthews, P. David, O. Guerin and F. Buchholz (2001). The swarm dynamics of northern krill (*Meganyctiphanes norvegica*) and pteropods (*Covolinia inflexa*) during vertical migration in the Ligurian Sea observed by an acoustic Doppler current profiler. *Deep-Sea Research I* **48**, 1671-1686.

Tarling, G.A., J.B.L. Matthews, R. Saborowski and F. Buchholz (1998). Vertical migratory behaviour of the euphausiid, *Meganyctiphanes norvegica*, and its dispersion in the Kattegat Channel. *Hydrobiologia* **376**, 331-341.

Tchernia, P. (1980). Descriptive regional oceanography. Oxford, Pergamon Press, 253 pp.

The_Ring_Group (1981). Gulf Stream cold-core rings: their physics, chemistry and biology. *Science* **212**, 1091-1100.

Thibault, D., R. Gaudy and J. Lefevre (1994). Zooplankton Biomass, Feeding and Metabolism in a Geostrophic Frontal Area (Almeria-Oran Front, Western Mediterranean) - Significance to Pelagic Food Webs. *Journal of Marine Systems* **5**, 3-5: 297-311.

Thorpe, S.A. and A.J. Hall (1987). Bubble clouds and temperature anomalies in the upper ocean. *Nature* **328**, 48-51.

Tintore, J., D. Gomis, S. Alonso and G. Parrilla (1991). Mesoscale dynamics and vertical motion in the Alboran Sea. *Journal of Physical Oceanography* **21**, 811-823.

Tintore, J., P.E. La Violette, I. Blade and A. Cruzado (1988). A study of an intense density front in the eastern Alboran Sea: The Almeria-Oran front. *Journal of Physical Oceanography* **18**, 1384-1397.

Tintore, J., A. Viudez, D. Gomis, S. Alonso and F.E. Werner (1994). Mesoscale variability and Q vector vertical motion in the Alboran Sea. *Coastal and Estuarine Studies* **46**, 47-71.

Tiselius, P. (1992). Behaviour of *Acartia tonsa* in patchy food environments. *Limnology and Oceanography* **37**, 1640-1651.

Trathan, P.N., J. Priddle, J.L. Watkins, D.G.M. Miller and A.W.A. Murray (1993). Spatial Variability of Antarctic Krill in Relation to Mesoscale Hydrography. *Marine Ecology-Progress Series* **98**, 1-2: 61-71.

Traykovski, L.V.M., T.K. Stanton, P. Wiebe and J.F. Lynch (1998). Model-based covariance mean variance classification techniques: Algorithm development and application to the acoustic classification of zooplankton. *IEEE Journal of Oceanic Engineering* **23**, 344-364.

Traynor, J.J. and J.E. Ehrenberg (1979). Evaluation of the dual beam fish target strength method. *Journal of Fisheries Research Board Canada* **36**, 9: 1065-1071.

Urick, R.J. (1983). Principles of underwater sound. New York, McGraw-Hill, 423 pp.

Van Cuyck, J.P., J.P. Sessarego, O. Guerin-Ancey and P.M. David (1993). Study of acoustical reflexion coefficient of a monospecific phytoplanktonic layer. *Compterendu de l'Academie des Sciences Paris, Life Sciences* **316**, 633-635.

Van Der Spoel, S. and R.P. Heyman (1983). A comparative atlas of zooplankton: biological patterns in the oceans. Berlin, Springer-Verlag, 186 pp.

Videau, C., A. Sournia, L. Prieur and M. Fiala (1994). Phytoplankton and Primary Production Characteristics at Selected Sites in the Geostrophic Almeria-Oran Front System (Sw Mediterranean-Sea). *Journal of Marine Systems* **5**, 3-5: 235-250.

Vinogradov, M.E. and N.M. Voronina (1961). Influence of the oxygen deficit on the distribution of plankton in the Arabian Sea. *Okeanologiya* **1**, 4: 670-678.

Vinogradov, M.Y., E.A. Shushkina, A.Y. Gorbunov and N.L. Shashkov (1991). Vertical distribution of the macro- and mesoplankton in the region of the Costa Rica Dome. *Oceanology* **26**, 222-228.

Viudez, A. and J. Tintore (1995). Time and space variability in the eastern Alboran Sea from March to May 1990. *Journal of Geophysical Research* **100**, 8571-8586.

Viudez, A., J. Tintore and R.L. Haney (1996). Circulation in the Alboran Sea as determined by quasi-synoptic hydrographic observations. Part 1: Three-dimensional structure of the two anticyclonic gyres. *Journal of Physical Oceanography* **26**, 684-705.

Wade, I.P. and K.J. Heywood (2001). Acoustic backscatter observations of zooplankton abundance and behaviour and the influence of oceanic fronts in the northeast Atlantic. *Deep-Sea Research II* **48**, 4-5: 899-924.

Waring, G.T., C.P. Fairfield, C.M. Ruhsam and M. Sano (1993). Sperm shales associated with Gulf Stream features off the northeastern USA shelf. *Fisheries Oceanography* **2**, 101-105.

Warren, B.A. (1992). Circulation of north Indian deep water in the Arabian Sea. In: Oceanography of the Indian Ocean. B. N. Desai (ed.), New Dehli, Oxford and IBH Publishing Co, 575-582.

Warren, B.A. (1994). Context of the suboxic layer in the Arabian Sea. In: Biogeochemistry of the Arabian Sea. D. Lal (ed.), Indian Academy of Sciences, 203-216.

Warren, B.A., H. Stommel and J.C. Swallow (1966). Watermasses and patterns of flow in the Somali basin during the southwest monsoon of 1964. *Deep-Sea Research I* **13**, 825-860:

Warren, J.D., T.K. Stanton, M.C. Benfield, P.H. Wiebe, D. Chu and M. Sutor (2001). *In situ* measurements of acoustic target strengths of gas-bearing siphonophores. *ICES Journal of Marine Science* **58**, 740-749.

Weeks, A.R., G. Griffiths, H. Roe, G. Moore, I.S. Robinson, A. Atkinson and R. Shreeve (1995). The distribution of acoustic backscatter from zooplankton compared with physical structure, phytoplankton and radiance during the spring bloom in the Bellingshausen Sea. *Deep-Sea Research Part II* **42**, 4-5: 997-1019.

Welschmeyer, N.A. (1994). Fluorometric analysis of chlorophyll-a in the presence of chlorophyll-b and pheopigments. *Limnology and Oceanography* **39**, 8: 1985-1992.

Wessel, J.H. and R.K. Johnson (1996). Commonality and uniqueness in the biogeography of Indian Ocean mesopelagic fishes. In: The Arabian Sea: living marine resources and the environment. M. F. Thompson and N. M. Tirmizi (ed.), Balkema, 295-308.

Wiebe, P.H. (1988). Functional regression equations for zooplankton displacement volume, wet weight, dry weight, and carbon: a correction. *Fishery Bulletin* **86**, 4: 833-835.

Wiebe, P.H. (1995). Developing a high-frequency system to remotely 'see' plankton distributions. *Oceanus* **38**, 1: 14-16.

Wiebe, P.H., S. Boyd and J.L. Cox (1975). Relationships between zooplankton displacement volume, wet weight, dry weight, and carbon. *Fishery Bulletin* **73**, 4: 777-787.

Wiebe, P.H., N.J. Copley and S.H. Boyd (1992). Coarse-scale horizontal patchiness and vertical migration of zooplankton in Gulf Stream warm-core ring 82-H. *Deep-Sea Research I* **39**, Suppl.: S247-S278.

Wiebe, P.H. and G. Flierl (1983). Euphausiid invasion/dispersal in Gulf Stream cold-core rings. *Australian Journal of Marine and Freshwater Research* **34**, 625-652.

Wiebe, P.H., C.H. Greene, T.K. Stanton and J. Burczynski (1990). Sound Scattering by Live Zooplankton and Micronekton - Empirical-Studies with a Dual-Beam Acoustical System. *Journal of the Acoustical Society of America* **88**, 5: 2346-2360.

Wiebe, P.H., D.G. Mountain, T.K. Stanton, C.H. Greene, G. Lough, S. Kaartvedt, J. Dawson and N. Copley (1996). Acoustical study of the spatial distribution of plankton on Georges Bank and the relationship between volume backscattering strength and the taxonomic composition of the plankton. *Deep-Sea Research II* **43**, 7-8: 1971-1998.

Wiebe, P.H., T.K. Stanton, M.C. Benfield, D.G. Mountain and C.H. Greene (1997). High-frequency acoustic volume backscattering in the Georges Bank coastal region and its interpretation using scattering models. *Institute of Electrical and Electronic Engineers Journal of Oceanic Engineering* **22**, 445-464.

Williams, R., N.R. Collins and D.V.P. Conway (1983). The Double Lhpr System, a High-Speed Microplankton and Macroplankton Sampler. *Deep-Sea Research I* **30**, 3: 331-342.

Williams, R. and D.V.P. Conway (1988). Vertical-Distribution and Seasonal Numerical Abundance of the Calanidae in Oceanic Waters to the Southwest of the British- Isles. *Hydrobiologia* **167**, 259-266.

Wilson, C.D. and E. Firing (1992). Sunrise swimmers bias acoustic Doppler current profiles. *Deep-Sea Research I* **39**, 885-892.

Wishner, K., E. Durban, A. Durbin, M. Macaulay, H. Winn and R. Kenney (1988). Copepod patches and right whales in the Great South Channel off New England. *Bulletin of Marine Science* **43**, 825-844.

Wishner, K., M. Gowing and C. Gelfman (1998). Zooplankton biomass in the upper 1000 m in the Arabian Sea: overall seasonal and geographic patterns, and relationship to oxygen gradients. *Deep-Sea Research II* **45**, 2405-2432.

Wishner, K., L. Levin, M. Gowing and L. Mullineaux (1990). Involvement of the oxygen minimum in benthic zonation on a deep seamount. *Nature* **346**, 57-59.

Wishner, K.F. and S.K. Allison (1986). The distribution and abundance of copepods in relation to the physical structure of the Gulf Stream. *Deep-Sea Research I* **33**, 705-731.

Woodward, W.E. and G.F. Appell (1986). Current velocity measurements using acoustic Doppler backscatter: a review. *IEEE Journal of Oceanic Engineering* **OE-11**, 3-6.

Wyrtki, K. (1962). The oxygen minima in relation to ocean circulation. *Deep-Sea Research I* **9**, 11-23.

Wyrtki, K. (1971). Oceanographic Atlas of the International Indian Ocean Expedition. US, National Science Foundation, Government Printing Office, 531pp.

Wyrtki, K. (1973). Physical oceanography of the Indian Ocean. In: The biology of the Indian Ocean. B. Zeitschel and S. A. Gerlach (ed.), Springer-Verlag, 18-36.

Yang, T.-H., N.C. Lai, J.B. Graham and G.N. Somero (1992). Respiratory, blood, and heart enzymatic adaptations of *Sebastolobus alascanus* (Scorpaenidae: Teleostei) to the oxygen minimum zone: A comparative study. *Biological Bulletin* **183**, 490-499.

Yayanos, A.A., A.A. Benson and J.C. Nevenzel (1978). The pressure-volume-temperature (PVT) properties of a lipid mixture from a marine copepod, *Calanus plumchrus*: implications for buoyancy and sound scattering. *Deep-Sea Research I* **25**, 257–268.

Yoder, J.A., L.P. Atkinson, S.S. Bishop, E.E. Hofman and T.N. Lee (1983). Effect of upwelling on phytoplankton productivity on the outer South-eastern US continental shelf. *Continental Shelf Research* **1**, 385-404.

Youssara, F. and R. Gaudy (2001). Variations of zooplankton in the frontal area of the Alboran Sea (Mediterranean Sea) in winter 1997. *Oceanologica Acta* **24**, 4: 361-376.

Zeitzschel, B. (1973). The biology of the Indian Ocean. London, Chapman & Hall Limited, 549 pp.

Zhou, M., W. Nordhausen and M. Huntley (1994). Adcp Measurements of the Distribution and Abundance of Euphausiids near the Antarctic Peninsula in Winter. *Deep-Sea Research I* **41**, 9: 1425-1445.

The following published papers were included in the bound thesis. These have not been digitised due to copyright restrictions, but the links are provided.

Fielding, S. Crisp, N. Allen, J.T. Hartman, M.C. Rabe, B. Roe, H.S.J. (2001) **Mesoscale subduction at the Almeria-Oran front** Journal of Marine Systems: 30 (3-4), 287-304 https://doi.org/10.1016/s0924-7963(01)00063-x Actions